Spring 2015

Physical basis of the power-law spatial scaling structure of peak discharges

Tibebu Bekele Ayalew
University of Iowa

PHYSICAL BASIS OF THE POWER-LAW SPATIAL SCALING STRUCTURE OF PEAK DISCHARGES

by

Tibebu Bekele Ayalew

A thesis submitted in partial fulfillment
of the requirements for the Doctor of Philosophy
degree in Civil and Environmental Engineering
in the Graduate College of
The University of Iowa

May 2015

Thesis Supervisors: Professor Witold F. Krajewski
Assistant Professor Ricardo Mantilla

Graduate College
The University of Iowa
Iowa City, Iowa

CERTIFICATE OF APPROVAL

_____

PH.D. THESIS

_____

This is to certify that the Ph.D. thesis of

Tibebu Bekele Ayalew

has been approved by the Examining Committee for
the thesis requirement for the Doctor of Philosophy degree
in Civil and Environmental Engineering at the May 2015 graduation.

Thesis Committee: _____
Witold F. Krajewski, Thesis Supervisor

_____
Ricardo Mantilla, Thesis Supervisor

_____
Allen Bradley

_____
Dale L. Zimmerman

_____
Gabriele Villarini

To my mom Atsede (አዳድዬ) and
To my late father Bekele (ጋሸዬ)

~አበባዬ...~
አበባዬን...
ውበቷ አድምቆት
ሊጋነቷ አሳምሯት
ድምቅቷ ሐብት ሆኗት
እምረቷ አሳድጎት
ግና...
ድንገት ፍቅር ሆና
ድንገት ረከሳ በሞት
ድንገት ህይወት ሆና
ድንገት ፅልመት ውጧት
በአርምሞ ሳያት
በፀጥታ ስከተላት
አንድን ቀን ደምቃ
ሌላን ቀን የመደብዘዟ
አንድን ቀን አብባ
ሌላን ቀን የመርገፏ
ተምሳሌትነቱ ለህይወቴ
ሀቅነቱ ለኔነቴ
ብርሐን ሆኖ
ህይወቴን በአበባዬ
አበባዬን በህይወቴ
መስ'ያት ነጎድኩኝ
ድንገት እስኪመጣ ሞቴ።
~~//~~

መጋቢት ፪፬÷፱፬
(አርባ ምንጭ)

… but I have long learned to distinguish that which is important from that which is urgent. True, it is urgent that man should eat, for else he cannot live and death abides no question. Yet love, the sense of life and the quest of God are more important.

Antoine de Saint-Exupéry
The Wisdom of the Sands

ACKNOWLEDGEMENTS

First and foremost, I offer my sincerest gratitude to my major supervisor, Prof. Witold F. Krajewski, for providing me the opportunity and the necessary guidance to work on the problem of flood prediction in ungauged basins. I am grateful for your dedication to our regular weekly meetings despite your numerous other commitments. I have enjoyed all our discussions and always left your office inspired. I have learnt from you not only about doing cutting edge science but also about many other things in life that I will always cherish. One simply could not wish for a better mentor.

I am also greatly indebted to my co-advisor, Prof. Ricardo Mantilla, for your exemplary guidance. Your passion for knowledge discovery is contagious. I will never forget the countless interesting discussions we had. I have met very few people that influenced my perspective on life and you are one of them. I would like to let you know that I am always striving to be better and to become the "permanent resident of the human network", as you so eloquently put it in one of our discussions. Thank you!

I also would like to extend my sincere gratitude to Professors Allen Bradley, Dale Zimmerman, and Gabriele Villarini for serving on my dissertation committee and for all your useful suggestions. Special mention goes to Prof. Dale Zimmerman for making yourself available and patiently working with me while drafting the last chapter of my dissertation (Chapter IX), which demonstrated the practical application of the findings I reported throughout the dissertation.

I have met great many people during my time at IIHR-Hydroscience and Engineering and because of them I have enjoyed every minute of my time at this great institute. The success of my dissertation is also not without the amazing help of Dr. Scott Small, for writing and patiently debugging the unbelievably fast research code, and

Radoslaw Goska, for making radar rainfall data easily accessible and for patiently working with me as I navigated through the baby stages of SQL programming. I am also thankful to Dr. Bong-Chul Seo for all the helps with the high resolution Iowa Flood Center (IFC) radar rainfall product. I would also like to thank Daniel Horna, Nicholas Thomas, Karl Brauer, Vijay Mishra, Chad Drake, and Mohamed Elsaadani for your friendship and all the fun times. I hope we will continue to keep in touch as we all embark on the next chapter of our professional career.

I also would like to thank my Ethiopian friends in Iowa, Arbsie and Berhan, for your amazing friendship and for being always there for me, Mimi, and Lina. Arbsie, I enjoyed all our interesting discussions and debates, sometimes heated but always respectful, on Ethiopian politics. I will miss those countless nights. I hope we will see a prosperous and democratic Ethiopia in our life time. Many thanks also goes to Wako for all your kindness. Though you arrived late in Iowa, I have learnt great many things from you.

My journey in my doctoral studies at the University of Iowa was punctuated by quite few life changing moments. I joined the graduate program few weeks after my daughter, Lina, was born. Seeing her grow up and hit her developmental milestones as books on infant development suggest was an amazing experience. It means that my time at the University of Iowa was not only counted by the classes I attended or the semesters I enrolled in or the papers I wrote but also by the milestones Lina was able to tick off of her menu. I feel as if we grew up together, learning new things and pushing ourselves to explore new frontiers. I regret, though, that I was not there to fully enjoy every minute of your progress for the commitment that I had for my own studies. But, always know that

you mean everything to me and I love you to pieces. Huge kudos goes to your mom, Mimi, who sacrificed a lot to the both of us. We love you more than you can imagine!

On the other side of the spectrum, my dad suddenly passed away mid-way through my study. It was the nadir of my life. I survived those dark moments through the help of my family and friends. My dad didn't go past elementary school but understood the value of education. He instilled in me an unquenchable curiosity and the discipline required to achieve my dreams. He also thought me not to put any limit to what I could achieve, challenged me to scale the heights, and to never give up. I wish you would have been around to see the progress I have made. I love you and I miss you!

ABSTRACT

Key theoretical and empirical results from the past two decades have established that peak discharges exhibit power-law, or scaling, relation with drainage area across multiple scales of time and space. This relationship takes the form $Q(A) = \alpha A^{\theta}$ where Q is peak discharge, A is the drainage area, θ is the flood scaling exponent, and α is the intercept. Motivated by seminal empirical studies that show that the flood scaling parameters α and θ change from one rainfall-runoff event to another, this dissertation explores how certain rainfall and catchment physical properties control the flood scaling exponent and intercept at the rainfall-runoff event scale using a combination of extensive numerical simulation experiments and analysis of observational data from the Iowa River basin, Iowa. Results show that θ generally decreases with increasing values of rainfall intensity, runoff coefficient, and hillslope overland flow velocity, whereas its value generally increases with increasing rainfall duration. Moreover, while the flood scaling intercept is primarily controlled by the excess rainfall intensity, it increases with increasing runoff coefficient and hillslope overland flow velocity. Results also show that the temporal intermittency structure of rainfall has a significant effect on the scaling structure of peak-discharges. These results highlight the fact that the flood scaling parameters are able to be estimated from the aforementioned catchment rainfall and physical variables, which can be measured either directly or indirectly using in situ or remote sensing techniques. The results of the study mark a step forward to provide a physically meaningful framework for regionalization of flood frequencies and hence to solve the long standing hydrologic problem of flood prediction in ungauged basins.

PUBLIC ABSTRACT

For decades, engineers have been challenged with estimating design floods of a given probability of occurrence, which is required while designing hydraulic structures. The problem is often solved using historical annual maximum peak discharge data obtained from a location upstream of the site of interest. However, as most of the basins in the world are ungauged, there are limited streamflow gauging sites from which the necessary information can be obtained. In the 1960's, the U.S. Geological Survey came up with a regional flood frequency estimation technique that can be used for flood prediction in ungauged basins. This purely statistical method often uses drainage area alone to predict design floods. Review of the regional equations show that the parameters of the power-law relation between peak discharge and drainage area change from one geographic region to another. Moreover, the regional flood frequency equations established for different regions of the U.S. kept changing every time they are updated to include the latest peak discharge observations. This shows the sensitivity of the method to the length of historical data, which has huge implications to the overall cost of hydraulic structures. The overarching goal of this dissertation is to contribute towards providing a physical foundation for the regional equations by investigating the physical mechanisms that control the scaling invariance of peak discharges with drainage area at the rainfall-runoff event scale. The dissertation also proposes and demonstrates a new flood forecasting framework that is based on the scaling theory of floods.

TABLE OF CONTENTS

LIST OF TABLES

LIST OF FIGURES

CHAPTER I

INTRODUCTION

1.1. Motivation

It seems that the rivers know the theory. It only remains to convince the engineers of the validity of this analysis. – Emil Gumbel

Regional flood frequency equations are extensively used for peak discharge prediction in ungauged and poorly gauged river basins. In the United States, the U.S. Geological Survey (USGS) pioneered the methodology used for regionalization of flood frequencies in the 1960's (Benson 1962; Benson 1964; Benson 1968), and the method has subsequently undergone several refinements (e.g., Hardison 1974; IACWD 1982; Tasker and Stedinger 1986). Regional flood frequency equations relate the peak discharge with rainfall and catchment physical properties such as drainage area, main channel slope, longest stream length, soil type, land use, and mean annual precipitation. Among these, drainage area is the most important and often used as the single explanatory variable to predict peak discharge *quantiles*. Observational data from across the world show that peak discharge *quantiles* exhibit scaling-invariance with drainage area and their relation can be described by the power-law $Q_p(A) = c(p)A^{\phi(p)}$, where $Q_p(A)$ is the peak discharge *quantile* for a given drainage area (A) and probability of exceedance (p), $c(p)$ is the intercept, and $\phi(p)$ is the flood scaling exponent. The peak discharge *quantiles* used to estimate $c(p)$ and $\phi(p)$ are obtained by fitting the Log-Pearson type III distribution to the annual maximum peak discharge time series obtained from gauging sites that are located in hydrologically similar regions (IACWD 1982). It is important to highlight that the peak discharge *quantile* scaling relationship is currently

used at the annual time scale to estimate peak discharge quantiles in ungauged basins that are nested within gauged basins from which historical peak discharge data that is required to estimate $c(p)$ and $\phi(p)$ is obtained. The interested reader is referred to Dawdy et al. (2012) for a detailed review of the history of regional flood frequency analysis and future directions.

A close examination of the regional flood-frequency methodology reveals that it has the following two major limitations: 1) peak discharge *quantiles* that are obtained from different gauging sites in hydrologically similar geographic regions do not necessarily come from the same rainfall-runoff event; in some cases they could actually come from events that occurred in different years, which leads to temporal mixing of peak discharge events that are not physically related and 2) peak discharge *quantiles* obtained from catchments that are not nested (i.e., catchments that don't share the same drainage network) but are located in hydrologically similar geographic regions are put together, and as a result, peak discharge *quantiles* that are a product of independent rainfall-runoff events that occurred in independent (unnested) catchments are mixed. Consequently, the methodology ignores the fundamental role that the scale-invariant drainage network plays in determining the magnitude of peak discharges across a range of scales in the basin (Gupta et al. 1996; Gupta et al. 2007; Mantilla et al. 2006; Menabde and Sivapalan 2001). As a result of the spatial and temporal mixing of independent peak discharges, the parameters of the power-law relationship between peak discharge *quantiles* and drainage area (i.e., $\alpha(p)$ and $\theta(p)$) that are extensively used in regional flood frequency equations lack physical meaning (Dawdy et al. 2012). Because of this and the lack of empirical data that is required to estimate $\alpha(p)$ and $\theta(p)$, the method

cannot be used for peak discharge estimation in ungauged basins located in ungauged regions.

The physics behind the scaling invariance of peak discharges with drainage area can be determined by analyzing peak discharges from nested watersheds that occur following a runoff generating rainfall event. Such an analysis would enable a precise description of the event-to-event variability of the flood scaling exponent and the intercept in terms of rainfall and catchment physical properties that govern the generation of peak discharges in space and time. The resulting insights are of paramount importance in our quest to solve the longstanding problem of hydrologic predictions in ungauged basins (PUB) (Sivapalan et al. 2003). In addition to being useful to develop a physically meaningful regionalization of flood frequency, such a framework will provide a flood prediction methodology that is not affected by climate change, as it does not depend on historical observations to predict future peak discharges (Dawdy et al. 2012; Gupta 2004; Gupta et al. 2010; Gupta et al. 2007). It can also provide a framework that can be used to verify the streamflow simulation skills of physics based rainfall-runoff models. To this end, a number of studies were undertaken in an effort to describe the flood scaling parameters in terms of rainfall and catchment physical properties (Di Lazzaro and Volpi 2011; Furey and Gupta 2005; Gupta 2004; Gupta et al. 1996; Gupta et al. 2010; Gupta et al. 2007; Mandapaka et al. 2009; Mantilla et al. 2006; Mantilla et al. 2011; Morrison and Smith 2001; Ogden and Dawdy 2003). These studies, which cover a range of theoretical and empirical studies, revealed that peak discharges from nested catchments exhibit scale-invariance with drainage area at the rainfall-runoff event scale and are able to connect both the intercept and the exponent to rainfall and catchment physical properties.

1.2. Research gaps and objectives

The literature review of the physical basis of the event-to-event variability of the flood scaling intercept and exponent, which is presented in Chapter-II, reveals the following major research gaps:

1) There is a lack of knowledge on whether or not the spatial-scaling structure of peak discharges at the individual rainfall-runoff event scale can be used to explain the spatial scaling structure of peak discharge quantiles at the annual time scale.
2) There is a limited knowledge on the effect of the interplay among catchment antecedent soil moisture state, rainfall intensity, duration, hillslope overland flow velocity, and channel flow velocity on the scaling structure of peak discharges. Moreover, there is no study that looked into how the temporal intermittency structure of rainfall affects the scaling structure of peak discharges.
3) The few empirical studies that demonstrated the occurrence of a scale invariant peak discharge spatial organization following a single rainfall event have done so using data from the 21 km^2 Goodwin Creek Experimental Watershed located in Mississippi, USA. There is a need to expand this analysis to larger river basins where flood with significant societal impacts often occur.
4) There is a limited understanding of how the interplay among rainfall intensity, duration, hillslope overland flow velocity, and channel flow velocity control the occurrence and property of a scale break in the power-law relationship between peak discharge and drainage area.

Motivated by the aforementioned research gaps, the overarching objective of my study is to contribute towards solving the longstanding problem of prediction in

ungauged basins (Sivapalan et al. 2003) by unveiling the physical connection between a host of rainfall and catchment physical properties and the flood scaling exponent and intercept at the rainfall-runoff event scale. In summary, the thesis is devoted to address the following key research questions:

1) Can regional flood frequency equations be understood in terms of the scaling invariance property of peak discharge with drainage area that is observed following the occurrence of a runoff generating rainfall event in a nested watershed (Chapter III)?
2) How does the interplay among rainfall and catchment physical properties control the spatial scaling structure of peak discharges (Chapters IV, V, and VI)?
3) How does the effect of certain rainfall and catchment physical properties on peak discharge at the rainfall-runoff event scale propagates to the annual time scale and, hence, affect flood frequency (Chapters VII and VIII)?
4) How can the spatial scaling properties of peak discharges observed following single rainfall-runoff events in nested watersheds be used for flood prediction (forecasting) across a range of spatial scales (Chapter IX)?

1.3. Thesis organization

The thesis is organized as follows. Chapter II presents the literature review where the research gaps stated above are discussed in greater detail. Chapter III strictly defines a hydrologic region as a nested watershed and explores if scale invariant peak discharges frequently occur in a mesoscale river basin at the rainfall-runoff event scale. The chapter also explores, provided that scaling invariance of peak discharges holds in a mesoscale river basin, the existence of a connection between the flood scaling parameters of peak

discharges resulting from individual rainfall-runoff events and the flood scaling parameters of peak discharge *quantiles*. Chapters IV and V investigate the physical basis behind the observed scaling invariance of peak discharge at the rainfall-runoff event scale using diagnostic numerical simulations of four different watersheds from the state of Iowa, US. Chapter VI provides empirical evidence for the simulation results obtained in Chapters IV and V and presents further insights into the effect of the temporal structure of rainfall on the spatial scaling structure of peak discharges. Chapter VII investigates how the drainage network geometry affects the magnitude of peak discharge at the rainfall-runoff event scale and how this effect propagates to the annual time scale affecting flood frequency. Chapter VIII expands on Chapter III and explores how the effect of the interplay among rainfall intensity and duration on peak discharge at the rainfall-runoff event scale affects the scaling of peak discharge quantiles. It also explores if a connection exists between event scale scaling and quantile based scaling of peak discharges that could help in regionalization of flood frequencies. Chapter IX proposes a flood forecasting framework that utilizes the insights obtained from the analysis of the scaling of peak discharges at the individual rainfall-runoff event scale. The predictive capability of the proposed framework is demonstrated using observed flood events that occurred in the Iowa River basin, Iowa. Chapter X synthesizes the findings of the thesis and provides concluding remarks on the main findings of the thesis, and ends with recommendations for future research. Figure I-1 provides a graphic summary of the thesis structure.

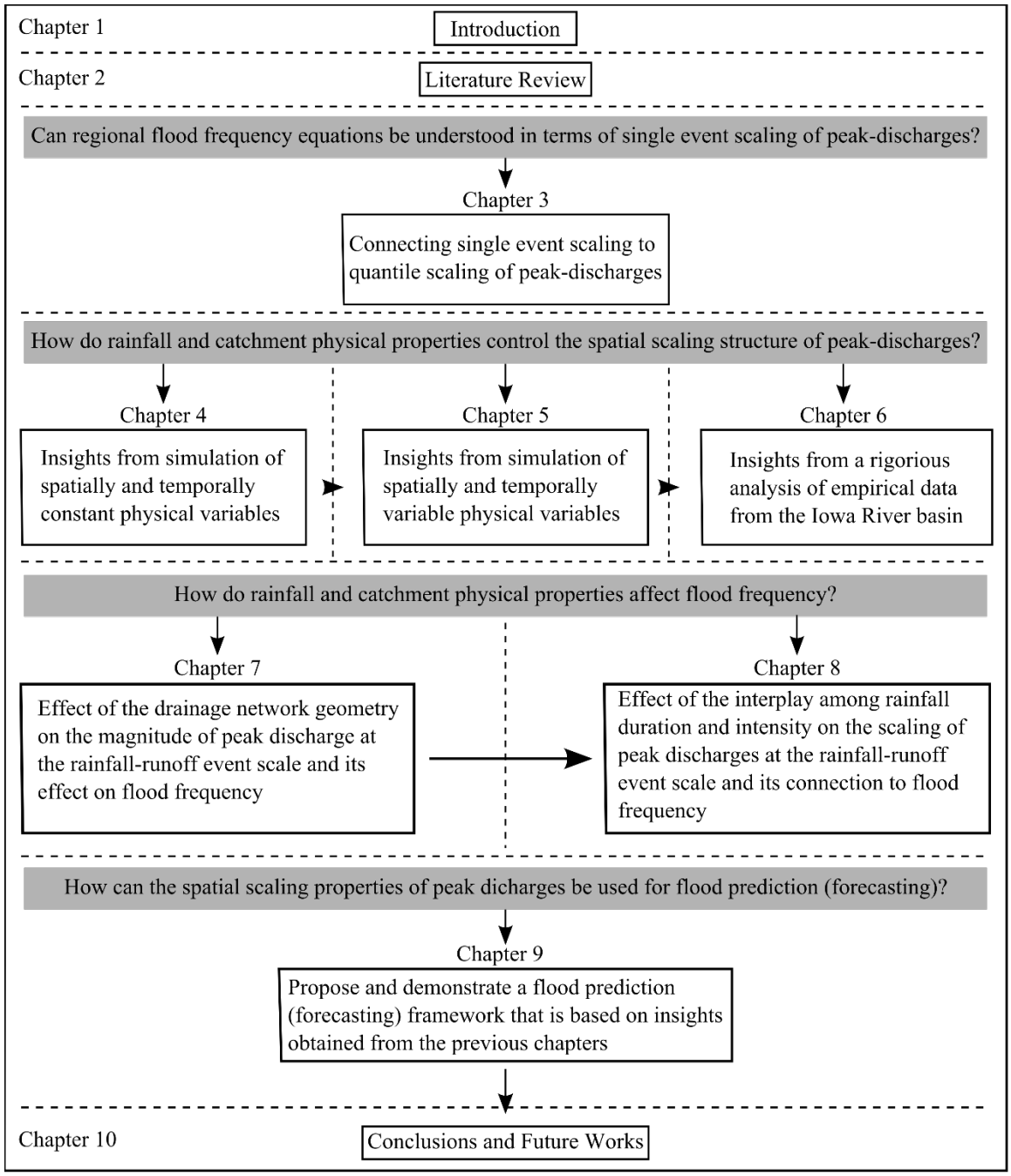

Figure I - 1. A schematic summary of the thesis structure.

CHAPTER II
LITERATURE REVIEW

2.1. A brief review of scaling laws in channel networks

Power-law relationships of the form $f(x) = ax^b$, which have an attribute of scaling invariance, have been shown to arise in numerous self-similar (self-affine) natural and artificial systems. Power-law patterns are well documented in biology, physics, chemistry, astronomy, geology, computer science, and finance, to name a few (e.g., Benz et al. 2008; Brown et al. 2004; Brown et al. 2002; Gabaix 2009; Mandelbrot 1983; Mitzenmacher 2003; Newman 2005; Schroeder 1991). Schroeder (1991) states that "self-similarity is one of the decisive symmetries that shape our universe and our efforts to comprehend it." In drainage basin hydrology, the channel network, along which the fundamental processes of transportation, aggregation, and attenuation of streamflows occur, is shown to be self-similar (Peckham 1995; Rodriguez-Iturbe and Rinaldo 1997; Tarboton et al. 1988). The self-similar property of channel networks is characterized by *Horton's* (1945) *laws of drainage composition*. These laws are stated as follows:

$$\frac{N_\omega}{N_{\omega+1}} \approx R_B \quad \text{or} \quad N_\omega \approx R_B^{\Omega-\omega} \qquad \text{Equation II-1}$$

$$\frac{L_\omega}{L_{\omega-1}} \approx R_L \quad \text{or} \quad L_\omega \approx L_1 R_L^{\omega-1} \qquad \text{Equation II-2}$$

$$\frac{A_\omega}{A_{\omega-1}} \approx R_A \quad \text{or} \quad A_\omega \approx A_1 R_A^{\omega-1} \qquad \text{Equation II-3}$$

where ω is the Horton-Strahler stream order, N_ω is the number of streams of order ω, R_B is termed as the bifurcation ratio; Ω is the order of the main stem of the river network and hence called the network order; L_ω is the mean length of streams of order ω; L_1 is

the mean length of streams of order 1; R_L is termed the length ratio; A_ω is the mean drainage area of catchments draining into streams of order ω; A_1 is the mean drainage area of catchments draining into streams of order 1; and R_A is termed as the area ratio. The laws stated in equations Equation II-1, 2, and 3 are specifically known as *Horton's law of stream numbers, Horton's law of stream lengths, and Horton's law of stream areas*, respectively. These laws serve as the governing principles of drainage basin structure (Kirchner 1993). A widely recognized power-law that emerges in drainage basins is the Hack's law $L \approx aA^{\varsigma}$, where L is mainstream length, A is the drainage area, and ς is the scaling exponent that typically ranges between 0.56 and 6.

The seminal work of Leopold and Maddock (1953) introduced the concept of *hydraulic geometry* and showed that, at a given channel cross-section, channel width (w), depth (d), flow velocity (v), and suspended-sediment load (S_L) vary as a power-law function of discharge (Q) as shown below.

$$w = aQ^b \qquad \text{Equation II-4}$$

$$d = cQ^f \qquad \text{Equation II-5}$$

$$v = kQ^m \qquad \text{Equation II-6}$$

$$S_L = pQ^j \qquad \text{Equation II-7}$$

where a, c, k, p, b, f, m, and j are numerical constants that are constrained by the set of equations $b + f + m = 1$ and $a \times c \times k = 1$, since $Q = wdv$. They also showed that these relationships hold true for different downstream locations that are related through discharges that have the same exceedance probability. These power-law equations have

found wide range of applications in river hydraulics (Ferguson 1986). A famous application is the streamflow rating curves that are used by the USGS to convert continuous streamflow stage measurements to discharge. Leopold and Miller (1956) later extended these hydraulic geometric relations to Horton laws and showed that river basin geomorphology, hydrology, and channel hydraulics are interconnected. Gupta and Mesa (2014) recently formulated Horton laws for the hydraulic-geometric variables and their scaling exponents using the self-similarity property of channel networks as a basis.

An important characterization of the drainage network structure for hydrologic application is provided by the geomorphological width function. The width function, which is defined as the total number of links at a given distance from the outlet, is connected to the streamflow response of a basin (Gupta et al. 1986; Gupta and Mesa 1988; Kirkby 1976; Mesa and Mifflin 1986). It is equivalent to the streamflow response that can be computed under the assumptions of spatially constant instantaneous rainfall; instantaneous injection of hillslope overland flow to adjacent channels, and the transport of channel flow with constant velocity and no attenuation (Gupta et al. 2010). The geomorphological theory of the instantaneous unit hydrograph (GIUH) has its roots in the physical understanding of the width function (Gupta and Waymire 1983; Gupta et al. 1980; Rodríguez-Iturbe and Valdés 1979).

Recent research has shown that the maxima of the width function that is evaluated at the bottom of complete order Horton-Strahler streams within a given watershed exhibits scaling invariance with drainage area (Veitzer and Gupta 2001). Moreover, empirical data shows that peak discharges, which are the subject of this dissertation, has a power-law relationship with drainage area over multiple scales of space and time (e.g.,

Eash 2001; Eaton et al. 2002; Furey and Gupta 2005; Goodrich et al. 1997; Gupta et al. 2010; Leopold et al. 1964; Lima and Lall 2010; Ogden and Dawdy 2003; Poveda et al. 2007; Robinson and Sivapalan 1997). The observed statistical self-similarity of peak discharges is believed to be a manifestation of the scale-invariant channel networks (Dawdy et al. 2012; Gupta 2004; Gupta et al. 2007; Gupta and Waymire 1998). Accordingly, I will give considerable emphasis to the role of the river network in all the empirical data analysis and diagnostic simulation exercises that I will conduct to reveal the rainfall and catchment physical properties that control the spatial scaling properties of peak discharges.

2.2. Evidence for peak discharge quantile scaling

Drainage area was first recognized as a peak discharge scaling parameter in the classical Rational Method (Mulvany 1850). In this method, for a given soil type (topography), rainfall intensity I and rainfall duration T, that is equivalent to the longest travel time in the watershed ("time of concentration," t_c), peak discharge scales linearly with drainage area at internal locations in the catchment and can be estimated using the formula $Q(A) = c_r \cdot I \cdot A$, where c_r is the runoff coefficient. Under this method, the flood scaling intercept corresponds to I_e ($I_e = c_r \cdot I$) and the scaling exponent $\theta = 1$. The method is still being used in engineering practice for the design of small drainage structures and is applicable to small catchments with drainage areas as large as 15 km^2 (Brutsaert 2005). At around the same time the Rational Method was outlined, (O'Connell 1868) proposed the power-law formula $Q(A) = cA^{0.5}$ that linked peak discharge to drainage area, where c is a coefficient related to the region.

In the early 1960s, the United States Geological Survey (USGS) adopted and popularized an empirical quantile regression method for regional flood frequency estimation that is being used throughout the world (Dawdy et al. 2012). These quantile regressions often use drainage area as the only predictor variable and follow the form $Q_p(A) = c(p)A^{\phi(p)}$, where both the intercept c and the exponent ϕ are functions of the probability of exceedance p. The flow quantile $Q_p(A)$ exhibits a log-log linear relationship with drainage areas located in a homogeneous region. This means that streams that belong to different drainage networks, and are therefore not nested but are located in a homogeneous region, exhibit similar peak discharge scaling structure. It is important to note here that the delineation of homogeneous regions is based on the residuals from regression analyses and on physiographic characteristics of river basins (Eash 2001).

Empirical evidence resulting from quantile regression analysis carried out by USGS shows the existence of two types of peak discharge scaling: simple scaling and multiscaling. Simple scaling describes the property that ϕ is independent of the probability of exceedance of peak discharge, whereas multiscaling describes the property that ϕ is either positively or negatively correlated with the probability of exceedance. Regional regression equations established by the USGS for different regions throughout the U.S. show that ϕ generally decreases with decreasing probability of exceedance, which implies multiscaling. Gupta and Dawdy (1995) suggested that the observed multiscaling property is a manifestation of the multiscaling property of rainfall and is generally observed in regions where rainfall-driven floods occur. They also suggested

that the simple scaling observed in snowmelt-generated floods arises from the simple scaling structure of the spatial variability in snowmelt patterns. However, empirical data analysis from the 21.2 km^2 Goodwin Creek Experimental Watershed has revealed that simple scaling can also occur in geographic regions where convective rainfall patterns occur frequently (Ogden and Dawdy 2003).

Goodrich et al. (1997) reported the first empirical evidence that showed peak discharge *quantiles* in nested watersheds exhibit self-similarity. They used empirical data from the semi-arid Walnut Gulch experimental watershed in Arizona, whose nested watersheds have drainage areas that range from 0.0018 to 149 km^2. Their peak discharge *quantile-based* empirical analysis revealed ϕ values of 0.85 and 0.90 for the 2-yr and 100-yr return periods for drainage areas up to 1km^2, whereas ϕ equals 0.55 and 0.58 for the 2-yr and 100-yr return periods for drainage areas greater than 1km^2, which suggests multiscaling. The fact that ϕ assumes different values for drainage areas above and below a certain critical drainage area, in this case 1km^2, suggests the existence of scale break. Ogden and Dawdy (2003) studied the scaling structure of peak discharge *quantiles* in a nested watershed where the spatial rainfall pattern is fairly uniform. They analyzed peak discharge data from the 21.2 km^2 Goodwin Creek experimental watershed (GCEW) located in Mississippi in the south-central United States. They examined 16 years of continuous rainfall and runoff data from subcatchments that have drainage areas ranging from 0.172 to 21.2 km^2 at the outlet. Their estimate of ϕ with the value of 0.77 was independent of the return period, which suggests simple scaling.

The *quantile-based* estimates of the flood scaling exponent ϕ discussed thus far offer little that would enhance the understanding of which aspects of the rainfall-runoff processes control the flood scaling intercept α and exponent θ during a single rainfall-runoff event. This is because, as discussed earlier, peak discharges used in the USGS's regional quantile regression approach likely correspond to different rainfall events which may also come from different watersheds that are not nested and, hence, belong to different drainage networks.

Research Gap 1: Although the regional flood frequency methods that are widely used in engineering practice in the United States and elsewhere in the world are known to be a statistical black-box (Dawdy et al. 2012), no meaningful attempt has been made to connect the physics of runoff generation at the individual rainfall-runoff event scale to the observed spatial scaling invariance of peak discharges at the annual time scale.

2.3. Evidence for peak discharge scaling following single rainfall-runoff events

2.3.1. Results from theoretical studies

Some of the first efforts to predict the flood scaling exponent θ from catchment physical variables that control the generation of peak discharges in space and time had the drainage network at the center of their theoretical investigations. The geomorphological theory of the instantaneous unit hydrograph (GIUH) (Gupta et al. 1980; Rodríguez-Iturbe and Valdés 1979), which for the first time connected the drainage network geometry to catchment runoff response, opened an avenue for such theoretical explorations. To this end, Gupta et al. (1996) made the first attempt to predict the scaling exponent θ from the self-similar properties of rainfall and drainage network. Their highly idealized setup, which included a spatially constant instantaneous rainfall, instantaneous delivery of runoff to channels, constant channel velocity, and the self-

similar Peano network, resulted in a derived power-law scaling of peak discharge with drainage area. They demonstrated that the flood scaling exponent can be described in terms of the *fractal dimension* of the spatial regions of a Peano basin that contributes to peak discharges at successively larger drainage areas. Relaxing the spatially constant rainfall assumption resulted in a flood-scaling exponent that is smaller than the one that was previously calculated using a spatially constant rainfall. Gupta and Waymire (1998) later used a more realistic random topology model (Shreve 1967) to demonstrate the role that rainfall duration plays in determining the flood-scaling exponent. They derived an analytical equation that relates mean peak discharge to drainage area A and rainfall duration T for a given excess rainfall depth P_e and showed that, as T approaches zero, θ assumes a value that ranges from 0 to 1 and can be estimated from the scaling exponent of the width function maxima (β). Their results show that if every link in the drainage network drains hillslopes that have the same drainage area, then the value of θ that results from a spatially uniform instantaneous rainfall input is the same as the scaling exponent of the maxima of the width function. Furthermore, they reported that when $T \to t_c$, $\theta \to 1$. The later result is essentially what the Rational formula predicts, with the flood scaling intercept α being the fraction of rainfall per unit area that appears as direct runoff at the catchment outlet.

Both Gupta et al. (1996) and Gupta and Waymire (1998) derived their results under the assumption that there is no attenuation of streamflow as it propagates downstream. Menabde and Sivapalan (2001) extended these studies to the more realistic Mandelbrot-Viseck tree (Mandelbrot and Vicsek 1989) over which the coupled mass and simplified momentum equations were solved at the hillslope-channel-link scale and investigated the

role of flow attenuation in channel networks. Their result showed the dependence of the flood scaling exponent on excess rainfall intensity and duration. They concluded that, as the rainfall duration approaches zero (i.e., instantaneous rainfall), the flood scaling exponent becomes less than the width function scaling exponent due to flow attenuation. Mantilla et al. (2006) expanded the analysis to real drainage networks and concluded that the flood scaling exponent is greater than the width function scaling exponent which contradicted results from earlier findings (Menabde and Sivapalan 2001; Menabde et al. 2001) that were obtained through the analysis of peak discharge spatial organization over idealized mean self-similar networks. Their result was further affirmed by Mandapaka et al. (2009) who, using the same methodology, extensively investigated the effect of the spatial variability of rainfall on the scaling structure of peak discharges in a real drainage basin.

Furey and Gupta (2007) investigated the role of P_e and T in determining α and θ. They devised, based on the theory of GIUH, an analytical formula that relates the expected value of peak discharge to P_e, T, and A. Their diagnosis of power-laws observed in 148 rainfall-runoff events from the GCEW further confirmed the systematic dependence of α and θ on P_e and T. They also reported the results from their preliminary analysis of the effect of channel velocity v_c and hillslope overland flow velocity v_h on α and θ and concluded that both α and θ can be affected by v_c and v_h. Their theoretical estimations of the peak discharge were comparable with empirical data from GCEW only when realistic v_h values were used, thereby confirming the importance of the hillslope residence time in determining the scaling structure of peak discharge.

However, their study did not investigate how the flood scaling intercept and exponent are affected by changes in hillslope overland flow velocity and channel velocity, which are manifestations of important catchment physical properties such as the antecedent moisture state, soil type, land use, and topography. Moreover, how the effect of both the channel and hillslope overland flow velocities on the spatial scaling of peak discharges is constrained by the interplay among rainfall intensity and duration that characterize a given rainfall event is not addressed.

The theoretical advancements discussed so far, with the exception of Furey and Gupta (2007), have all neglected the role of hillslope residence time and assumed that runoff generated on hillslopes enters the drainage network instantaneously. An interesting line of research has focused on determining the relative role of hillslope and channel network processes at different catchment scales. Robinson et al. (1995) argued that hillslope processes dominate the runoff response of small catchments, while the network geomorphology dominates the runoff response at larger catchment scales. They reported that the scale at which the catchment runoff response transitions from hillslope-dominated to one that is dominated by the network geomorphology is on the order of 10 km^2. D'Odorico and Rigon (2003), building on the theory of GIUH, also suggested that the contribution of hillslope residence time in the runoff dispersion is significant at smaller watersheds and can be neglected at larger scales. They also suggested that the role of the hillslope is dependent on the catchment moisture condition and becomes significant due to the increased residence time when the catchment is saturated. Contrary to these findings, Saco and Kumar (2004) showed that hillslopes play a significant role in shaping the runoff response at all scales. Most importantly, they showed that, when

hillslope overland flow velocities are smaller than channel velocities, which is often the case, the effect of hillslope overland flow velocity through kinematic dispersion becomes more important than geomorphic dispersion. Botter and Rinaldo (2003) analyzed the role of hillslopes in 150 sub-basins of the Brenta River in Italy that have sizes ranging from 4 to 1500 km^2 and further confirmed that v_h has a significant role in determining the runoff response at all scales.

In a study that directly addressed the effect of hillslope overland flow velocity on the spatial scaling structure of peak discharges, Di Lazzaro and Volpi (2011) argued that the spatial variability of hillslope velocity breaks the scaling invariance property of peak discharges. Their analytic approach was also based on the theory of GIUH. They applied the methodology to 13 different river basins that have drainage areas ranging from 218 to 4116 km^2 and are located in the Tiber catchment in central Italy. They extracted the drainage network from a 20×20 m digital elevation model and calculated both v_c and v_h for each basin using observed rainfall-runoff data in the catchment. They finally estimated peak discharge values at the outlet of each basin to study their scaling structure. Their result showed that peak discharge estimates became scale invariant and followed a power-law with $\theta = 0.52$ when the instantaneous rainfall input and both v_c and v_h are all assumed to be uniform across all basins. However, scale invariance of peak flow does not hold when they apply different v_h values to each basin while allowing both instantaneous rainfall input and v_c values to remain uniform across all basins. Although the applied v_h values were different from basin to basin, they were constant over a single basin. Considering that the study basins were not nested, it is impossible to

conclude from this work how the aggregated effect of spatially variable v_h affects peak discharges at successively larger scales.

Research Gap 2: It is now very clear that the runoff response at all scales is not only shaped by the drainage network and v_c but also by v_h. The review of the literature also showed that the effect of the interplay among I_e, T, v_h, and v_c on the scaling structure is not fully addressed. Moreover, no study has addressed the role of catchment antecedent soil moisture state in shaping the spatial scaling structure of peak-discharges. This is important because, in reality, these catchment processes are interdependent, and understanding their relative roles in determining the spatial scaling structure of peak discharges provides further insight into our quest to estimate α and θ from catchment variables that can be either measured or estimated.

2.3.2. Results from empirical study

The first rainfall-runoff event-based empirical study of peak discharge comes from Ogden and Dawdy (2003), who studied the scaling structure of peak discharges in the nested Goodwin Creek Experimental Watershed where the spatial rainfall pattern is fairly uniform. They analyzed 226 rainfall-runoff events that occurred in the watershed over a period of 16 years. These events occurred over a time scale that range from few hours to a day. Their results showed that the estimated θ values were different for different rainfall-runoff events and generally varied between 0.6 and 1. The event-to-event variability of θ was also shown to decrease as the magnitude of peak discharge at the outlet increases. This is because, they argued, more intense rainfall events that are responsible for larger peak discharge events have less spatial variability when compared with less intense rainfall events.

Furey and Gupta (2005), motivated by the findings of Ogden and Dawdy (2003), undertook a rainfall-runoff event-based analysis of peak discharge scaling structure in the

GCEW with the main objective of understanding which rainfall and catchment physical properties are responsible for the event-to-event variability of both α and θ. Their study, which was based on 148 rainfall-runoff events, showed that θ increases with increasing rainfall duration T, whereas α increases with increasing excess rainfall depth P_e. They explained that the significant event-to-event variability of θ observed at smaller peak discharge values is due to the variability in the antecedent soil moisture state that is strongly seasonal and the increased spatial rainfall variability associated with less intense rainfall events.

In a related study, Gupta et al. (2007) reported that peak discharges from the semiarid Walnut Gulch basin (A=150 km^2) in Arizona also follow power-law scaling with drainage area at the individual rainfall-runoff event scale. Recently, Gupta et al. (2010) analyzed the devastating June 2008 flood event in the Iowa River basin (A=32,400 km^2) and demonstrated that power-law scaling holds following rainfall-runoff events in a mesoscale catchment. Moreover, the predicted flood scaling exponent of 0.79 is different from the width function maxima scaling exponent of 0.47, which was estimated for the same river basin. This indicates that the scaling exponent is controlled by other physical factors in the basin in addition to the drainage network along which the spatial aggregation and attenuation of flows occur. The findings of Ogden and Dawdy (2003), Furey and Gupta (2005), Gupta et al. (2007), and Gupta et al. (2010) collectively represent mounting empirical evidences for the existence of scaling invariance of peak discharge with drainage area at the rainfall-runoff event scale and that the scaling parameters are controlled by rainfall and catchment physical properties that vary from event to event. However, our ability to exploit this fundamental hydrologic discovery for

predictive purposes in ungauged and scarcely-gauged catchments depends on whether or not we succeed to physically describe both α and θ in terms of measurable catchment physical variables.

Research Gap 3: Furey and Gupta (2005, 2007) undertook the only empirically-based effort to connect the event-to-event variability of the flood scaling exponent to rainfall and catchment physical properties using data from the 21 km^2 GCEW. In light of this, there is a need to expand the analysis to larger river basins at which scale devastating flood events often occur. In addition to testing the validity of existing theoretical predictions, a similar empirically-based analysis using data from large river basins would enable us to unveil additional insights into catchment physical processes that govern the generation of scale invariant peak discharges in space and time.

2.4. Existence of scale break

In the context of statistical scaling of peak discharges, a scale break occurs when the log-log linear relationship between peak discharge and drainage area exhibits different flood scaling exponents above and below a certain critical drainage area. Empirical data suggests the existence of scale break in some catchments. Using a *quantile-based* analysis of annual peak discharge data from the nested Walnut Gulch Experimental Watershed, Goodrich et al. (1997) showed the existence of scale break at about 1 km^2 in the watershed. They attributed the observed scale break to partial area storm coverage and ephemeral channel losses through infiltration as the stream flow propagates downstream. Asquith and Slade (1997), also using a *quantile-based* regional regression analysis, reported the existence of a scale break for watersheds in Texas, US, that happens at about 83 km^2 for the 100 year flood. Contrary to the aforementioned findings, no scale break was reported in the *event* and *quantile-based* analysis of empirical data from the GCEW (Furey and Gupta 2005; Ogden and Dawdy 2003). This leads to the

questions: why is a scale break not observed in GCEW? Is that because the watershed is too small (A~21 km^2) to detect a scale break? Or is that because of the difference in rainfall patterns and runoff generating mechanisms across different geographic regions? If the answer to the later question is yes, what is the physical basis for the observed scale break? There is limited literature that addresses these questions.

Gupta and Waymire (1998) investigated the effect of rainfall duration on the scaling structure of peak discharges and showed how a scale break in the log-log linear relationship between peak discharge and drainage area can result as a product of rainfall duration that is shorter than the catchment time of concentration. They showed that the power-law scaling of peak discharge with drainage area is dominated by the rainfall-runoff variability at smaller spatial scales, whereas it is dominated by the drainage network structure and flow dynamics at larger spatial scales. Based on this observation, they theorized that the transition between the two processes marks the scale at which a scale break occurs. It is important to note here that they derived their results under the assumption that there is no attenuation of streamflow as it propagates downstream. Menabde and Sivapalan (2001) extended these studies to the more realistic Mandelbrot-Viseck tree over which the coupled mass and simplified momentum equations were solved at the hillslope-channel-link scale and investigated the role of flow attenuation in channel networks. Their results also showed the existence of scale break whose spatial scale of occurrence is controlled by rainfall duration. Mandapaka et al. (2009) expanded the analysis to a real river network and showed that, under the assumption of rainfall that is either spatially constant or spatially variable according to the Gaussian distribution, the spatial scale at which a scale break occurs varies as a function of rainfall duration when

linear channel velocity formulation is used whereas it varies as a function of the interplay among rainfall duration and intensity when a nonlinear channel velocity formulation is used. Interestingly, they also reported that the scale break disappears when a realistic rainfall field that is either obtained from radar rainfall data or is randomly generated using a space-time rainfall model is used as input. This later result suggests the role the space-time structure of rainfall plays in determining the spatial scaling structure of peak discharges.

Research Gap 4: The literature review indicates that all of the studies that used a numerical simulation approach to address the issue of scale break ignored the role of hillslope residence time in determining the spatial scaling structure of peak-discharges (Gupta and Waymire 1998; Mandapaka et al. 2009; Menabde and Sivapalan 2001). This highlights the need for a comprehensive assessment of the effect of the interplay among rainfall intensity, duration, hillslope overland flow velocity, and channel flow velocity on the occurrence and property of a scale break.

CHAPTER III

SCALING INVARIANCE OF PEAK DISCHARGES IN A MESOSCALE RIVER BASIN

3.1. Introduction

Ogden and Dawdy (2003) reported from the analysis of 223 rainfall-runoff events observed in the 21 km^2 GCEW that the flood scaling intercept and exponent varies from event to event over a range of 0.6 to 1.0. This result provided the first empirical evidence for the existence of a scale invariant spatial organization of peak discharges at the rainfall-runoff event scale. The event-to-event variability of the flood scaling intercept and exponent are a direct consequence of the event-to-event variability of rainfall and catchment physical properties that govern the generation of runoff in space and time. While both the flood scaling exponent and intercept of peak discharges resulting from a single rainfall-runoff event vary from event to event, their annual maximum peak discharge *quantile-based* analysis of the same dataset revealed that the flood *quantile* scaling exponent ϕ is constant (~0.77) for all the return periods considered suggesting simple scaling. This leads me to ask the question: if the rainfall and other catchment physical variables that gave rise to the annual maximum peak discharges at each of the gauging sites are different from year to year, how can the exponent remain the same? Can similar observations be made in other river basins? To date, no study is conducted if the observations from the GCEW also hold in mesoscale river basins where peak flood prediction is of paramount societal importance. A significant step in this direction is the study by Gupta et al. (2010) who showed that scaling invariance of peak discharge holds

for the historical flood event of June 2008 that occurred in the mesoscale Iowa River basin (Mutel 2010; Smith et al. 2013).

The main objectives of this chapter is to test if scaling-invariance of peak discharge with drainage area is observed in the mesoscale Iowa River basin (A=32,400 km^2) not only during rare flood events such as the one observed following the 2008 flood event but also during more frequent runoff generating rainfall events. Moreover, I will test if a connection can be made between scaling of peak discharges originating from single rainfall-runoff events and scaling of peak discharge *quantiles*. The reminder of the chapter is organized as follows. I begin by describing the study area and the sources of data used in this study. This is followed by a detailed description of the methodology used to identify rainfall-runoff events. I follow this by presenting the results and discussing their implication on the potential use of the *scaling theory of floods* in ungauged basins. I conclude the chapter by summarizing the major findings.

3.2. Study Area and Data Source

The Iowa River basin, which is located in eastern Iowa, US, drains a total area of about 32,400 km^2 before it joins the Mississippi River. The average annual temperature in the region ranges between 7 and 11 °C with July being the hottest month with mean daily highs of up to 28 ºC. The region gets mean annual precipitation of 965 mm with June being the wettest month (118 mm) and, as a result, floods are most frequent in June (Villarini et al. 2011). Floods also occur between Mid-March and early April as a combined result of snowmelt and rain on frozen soils (source: National Climatic Data Center (NCDC)). The region has recently suffered from frequent flooding with three of the top four peak discharge magnitudes of the past 112 years occurring at the catchment

outlet in June 2008, July 2014, and April 2013. When it comes to the landscape, the region has undergone extensive land cover change over the past century and it is now predominantly covered by cropland that is dominated by corn and soybeans (Gallant et al. 2011; Schilling et al. 2008).

I used a 30 m digital elevation model (DEM) obtained from the USGS to extract the drainage network. Geomorphic analysis of the drainage network show that the exponent that describes the power-law scaling of the width function maxima with drainage area is 0.45. The width function is calculated as the total number of channel-links at a given distance from the outlet of a catchment. Gupta et al. (2010) defines the width function as being equivalent to the streamflow response to an instantaneous rainfall that is instantaneously injected to channel-links and moves along the drainage network with constant velocity and without attenuation. Results from Mandapaka et al. (2009) and Mantilla et al. (2006) show that the scaling exponent of the width function maxima is the lower bound of the flood scaling exponent.

I used streamflow estimates provided by the USGS through their web interface to identify peak discharge events. These gauging sites provide instantaneous discharge data at a temporal resolution that ranges from 15 to 30 minutes. The total number of functioning streamflow gauging sites in the basin varies from year to year and from event-to-event within a given year. Accordingly, the total number of streamflow gauging sites used in our analysis varies from 30 to 42 and their corresponding drainage area range from 7 to 32,400 km^2. Moreover, I neglect two gauging sites that are located downstream of the Coralville dam which regulates a drainage area of 8070 km^2 along the main stem of the Iowa River. One of the gauging sites is located immediately

downstream of the dam whereas the other is located in Iowa City which is located 14 km further downstream. The nearest gauging site to the dam that we used in our analysis is located about 60 km downstream from the dam. I neglect the effect of the dam on the observed peak discharge at this gauging site and at those sites located further downstream by citing Smith et al. (2010) who reported that reservoirs have limited effect on the observed flood frequency for locations far downstream. The study area and the geographic locations of the gauging sites within the study area are shown in Figure III-1.

The streamflow time series is complemented by the Stage-IV radar rainfall product availability of which constrains my analysis to the 12 year period between 2002 and 2013. The radar rainfall product has a spatial resolution of 4×4 km and a temporal resolution of 1 hour. The product, which is provided nationally on the Hydrologic Rainfall Analysis Project (HRAP) grid, is extensively used for hydrologic modelling purposes in the Iowa River basin and elsewhere with good success (e.g., Cunha et al. 2012; Kalin and Hantush 2006).

3.3. Selection of Rainfall-Runoff Events

The first step in selecting rainfall-runoff events is to identify the time window that separates "independent" peak discharge events at the basin outlet. The term "independent" is used here in the approximate sense because the long memory of the basin means that peak discharge events happening in a single season are not strictly independent. Bearing this in mind, we used the basin's time of concentration, which is the time required for a water parcel to travel along a hillslope and the river network from the farthermost location in the basin to the outlet, as the minimum size of the time window that separates independent peak discharge events. I estimated the basin's time of

concentration using the respective channel flow velocity and hillslope overland flow velocity values of 0.5 and 0.02 m/s and found that for the Iowa River basin it is about 15 days. These channel and overland flow velocity values are within the range of what is observed in field measurements (Grimaldi et al. 2010; Gupta and Waymire 1998; Leopold et al. 1964). This means that rainfall events that occur more than 15 days before a peak discharge is observed at the basin outlet do not contribute directly to the observed peak discharge. Note here that I am neglecting the contribution of the base flow which comes from rainfall events that occurred within the basin way beyond the 15 days window that I am using to define a rainfall-runoff event.

3.4. Peak discharge Selection

Once the time window that separates independent rainfall-runoff events was estimated, I used the following two criteria to identify peak discharges corresponding to a single event: (1) there is a single-peaked hydrograph at the outlet and (2) all the streamflow gauging sites exhibit a significant streamflow response at some point during the 15 days window leading up to the time when a peak discharge is observed at the outlet. The second criterion ensures that the entire basin received a runoff generating rainfall event at some point during the 15 days window. Finally, I estimated the flood scaling parameters using Ordinary Least Squares (OLS) regression. I used the coefficient of determination from the OLS regression between peak discharge and drainage area as an additional criterion and neglected those events for which the coefficient of determination was less than 0.7.

3.5. Results

3.5.1. Analysis of peak discharge scaling at the rainfall-runoff event scale

Based on the strict criteria of rainfall-runoff event selection discussed in the previous section, I was able to identify, over the 12 year period, 50 events that exhibit scaling invariance. These results indicate that scaling invariance of peak discharge with drainage area often occurs at the rainfall-runoff event scale in a mesoscale river basin such as the Iowa River basin. This is the first empirical observation of its kind. The analysis also show that scaling invariance of peak discharge fails when only part of the basin gets rainfall during the 15 day time window. This is demonstrated in Figure III-2 and 3 where two different rainfall-runoff events are presented to show when scaling invariant peak discharge occurs and does not occur.

Figure III-4 shows four examples from the 50 events I have identified. As expected, the flood scaling exponent and intercept change from event to event. The temporal distribution of the flood scaling parameters estimated for the 50 events is presented in Figure III-5(a) and (b). It can be seen that no significant temporal trend is observed for the months considered. The results also show that the flood scaling exponent ranges between 0.5 and 1.3 leading to two important insights. First, the flood scaling exponent can be greater than one. This is contrary to results from theoretical predictions that set the upper bound of the flood scaling exponent to unity (Gupta and Waymire 1998). Empirical results from the GCEW also show that the flood scaling exponent is always less than one (Furey and Gupta 2005; Ogden and Dawdy 2003). The fact that the flood scaling exponent can be greater than one in the Iowa River basin whereas it is always less than one in the GCEW can be attributed to the spatial variability

of rainfall. Analysis of rainfall data from the GCEW shows that rainfall can be assumed to be spatially uniform due to the small size of the catchment which is less than the estimated correlation distance of rainfall occurring in the catchment (Ogden and Dawdy 2003). However, such uniformity of rainfall cannot be expected over the mesoscale Iowa River basin. The second important insight that we gain from these results is that the flood scaling exponent is always greater than the width function maxima scaling exponent of the basin's drainage network, which is found to be 0.45 (Figure III-1 c). This means that the lower bound of the flood scaling exponent is the width function maxima scaling exponent.

3.5.2. Analysis of peak discharge quantiles

In the previous section, I have shown that scale invariant spatial organization of peak discharges often occur in a mesoscale river basin such as the Iowa River basin following single rainfall-runoff events. An important additional question is to test if the scaling exponents and intercepts of peak discharges obtained from individual rainfall-runoff events can be connected to the scaling exponents and intercepts of peak discharge *quantiles*. Figure III-6 shows all the 50 peak discharge events observed at all the gauging sites in the basin. These events are not annual maximums and hence can be considered as being equivalent to peak discharges above a certain threshold, with the threshold in this case being the strict criteria set out in earlier sections to define rainfall-runoff events in a mesoscale river basin. The grey lines in Figure III-6 trace the OLS regression line fitted to peak discharges coming from individual rainfall-runoff events. The dark black lines show the OLS regression line fitted to the lowest, median, and highest peak discharge *quantiles*.

I followed the following two steps to test if a connection exists between the scaling of basin wide peak discharges resulting from single rainfall-runoff events and scaling of peak discharge *quantiles*. First, I calculated the probability of exceedance of the pair of scaling exponent and intercept corresponding to the 50 basin wide individual rainfall-runoff events using the probability of exceedance of the peak discharge observed at the outlet of the basin (Wapello) as a proxy. Second, I calculated two types of peak discharge *quantiles* using Weibull's plotting position formula. I call them Type-I and Type-II peak discharge *quantiles*. Type-I peak discharge *quantiles* are based on the 50 individual rainfall-runoff events. In this case, the 50 peak discharge events at each gauging sites are sorted in an increasing order and assigned a probability of exceedance according to their rank. This will lead to the scenario that peak discharges at different gauging sites that have the same probability of exceedance can come from different rainfall-runoff events. Type-II peak discharge *quantiles* are based on 12 annual maximum peak discharges that are observed at each gauging site over the 12 year period between 2002 and 2013. Recall that the 50 individual basin wide rainfall-runoff events were also obtained over the same 12 year period. The corresponding peak discharge *quantile* scaling exponents and intercepts for Type-I and Type-II peak discharge *quantile*s are then estimated by fitting an OLS regression line to logarithms of peak discharges that have the same exceedance probability and the logarithms of the corresponding drainage area, $log\ (A_j)$ where j denotes a stream flow gauging site. For the sake of comparison, I have also included the scaling exponent and intercept I calculated for annual maximum peak discharge *quantiles* (Type-II *quantiles*) that are observed over the 50 year period between 1963 and 2013. This compares to the regional

flood frequency equations the USGS estimated for the hydrologic region to which the Iowa River basin belongs (Eash 2001).

Figure III-7 shows superposition of the event based and *quantile* based estimates of the flood scaling exponents and intercepts as a function of the probability of exceedance of the peak discharges observed at the catchment outlet. It can be seen that the peak discharge *quantile* scaling exponent increases with increasing probability of exceedance while the intercept decreases with increasing probability of exceedance. The fact that the scaling exponent of peak discharge *quantiles* changes with probability of exceedance suggests that peak discharges from the Iowa River basin follow multiscaling. This result stands contrary to the results obtained from the GCEW where the peak discharge *quantile* scaling exponent remains constant irrespective of the probability of exceedance (Ogden and Dawdy 2003).

The results presented in Figure III-7 also show that the exponents ϕ and intercepts c of Type-I *quantiles* traces midway through the event based estimates of the exponent θ and intercept α. This connection between the scaling parameters corresponding to peak discharges resulting from basin wide single rainfall-runoff events and Type-I *quantiles* is made possible because the analysis is made in a nested watershed and peak discharges used for both sets of analysis are selected at the rainfall runoff event scale. The results also show that Type-II (annual maximum peak discharge) *quantile* based estimates of the exponent is less than the event and Type-I *quantile* based estimates of the exponent. The opposite is true for the intercepts estimated for Type-II *quantiles*. It appears that the relatively small values of the exponents estimated for Type-II *quantiles* is compensated

by the corresponding values of the intercepts that are relatively higher than the intercepts estimated for the events and Type-I *quantiles*.

The observed difference between single rainfall-runoff event based and *quantile* (Type-I and Type-II) based estimates of the scaling intercept and exponent does not necessarily mean that one is a better prediction framework than the other. While both can be used to predict peak discharge events and *quantiles* across scales, the degree of their applicability to solve the problem of peak discharge prediction in ungauged basins sets them apart. It is important to stress here that the *quantile* based estimates are used to predict peak discharges for ungauged basins located within gauged region. In such cases, they are used to predict future floods in terms of their probability of exceedance under the assumption that that the hydroclimate system has been stationary and will remain so in the future. However, this assumption is no longer valid as mounting evidence suggests that the climate is changing. Moreover, the *quantile* based estimates cannot be used for predictions in basins that are located within ungauged regions because of the lack of data required to estimate the flood scaling intercept and exponent. The promise of the event based peak discharge scaling analysis is that it can be used for prediction in ungauged basins embedded in ungauged regions. This promise is hinged on the hope that the event based scaling intercept and exponent can be predicted from rainfall and catchment physical processes that control the generation of peak flows in space and time. This means that historical peak discharge data is not required to predict the scaling exponent and intercept. As a result, it can be used under the changing climate. It is this exciting promise that motivated this dissertation. The following 3 chapters are devoted to

understand the observed event-to-event variability of the flood scaling exponent and intercept in terms of catchment physical processes.

3.6. Conclusion

The main objective of this chapter is to test if scaling invariance of peak discharge with drainage area can be observed following runoff generating rainfall events in a mesoscale river basin. To this end, I analyzed 50 rainfall-runoff events from the Iowa River basin (A=32,400 km^2). I selected these events in such a way that a single-peaked hydrograph is observed at the catchment outlet and that all the internal gauging sites exhibit a significant streamflow response at some point during a 15 days period leading up to the time when the peak discharge at the outlet is observed. This duration corresponds to the basin's time of concentration.

The results indicate that scaling invariance of peak discharge with drainage area frequently occurs in a mesoscale river basin such as the Iowa River basin at the rainfall-runoff event scale and the corresponding flood scaling parameters change from event-to-event. This finding extends the spatial scale of the only two other empirical findings obtained from the 21 km^2 Goodwin Creek Experimental Watershed (GCEW) in Mississippi (Furey and Gupta 2005; Ogden and Dawdy 2003) and the 148 km^2 Walnut Gulch Experimental Watershed (WGEW) in Arizona (Gupta et al. 2007).

The results also show that a connection can be made between the scaling parameters of peak discharges resulting from single basin wide rainfall-runoff events and peak discharge *quantiles* as long as the analysis is made using single rainfall-runoff event based peak discharges obtained from a nested basin. However, no apparent connection is evident between scaling exponent and intercept of peak-discharges obtained from single

rainfall-runoff events and the scaling exponent and intercept of annual maximum peak discharge *quantiles*.

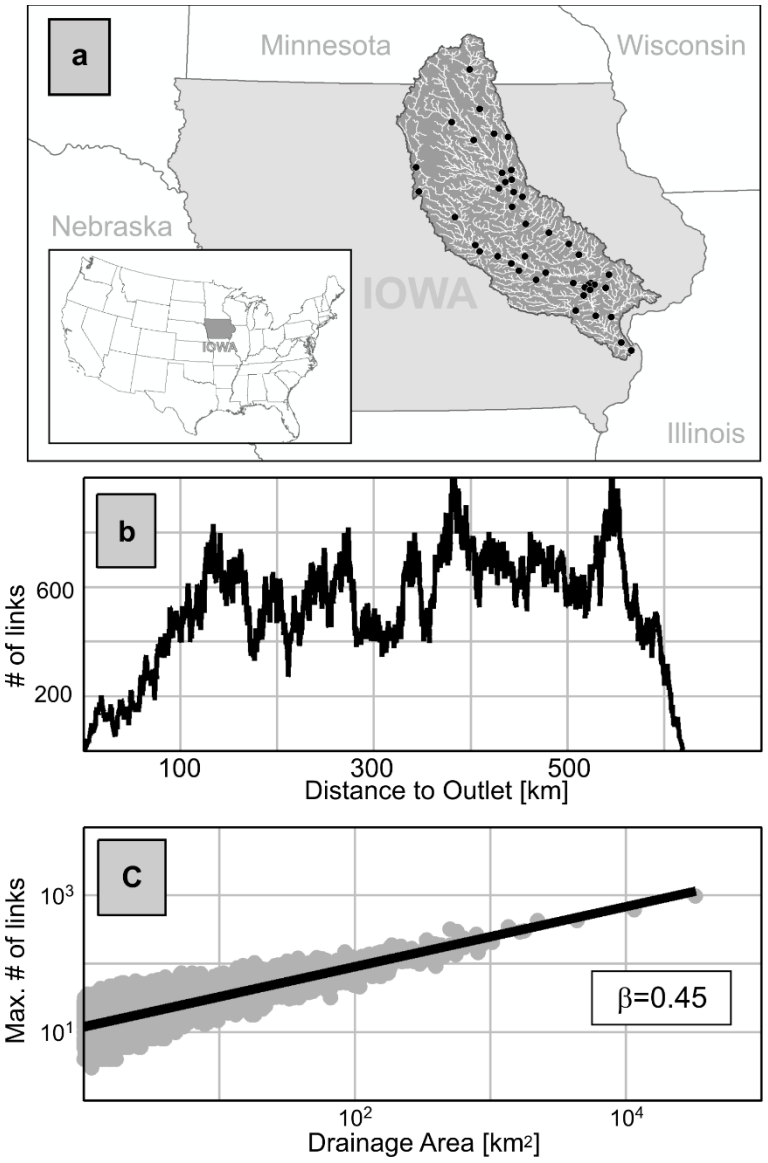

Figure III - 1. (a) The Iowa River basin and the geographic locations of the USGS gauging stations (black circles), (b) the width function evaluated at the outlet of the basin, and (c) scaling plot of the maxima of the width function that are evaluated at the bottom of the width function that are evaluated at the bottom of complete order Horton-Strahler streams in the basin.

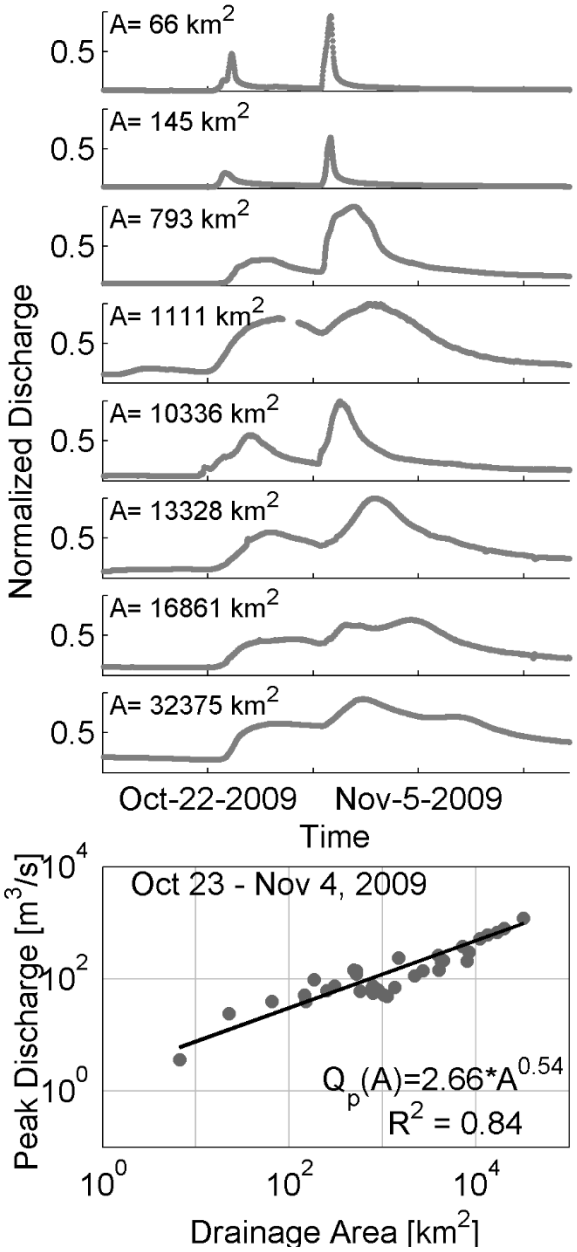

Figure III - 2. Example streamflow time series from representative USGS gauging sites in the basin (top panels) and the associated peak-discharge scaling plot (bottom panel) for the case where the entire basin got rainfall at some point during the 15 day travel time window. The streamflow time series is normalized by the annual maximum flow for each gauging site.

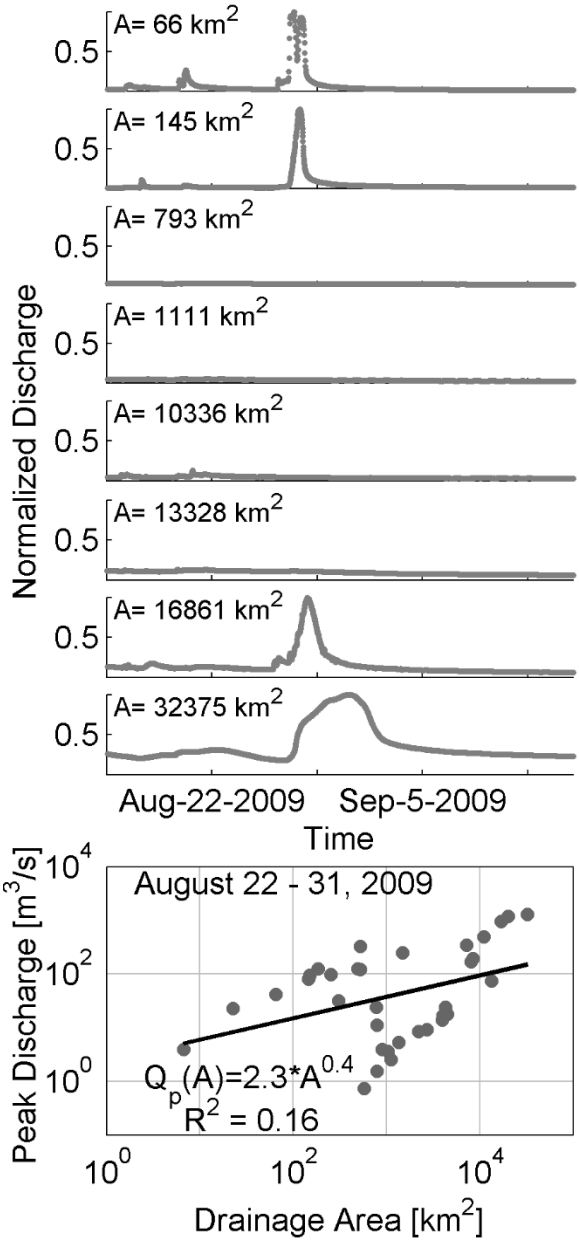

Figure III - 3. Example streamflow time series from representative USGS gauging sites in the basin (top panels) and the associated peak-discharge scaling plot (bottom panel) for the case where only a portion of the basin got rainfall at some point during the 15 day travel time window. The streamflow time series is normalized by the annual maximum flow for each gauging site.

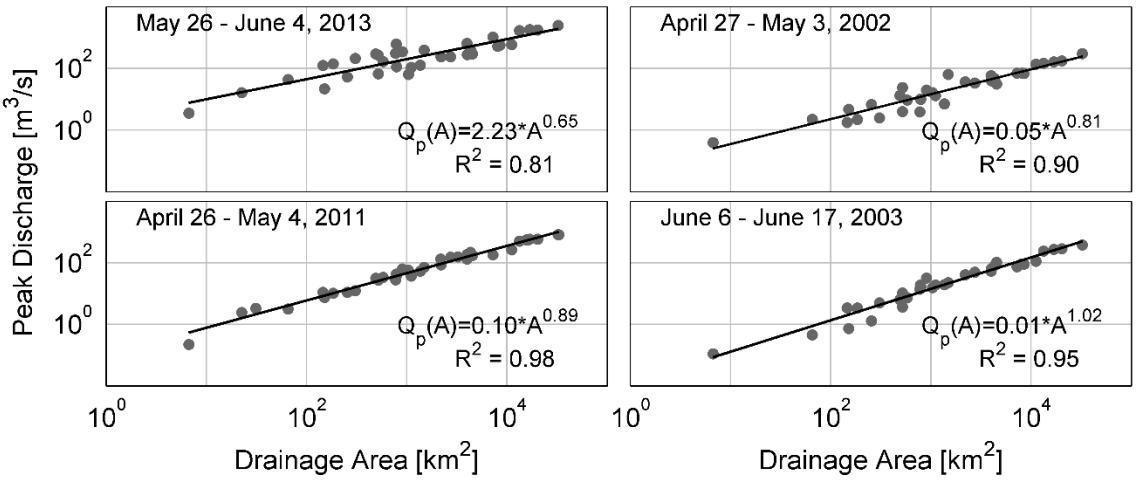

Figure III - 4. Observed spatial scaling of peak-discharges with drainage area for four events in the Iowa River basin.

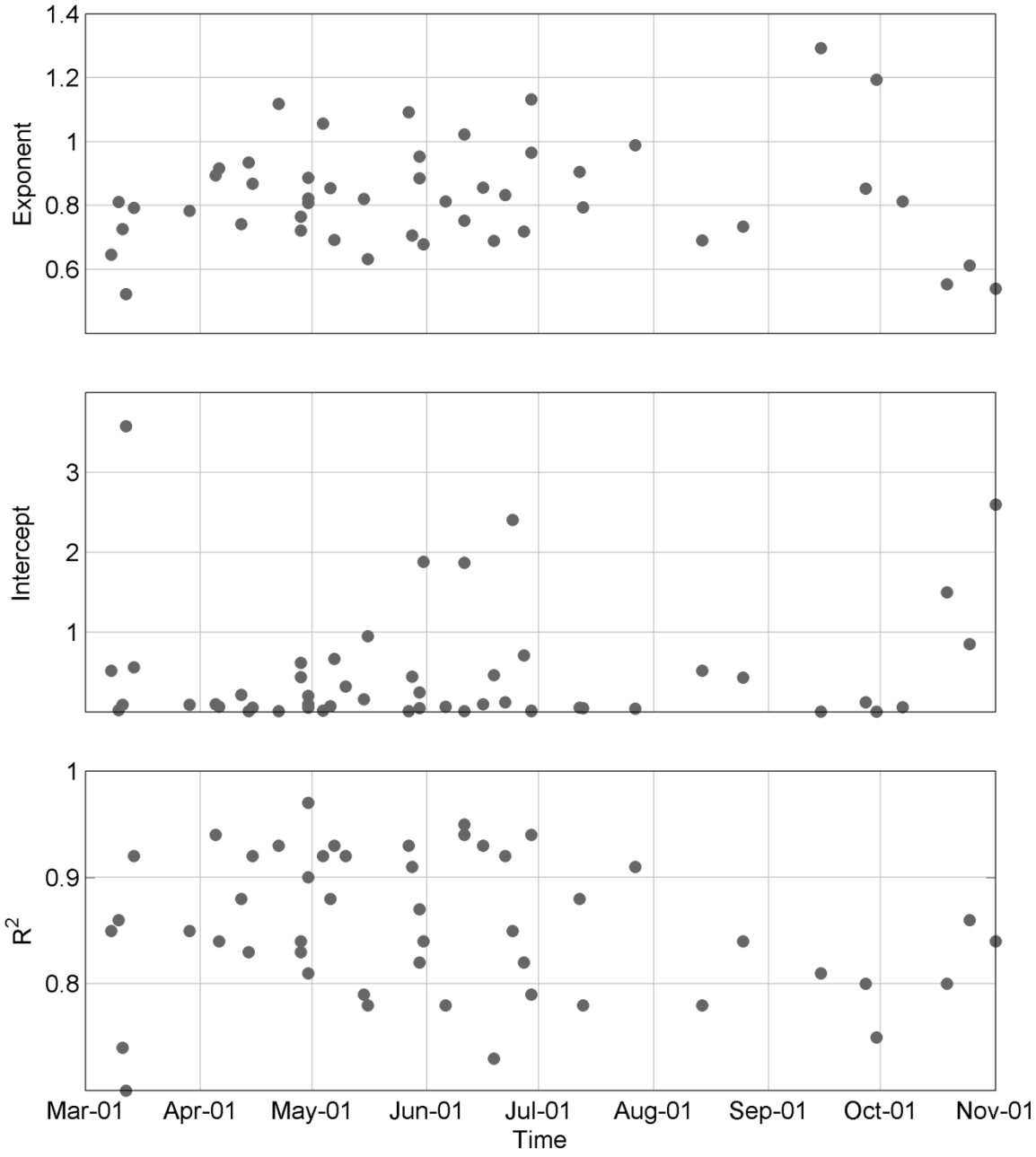

Figure III - 5. Temporal distribution of the flood scaling exponent, intercept, and the coefficient of determination corresponding to the 50 rainfall-runoff events.

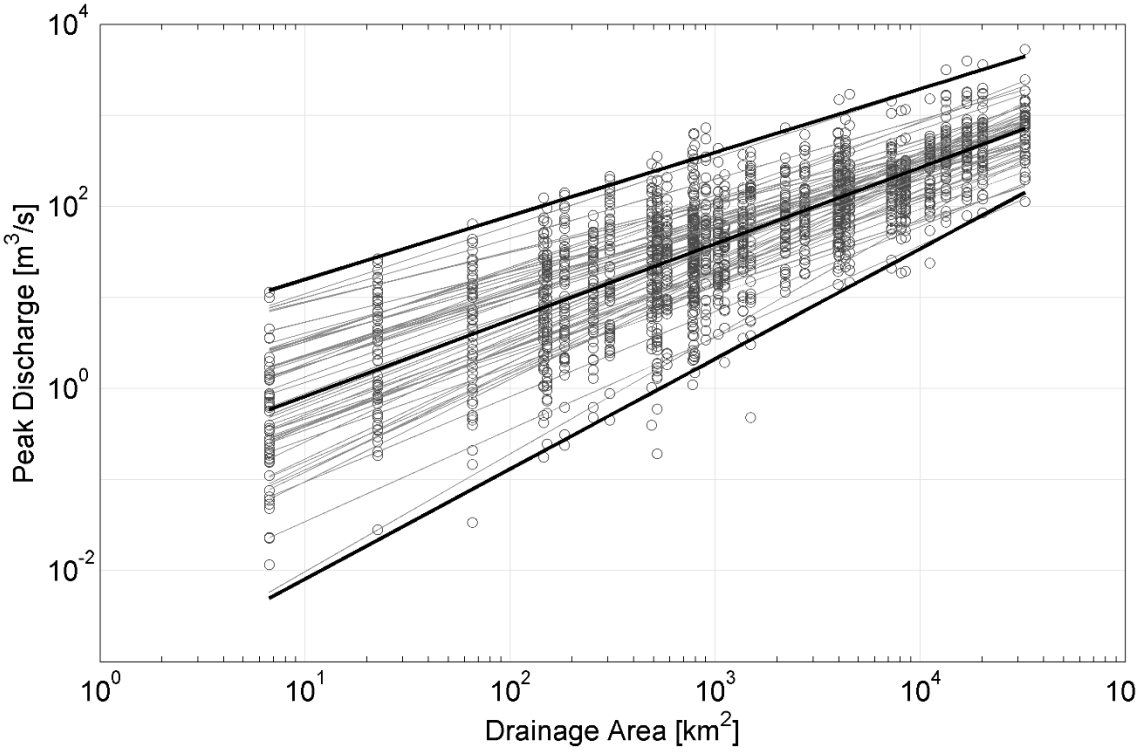

Figure III - 6. Plot of the 50 peak discharge events observed at each gauging site. The light grey line traces the OLS regression fitted through peak discharges coming from the same rainfall-runoff event. The dark line traces OLS regression line fitted to example Type-I quantiles (minimum, median, and maximum of peak discharges observed at each gauging site).

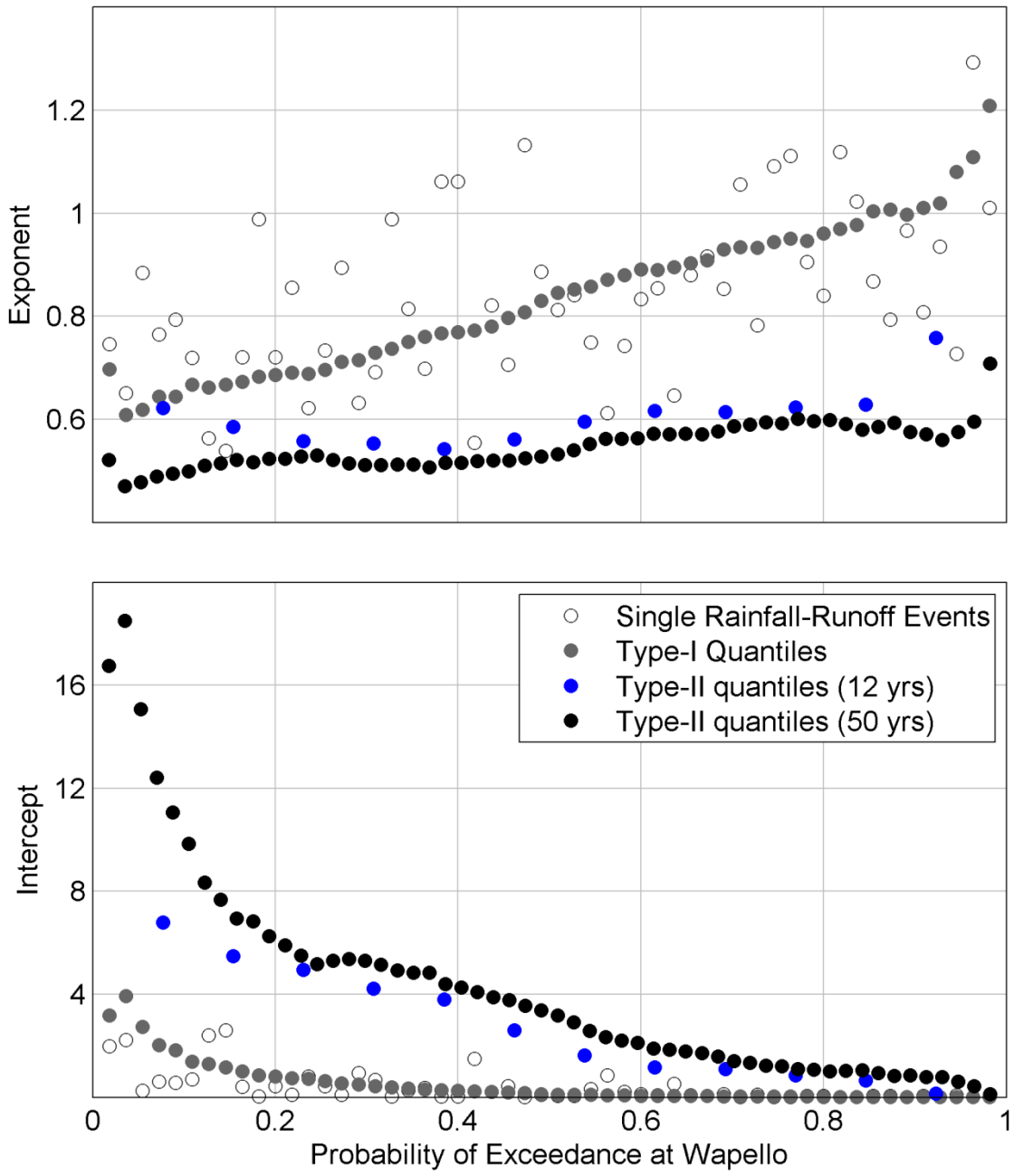

Figure III - 7. Comparison of flood scaling exponent and intercepts obtained from single rainfall-runoff events (grey hollow circles), Type-I quantiles (grey filled circles), and Type-II quantiles (blue circles). For the sake of comparison, flood scaling exponents and intercepts calculated for 50 years of annual maximum peak discharge data is also included (black filled circles). These are also categorized as Type-II quantiles.

CHAPTER IV

CONNECTING THE POWER-LAW SCALING STRUCTURE OF PEAK DISCHARGES TO SPATIALLY UNIFORM RAINFALL AND CATCHMENT PHYSICAL PROPERTIES [1]

4.1. Introduction

This chapter is devoted to understanding the role of the drainage network and the interplay among rainfall intensity (I), duration (T), channel flow velocity (v_c), and hillslope overland flow velocity (v_h) in determining the scaling structure of peak discharges at the rainfall-runoff event scale. My approach involves simulation using the drainage network based hydrologic model CUENCAS (Mantilla and Gupta 2005). I systematically altered the aforementioned catchment process variables to gain insight into their effects on the scaling structure of peak discharges. To this end, I carried out systematic simulation experiments in multiple watersheds to determine whether or not my findings hold for watersheds that have different shapes, sizes, and width functions.

Although the work reported in this chapter is closely connected to that of Furey and Gupta (2007), we use a drainage network-based hydrologic model simulation to provide an in-depth insight into the role of the interplay among , T, v_h, and v_c in controlling α and θ, which Furey and Gupta (2007) did not fully address. A further understanding of this problem is important because, in reality, these catchment processes are interdependent, and understanding their relative roles in determining the peak discharge

[1] Adapted from Ayalew, T. B., Krajewski, W. F., Mantilla, R., and Small, S. J. (2014). "Exploring the Effects of Hillslope-Channel Link Dynamics and Excess Rainfall Properties on the Scaling Structure of Peak-Discharge." Advances in Water Resources, 64, 9-20.

scaling structure provides further insight into our quest to estimate α and θ from catchment variables that can be either directly measured or estimated.

The chapter is organized as follows. In the next section I discuss the study areas and the research methodology in greater detail. This section outlines the drainage network based hydrologic model called CUENCAS and the three different watersheds I studied. I also discuss the physical assumptions I have made, the associated limitation of the study, and the systematic setup of the simulation experiments. This is followed by my presentation of results and a discussion on their implications for peak discharge estimation across scales. I conclude the chapter with a summary of the main findings.

4.2. Methodology

4.2.1. Study watersheds

I selected three different watersheds in Iowa: Clear Creek, Old Mans Creek, and Boone River, which have drainage areas of 254, 520, and 1082 km^2, respectively. I extracted their respective drainage networks and hillslopes from a one arc-second (~30 m) digital elevation model (DEM) obtained from the USGS. The smallest subcatchment that drains first order streams in all of the watersheds was on the order of 0.01 km^2. Choosing these three different watersheds allow me to test the dependence of my findings on the river network structure as well as on the size and shape of drainage basins.

The geometry of the drainage network determines the property of the streamflow response (hydrograph) at different locations in the catchment (Gupta et al. 1980; Rinaldo and Rodriguez-Iturbe 1996; Rodríguez-Iturbe and Valdés 1979). Its manifestation in the streamflow response can best be described by the width function which is defined as the

number of channel-links at a given distance from the outlet of a catchment. The width function will have the same shape as the discharge hydrograph under the conditions that (1) rainfall is spatially uniform and it occurs over a short duration, (2) runoff generated on hillslopes instantaneously joins the drainage network, and (3) water moves through the drainage network at a constant velocity and without attenuation (Gupta et al. 2010). My analysis of the peak of the width function that is calculated at the bottom of complete order Horton-Strahler streams shows that it is scale invariant and can be estimated as a function of drainage area using a power-law. This originates from the fractal property of the drainage network and is widely reported in the literature (e.g., Tarboton et al. 1988; Veitzer and Gupta 2001). To this end, the respective values of the intercept c and the exponent β of the width function maxima were 4.88 and 0.46 for Clear Creek, 5.18 and 0.44 for Old Mans Creek, and 3.98 and 0.47 for Boone River. Figure IV-1 shows plots of each of the watersheds, their width function evaluated at the outlet, and the scaling of the width function maxima evaluated at the bottom of complete order Horton-Strahler streams. Note that, based on the catchment outline shape and the width function, Clear Creek and Old Mans Creek appear similar to each other while Boone River appears to be different from both.

4.2.2. Numerical framework

I carried out my simulation-based study using the hydrologic model CUENCAS (Mantilla and Gupta 2005), which can be viewed as a contemporary numerical rainfall-runoff simulation laboratory that has a drainage network at its core. Unlike many grid-based distributed rainfall-runoff models that are being used by the hydrologic community, CUENCAS decomposes the landscape into hillslope-channel-link

components and applies the mass and momentum conservation equations at the hillslope-channel-link scale. The model is implemented in a parallel computing framework by exploiting the tree-like structure of the river network which resulted in a significant reduction in computational time (Small et al. 2013).

The fact that the drainage network is central to the modeling framework in CUENCAS makes it an ideal tool for my study. This is because, as discussed earlier, the drainage network plays a dominant role in determining the shape of the discharge hydrograph and the magnitude of its peak at all scales. As such, its accurate representation and modeling is important to understanding how peak discharges are organized at different scales and how their scaling property is controlled by different catchment physical properties. CUENCAS is extensively tested in multiple watersheds with drainage areas ranging up to 20 000 km^2 and is found to produce reasonable results (Cunha et al. 2011; Cunha et al. 2012).

For the purpose of this study, I use a simplified version of CUENCAS where hillslope and channel processes are conceptualized using few parameters while adequately reproducing observed streamflow time series. My deliberate choice of simple model derives from the fact that more complex models are characterized by a large number of parameters, which would make it difficult to separately study the effect of important catchment process variables on the scaling structure of peak discharges. Figure IV-2 shows a sketch of the hillslope-channel-link control volume at which scale relevant equations are written.

For a single hillslope-channel-link control volume, which serves as a local control volume, the mass conservation equation for a given channel-link is written as:

$$\frac{dS_i(t)}{dt} = q_{si}(t) + q_{gi}(t) + \sum q_j(t) - q_i(t) \qquad \text{Equation IV-1}$$

where $S_i(t)[L^3]$ is the channel storage at channel-link i, $q_{si}(t)[L^3T^{-1}]$ is surface runoff to the link, $q_{gi}(t)[L^3T^{-1}]$ is subsurface stormflow to the channel-link, $\sum q_j(t)$ $[L^3T^{-1}]$ is the summation of inflows from upstream channel-links indexed by j, $q_i(t)[L^3T^{-1}]$is the outflow from the channel-link, and $t[T]$ is time. The hillslope overland flow rate into a channel-link is calculated by assuming that overland storage depth is uniform over the hillslope and using the set of equations:

$$S_{si}(t) = A_h d(t) \qquad \text{Equation IV-2}$$

$$q_{si}(t) = v_h L d(t) \qquad \text{Equation IV-3}$$

where $S_{si}(t)[L^3]$ is the proportion of rainfall that is stored on the surface of the hillslope at a given time, $A_h[L^2]$is the hillslope area, $d(t)$is the time dependent overland flow depth, $v_h[LT^{-1}]$is the hillslope overland flow velocity, $L[L]$ is the length of the channel-link, and $q_{si}(t)$ is as defined earlier. Solving equations IV-2 and IV-3 simultaneously yields:

$$q_{si}(t) = v_h \frac{L}{A_h} S_{si}(t) \qquad \text{Equation IV-4}$$

Rewriting equations IV-2 and IV-3 for the subsurface flow case and solving them simultaneously yields:

$$q_{gi}(t) = v_g \frac{L}{A_h} S_{gi}(t) \qquad \text{Equation IV-5}$$

where $v_g\,[LT^{-1}]$ is the subsurface flow velocity, and $S_{gi}(t)[L^3]$ is the proportion of rainfall that is stored in the subsurface of the hillslope. The rate of change of surface and subsurface storage is further calculated by assuming that rainfall is partitioned into surface and subsurface storage according to the runoff coefficient c_r and using the following set of ordinary differential equations:

$$\frac{dS_{si}}{dt} = c_r A_h I_i(t) - q_{si}(t) \qquad \text{Equation IV-6}$$

$$\frac{dS_{gi}}{dt} = (1 - c_r) A_h I_i(t) - q_{gi}(t) \qquad \text{Equation IV-7}$$

where c_r is the runoff coefficient and $I_i(t)\,[LT^{-1}]$ is the rainfall intensity.

The outflow from a channel-link, $q_i(t)$, is calculated by assuming that the channel cross-sectional area and flow depth is uniform over the channel-link and using the following set of equations:

$$S_i(t) = a_c L \qquad \text{Equation IV-8}$$

$$q_i(t) = a_c v_c(t) \qquad \text{Equation IV-9}$$

where $S_i(t)[L^3]$ is the channel storage at link i, $a_c[L^2]$ is the channel-link cross-section area, $v_c[LT^{-1}]$ is the channel flow velocity, and the rest is as defined earlier. Combining equations IV-8 and IV-9 yields:

$$q_i(t) = v_c(t) \cdot \frac{S_i(t)}{L} \qquad \text{Equation IV-10}$$

Equation IV-10 is not yet complete since v_c is unknown. We used the following equation to estimate v_c:

$$v_c(t) = v_r \cdot \left(\frac{q_i(t)}{Q_r}\right)^{\lambda_1} \cdot \left(\frac{A}{A_r}\right)^{\lambda_2} \qquad \text{Equation IV-11}$$

where $v_r[LT^{-1}]$ is the reference channel velocity, $q_i(t)[L^3T^{-1}]$ is the discharge from the link, $A[L^2]$ is the drainage area upstream of the outlet of link i, and $Q_r[L^3T^{-1}]$ and $A_r[L^2]$ are the reference discharge and drainage area, whose values are taken in this study to be 1m/s and 1km^2, respectively. The parameters λ_1 and λ_2 are the scaling exponents for discharge and drainage area, respectively. The derivation of equation IV-11 is rooted in the assumption that channel velocity scales as a function of drainage area and discharge. The interested reader is encouraged to refer to Mantilla (2007) for the theoretical background and its detailed derivation.

Finally, the outflow from the link is calculated by combining equations IV-10 and IV-11 and solving for $q_i(t)$. The result leads to a channel storage-discharge relationship

which can be considered as a simplified form of momentum conservation equation and is written as follows:

$$q_i(t) = \left(v_r \frac{S_i(t)}{L} \left(\frac{A}{A_r} \right)^{\lambda_2} \right)^{\frac{1}{1-\lambda_1}} \qquad \text{Equation IV-12}$$

Solving the above set of equations over the drainage network results in channel flows that mimic the dispersion and attenuation of flows as the flood wave propagates downstream.

In order to illustrate the model's capability to reproduce observed streamflow data I simulated observed rainfall-runoff events in all the three study catchments using Stage-IV radar rainfall data as input. The Stage-IV product is widely used in hydrologic applications. It provides hourly radar-rainfall estimates that are adjusted by rain gauge data in real time(Habib et al. 2013; Kitzmiller et al. 2013). While quality and accuracy of the product may vary across the U.S., over Iowa the multiplicative bias is close to unity (Seo and Krajewski 2011). For all the catchments, we also used a spatially uniform v_r, $\lambda_1, \lambda_2, v_h$, and c_r values of 0.25m/s, 0.3, -0.1, 0.01m/s, and 0.3, respectively. The simulation results, which are shown in Figure IV-3, indicate that the model is capable of reproducing real events and hence fits the purpose of our study.

4.2.3. Scope of the study

The rainfall-runoff simulation-based study that I report in this chapter uses the following assumptions: (1) rainfall is spatially uniform and its intensity I is constant over its duration T; (2) the entire watershed has the same soil moisture deficit; (3) v_h is constant both in space and time, and (4) v_c is either constant both in space and time or

variable as a nonlinear function of drainage area and discharge. Relevant theoretical accomplishments were advanced using similar assumptions at comparable or even higher scales (e.g., Botter and Rinaldo 2003; Di Lazzaro and Volpi 2011; Menabde and Sivapalan 2001). These simplifying assumptions are the main limitations of the study reported in this chapter. This is because spatially uniform and temporally constant I, c_r, v_h and v_c seem unrealistic at the scale of the watersheds we investigated. However, these assumptions are helpful to separately study the role of these important rainfall and catchment physical variables in shaping the scaling structure of peak discharges. Thus, the results reported in this chapter should be taken within the context of these assumptions. Chapter 5 builds on the findings of this chapter by relaxing some of these assumptions.

4.2.4. Experimental setup

I systematically organized the simulation experiment into four distinctive groups in order to separately study the effect of variation in one variable on both α and θ by keeping the other variables constant. I used both the constant and nonlinear channel velocity formulations in each group. For the constant channel velocity case, I set $\lambda_1 = \lambda_2 = 0$ and used $v_c = v_r$ values that range from 0.1 to 2 m/s with a typical value of 0.5 m/s and applied it uniformly both in space and time. When experimenting with nonlinear channel velocity as described by equation IV-11, I used v_r values that range from 0.1 to 2 m/s and set $\lambda_1 = 0.3$ and $\lambda_2 = -0.1$. These λ_1 and λ_2 values are supported by field data (Cunha et al. 2011; Mantilla 2007) and, as shown in Figure IV-3, are also appropriate for our study catchments. For a given v_r, these λ_1 and λ_2 values generally

lead to v_c values that, in addition to increasing with increasing rainfall intensity, increase in the downstream direction. Figure IV-4 shows the range v_c values will assume at different scales and for different values of v_r and I. For this study, when experimenting with nonlinear channel velocity, I take v_r =0.25 m/s as the typical value and the resulting v_c values are in the range of 0.1 to 1 m/s. These scale dependent v_c values are also reported in the literature (Leopold et al. 1964).

When modeling the hillslope response, I used a spatially uniform and temporally constant v_h value that range from 0.001 to 0.1 m/s with a typical value of 0.01 m/s. These values are also supported by results from field studies (Botter and Rinaldo 2003; Di Lazzaro and Volpi 2011; Grimaldi et al. 2010; Huff et al. 1982). Gupta and Waymire (1998) also reported that the maximum value v_h could attain is in the range of 0.03 m/s. In addition, we also assumed a constant subsurface flow velocity value of $v_g = 0.005 m/s$ which is in the range of what is observed in tracer-based field studies (Anderson et al. 2009; Anderson et al. 1997). Furthermore, a spatially uniform and temporally constant runoff coefficient value of $c_r = 0.5$ was also used for all the simulations. This c_r value was determined in an ad-hoc fashion and is immaterial for our study. A detailed summary of the simulation experiments is outlined in Table IV-1.

Peak discharge estimates were extracted at the bottom of complete order Horton-Strahler streams whose drainage areas are known from the analysis of the DEM in CUENCAS. I then used the ordinary least-squares (OLS) regression method in the log-log scale to parameterize the power-law relationship between peak discharge and

drainage area. I used the OLS regression even though I recognize that the residuals are correlated in violation of one of the OLS regression assumptions. This arises because, in a nested watershed, peak discharges in higher order Horton-Strahler streams are dependent on peak discharges from lower order streams that drain into them. However, since the purpose of my study is to identify systematic trends of α and θ in response to changes in the magnitude of important catchment physical parameters (and not to develop a predictive model), OLS remains a valid method of regression analysis.

4.3. Results and discussion

4.3.1. Effect of rainfall duration and intensity on the scaling structure

I began by investigating the effect of rainfall duration T on the scaling exponent θ. For this experiment, I used a spatially uniform rainfall depth of 25 mm, which is equivalent to the 1-year, 1-h rainfall for the study sites (Huff and Angel 1992). I applied this rainfall depth over the following values of T: 5-min, 10-min, 15-min, 30-min, 1-hr, 2-hr, 3-hr, 6-hr, 12-hr, 18-hr, 1-day, and 2-day. This arrangement means that I decreases as T increases while the rainfall volume remains constant. Additionally, I used the constant channel velocity formulation with v_c and v_h values of 0.5 m/s and 0.01 m/s, respectively. In order to separately study the effect of rainfall duration, I repeated the above experiment by keeping the rainfall intensity constant at 25 mm/h for all durations considered here. The result, which is presented in Figure IV-5, shows how α and θ systematically change with I and T. It reveals that, under the assumptions we employed here, θ starts at a value greater than the scaling exponent of the width function maxima β for small values of T and systematically converges to a value closer to 1 as T

increases. This property is previously observed in empirical studies (Furey and Gupta 2005) and in theoretical results (Furey and Gupta 2007; Gupta and Waymire 1998). The value of θ, under the present constant channel velocity assumption, is independent of the rainfall intensity and is determined solely by T, which is evident in Figure IV-5 where I values of $I = 25/T$ mm/h (top panels) and $I = 25$ mm/h for all T (bottom panels) lead to the same θ values.

Plots of hydrographs at the bottom of selected complete order Horton-Strahler streams (not shown here) revealed that θ converges to 1 only when the rainfall duration equals or exceeds the time of concentration for the subsurface stormflow. This duration is in the order of few weeks at the scale of the catchments I studied. This long duration is the result of the considerably low subsurface flow velocity. The corresponding time of concentration for overland flow calculated using the constant v_c and v_h values discussed above was about 60-hour, 80-hour, and 100-hour for the Clear Creek, Old Mans Creek, and Boone River, respectively. Since a rainfall duration that is in the order of few weeks is highly unrealistic, we conclude that $\theta = 1$ is the upper bound value for the scaling exponent when both rainfall and catchment antecedent moisture state are spatially uniform and temporally constant. Furthermore, the fact that θ increases with T convincingly lends itself to the argument that, under a given set of v_c and v_h, longer T values increase the proportion of subcatchments that contribute to the peak discharge at the outlet, which is reflected in the increasing magnitude of θ (Gupta and Waymire 1998).

The result presented in Figure IV-5 (top panels) also shows that, for a fixed rainfall depth, α decreases with decreasing I. Moreover, Figure IV-5 (bottom panels) shows, for a fixed I, α increases with increasing T. These results clearly show that, for given v_c and v_h values, α is controlled by both I and T. Building on a similar results to those shown in Figure IV-5 (top panels), Furey and Gupta (2007) suggested a decreasing concave relationship between α and T for a fixed P. However, I underscore the observed decreasing concave relationship as due to the resulting concave (inverse) relationship between I and T for a fixed P. Figure IV-5 (bottom panels) clearly shows that if I is fixed, there is an increasing convex relationship between α and T. To further elucidate this, in the subsequent sections we demonstrate that, under realistic assumptions of v_c and v_h, α is an increasing function of I for a given rainfall duration T. This means that the decrease in α with increasing T observed in empirical data (Furey and Gupta 2005) can be partially explained by the generally decreasing relationship of I with increasing T, which is also observed in empirical data (e.g., Huff and Angel 1992).

To further understand the effect of T and I on α and θ, I set up simulation experiments where I used a constant $T = 1\,\text{hr}$ and systematically increased I. I used both the constant and nonlinear channel velocity assumptions. I also experimented with a range of other values of T and obtained the same result. The results presented in Figure IV-6(top panels) show that, for the constant channel velocity case, θ is independent of I and remains constant despite the increasing I. This means that the scaling structure follows simple scaling when both hillslope overland flow and channel flow velocity are assumed to be constant both in space and time. We can also see in the same Figure

(bottom panels) that, for the nonlinear channel velocity case, θ increases with increasing I suggesting multiscaling. This is due to the fact that, under nonlinear velocity assumption, channel velocity increases as I increases. And for a given T, the increased v_c further leads to an increase in the proportion of subwatersheds connected to the outlet which is in turn reflected in the increased θ. More interestingly, θ appears to asymptotically converge to some limiting value, determined by v_c and *T*, as I increases. This suggests that even when v_c is nonlinear and varies in both space and time, simple scaling is potentially sufficient for explaining the scaling structure of extreme flood events. Figure IV-6 also shows that, when the rainfall duration is fixed, α is a linear function of I for both the constant and nonlinear channel velocity cases. This is because of the increasing rainfall volume which is in turn reflected in the increasing peak discharge at all scales. The linearity of α as a function of I, irrespective of the channel velocity formulation, is a direct consequence of the linear response of hillslopes represented in the model.

The results presented in this section also show that both the Clear Creek and Old Mans Creek catchments exhibit similar α and θ values that are significantly different from those estimated for Boone River (Figure IV-5 and IV-6). This is explained by the shape of the boundaries and the width function of the respective catchments. Both Clear Creek and Old Mans Creek catchments have elongated shapes and, as a result, exhibit quite similar width functions, whereas the Boone River catchment has a circular shape and, consequently, a markedly different width function. Because the results for all three watersheds exhibit essentially the same trends and properties of α and θ as a function of

the catchment physical variables I investigated, the rest of the chapter will only present (unless otherwise stated) the results for the Clear Creek catchment.

4.3.2. Effect of channel velocity on the scaling structure

In a given catchment, v_c varies from location to location depending on the local channel geometry, slope, roughness, and discharge. In this section, I investigate how changes in v_c affect θ. I ignore the velocity fluctuations across the channel as well as those at small scale (e.g. single channel-link). In the scenario considered herein, I used a constant v_h value of 0.01 m/s and considered two v_c cases. In the first case, I used a constant v_c that was selected from the range of 0.1 to 2 m/s. I kept $\lambda_1 = \lambda_2 = 0$ which means that v_c is constant both in space and time. In the second case, I used the nonlinear channel velocity formulation (see Eq. 11) and varied v_r between 0.1 and 2 m/s and kept $\lambda_1 = 0.3$ and $\lambda_2 = -0.1$. In this case, as a result of the nonlinear relationship between channel velocity and discharge, v_c varies both in space and time with a generally increasing trend in the downstream direction. In both cases, I applied a spatially uniform rainfall depth of 25 mm over T values that ranged from 5-min to 12-hours. This implies that I decreases as T increases.

The results, shown in Figure IV-7(a and c), reveal that increasing v_c leads to an increase in θ with its effect being significant at shorter T values. This is explained by the fact that v_c reflects how the catchment retards the runoff response. To this end, for a given T, an increase in the magnitude of v_c yields an increase in the proportion of

subcatchments contributing to the peak discharge at the outlet, which eventually leads to an increase in θ. The effect of increasing v_c is less significant for longer T because the catchment already has sufficient time for a larger proportion of the catchment to contribute to the peak discharge regardless of the effect of increasing v_c. An interesting finding here is that as v_c increases, θ converges to a certain limiting value that is largely determined by T. This is similar to the effect of increasing I under the assumption of nonlinear v_c (Figure IV-6 (bottom panels)).

Channel velocity also controls α in the same way it controls θ, as discussed above. An increase in v_c leads to an increase in the magnitude of α until a certain limiting value, with its effect particularly significant as T gets shorter. This limiting value is associated with the maximum discharge the catchment can attain under given values of I and T. As previously discussed, increasing v_c leads to an increase in the proportion of the catchment that contributes to the peak discharge at larger scales. This causes an increase in the magnitude of the peak discharge that is reflected in the increasing magnitude of α. When T is limiting, there is a maximum limit on the proportion of the catchment that contributes to peak discharge. This limiting value explains the asymptotic behavior of both α and θ under increasing v_c at shorter values of T. This finding highlights the dependence of both α and θ on v_c in addition to their already acknowledged dependence on I and T. In the following section I also show that hillslope

dynamics play an even more significant role in determining the magnitude of both α and θ.

4.3.3. Effect of hillsope overland flow velocity on the scaling structure

Recent studies suggest that hillslopes play a significant role in determining the runoff response of a catchment (Botter and Rinaldo 2003; Furey and Gupta 2007; Saco and Kumar 2004). Furey and Gupta (2007) represent the only study that report the role of hillslopes in determining the scaling structure of peak discharges from nested watersheds during a single rainfall-runoff event. I continue on this trajectory and further investigate the significant role hillslopes play in determining the scaling structure of peak discharges. In this phase of my study, I first used a constant v_c of 0.5 m/s and varied v_h in the range of 0.001 and 0.1 m/s among different simulations. I followed this by repeating the simulation experiment using the nonlinear channel velocity formulation by setting $v_r = 0.25$m/s, $\lambda_1 = 0.3$ and $\lambda_2 = -0.1$. In both cases, I used a rainfall depth of 25 mm that is applied over T values ranging from 5-min to 12-hours. The results revealed how the interplay between T and v_h affect the peak discharge scaling statistics.

The results presented in Figure IV-8 reveal that, for the constant v_c case, θ decreases with increasing v_h when $T < 1$hr, whereas it increases with increasing v_h when $T \geq 1$hr. This is because, although the increase in v_h leads to smaller catchments to discharge water at a higher rate per unit area than larger catchments, their contribution to discharge at larger scales is determined by T, which controls the time available for peak discharges from smaller scales to be transported and contribute to peak discharges at larger scales.

This means that when T gets shorter, the impact of increasing v_h is reflected in the increased peak discharge rate per unit drainage area at smaller subcatchments that is higher than the corresponding rate at larger scale subcatchments. Additionally, shorter rainfall durations and higher hillslope overland flow velocity values will satisfy, as discussed in section 4.2.1, the first two conditions required for the discharge hydrograph to resemble the width function of the catchment at all scales. Consequently, the exponent θ decreases with increasing v_h and converges to the scaling exponent β of the width function maxima. This convergence to β is not seen in Figure IV-8 because we allowed for flow attenuation to occur in the drainage network, effectively invalidating the third condition required for the discharge hydrograph to resemble the width function of the catchment. Following the assumptions employed in this study, these results indicate that the lower limit of θ is β.

It can also be seen in Figure IV-8 that θ increases with increasing v_h when T get longer. This is because, as T gets longer, there will be sufficient time available for a larger proportion of subcatchments to contribute to peak discharges at larger scales. In this case, increasing v_h further increases the proportion of the catchment that contributes to peak discharge at larger scales, which is reflected in the increasing values of θ. Furthermore, the value of T, above and below which we see contrasting effects of v_h on θ, is also controlled by the magnitude of v_c. It can be seen that its value increased to 2-hr when the nonlinear v_c was used (Figure IV-8 (c)). This is because, at smaller scales, the nonlinear channel velocity formulation leads to v_c values that are generally smaller

than the corresponding $v_c = 0.5$ m/s that is used for the constant channel velocity case (see Figure IV-4). This simply means that higher v_c and v_h values shorten the time required for a larger proportion of the watershed to contribute to peak discharge at higher scales. Although not shown here, this magnitude of T is the same for all the three catchments. However, it is likely that it will assume higher values as the catchment becomes bigger than those considered in this study.

As shown in Figure IV-8 (b and d), it can also be seen that α increases with increasing v_h as well as with increasing I. We should note that, due to the constant P applied, I increases with decreasing T. An important result here is that in addition to I, v_h plays a more dominant role in controlling α than v_c does. This is because v_h controls the rate at which excess rainfall is delivered to the channel network whereas v_c determines how the water traffic aggregates at successively larger scales. This is evident in Figure IV-7(b and d) where an increase in v_c for a given v_h leads to a smaller increase in α than the increase of α due to the effect of v_h for a given v_c, as can be seen in Figure IV-8(b and d). I checked this for various combinations of v_h and v_c and found similar results. This observation highlights the dominant role of hillslope processes in determining both α and θ.

4.3.4. Hillslope overland flow velocity and scale break

In the context of statistical scaling of peak discharge, a scale break occurs when the log-log linear relationship between peak discharge and drainage area exhibits different slopes (θ) above and below a certain critical drainage area value. Empirical data

suggests the existence of scale break in some catchments. Using a quantile-based analysis of annual peak discharge data, Goodrich et al. (1997) showed the existence of scale break at about 1 km^2 in the Walnut Gulch basin. Asquith and Slade (1997), also using a quantile-based regional regression analysis, reported the existence of scale break for watersheds in Texas (U.S.) that happens at about 83 km^2 for the 100 year flood. Because these empirical studies were not event based, it is difficult to physically describe the reasons for the observed scale break. To this end, a number of event-based theoretical studies have been conducted that either directly or indirectly addressed the issue of scale break (Gupta and Waymire 1998; Mandapaka et al. 2009; Mantilla et al. 2006; Menabde and Sivapalan 2001). All these important theoretical contributions assume that runoff generated on hillslopes instantaneously enters the river network and studied the property of the scale break as a function of rainfall duration only. In this study, I relax the assumption of instantaneous runoff delivery to the river network by making use of appropriate hillslope overland flow velocities and investigate the role the interplay among v_h, v_c, and T plays in determining the occurrence and property of scale break.

To separately study how hillslope overland flow velocity affects the scale break, I setup a simulation where I set the rainfall duration $T = 1$hour, its intensity $I = 25$mm/h, and used the constant channel velocity parameters $v_c = 0.5$ m/s, $\lambda_1 = 0$ and $\lambda_2 = 0$. I then varied the hillslope overland flow velocity v_h between 0.01 and 1 m/s per simulation. The results presented in Figure IV-9 show how v_h affect the scale break in each of the three catchments. For the sake of comparison, we superimposed peak discharge

estimates (black lines) calculated using the rational formula ($Q_p(A) = c_r \cdot I \cdot A$) for which $\theta = 1$. These results clearly show that, for a rainfall duration of $T = 1$ hour, a scale break occurs at around 1 km^2 and is caused when part of the catchment that is drained by lower order streams achieves saturation, i.e., converge to the $\theta = 1$ line. It can be seen that higher than average v_h values are responsible for the quick saturation of smaller subcatchments resulting in the decreasing scatter of peak discharge with increasing v_h.

The same experiment was repeated where I investigated the role of the interplay among rainfall duration and channel velocity on the occurrence and property of scale break. In order to achieve this, I set $v_h = 1$ m/s and varied v_c between 0.5 and 1.5 m/s while always keeping $\lambda_1 = 0$ and $\lambda_2 = 0$. Moreover, the rainfall depth was kept constant at 25 mm and was applied over durations T between 5-min and 12-hr. Since the results from the three catchments exhibit similar properties, I will only discuss those results from the Clear Creek catchment. Also, I only present the results for the constant channel velocity case since the results are similar to the case when the channel velocity is a nonlinear function of discharge and drainage area.

The results presented in Figure IV-10 reveal that the critical catchment area at which the scale break is observed generally increases with increasing T. This is explained by the fact that, under a given set of v_h and v_c, subcatchments whose drainage area is less than the critical area have already achieved saturation, and as such an increase in T would only result in an increased proportion of the catchment achieving saturation. Although not presented here, under the present channel and hillslope overland flow velocity values

of $v_c = 0.5m/s$ and $v_h = 1m/s$, the scale break disappears when $T \geq 24hr$, $T \geq 36hr$, and $T \geq 32hr$ for the Clear Creek, Old Mans Creek, and Boone River, respectively. No noticeable scale break is observed when $T = 5\min$ which is because the rainfall duration is not long enough for smaller subcatchments to achieve saturation and, as previously discussed, the discharge hydrograph at all scales resembles the corresponding width function. Another important feature of the results presented in Figure IV-10 is that the channel velocity also plays a role in determining the scale at which the scale break occurs. These results show that an increase in v_c also leads to an increase in the scale at which the scale break occurs. This happens because an increase in v_c results in a decrease in t_c, which means that more subcatchments achieve saturation for a given T. In conclusion, the results discussed so far indicate that the occurrence of a scale break is dictated by the interplay among v_h, v_c, and T. Among these, v_h plays the dominant role.

4.4. Summary and conclusions

In this chapter, the role of the interplay among rainfall intensity (I), duration (T), hillslope overland flow velocity (v_h), and channel velocity (v_c) in determining the scaling structure of peak discharge is investigated. I used the drainage network-based hydrologic model CUENCAS (Mantilla and Gupta 2005), which decomposes a given catchment into a hillslope-channel-link system at which scale it solves the mass and a simplified momentum conservation equations. I applied the model to three different catchments in the state of Iowa in central U.S. and systematically set up approximately

1000 different event-based simulations per each catchment. These simulations were carried out under the assumption that: (1) rainfall is spatially uniform and $\boldsymbol{I}$ is constant over T; (2) the entire catchment has the same soil moisture deficit; (3) v_h is constant both in space and time; and (4) v_c is either constant in space and time for the constant channel velocity case or it varies in space and time for the nonlinear channel velocity case. These assumptions were necessary prerequisites to gain a first-order understanding of which catchment physical variables determine the scaling structure of peak discharge observed in empirical data.

Analysis of the simulation results reveal that peak discharge exhibits a log-log linear relationship with drainage area for all the three catchments that are investigated and for all combinations of $\boldsymbol{I}$, T , v_h, and v_c values that are considered. The results show that when a spatially uniform and temporally constant v_c is used, peak discharge follows simple scaling. Moreover, the results show that the use of a nonlinear channel velocity formulation, which leads to spatially and temporally variable v_c values, leads to exponents that are a function of rainfall intensity, which provides an important insight into the multiscaling of peak discharge generally observed in empirical flood quantile data analyses. Another interesting result is the dependence of the intercept (α) and the scaling exponent (θ) on the spatial organization of the drainage network, which is reflected in the catchment width function. We showed that under similar values of $\boldsymbol{I}$, T, v_h, and v_c, our estimates of α and θ for the Boone River catchment are significantly different from those estimated for the Clear Creek and Old Mans Creek catchments. This

is because the width function of the Boone River catchment is significantly different from the width functions of Clear Creek and Old Mans Creek, which are similar to each other.

The results further showed that α reflects the magnitude of the peak discharge, whereas θ reflects the proportion of the catchment that contributes to the peak discharge at the outlet. This means that α is controlled by the rainfall and catchment physical properties that affect the magnitude of the peak discharge and θ is controlled by the rainfall and catchment physical properties that affect the proportion of the catchment that contribute to the peak discharge at the outlet irrespective of its magnitude. To this end, I showed that, for a given catchment, T and v_h play a dominant role in controlling θ, followed by v_c and $\boldsymbol{I}$. I also showed that, for a given catchment, α is controlled by the interplay among $\boldsymbol{I}$, T, v_h, and v_c with v_c playing the least dominant role. These results reveal that, under the assumptions we used, the scaling structure is controlled by the interplay among $\boldsymbol{I}$, T, v_h, and v_c. The variation of α and θ observed in empirical data across multiple watersheds can therefore be explained by the drainage network structure, the local climate that determines the properties of $\boldsymbol{I}$ and T, the local topography, soil type, land use, and land cover that controls v_h and v_c. The event-to-event variability of α and θ can also be described based on the event-to-event variability of rainfall, the antecedent catchment moisture state, and nonlinearities related to v_h and v_c.

Under the assumptions I used, the results also reveal that the interplay between T and v_h determines if and when a scale break happens whereas the scale at which the

break happens is controlled by the interplay among T, v_h, and v_c. Most importantly, a scale break happens when runoff generated on hillslopes quickly enters the drainage network and, for catchment scales we investigated, when $T \leq 12$ hr. These results show the importance of understanding the hillslope scale processes in order to predict both α and θ in a physically meaningful way.

Table IV - 1. Summary of the simulation experiments

Objective of the experiment	Channel velocity formulation	Parameter varied	Parameters kept constant
Study the effect of rainfall intensity and duration	Constant	$5\,\text{min} \le T \le 2\text{day}$	$\text{P} = 25\text{mm}$, $v_r = 0.5\text{m/s}$ $\text{v}_\text{h} = 0.01\text{m/s}$
		$15 < \text{I} < 75\text{mm/hr}$	$T = 60\,\text{min}$, $v_r = 0.5\text{m/s}$ $\text{v}_\text{h} = 0.01\text{m/s}$
	Nonlinear	$5\,\text{min} \le \text{T} \le 2\text{day}$	$\text{P} = 25\text{mm}$, $v_r = 0.25\text{m/s}$ $\text{v}_\text{h} = 0.01\text{m/s}$
		$15 < \text{I} < 75\text{mm/hr}$	$T = 60\,\text{min}$, $v_r = 0.25\text{m/s}$ $\text{v}_\text{h} = 0.01\text{m/s}$
Study the effect of channel velocity	Constant	$5\,\text{min} \le \text{T} \le 12\text{hr}$ $0.1 \le v_r \le 2\text{m/s}$	$\text{P} = 25\text{mm}$ $\text{v}_\text{h} = 0.01\text{m/s}$
	Nonlinear		
Study the effect of hillslope overland flow velocity	Constant	$5\,\text{min} \le \text{T} \le 12\text{hr}$ $0.001 \le \text{v}_\text{h} \le 0.1\text{m/s}$	$\text{P} = 25\text{mm}$
	Nonlinear		
Study the relationship between v_h, v_c, T, and scale break	Constant	$5\,\text{min} \le \text{T} \le 12\text{hr}$ $0.01 \le \text{v}_\text{h} \le 1\text{m/s}$ $0.1 \le v_r \le 2\text{m/s}$	
	Nonlinear		

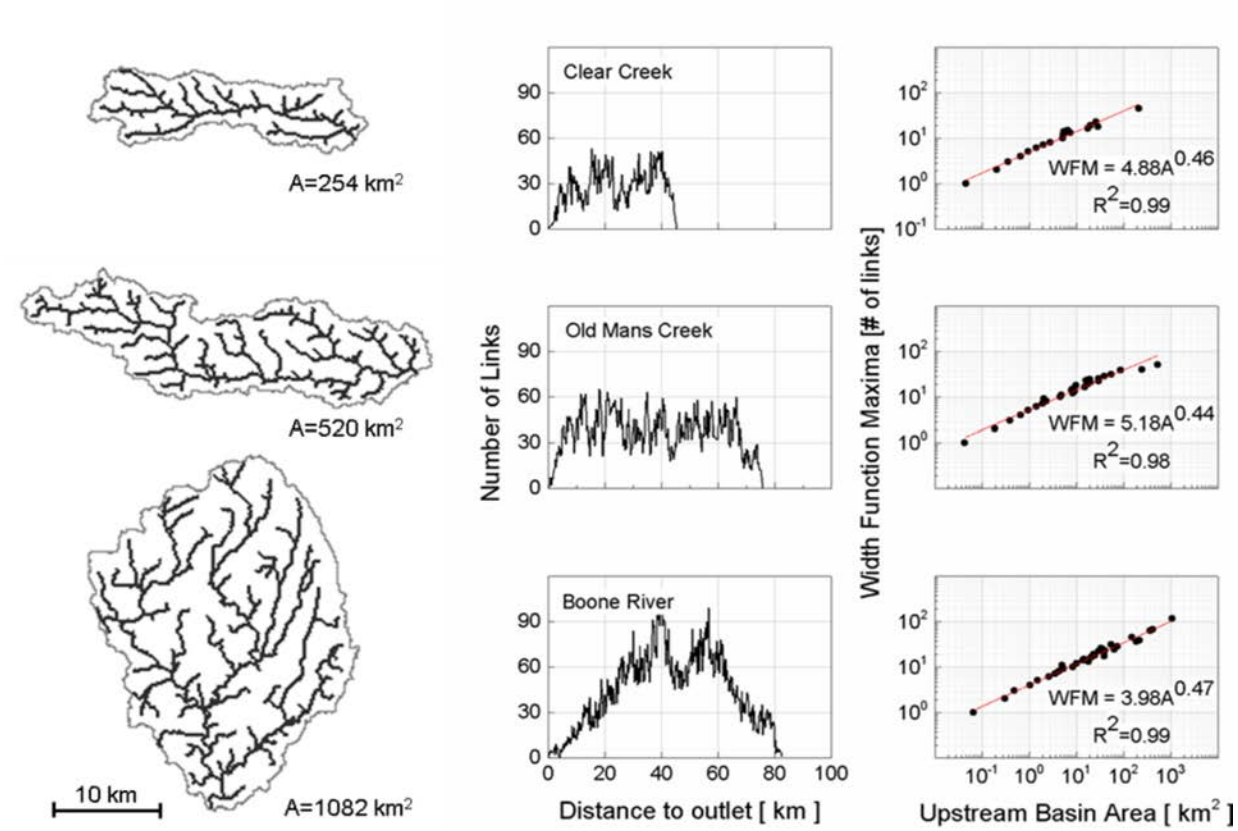

Figure IV - 1. Plot of the drainage network, the width function, and scaling of the width function maxima for Clear Creek, Old Mans Creek, and Boone River catchments. For the sake of clarity, only streams of order 4 and higher are shown for the drainage network.

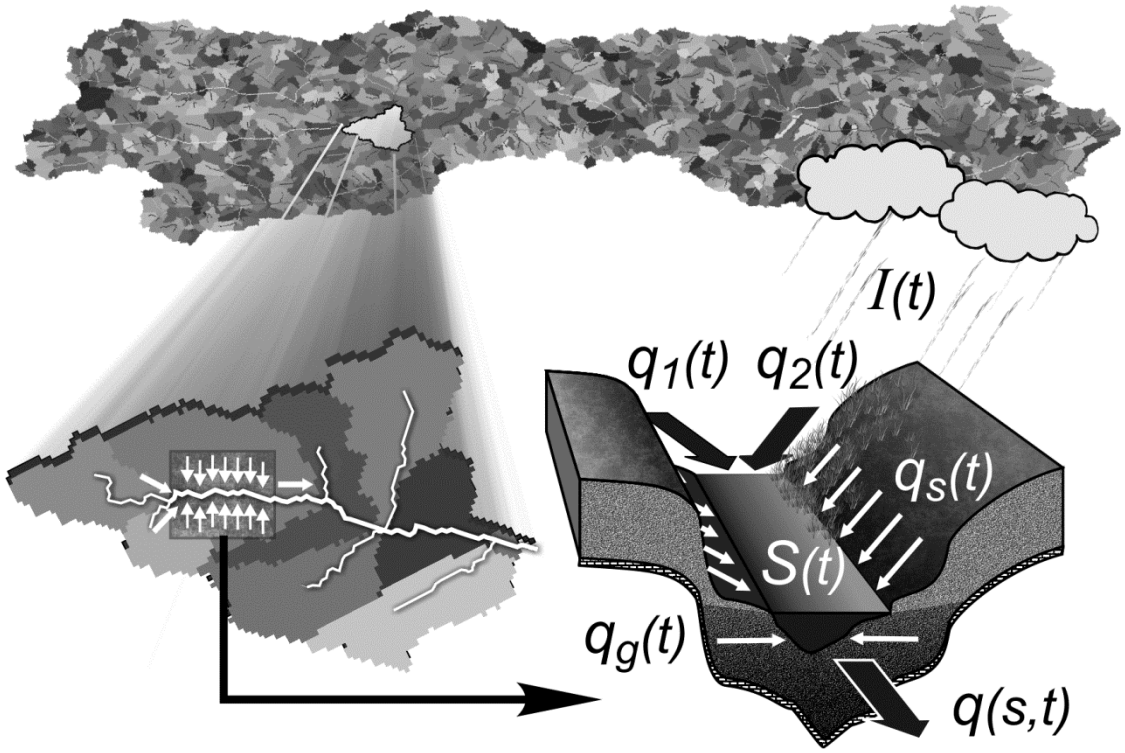

Figure IV - 2. Sketch depicting the decomposition of the Clear Creek catchment into hillslope-channel-link system. The hillslope-channel-link control volume is also shown.

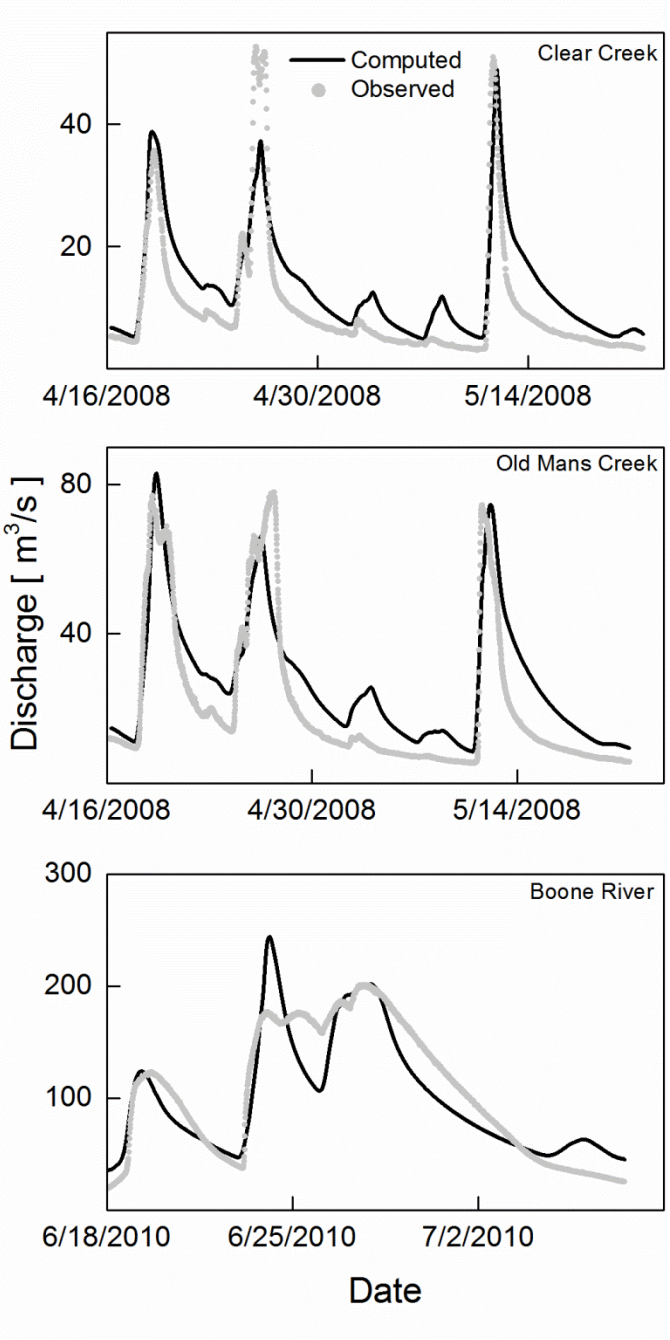

Figure IV - 3. Plot of Observed versus Simulated Hydrographs.

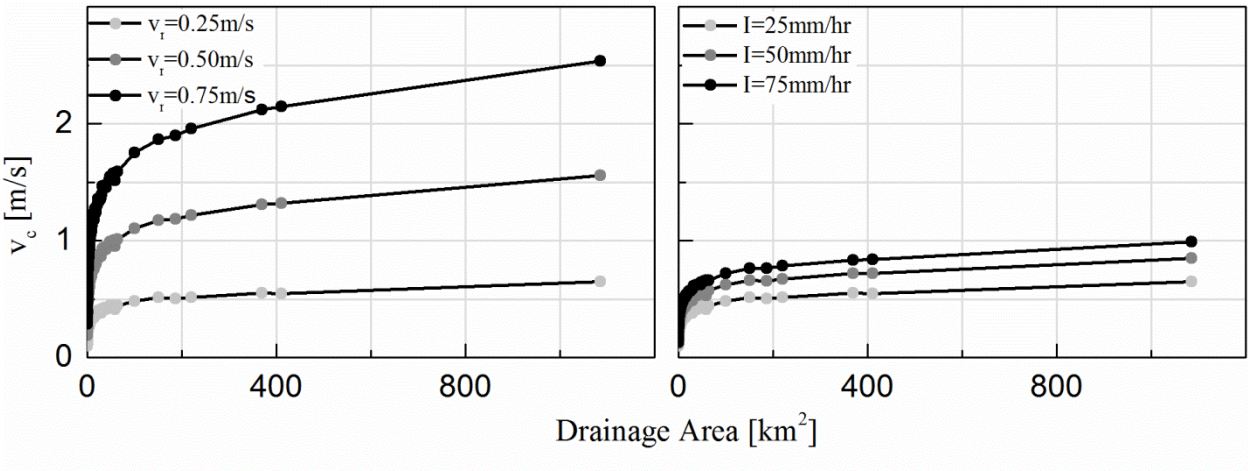

Figure IV - 4. Change of the channel velocity v_c as a function of v_r and A for a fixed $I = 25\text{mm/hr}$ (left) and its change as a function of I and A for a fixed $v_r = 0.25\text{m/s}$ (right).

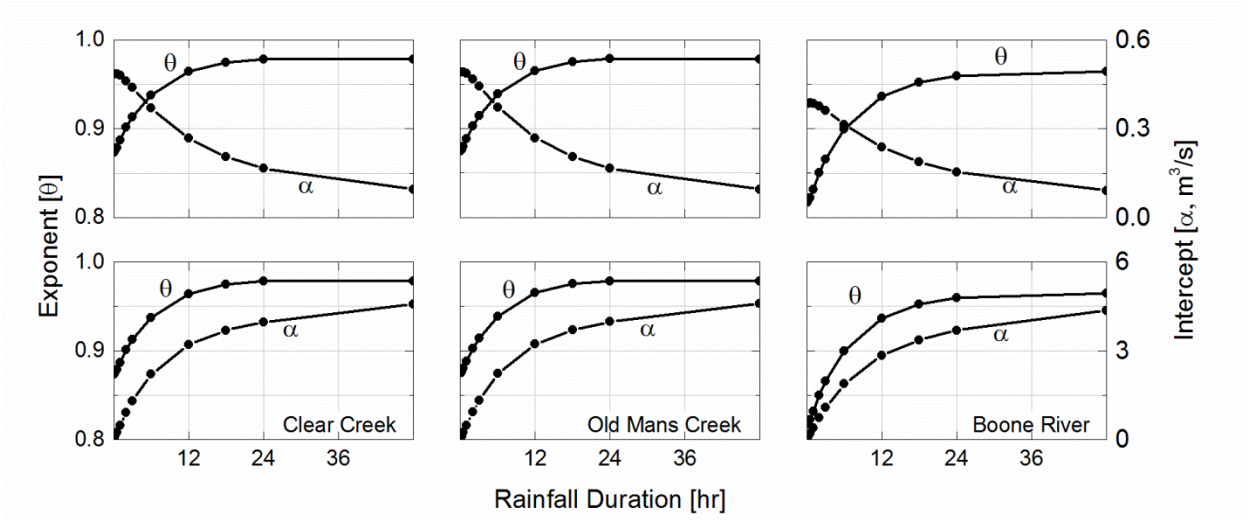

Figure IV - 5. Systematic dependence of both the intercept α and the scaling exponent θ on excess rainfall duration T and intensity I (top panels) for a fixed excess rainfall P where $I = P/T$ and (bottom panels) for a fixed I.

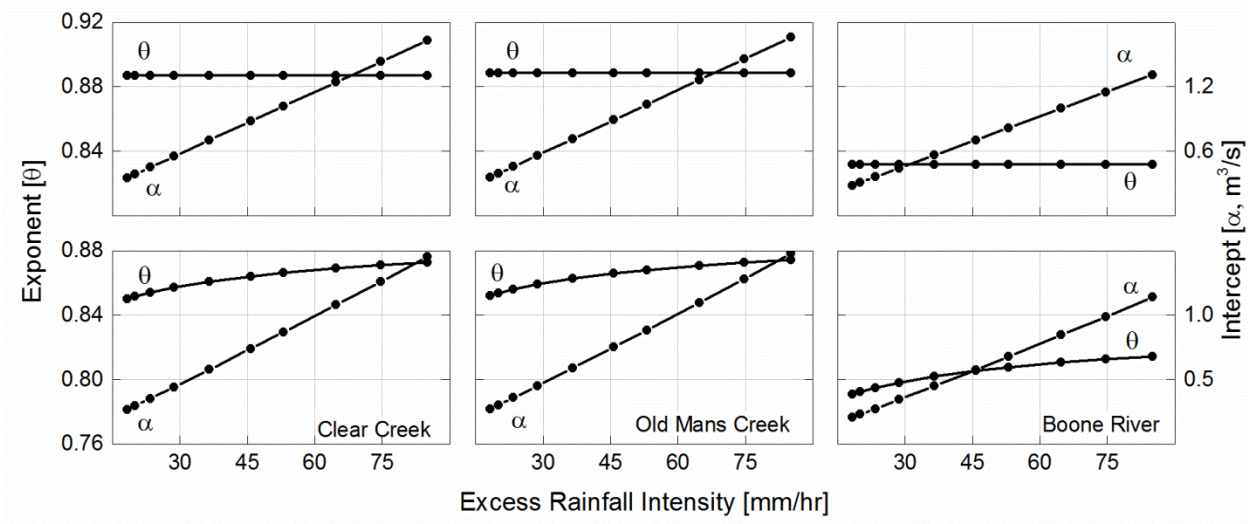

Figure IV - 6.. Systematic dependence of the intercept α and the scaling exponent θ on excess rainfall intensity I for both the constant channel velocity (top panels) and nonlinear channel velocity cases (bottom panels). The rainfall had a constant duration of 1 hr.

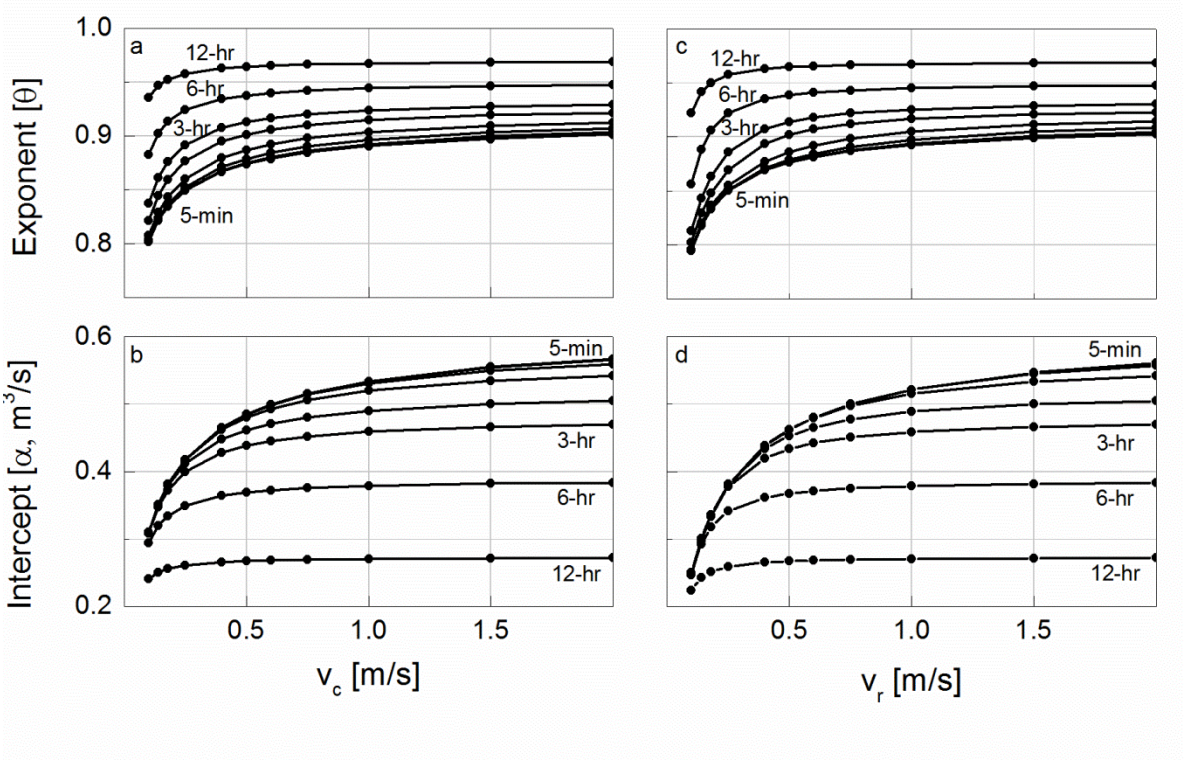

Figure IV - 7. Dependence of the intercept α and the scaling exponent θ on channel velocity v_c for the constant channel velocity case (a and b) and for the nonlinear channel velocity case (c and d). The respective values of rainfall duration T shown here are 5-min, 10-min, 15-min, 30-min, 1-hr, 2-hr, 3-hr, 6-hr, and 12-hr.

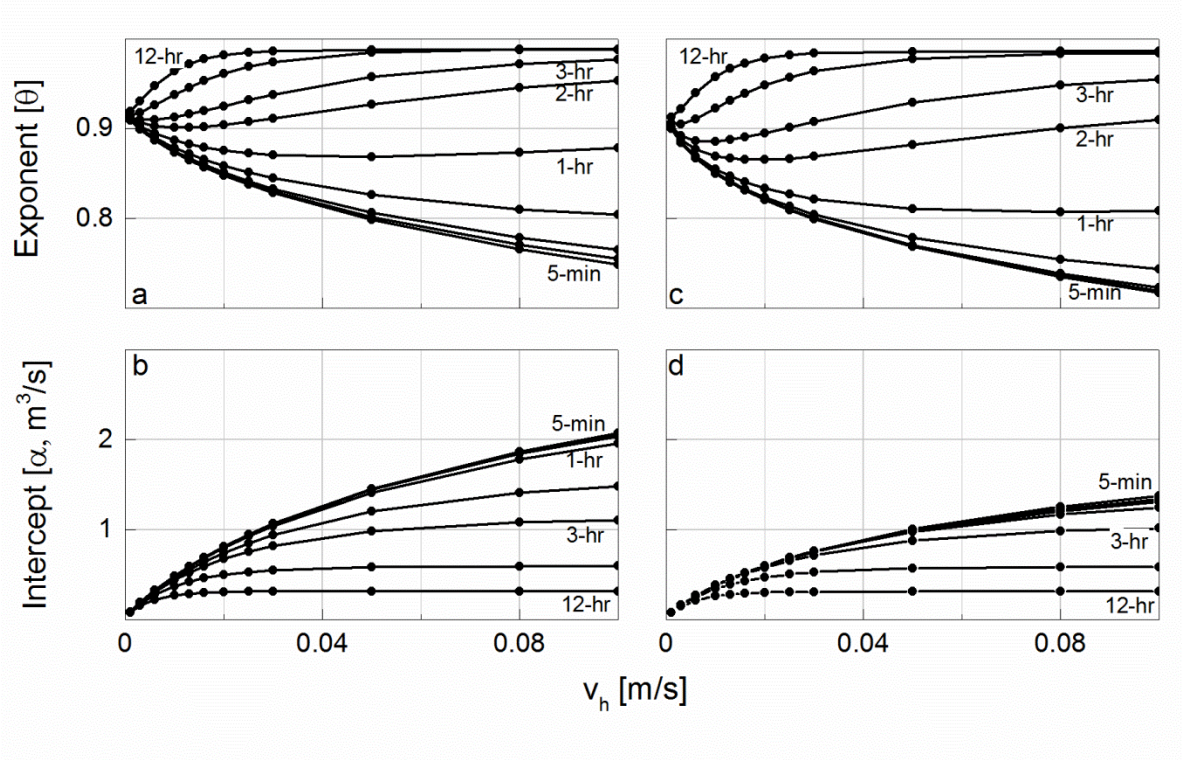

Figure IV - 8.. Dependence of the intercept α and the scaling exponent on hillslope overland flow velocity v_h for the constant channel velocity case (a and b) and for the nonlinear channel velocity case (c and d). The respective values of rainfall duration T shown here are 5-min, 10-min, 15-min, 30-min, 1-hr, 2-hr, 3-hr, 6-hr, and 12-hr.

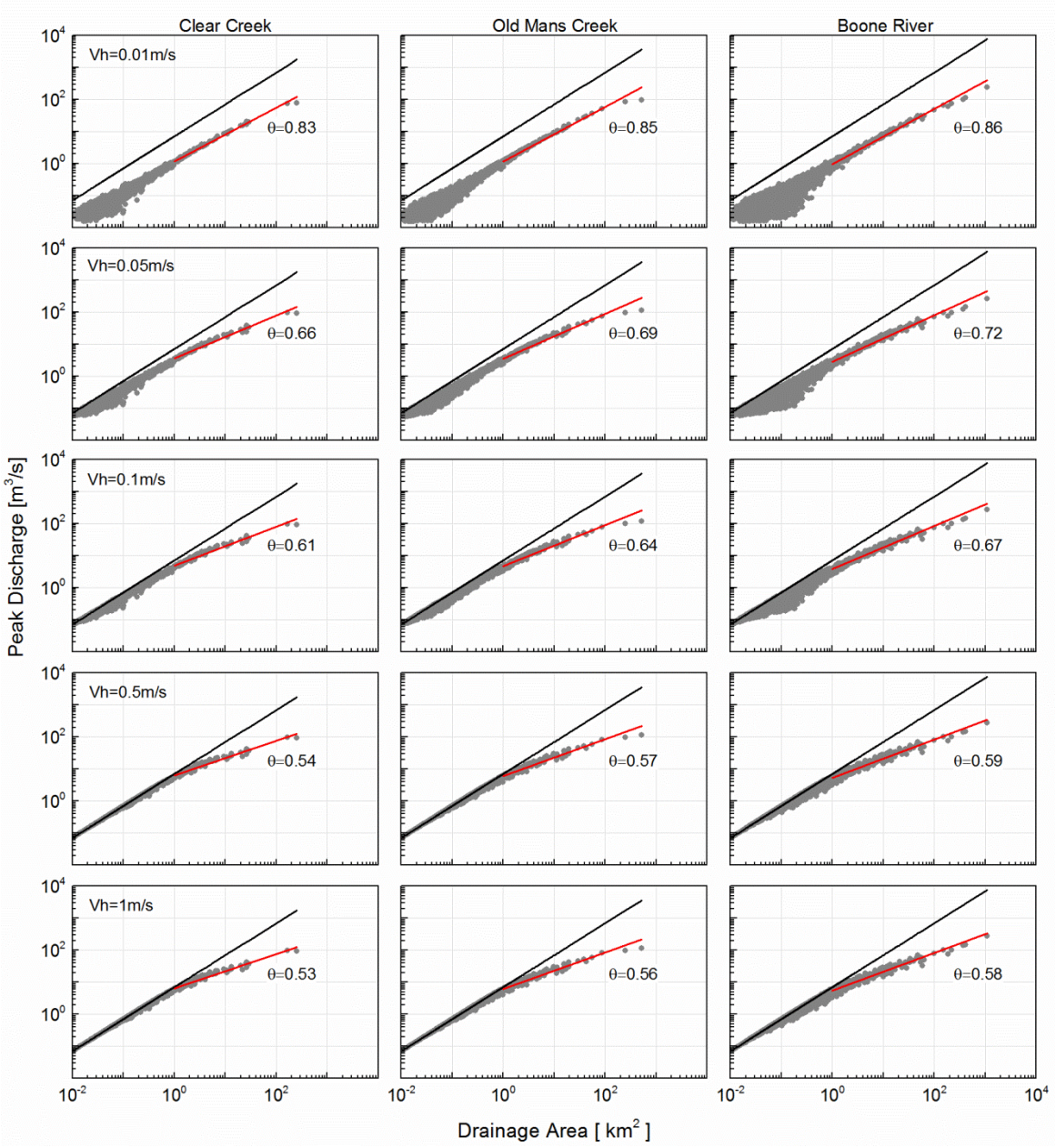

Figure IV - 9. Plot of peak-discharge as a function of drainage area in the three catchments for T =1 hr and different v_h values. The solid black line represents the peak discharge calculated using the rational formula for which $\theta = 1$. The red line is a regression line fitted to those peak discharge values coming from subcatchments with drainage area greater than 1km^2.

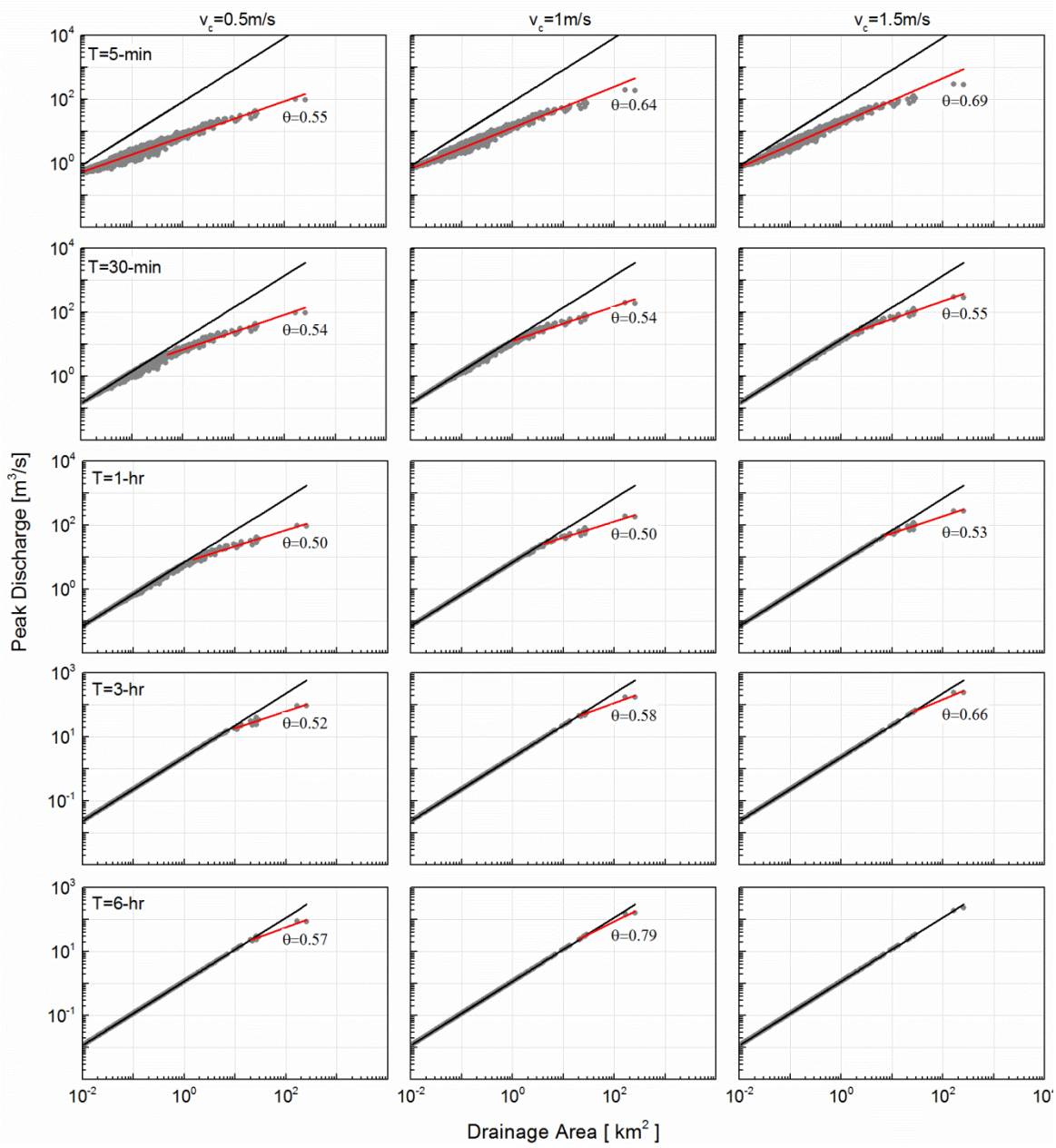

Figure IV - 10. Plot of peak-discharge as a function of drainage area in the Clear Creek catchment for $v_h = 1\text{m/s}$ and different T and v_c values. The solid black line represents peak discharge calculated using the rational formula for which $\theta = 1$. The red line is a regression line fitted through those peak discharges that depart from the $\theta = 1$ line.

CHAPTER V

HOW DO SPATIALLY VARIABLE RAINFALL AND CATCHMENT PHYSICAL PROPERTIES CONTROL THE POWER-LAW SCALING STRUCTURE OF PEAK DISCHARGES? [2]

5.1. Introduction

The main limitations of the results reported in chapter IV come from the simplifying assumptions I made in order to separately understand the effect of rainfall and catchment physical variables on the scaling structure of peak discharges. In doing so, we gained significant insight into their respective roles. However, at the catchment spatial scales I investigated, both rainfall and the catchment antecedent moisture state are not constant both in space and time. The same goes for v_h and v_c. I already showed that the aggregated effect of a spatially and temporally variable v_c leads to a scale invariant peak discharge spatial organization. The main objective of this chapter is, therefore, to build upon the findings reported in chapter IV by: (1) expanding the analysis to a larger catchment than those considered in chapter IV, (2) relaxing the assumptions of spatially constant rainfall, antecedent soil moisture, and hillslope overland flow velocity by setting these variables to be spatially variable, (3) expanding the analysis to investigate the role of catchment antecedent moisture state by using the runoff coefficient as a proxy, (4) introducing a nonlinear hillslope model in which the hillslope overland flow velocity is dynamically calculated as a function of hillslope overland storage using the Manning's equation, and (5) investigating the effect of rainfall movement speed and direction on the

[2] Adapted from Ayalew, T. B., Krajewski, W. F., and Mantilla, R. (2014). "Connecting the power-law scaling structure of peak-discharges to spatially variable rainfall and catchment physical properties." *Advances in Water Resources*, 71(0), 32-43.

runoff response across scales. To this end, I undertook a number of systematic simulation experiments to describe the dependence of the flood-scaling exponent θ and intercept α on the significant, aforementioned catchment physical variables.

The chapter is organized as follows. First, I describe the study catchment and the application of the model to observed rainfall events, which justifies the model's use as a simulation tool. I will then discuss the scope and limitations of the study conducted in this chapter, followed by an in-depth discussion of the results within the framework of the *scaling theory* of floods. I conclude with a summary of the major findings.

5.2. Study area and model application to real events

To demonstrate the "reasonableness" of the model and its ability to reproduce observed streamflow time series across scales, I applied CUENCAS to the Cedar River basin in Cedar Rapids, Iowa, which has a drainage area of 16,861 km^2. The basin is located in eastern Iowa in the Midwestern United States in the Upper Mississippi River basin. This region experienced the devastating flood events of June 2008 (Mutel 2010; Smith et al. 2013). Figure V-1a and b show the location of the Cedar River in Iowa and its drainage network, respectively. Figure V-1c shows the width function of the river at the catchment outlet. The width function represents the catchment runoff response under the highly idealized conditions of equal area hillslopes, spatially constant instantaneous rainfall input that is directly delivered to the channel network, constant channel flow velocity, and no channel flow attenuation (Gupta et al. 2010). Figure V-1d shows how the peaks of the width functions, evaluated at the bottom of complete order Horton-Strahler streams, scale as a function of drainage area with a scaling exponent (β) of 0.47. In fact, the early efforts to estimate the scaling parameters of peak discharge used the

scaling properties of the width function as a key explanatory variable (Gupta et al. 1996; Mantilla et al. 2006; Mantilla et al. 2011; Menabde and Sivapalan 2001; Veitzer and Gupta 2001).

We simulated the 2008 flood event in the Cedar River using the Stage IV radar rainfall product (Kitzmiller et al. 2013) as an input. This radar rainfall product has a spatial and temporal resolution of about 4-km and 1-hr, respectively. Furthermore, we set the values of C_r, v_h, v_r, λ_1, and λ_2 to 0.8, 0.02 m/s, 0.4 m/s, 0.25, and -0.2, respectively. Figure V-2a shows a comparison of observed and simulated streamflow time series at six different USGS streamflow gauging sites that represent different spatial scales in the catchment. Gupta et al. (2010) previously studied the power-law scaling property of the 2008 flood event, shown in Figure V-2b, using observed streamflow data from the Iowa River basin, which has a drainage area of 32,400 km^2. To compare the scaling property of simulated peak discharge with observation, I extracted simulated peak discharge estimates at the bottom of complete order Horton-Strahler streams and plotted them against their respective drainage areas, as shown in Figure 3(c). Note here that the Cedar River is a tributary of the Iowa River, which drains into the Mississippi River. The simulation results show that the model reasonably reproduced both the streamflow time series and the power-law scaling statistics of peak discharges in the catchment. The minor discrepancy between the observed and simulated values of α and θ is to be expected considering uncertainties due to the rainfall input data, the model structure, model parameters, and sample size bias in observations (see also Cunha et al. 2012; Seo et al. 2013).

5.3. Scope of the chapter

This chapter builds on the findings reported in chapter IV, which were obtained under the assumptions that rainfall, runoff coefficient, and hillslope overland flow velocity are constant both in space and time. In this chapter, I relax these assumptions by allowing all of the parameters to vary randomly in space (i.e., from hillslope to hillslope) statistically by sampling rainfall intensity from an exponential distribution and the remaining parameter values from a lognormal distribution. Using the Manning's equation and randomly varying the Manning's n value in space, I also introduce a nonlinear hillslope case in which the hillslope overland flow velocity varies both in space and time. However, I maintain the assumption that, for a given hillslope, both rainfall intensity and the runoff coefficient are time invariant.

My assumption of random spatial variability of rainfall and catchment physical variables is by no means an accurate representation of the physical reality because rainfall, the runoff coefficient, land use, and topography are known to exhibit some form of spatial organization. However, through this simplification, I systematically build our process understanding before embarking on a similar investigation based on a complex representation of the rainfall-runoff process. Note that the purely random variability of rainfall, the runoff coefficient, and the hillslope overland flow velocity I simulate here represents the opposite bound of the earlier (chapter IV) assumption in which these parameters were considered to be constant both in space and time. Accordingly, the results of this study should be taken within the context of these assumptions.

The simulation experiments were organized in such a way that the effect of one variable on α and θ is investigated by fixing other variables to their respective values

that were randomly sampled from a distribution whose mean is obtained from the set of parameters that resulted in a good agreement between model simulated flows and observational data. The ranges of parameter values used for each simulation experiment are summarized in Table 1. These values are selected based on observational data that are reported in the literature (Botter and Rinaldo 2003; Di Lazzaro and Volpi 2011; Huff and Angel 1992; Leopold et al. 1964).

5.4. Results and Discussion

The first objective is discuss how the peak discharge scaling parameters were calculated and also to revisit the concept of scale break, which is necessary in order to understand the results that will be discussed in the subsequent sections. The peak discharge scaling intercept α and exponent θ for each of the simulations were calculated using Ordinary Least Square (OLS) regression in the log-log space. I used peak discharge estimates at the bottom of complete order Horton-Strahler streams whose respective drainage area was processed in CUENCAS (Mantilla and Gupta 2005) and considered only those complete order streams that have a drainage area of greater than 1 km^2. This decision is based on the visual inspection of peak discharge versus drainage area plots, which showed a significant scatter of peak discharges for those subcatchments that have a drainage area of less than 1 km^2. Plots of peak discharge versus drainage area also revealed the existence of a scale break, and the spatial scale of its occurrence (A_c) varies among different simulations that have different input parameters. I have already shown in chapter IV that the magnitude of A_c is dependent on the interplay among rainfall duration, channel flow velocity, and hillslope overland flow velocity. In this chapter, I determined the magnitude of A_c for each simulation and separately calculated

the scaling parameters for the group of subcatchments whose drainage areas are greater and smaller than A_c.

I determined the spatial scale at which a scale break occurs (i.e., A_c) using the statistical method proposed by Main et al. (1999). I call the scaling parameters α_1 and θ_1 for those groups of subcatchments in which $A \le A_c$, whereas I call them α_2 and θ_2 for those groups of subcatchments where $A > A_c$. Figure V-3 shows a scaling plot for peak discharges following rainfall events that have different durations. In all of the cases, the spatially variable input parameter values are sampled from $P(mm) \sim Exp(1/25)$, $C_r \sim Logn(0.5, 0.25^2)$, and $v_h(m/s) \sim Logn(0.02, 0.01^2)$. Simulation results show that A_c increases with increasing rainfall duration, and it occurs between 15 and 450 km^2 for the set of parameters used in this study. I will further discuss how rainfall duration controls both α and θ in the subsequent sections.

5.4.1. Effect of spatial variability of input parameters on the runoff response

In this section, I show how the runoff response at different spatial scales is affected by the hillslope-scale spatial variability of rainfall, the runoff coefficient, and the hillslope overland flow velocity. The results presented in Figure V-4 show five separate simulation cases. Figures V-4a, b, c, and d illustrate the respective cases when only P, C_r, v_h, or n is spatially variable while other parameters are kept spatially constant. Figure V-4e represents the case in which all parameters (P, C_r, and v_h) are spatially variable. For each case, I simulated 100 independent realizations of the input parameters. The dark black line shown on all of the plots represents the case in which spatially

constant values of $E[I]$, $E[C_r]$, and $E[v_h]$ (or $E[n]$) are used as an input. In all cases, I used the nonlinear channel velocity formulation. These results indicate that the effect of the spatial variability of the model's input parameters on the simulated runoff response is significant at smaller catchment spatial scales and decrease with increasing catchment area. Carpenter and Georgakakos (2004) arrived at a similar conclusion using a different modeling framework.

Visual inspection also reveals that, of all the simulation results presented in Figure V-4, the spatial variability of v_h (or n) tends to exhibit a different effect on the runoff response of small to medium sized catchments when compared to the effects of the spatial variability of P and C_r. It can be seen (Figure V-4c and d) that the spatial variability of the hillslope overland flow velocity leads to a higher dispersion of the runoff response at smaller scales. Moreover, the runoff response tends to converge to a different hydrograph that has a reduced peak value and a longer tail than the one obtained by simulating the basin using average rainfall and model parameter values that are spatially constant (i.e., the black line). Grimaldi et al. (2010) showed a similar result by applying a different modeling framework to different catchments that have drainage areas ranging from 35 to 131 km^2. Their approach used a constant channel flow velocity and a spatially variable hillslope overland flow velocity that was calculated using the Manning's equation, whose parameters are obtained from terrain and land use data. The results presented in Figure V-4 suggest that the spatial variability of the hillslope overland flow velocity has a significant impact on the runoff response in small to medium sized catchments, and the effect reduces with increasing drainage area.

The fact that, with increasing spatial scale, the mean hydrograph of different realizations converges to the hydrograph obtained using spatially constant mean parameter values shows that predictions in large scale catchments appear to be simpler than in smaller scale catchments, as long as we get the spatial mean parameter values correct. This observation can be tied to the observed process simplicity in empirical data with increasing spatial scale (e.g., Goodrich et al. 1997; Gupta et al. 2010; Ogden and Dawdy 2003).

5.4.2. Effect of hillslope overland flow velocity

The role hillslope overland flow velocity plays in affecting the runoff response at different catchment scales has been the subject of past research, and contrasting results exist in the literature. Robinson et al. (1995) argued that hillslope processes dominate the runoff response of small catchments, while the network geomorphology dominates the runoff response at larger catchment scales. They reported that the scale at which the catchment runoff response transitions from one that is hillslope-dominated to one that is dominated by the network geomorphology is on the order of 10 km^2. D'Odorico and Rigon (2003), building on the theory of GIUH, also suggested that the contribution of hillslope residence time to the runoff dispersion is significant at smaller watersheds and negligible at larger scales. They also suggested that the role of the hillslope is dependent on the catchment moisture condition and becomes significant due to the increased residence time when the catchment is saturated. Contrary to these findings, Saco and Kumar (2004) showed that hillslopes play a significant role in shaping the runoff response at all scales. Most importantly, they showed that when hillslope velocities are smaller than channel velocities, which is often the case, the effect of hillslope overland

flow velocity through kinematic dispersion becomes more important than geomorphic dispersion. Botter and Rinaldo (2003) analyzed the role of hillslopes in 150 sub-basins of the Brenta River in Italy that range in size from 4 to 1500 km^2 and showed that v_h plays a significant role in determining the runoff response at all scales.

My findings, albeit using a different methodology that is based on the numerical simulation of hillslope-channel-link dynamics, highlight that the role that v_h plays in determining the runoff response is a function of spatial scale and rainfall duration. The results presented in Figure V-5a and b, which are obtained by increasing v_h 100 fold between two different simulations, show that v_h has a more significant effect on the runoff response when the rainfall duration is short than when the rainfall duration is longer. In both cases, the effect of v_h on the runoff response decreases with increasing spatial scale. Furthermore, we see in Figure V-5a that there is a significant dispersion of peak discharge estimates when the v_h value is high and the rainfall duration is short. This dispersion is a manifestation of the geomorphic dispersion (see Figure V-1d) that dominates the runoff response when the hillslope residence time is significantly reduced through a combination of very high v_h and short rainfall duration.

My results also suggest, as shown in Figure V-5c and d, that channel flow velocity v_c plays a significant role in determining the runoff response with increasing spatial scale, which indicates that v_c and v_h have contrasting effects across scales. The reason behind the increasing significance of v_c with increasing catchment scale is that increasing v_c significantly increases the proportion of hillslopes connected to the outlet due to the

reduced travel time. The role of v_c is less significant at smaller catchment scales because the reduced time of concentration due to an increase in channel velocity is countered by the competing rainfall duration that itself determines the time available for the connectivity of hillslopes to the outlet of smaller scale subcatchments to occur. Building on a similar result, have shown in chapter IV that both α and θ increase with increasing v_c.

I explored the sensitivity of α and θ to a spatially variable v_h by systematically increasing the mean of the lognormal distribution from which v_h is sampled while keeping the coefficient of variation c_v constant at 0.5. For the nonlinear hillslope case, we calculated v_h using Manning's equation and sampling Manning's n from a lognormal distribution with a specified mean and $c_v = 0.5$. Rainfall P and runoff coefficient C_r were sampled from $P(mm) \sim Exp(1/25)$ and $C_r \sim Logn(0.5, 0.25^2)$, respectively. My analysis of the aggregated runoff response at the bottom of the complete order Horton-Strahler streams indicate that scale-invariance of peak discharge with drainage area is preserved. This result is contrary to the findings of Di Lazzaro and Volpi (2011), who argued that the spatial variability of hillslope velocity breaks the scale-invariance property of peak discharges. However, since the study catchments they used were not nested, it is difficult to conclude from their work how the aggregated effect of spatially variable v_h affects peak discharges at successively larger scales.

The results presented in Figure V-6 show how both constant and nonlinear v_h affect the scaling structure of peak discharge by systematically controlling the magnitudes of

α_1, θ_1, α_2, and θ_2. The scaling parameters were calculated by taking the average of the scaling parameters computed from 100 independent realizations of P, C_r, and v_h. It can be seen that θ_1 and θ_2 generally decrease with increasing $E[v_h]$ and appear to converge to some limiting value that is also controlled by the rainfall duration. As shown in Figure V-5a and b, this is because an increase in hillslope overland flow velocity leads to a greater increase of peak discharge per unit drainage area at smaller catchment scales than at larger catchment scales, thereby reducing the magnitude of the flood scaling exponent. It can also be seen that at $T = 12$ hr, θ_1 initially decreases with increasing $E[v_h]$, recovers back to increase with increasing $E[v_h]$, and finally converges to unity as the time of concentration is equaled or exceeded. The same is not observed for θ_2, even at $T = 48$ hr, because of the generally longer time of concentration in larger catchments. To add perspective to our analysis, the time of concentration at the outlet of the study catchment is about 12 days, whereas it is about 18 hours in a typical 64 km^2 catchment. These concentration time estimates were calculated using constant $v_c = 0.4$ m/s and $v_h = 0.01$ m/s values. Note also that θ_1 is for those sets of subcatchments whose minimum area is 1 km^2 and whose maximum area is in the range of 15 - 450 km^2, depending on the specific combination of T and v_h. An important insight that emerges from these results is that the effect of v_h on both α and θ is significant at shorter rainfall durations, and its effect dampens as the rainfall duration increases depending on the size of the catchment.

The results also show that, irrespective of whether the hillslope is linear or nonlinear, both the intercepts α_1 and α_2 generally increase with increasing $E[v_h]$ because, as

shown in Figure 6 (a and b), an increase in $E[v_h]$ leads to smaller catchments to discharge water at a higher rate per unit drainage area than larger catchments. It is also shown in Figure V-6 that both α_1 and α_2 increase with decreasing rainfall duration. This inverse relationship is explained by the increasing rainfall intensity with decreasing duration for a fixed rainfall volume $E[P]$. This will be discussed in greater detail in the following sections. A similar result was reported in chapter IV where a linear hillslope is used under the assumption of a spatially constant P, C_r, and v_h.

5.4.3. Effects of the runoff coefficient

The runoff coefficient varies both in space and time. Its spatial variability is mainly due to the spatial variability of rainfall (Merz et al. 2006), whereas its temporal variability is mainly due to the antecedent moisture condition that is itself tied to the temporal variability of rainfall and evapotranspiration (Merz and Blöschl 2009). Land use, soil types, and geology play a less significant role in determining the runoff coefficient at the catchment scale (Merz and Blöschl 2009; Merz et al. 2006). In this chapter, a spatially variable runoff coefficient is used to partition the input rainfall into surface and subsurface flow, which essentially makes saturation-excess overland flow the only runoff production mechanism. I neglected the temporal variability of the runoff coefficient by assuming that it is constant at the event scale. Furthermore, its spatial variability is modeled as a purely random process by sampling from a uniform distribution. However, the latter assumption is not realistic, as the runoff coefficient follows a spatially organized structure. However, Merz and Plate (1997) showed that the assumptions of spatially random and spatially structured soil moisture, which can be considered as a

proxy for the runoff coefficient, seem to yield comparable runoff estimates with increasing spatial scale in a catchment whose drainage area is 6.3 km^2.

The results presented in Figure V-7 show how, for a given rainfall event that is described by its intensity and duration, the runoff coefficient can lead to a range of flood scaling parameters. This means that the catchment antecedent moisture state, which mainly controls the runoff coefficient, plays a significant role in determining the scaling structure of peak discharges. In particular, we can see that θ_2 generally decreases with an increasing $E[C_r]$ for both the linear hillslope (Figure V-7, second column) and nonlinear hillslope (Figure V-7, fourth column) cases. The reason why the scaling exponent decreases with an increasing runoff coefficient is that an increase in the runoff coefficient increases the proportion of water on the hillslope that is transported more quickly (since $v_h >> v_g$). This means that increasing the runoff coefficient is equivalent to increasing v_h, which is why the runoff coefficient affects the power-law scaling parameters in such a way that is comparable to the effect of v_h, as is presented in Figure V-6. Furthermore, it is shown in Figure V-7 that the effect of the runoff coefficient on the power-law scaling parameters is significant when the rainfall intensity is higher (smaller rainfall duration) and the hillslope is nonlinear. This is because, in the nonlinear hillslope case, v_h increases with an increasing rainfall intensity and runoff coefficient, which increase the hillslope surface storage.

It is also evident in Figure V-7 that the exponent θ_1, which describes the scaling property of peak discharges in smaller catchments, is affected by the runoff coefficient only slightly when the hillslope is linear (Figure V-7, first column), whereas it is affected

comparatively more significantly when the hillslope is nonlinear (Figure V-7, third column). This is attributed to, as discussed earlier, the difference in the range of v_h values among the two hillslope models. In all cases, α_1 and α_2 increase with an increasing runoff coefficient, which is simply a reflection of the increased peak discharge that results from a higher runoff coefficient. It can also be seen that α_2 is a nonlinear function of the runoff coefficient when the hillslope is nonlinear.

5.4.4. Effects of rainfall duration and intensity

Empirical evidence from the 21 km^2 GCEW catchment suggests that rainfall duration controls the flood-scaling exponent, whereas rainfall intensity controls the intercept (Furey and Gupta 2005). The mechanism by which the rainfall duration controls the flood-scaling exponent is that it determines the proportion of subcatchments that contribute to peak discharge (Gupta and Waymire 1998). Under the assumption of a spatially constant rainfall, I have showed in chapter IV that the scaling exponent converges to unity as the rainfall duration approaches or exceeds the catchment's time of concentration, which is itself a function of the size of the catchment, hillslope overland flow velocity, and channel velocity. This is also one of the principles on which the Rational Formula was built (Mulvany 1850), which is being used for peak discharge estimation in small scale catchments.

In this chapter, I expanded the analysis to a spatially variable rainfall, runoff coefficient, and hillslope overland flow velocity. The scale of the watershed is also greatly extended. The results presented in Figure V-8 show that both θ_1 and θ_2 increase with increasing rainfall duration, which is consistent with earlier studies (Furey and

Gupta 2005; Furey and Gupta 2007). It is also evident in Figure V-8 that θ_1 is generally greater than θ_2 and that it asymptotically converges to unity quickly because of the shorter time of concentration in the smaller catchments. The results also show that both α_1 and α_2 decrease with increasing rainfall duration. It is important to note here that, in this experimental setup, increasing rainfall duration leads to a decreasing rainfall intensity since the rainfall depth is kept constant ($P(\text{mm}) \sim Exp(1/25)$).

I further investigated the role played by the rainfall intensity in determining the power-law scaling parameters. I varied the rainfall intensity among different simulations and fixed the rainfall duration at $T = 60\,\text{min}$. Furthermore, I used both constant and nonlinear hillslope overland flow velocity and channel flow velocity formulations in order to separately address the role played by the hillslope and channel flow nonlinearities in determining the runoff response at multiple spatial scales. The results show that, for the linear hillslope case (Figure 10, top row), both θ_1 and θ_2 nonlinearly increase with increasing spatial average rainfall intensity $E[I]$ when using the nonlinear channel velocity formulation (Figure V-9a and b), whereas both θ_1 and θ_2 remain independent of rainfall intensity when using constant channel velocity (Figure V-9c and d). However, both θ_1 and θ_2 decrease as a nonlinear function of rainfall intensity when the hillslope is nonlinear (Figure V-9, bottom row), irrespective of the linearity or nonlinearity of the channel flow velocity.

The results also show that, when the hillslope is linear (Figure V-8, top row), both α_1 and α_2 vary linearly with rainfall intensity regardless of whether the channel velocity is constant or nonlinear. However, it can also be seen that both α_1 and α_2 are nonlinear

functions of rainfall intensity irrespective of whether the channel velocity is constant or nonlinear. These results suggest that nonlinearities in the catchment runoff response are dictated by nonlinearities in the hillslope rather than by nonlinearities in channel flow routing.

5.4.5. Effects of rainfall movement direction and speed

In mesoscale catchments such as the one used in our present study, storms that have smaller size than the catchment are the norm rather than the exception. Several studies have shown that rainfall movement speed and direction with respect to the direction of streamflow have a significant effect on the timing and peak discharge magnitude at the catchment outlet (De Lima and Singh 2002; Niemczynowicz 1984; Ogden et al. 1995; Seo et al. 2012). These studies independently concluded that a storm moving in the downstream direction with speed comparable to the channel flow velocity leads to peak discharge that is significantly greater than peak discharge that can result from either a stationary storm that covers the entire catchment or a storm that moves in the upstream direction. In addition to storms moving upstream or downstream, storms can also pass through different sections of a given basin. For example, consecutive storms passing through successive downstream sections of the basin represent one of the drivers behind the devastating flood event of June 2008 in the Cedar River basin (Krajewski and Mantilla 2010).

In this section, I consider the case where consecutive storms pass through different parts of the basin at different time intervals (lag times). A storm is then said to be moving in the downstream (upstream) direction when consecutive storms pass through successive downstream (upstream) sections of the catchment. Obviously, this setup also

mimics a storm that is actually moving either downstream or upstream with the speed of movement determined by the lag time between successive storms. I set up the simulation experiment so that the study basin is partitioned into six travel time zones according to the geometric distance of hillslopes from the basin outlet (Figure V-10a). This particular partitioning is based on the assumption that the average storm that moves across the catchment has a width of 40 km. We set a rainfall event to move either in the upstream or downstream direction in such a way that it arrives in a given travel time zone at time t and stays there for a certain duration T. Hillslopes located in the next upstream or downstream travel time zone will begin to get rain after a certain lag time t_{lag} after t. Note that t_{lag} can also be used as a proxy to rainfall movement speed. For example, $t_{lag} = 1\,\text{hr}$ is equivalent to a storm speed of 41 km/hr in the upstream or downstream direction. This arrangement means that neighboring travel time zones could receive rain in overlapping times for those cases where $T > t_{lag}$. Furthermore, we used a spatially variable rainfall, runoff coefficient, and hillslope overland flow velocity.

The results presented in Figure V-10b and c show the results for the case in which the rainfall duration over each partition is $T = 1\,\text{hr}$. Although not shown here, similar results were obtained for other rainfall durations. These results show that the runoff response at different scales is affected differently by the rainfall movement direction and speed. When the rainfall is moving in the upstream direction, the highest peak discharge at all scales is caused by the fastest moving rainfall ($t_{lag} = 0.5\,\text{hr}$). Furthermore, multiple peaks are observed when the rainfall is moving slowly in the upstream direction, and the number of peaks is equivalent to the number of partitions in the catchment

(subcatchment). The time between these multiple peaks in a given catchment is dictated by the rainfall speed. The results also show that, when rainfall is moving in the downstream direction (Figure V-10c), the storm speed that leads to the highest peak discharge is scale dependent. These results demonstrate that rainfall that moves in the downstream direction with the "perfect speed" can lead to major flooding.

Analysis of peak discharges indicates that the scale-invariance of peak discharge with drainage area is preserved under a moving rainfall, irrespective of its movement direction. However, the correlation coefficient between the peak discharge and drainage area decreases with decreasing rainfall speed (i.e. higher t_{lag} values). The decrease in the coefficient of correlation is more significant when a storm is moving in the upstream direction, and it improves as the rainfall duration increases. The reason behind the decrease in the coefficient of correlation is that the slow movement of rainfall leads to localized runoff-responses that do not contribute to the runoff-response at larger scales, and as a result, at larger scales, the area within the catchment that contributes to the peak discharge is smaller than the actual catchment area that is used in the power-law formula.

The results presented in Figure V-11 show that, for a given rainfall speed defined by t_{lag}, the flood-scaling exponent θ_2 increases with increasing rainfall duration, which is in agreement with results obtained earlier under the assumption of a spatially variable rainfall that covers the entire catchment. The intercept α_2 also decreases with increasing rainfall duration (decreasing rainfall intensity). The effect of rainfall speed on both α_2, and θ_2 appears to be less significant when the rain is moving in the upstream direction. However, it becomes significant when rainfall moves in the downstream direction. It can be seen in Figure V-11d that, within the range of t_{lag} that we considered, θ_2 increases

with increasing t_{lag}, whereas α_2 decreases with increasing t_{lag}. Higher t_{lag} values than those considered here lead to disconnected runoff-responses at different scales, thereby invalidating the occurrence of spatial aggregation of flows which is a prerequisite for the power-law scaling structure to hold. Both α_1, and θ_1 are not affected by the storm movement direction and speed because they represent those subcatchments whose drainage area is smaller than the spatial extent of the storm.

5.5. Summary and conclusions

In this chapter, I used a diagnostic numerical simulation methodology that is based on an accurate representation of the drainage network to investigate the role played by rainfall and catchment physical properties in shaping the power-law scaling structure of peak discharge with drainage area. My simulation methodology implemented a simple hillslope model with three physically meaningful parameters (C_r, v_h, and v_g) when using a linear hillslope response and with four parameters (C_r, n, S_o, and v_g) when using a nonlinear hillslope response. This simplification warrants a concise, first-order understanding of the problem that would be difficult to achieve using an over-parameterized complex model. Furthermore, I assumed that rainfall is spatially variable according to the exponential distribution, whereas hillslope overland flow velocity and runoff coefficient are spatially variable according to the lognormal distribution. Although not reported in this dissertation, I also experimented with spatially variable rainfall and hillslope parameters that are sampled from a uniform distribution and found similar results.

The key results of this chapter can be summarized as follows:

1) The effect of the random spatial variability of rainfall, runoff coefficient, and hillslope overland flow velocity on the runoff response decreases with increasing spatial scale. The results show that, at some scale (~500 km^2), hydrographs resulting from a spatially variable hillslope overland flow velocity appear to converge to a mean hydrograph that has a lesser peak and longer tail than the hydrograph obtained using a spatially-constant mean hillslope overland flow velocity. However, convergence to the mean hydrograph occurs as the drainage area increases. This means that peak discharge prediction at larger catchment scales is possible with spatially uniform rainfall and model parameters as long as their spatially averaged mean values are accurately estimated.
2) The effect of the hillslope overland flow velocity on the runoff response decreases with increasing spatial scale, whereas the effect of channel flow velocity increases with increasing spatial scale. However, the significance of the effect of both hillslope overland flow velocity and channel flow velocity on the runoff response across scales is controlled by rainfall duration, which dampens their effect as it lengthens. These mechanisms are the reason why, at relatively shorter rainfall durations, increasing the hillslope overland flow velocity leads to a decrease in the flood-scaling exponent, whereas increasing the channel flow velocity has the opposite effect. As the rainfall duration gets longer, more and more hillslopes (subcatchments) achieve saturation irrespective of the reduced time of concentration due to increased hillslope and channel flow velocities. This condition is reflected in the reduced effect of hillslope and channel flow velocities on the flood-scaling exponent. Furthermore, increasing the runoff coefficient

appears to affect the flood-scaling exponent in a way that is similar to the hillslope overland flow velocity. To conclude, the results show that hillslope overland flow velocity dominates small scale catchment responses whereas channel flow velocity significantly affects large scale catchment responses.

3) Rainfall duration controls the scaling structure of peak discharge by controlling the proportion of subcatchments that achieve saturation and that contribute to the peak discharge at the outlet. As such, under the assumption that rainfall covers the entire catchment, the flood-scaling exponent increases with increasing rainfall duration and converges to unity when the rainfall duration approaches or exceeds the catchment time of concentration, which is controlled by the drainage area, channel flow velocity, and, to a lesser extent, by hillslope overland flow velocity. Furthermore, increasing rainfall duration leads to a decrease in the variance (scatter around the regression line) of peak discharge that is mainly introduced by the variance of the width function maxima. Rainfall intensity, an additional rainfall property, affects the scaling structure of peak discharge through its indirect effect on the magnitude of hillslope overland flow velocity and channel velocity. Rainfall intensity does not have any effect on the flood-scaling exponent when both the hillslope and channel flow velocity are constant.

4) Rainfall movement direction and speed have an effect on the runoff response at different scales. Rainfall moving in the downstream direction increases the magnitude of peak discharge through its synchronization with travel time zones. When rainfall moves in the downstream direction, the rainfall speed that leads to the highest possible peak discharge is scale dependent. Also, scale-invariance of

peak discharge with drainage area holds irrespective of the rainfall movement direction, and the flood-scaling parameters are controlled by the rainfall duration and, when it is moving in the downstream direction, by the storm movement speed.

Table V - 1. Summary of the range of input parameters used for each simulation experiment.

Study Objective	Hillslope type	Range over which input parameters are varied
Effect of overland flow velocity	Linear	$v_h(m/s) \sim Logn\left(E[v_h], \left(0.5 * E[v_h]\right)^2\right)$ where $0.001 \le E[v_h] \le 0.1$
	Nonlinear	$n \sim Logn\left(E[n], \left(0.5 * E[n]\right)^2\right)$ where $0.01 \le E[n] \le 0.1$
Effect of runoff coefficient	Linear	$C_r \sim Logn\left(E[C_r], \left(0.5 * E[C_r]\right)^2\right)$ where $0.1 \le E[C_r] \le 0.9$
	Nonlinear	
Effect of rainfall duration	Linear	$5\ \text{min} \le T \le 48\ \text{hr}$
	Nonlinear	
Effect of rainfall intensity	Linear	$I(mm/hr) \sim Exp\left(\frac{1}{E[I]}\right)$ where $5 \le E[I] \le 100$ and $T = 60\ \text{min}$
	Nonlinear	
Unless otherwise stated, the following set of parameter values were used in all of the experiments: • $P(mm) \sim Exp(1/25)$ applied over durations $5\ \text{min} \le T \le 48\ \text{hr}$, • $C_r \sim Logn(0.5, 0.25^2)$, • $v_h(m/s) \sim Logn\left(0.02, 0.01^2\right)$ for the linear hillslope case and, • $n \sim Logn\left(0.035, 0.0175^2\right)$ and $S_o(m/m) = 0.001$ for the nonlinear hillslope case.		

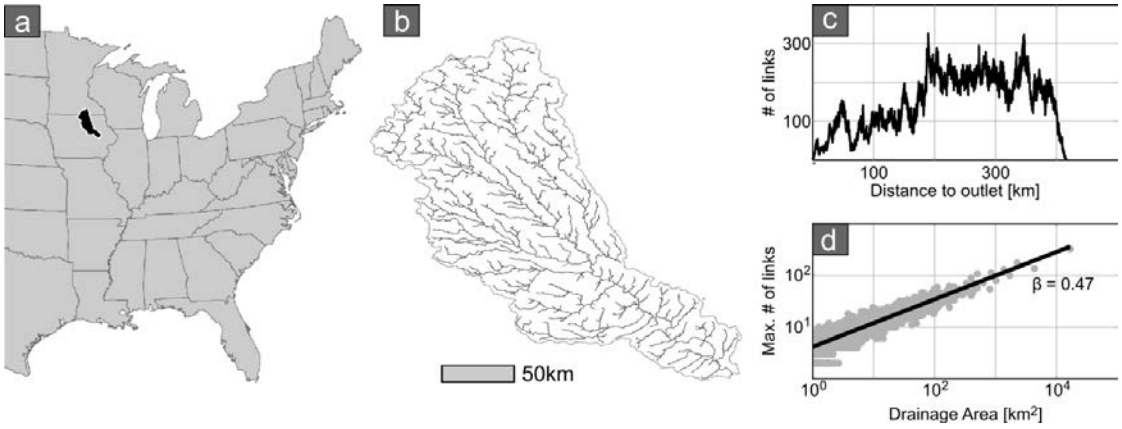

Figure V - 1. Cedar River basin, its drainage network (stream order 5 and above), its width function evaluated at the outlet, and scaling of the width function maxima with drainage area.

3

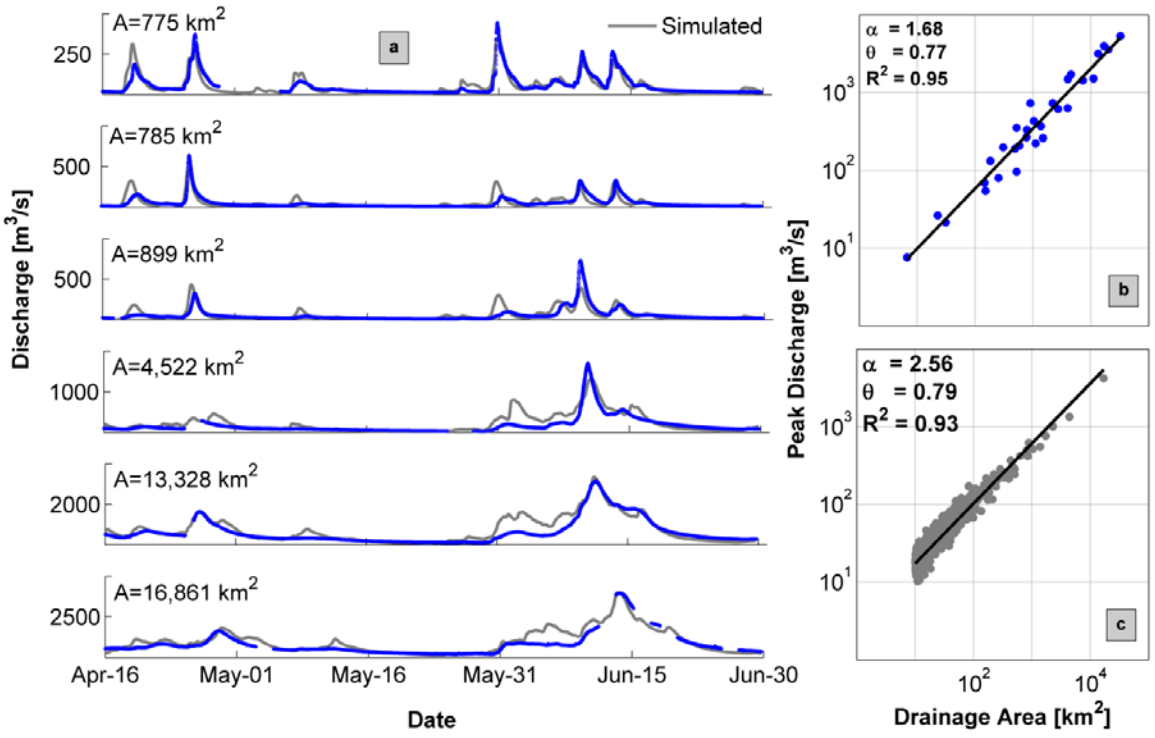

Figure V - 2. (a) Comparison of observed and simulated streamflow time series at different spatial scales in the river basin and (b) observed and (c) simulated peak-discharge scaling plots.

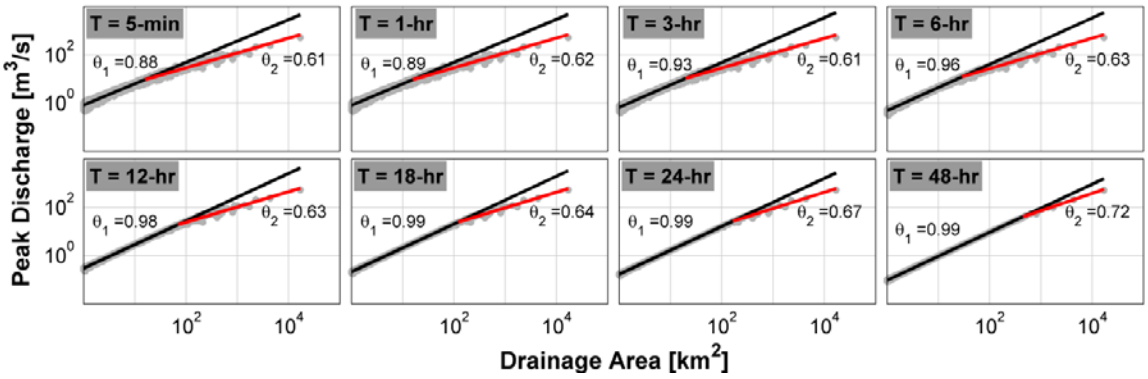

Figure V - 3. Scaling structure of peak-discharge for different rainfall durations.

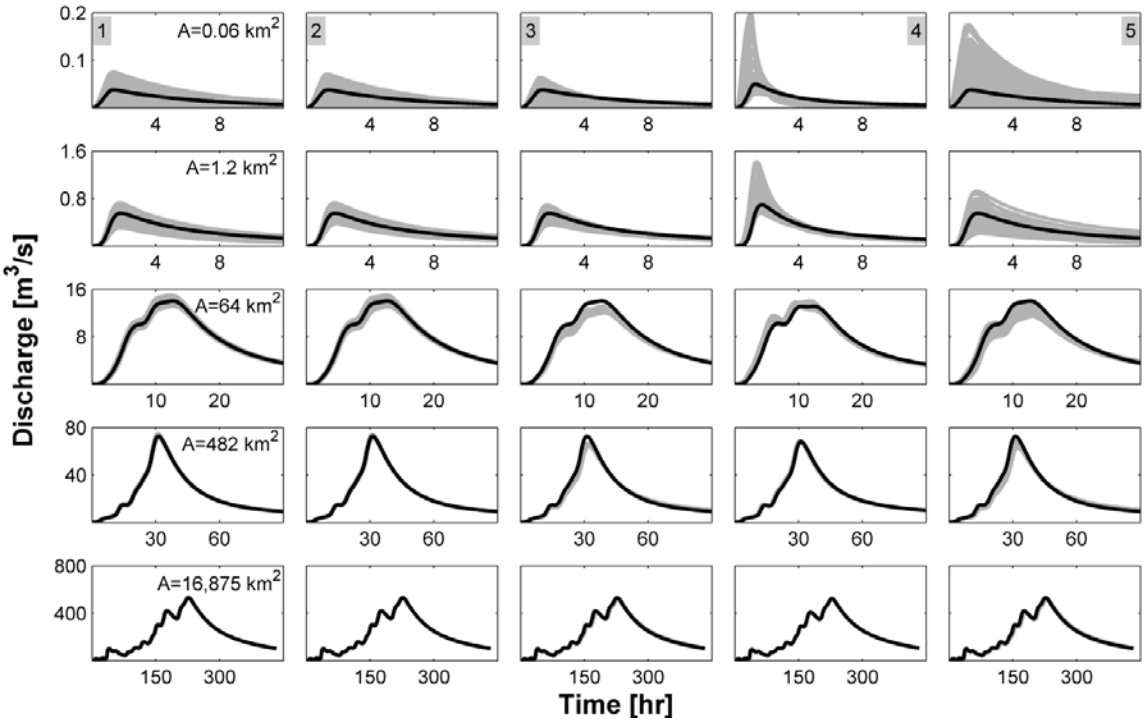

Figure V - 4. Effect of spatial variability of (1) rainfall, (2) runoff coefficient, (3) hillslope overland flow velocity, (4) manning's n, and (5) rainfall, runoff coefficient, and hillslope overland flow velocity. Each row represents different spatial scales as shown in column one.

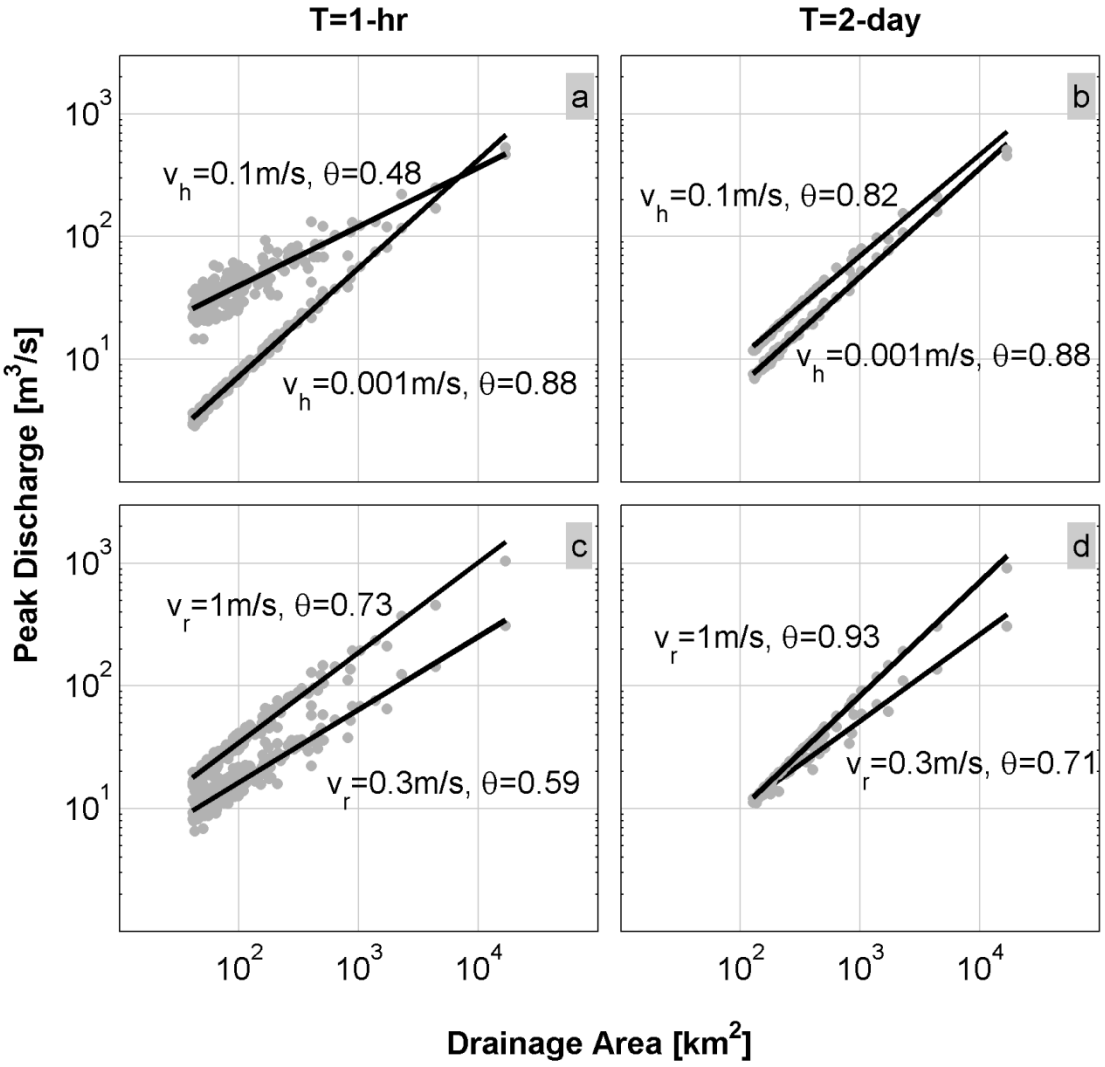

Figure V - 5. Effect of hillslope overland flow velocity (top row) and channel routing velocity (bottom row) on the scaling structure of peak-discharge.

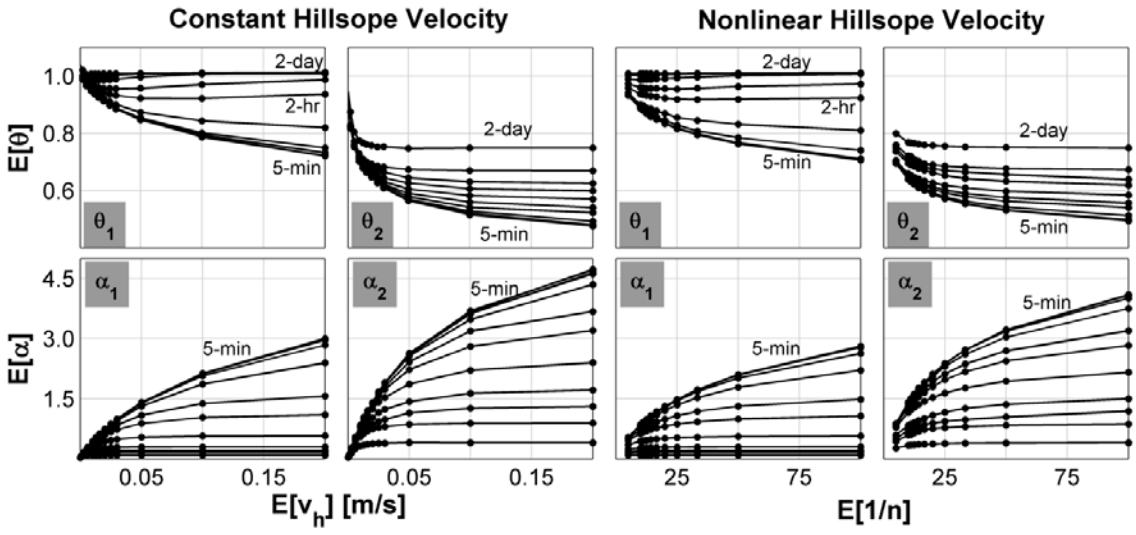

Figure V - 6. Effect of constant (first two columns) and nonlinear (last two columns) hillslope overland flow velocity on the intercept and exponent. Each black circle is an average θ or α calculated using 100 realizations of P, C_r, and v_h. Each line represents rainfall duration of 5min, 10min. 15min, 30min, 1hr, 2hr, 3hr, 6hr, 12hr, 1day and 2day, respectively.

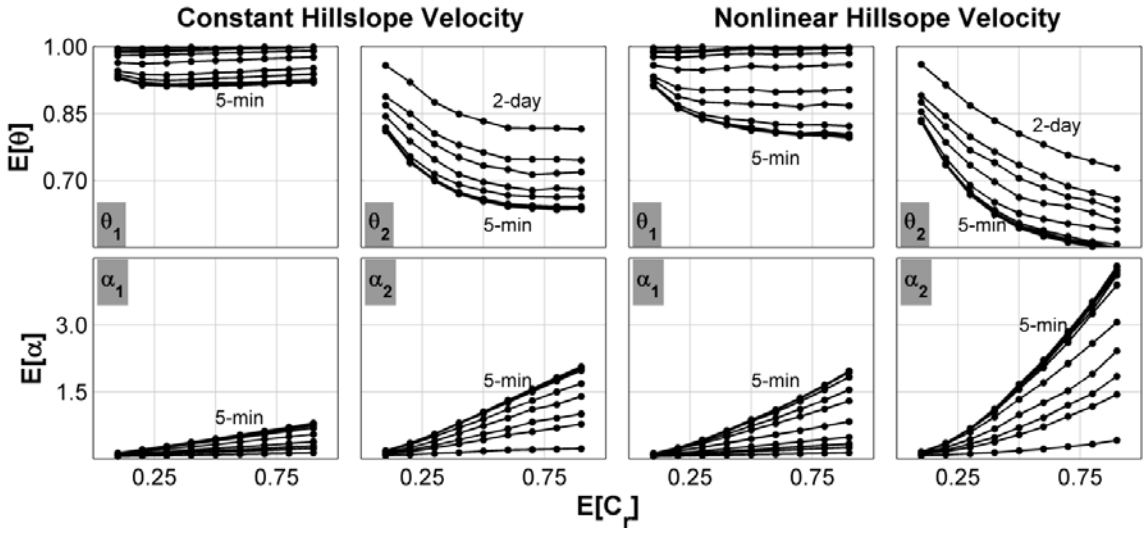

Figure V - 7. Effect of runoff coefficient on the intercept and exponent for constant (first two columns) and nonlinear hillslope overland flow velocity (last two columns). Each black circle is an average θ or α calculated using 100 realizations of P, C_r, and v_h. Each line represents rainfall duration of 5min, 10min. 15min, 30min, 1hr, 2hr, 3hr, 6hr, 12hr, 1day and 2day, respectively.

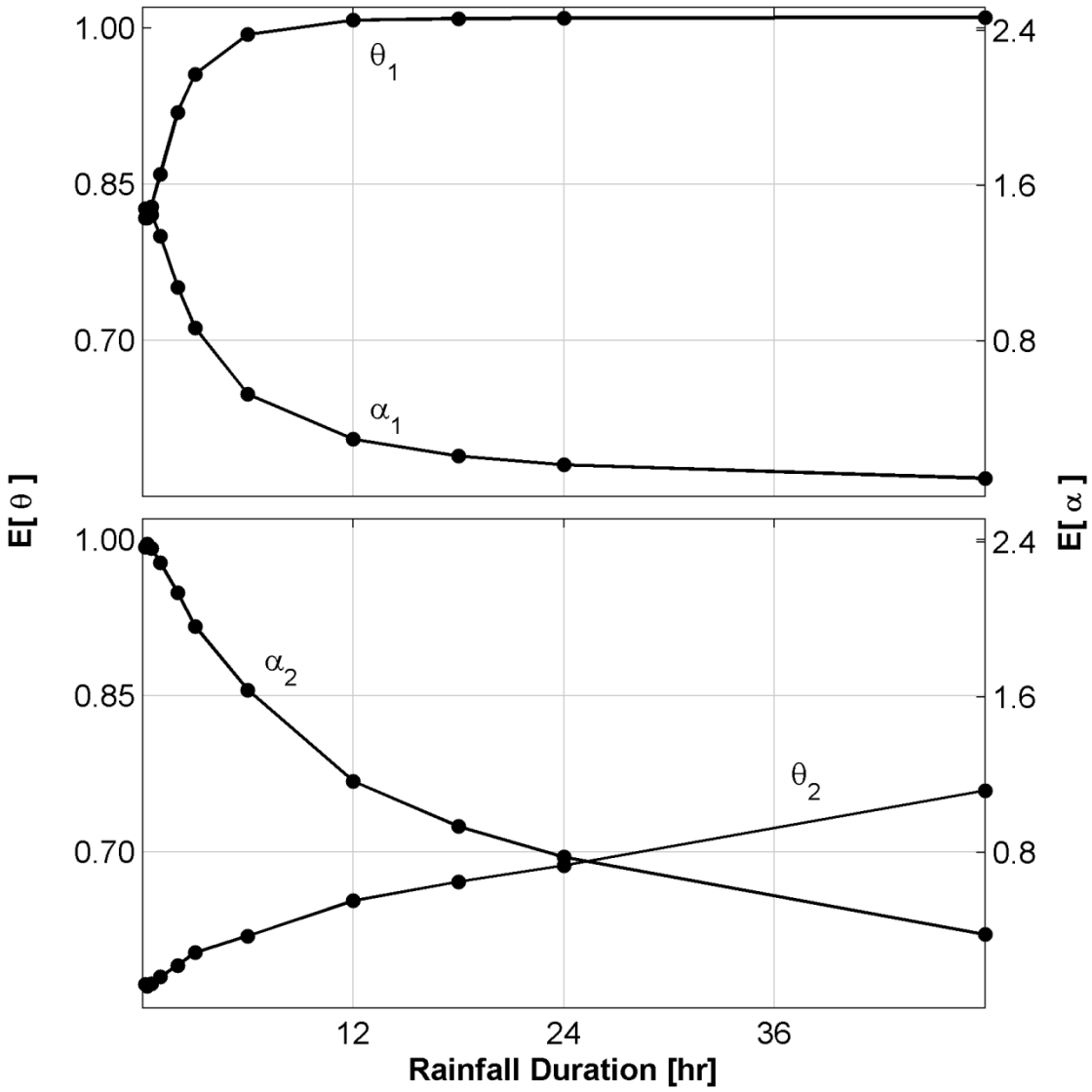

Figure V - 8. Effect of rainfall duration on the intercept and exponent. Each black circle is an average θ or α calculated from 100 realizations of P, C_r, and v_h.

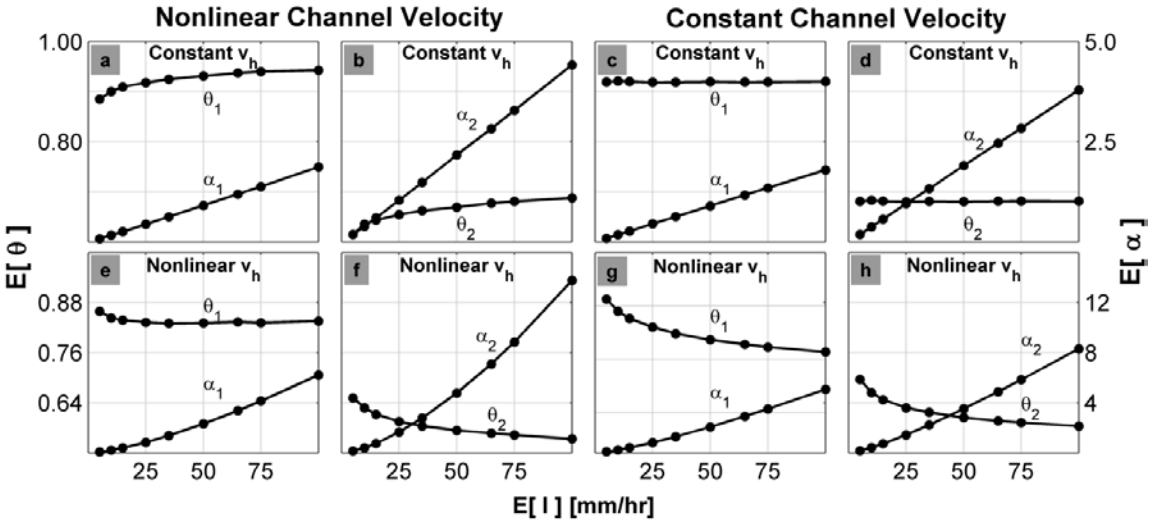

Figure V - 9. Effect of rainfall intensity on the flood scaling exponent and intercept for constant (top row) and nonlinear hillslope overland flow velocity (bottom row). The first two columns (a, b, e, f) represent results when nonlinear channel velocity is used, whereas the last two columns (c, d, g, h) show results when constant channel velocity is used. Each black circle is an average θ or α calculated using 100 realizations of P, C_r, and v_h.

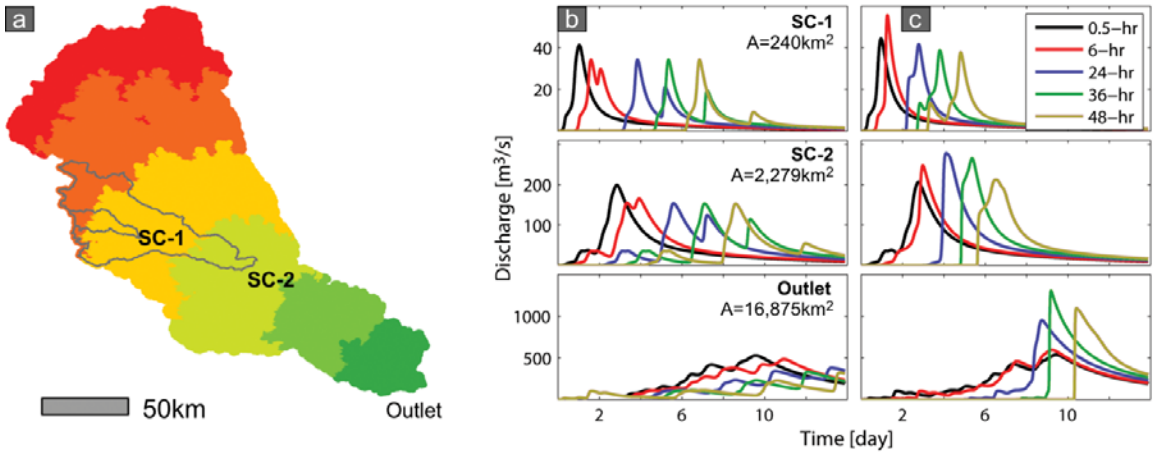

Figure V - 10. Effects of storm movement direction and lag times (shown in the legend) on the runoff response at different scales in the catchment. Shown in the figure are (a) the catchment partitioning, (b) hydrographs at the outlet resulting from a rainfall moving upstream, and (c) hydrographs resulting from a rainfall moving downstream.

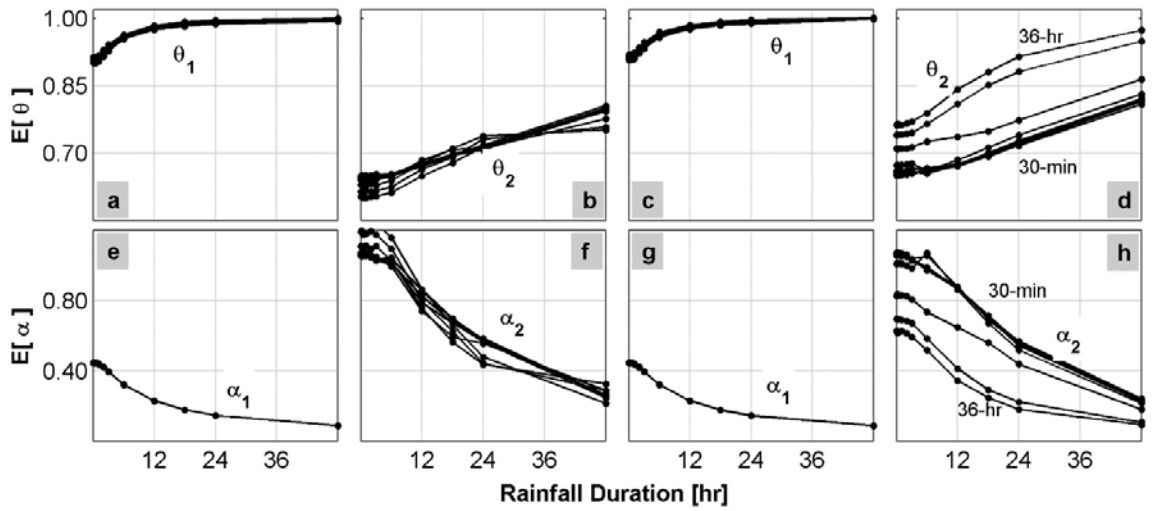

Figure V - 11. Effect of storm movement in the upstream direction (a, b, e, and f) and downstream direction (c, d, g, and h) on the flood scaling exponent and intercept. Storm lag times are indicated on the right-most column. Storm lag times are arranged in the following order: 30-min, 3-hr, 6-hr, 12-hr, 24-hr, and 36-hr. Each black circle is an average θ or α calculated from 100 realizations of P, C_r, and v_h.

CHAPTER VI

EMPIRICALLY BASED ANALYSIS OF THE EFFECTS OF EXCESS RAINFALL PROPERTIES ON THE SCALING STRUCTURE OF PEAK DISCHARGES [3]

6.1. Introduction

Although significant theoretical advances have been made in linking the intercept and the flood scaling exponent to rainfall and catchment physical properties that vary from event-to-event, little progress has been made in testing the theories using empirical data. Furey and Gupta (2005) made the first attempt to connect the flood scaling exponent and intercept to rainfall properties. They analyzed 148 rainfall-runoff events from the GCEW and showed that the exponent varies as a function of rainfall duration whereas the intercept varies as a function of excess rainfall intensity. Furey and Gupta (2007) affirmed these results through a detailed diagnostic study of the same dataset. While these studies highlighted the respective dependence of the exponent and the intercept on the excess rainfall duration and intensity, more is needed to be done to test whether or not these findings hold true in bigger catchments and also investigate interplay of these parameters with other catchment physical variables. There is yet no study that demonstrated if the findings from the 21 km^2 GCEW (Furey and Gupta 2005; Furey and Gupta 2007) hold true in a larger watershed. Such a study would go a long way in establishing the physical connection between the flood scaling parameters and rainfall and catchment physical properties that vary from event-to-event. I address this need in this chapter.

[3] Adapted from Ayalew, T. B., Krajewski, W. F., and Mantilla, R. (2015). "Analyzing the effects of excess rainfall properties on the scaling structure of peak-discharges: Insights from a mesoscale river basin." *Water Resources Research*.

The chapter is organized as follows. I begin by discussing the methodology I used to identify and characterize the rainfall events that are associated with the 52 basin wide peak-discharge events discussed in Chapter-III. I also discuss the methodology used to characterize the catchment soil moisture state. This is followed by a discussion of the results. I conclude the chapter by summarizing the major findings.

6.2. Methodology

The methodology used to identify peak-discharge events in the Iowa River basin is already discussed in greater detail in Chapter-III. Recall that I was able to identify 52 basin wide peak-discharge events that exhibit scaling invariance with drainage area at the rainfall-runoff event scale. These events occurred over the 12 year period between 2002 and 2012. In this section, I describe the procedures I designed to identify and characterize the rainfall events that led to these peak discharge events.

6.2.1. Rainfall event selection and characterization

I selected and analyzed rainfall data corresponding to the peak discharge events using the assumption that it occurs over the time window that starts two to five days before the first peak discharge is observed in the catchment and lasts until the time when the peak discharge at the catchment outlet is observed. The first peak discharge is observed in one of the small scale subcatchments whose concentration time ranges between two and five days. Therefore, the two to five day advance time window before the first peak discharge is observed in the basin is a reasonable estimate of the time when the rainfall event begins. The rainfall event ends at the time when the peak discharge at the outlet is observed. Any rainfall that is observed over this time window constitutes the rainfall event that generated the observed peak discharges in the study basin. The

maximum overall time window over which the excess rainfall occurs is 15 days, which is equivalent to the basin's concentration time.

To examine the dependence of the flood scaling parameters on the properties of rainfall, We need to first establish the excess rainfall time series corresponding to the observed peak discharges in the basin. The estimation of the excess rainfall time series is achieved by using the runoff coefficient to partition rainfall into excess rainfall and "lost" rainfall (i.e., evapotranspiration, percolation, etc.). To this end, I estimated a monthly runoff coefficient time series for the twelve-year period since 2002. To accomplish this, I performed a water balance analysis at the monthly time scale and estimated the runoff coefficient as the ratio of the observed monthly runoff volume at the catchment outlet to the rainfall volume that is integrated over the entire catchment and the same time period. As discussed earlier, I used the Stage-IV radar rainfall product as the rainfall data source. The Iowa River basin is covered by 1,788 HRAP grid cells (~4×4 km2) over which hourly rainfall accumulation data is provided. Although the runoff coefficient is known to vary both in space and time from event to event as a result of the spatio-temporal variability of rainfall and other catchment physical variables (Merz and Blöschl 2009; Merz et al. 2006), I considered the runoff coefficient as constant both in space and time for a given month. I used this resulting runoff coefficient time series to construct the hourly excess rainfall time series for each of the HRAP grid cells. Finally, I constructed a spatially averaged excess rainfall time series from the excess rainfall intensities calculated at each pixel.

I characterized the selected excess rainfall time series using two metrics: rainfall volume and duration. The rainfall event volume is easily calculated by integrating the

excess rainfall time series over the time window in which it is observed. However, estimating the rainfall duration is not as easy due to the temporal intermittency of rainfall. To circumvent this problem, I calculated the following basic characteristics (temporal moments) of the mean areal excess rainfall time series:

$$V = \sum_{t=0}^{T} I(t)\Delta t \qquad \text{Equation VI-1}$$

$$\mu = \frac{1}{V}\sum_{t=0}^{T} t \cdot I(t)\Delta t \qquad \text{Equation VI- 2}$$

$$\sigma^2 = \frac{1}{V}\sum_{t=0}^{T} (t-\mu)^2 \cdot I(t)\Delta t \qquad \text{Equation VI- 3}$$

where V is the rainfall volume, $I(t)$ is the excess rainfall intensity, t is time, and T is the time at which the peak discharge at the catchment outlet is observed. Recall that $t = 0$ starts two to five days before the first peak discharge is observed in the basin, which is observed at the outlet of one of the small scale gauged subcatchments in the basin. The choice of two to five days is based on a conservative estimate of the time of concentration of smaller subcatchments in the basin. For example, the smallest gauged subcatchment in the Iowa River basin has a 6 hr time of concentration. Note also that μ describes the mean time of the excess rainfall, whereas σ^2 describes how the excess rainfall is spread around the time when the peak excess rainfall intensity is observed, making it a better measure of the excess rainfall duration. Hence, I decided to use σ as a surrogate to estimate excess rainfall event duration. A more sophisticated characterization of the rainfall events (e.g., fractal-based) is difficult, and perhaps unnecessary, due to the shortness of the series. Figure VI-1 shows an example rainfall,

runoff event time series for selected streamflow gauging sites and the associated peak discharge scaling plot.

6.3. Results and discussion

6.3.1. Effects of excess rainfall on the intercept

I begin by discussing my findings regarding the effects of excess rainfall properties on the flood scaling intercept (α) shown in equation (2). It is important to recall that the physical meaning of the flood scaling intercept is that it is equivalent to the peak discharge at $1km^2$, when metric units are used. This means that the flood scaling intercept is expected to have a positive correlation with excess rainfall depth. Similarly, excess rainfall depth is a result of a host of rainfall and catchment physical properties such as rainfall intensity, soil type, land use, and antecedent soil moisture, which itself is a function of antecedent rainfall and a host of other catchment physical properties. Figure VI-2 shows how the natural logarithm of the flood scaling intercept varies with the natural logarithm of excess rainfall depth. It can be seen that the flood scaling intercept appears to increase with increasing excess rainfall depth. This result further confirms the results found in the theoretical studies of simulated hypothetical rainfall-runoff events from subcatchments of the study basin (Ayalew et al. 2014; Ayalew et al. 2014) and analysis of empirical data from the 21 km^2 GCEW (Furey and Gupta 2005; Furey and Gupta 2007).

Any insight that can be gained from Figure VI-2 is based purely on visual examination of the plot and it is important to explore if the observed relationship between excess rainfall depth and the flood scaling intercept is statistically significant. Moreover, We need to explore if the observed scatter in the relationship between the flood scaling

intercept and excess rainfall depth can be explained by other properties of rainfall. To this end, I conducted a multiple linear regression analysis where the natural logarithm of the flood scaling intercept is regressed against the natural logarithms of excess rainfall depth and duration. The results presented in Table VI-1 show that the event to event variability of the flood scaling intercept can be partially described by excess rainfall depth and duration in a statistically significant way (at a 99% confidence level). The Shapiro-Wilk test ($W = 0.98$, p-value = 0.76) indicates that the residuals of the regression model presented in Table 1 are normally distributed. The plots of the residuals against the fitted flood scaling intercept, excess rainfall depth and duration, which are not shown here for the sake of brevity, indicate that the residuals have constant variance. These diagnostics confirm the robustness of the multiple linear regression model presented in Table 1.

The results presented in Table VI-1 show how excess rainfall depth and duration can be linearly combined to predict the flood scaling intercept. However, We still need to confirm how the excess rainfall depth and duration individually affect the flood scaling intercept. This can be achieved by constructing partial regression plots. Partial regression plots can be used to examine the relationship between the dependent variable and a specific independent variable (Faraway 2004). The following procedure is used to make the partial regression plots that show the individual relationship between the flood scaling intercept and the excess rainfall depth and duration. First, the natural logarithm of the flood scaling intercept is regressed on the natural logarithm of the excess rainfall duration. Second, the natural logarithm of the excess rainfall depth is regressed on the natural logarithm of the excess rainfall duration. Finally, the residuals from the first step

are plotted against the residuals from the second step. The resulting plot shows the relationship between the flood scaling intercept and excess rainfall depth with the effect of excess rainfall duration taken out. A similar procedure is followed to establish the partial regression plot of the intercept and excess rainfall duration.

The results presented in Figure VI-3 summarize the results from the partial regression analysis. In particular, Figure VI-3a confirms that the flood scaling intercept increases with increasing excess rainfall depth. The slope of the regression line shown in the same figure is statistically significant at a 99% confidence level and is equivalent to the corresponding slope (coefficient) reported in Table VI-1. Figure VI-3b shows that the flood scaling intercept decreases with increasing excess rainfall duration and the relationship is statistically significant at a 99% confidence level. Again, the coefficient of the regression line depicted in Figure VI-3b is the same as the corresponding coefficient reported in Table VI-1. This later result reinforces theoretical (Ayalew et al. 2014; Ayalew et al. 2014) and empirical (Furey and Gupta 2005; Furey and Gupta 2007) findings that showed that the flood scaling intercept decreases with increasing excess rainfall duration. Ayalew et al. (2014) attributed this to an observed trend in empirical data that shows that rainfall intensity decreases with increasing rainfall duration (Huff and Angel 1992).

6.3.2. Effects of excess rainfall on the flood scaling exponent

We turn attention now to factors that control the flood scaling exponent (θ). In Figure VI-4, We show that the flood scaling exponent generally increases with increasing rainfall duration. The simulation results presented in previous chapters as well as a number of other theoretical results have shown that the flood scaling exponent increases

with increasing rainfall duration, and it is attributed to the fact that the proportion of the watershed that contributes to the peak discharge at the outlet increases as the excess rainfall duration increases (Gupta and Waymire 1998; Mandapaka et al. 2009; Menabde and Sivapalan 2001).

The results presented in Figure VI-4 show that the flood scaling exponent is always greater than the width function scaling exponent (β), which is 0.45 for the study basin. This particular result further confirms my findings reported in chapter IV and V where I showed $\theta > \beta$. A similar finding is also reported elsewhere (Mandapaka et al. 2009; Mantilla et al. 2006). An additional insight that emerges from these results is that, contrary to findings from simulation-based studies that put the upper limit of the flood scaling exponent to one (e.g., Gupta and Waymire 1998; Menabde and Sivapalan 2001), the flood scaling exponent can be greater than one. The reason behind this discrepancy is the main simplifying assumption that the simulation-based studies used, which is that excess rainfall is continuous both in space and time and has constant intensity over its duration. These assumptions do not hold true in reality because rainfall exhibits temporal and spatial variability. By relaxing the spatial uniformity of excess rainfall assumption, I have shown in Chapter-V that the spatial variability of rainfall coupled with its duration can lead to a flood scaling exponent that is greater than one.

The scatter plot presented in Figure VI-4 combine all classes of excess rainfall depth and duration into a single group. I conducted multiple linear regression to test if the dependence of the flood scaling exponent on excess rainfall duration and depth is statistically significant. Table VI-2 presents the results from the multiple linear

regression analysis where the flood scaling exponent is regressed against the natural logarithms of excess rainfall duration and depth. It can be seen that part of the event to event variability of the flood scaling exponent can be described by the excess rainfall duration and depth in a statistically significant way (at a 99% confidence level). The robustness of the regression model is confirmed using a series of diagnostic tests. The Shapiro-Wilk test (W = 0.99, p-value = 0.90) conducted on the residuals indicates that the residuals are normally distributed. Similarly, the plots of the residuals against the fitted flood scaling exponent, excess rainfall depth and duration, which are not shown here for the sake of brevity, support the assumption of homogeneous variance of the residuals.

In order to separately study the effect of excess rainfall duration and depth on the flood scaling exponent, I conducted a partial regression analysis following the procedure outlined in Faraway (2004) and summarized in section 4.1 of this paper. The partial regression plot presented in Figure VI-5a show that the flood scaling exponent decreases with increasing excess rainfall depth after the effect of excess rainfall duration is taken out. These results also support the findings I reported in Chapter-V, where I have shown that the exponent decreases with increasing excess rainfall depth due to its direct effect on the hillslope overland flow velocity. Specifically, my simulation based study of Chapter-V demonstrated that rainfall and catchment physical properties that lead to an increase in the hillslope overland flow velocity lead to a decrease in the flood scaling exponent. This is because the effect of hillslope overland flow velocity on peak discharges decreases with increasing catchment scale. In other words, the rate at which peak discharges increase with increasing hillslope overland flow velocity is greater at smaller catchment scales than at larger catchment scales, which in turn leads to a

decrease in the flood scaling exponent. This explains the physical reason behind the results presented in Figure VI-5a. The interested reader can refer to Chapter-V for a detailed discussion on how the interplay among hillslope overland flow velocity and rainfall duration affect the flood scaling exponent. In addition, the partial regression plot presented in Figure VI-5b show that the flood scaling exponent increases with increasing excess rainfall duration after the effect of excess rainfall depth is taken out, which again confirms results from the theoretical (Gupta and Waymire 1998; Menabde and Sivapalan 2001) and empirical studies of Furey and Gupta (2005); Furey and Gupta (2007) that were conducted using data from the 21 km^2 GCEW. An interesting connection that can be made here based on the results presented in Figure VI-4a and VI-5a is that rare flood events are described by bigger flood scaling intercept and smaller flood scaling exponent. Regional flood frequency studies often show a similar trend (e.g., Eash 2001; Gupta and Dawdy 1995). These reports show that the flood *quantile* scaling intercept and exponent shown in equation (1) respectively increase and decrease with decreasing probability of exceedance.

6.3.3. Effects of rainfall temporal intermittency on the scaling structure of peak discharge

The data analyses results presented thus far show that the flood scaling exponent increases with increasing excess rainfall duration and with decreasing excess rainfall depth. Similarly, the flood scaling intercept generally increases with increasing excess rainfall depth and with decreasing excess rainfall duration. However, these trends are dominated by a significant scatter. The scatter could be attributed to how accurately I estimated the excess rainfall depth, which is undermined by two factors. First, I have assumed that the runoff coefficient is constant both in space and time over a given month.

This assumption will certainly introduce some error into my excess rainfall estimation. Second, I used radar-rainfall data to estimate both the monthly runoff coefficients and the hourly excess rainfall time series. The radar-rainfall estimate has its own error (Ciach et al. 2007; Villarini and Krajewski 2010) that will eventually propagate into our excess rainfall estimation. Although the excess rainfall depth estimation error may explain some of the scatter, it is important to investigate the role of additional rainfall and catchment properties in determining the scaling structure of peak discharges.

A close examination of the results presented in Figure VI-5 indicated that, as a consequence of the scatter, two events that have different excess rainfall duration can have a similar flood scaling exponent, and two events that have the same excess rainfall duration can have a different flood scaling exponent. The same can be said about the intercept. Although the multiple linear regression results shown in Figures VI-3 and VI-5 show the dependence of the flood scaling exponent and intercept on excess rainfall depth and duration, they also exhibit a significant scatter. These results call for the search of additional rainfall and catchment physical properties that could improve the prediction of the flood scaling exponent and intercept. To this end, I examined the excess rainfall time series corresponding to each of the 52 rainfall-runoff events and found that the temporal intermittency structure could play a significant role in determining the magnitudes of the flood scaling exponent and intercept. Figure VI-6 presents an example case where two completely different rainfall time series, one occurring over a period of 12 days (Figure VI-6a) and the other occurring over a period of 8 days (Figure VI-6b), lead to comparable flood scaling exponents. The obvious difference in the two rainfall events is the temporal structure of the storms, which is evident in the significant intra-storm dry period shown in

Figure VI-6a. This suggests that the temporal intermittency of rainfall could play a significant role in determining the scaling structure of peak discharges. This section is devoted to investigating this important issue using numerical simulation of hypothetical rainfall-runoff events in the Iowa River basin.

To investigate the effect of the temporal intermittency of excess rainfall on the flood scaling structure, I used the model described in Chapter-IV to simulate the Iowa River basin using a hypothetical rainfall time series as input. I set up the simulation experiment in such a way that the temporal intermittency structure of rainfall is conceptualized using two storm cells that have the same intensity and duration (T) and are separated by a dry period (t_{dry}) (see a schematic in Figure VI-7). Conceptualizing a rainfall event as a convolution of a random number of storm cells that have a random duration and that could be separated by a random dry period is a common practice in synthetic rainfall time series generation (e.g., Cowpertwait et al. 2007; Rodriguez-Iturbe et al. 1987). I undertook a number of simulations by varying the duration of the individual storm cells and the intra-storm dry period. I set the total excess depth to be constant (25 mm) with the two storm cells each having a rainfall depth of 12.5 mm. This means that the intensity of the individual storm cells decreases with increasing storm cell duration. Since I used a constant runoff coefficient value of 0.5, the excess rainfall depth for the entire event is 12.5 mm. This configuration will enable us to understand how the intra-storm dry period and the duration and intensity of the individual storm cells control the flood scaling structure for a fixed rainfall volume. In this experiment, rainfall is assumed to be spatially constant, and its temporal structure is the same throughout the basin.

Figure VI-8 shows the streamflow response as a function of the catchment spatial scale and the intra-storm dry period. Two storm cells lead to either one or two peak discharge events, depending on the magnitude of the intra-storm dry period and the spatial scale of the catchment. The intra-storm dry period that leads to independent peak discharge events in watersheds that have spatial scales of 10, 100, 1000, and 32400 km^2 is on the order of 1, 5, 10, and 30 days, respectively, which means that the effect of the intra-storm dry period on peak discharge is scale dependent. For example, We can see in Figure VI-8 that when $t_{dry} = 1$ day, the respective peak discharge at catchment scales of 10, 100, 1000, and 32400 km^2 has decreased by 50, 50, 25, and 5% in comparison to when $t_{dry} = 0$. Accordingly, the flood scaling exponent corresponding to $t_{dry} = 1$ day should be greater than the flood scaling exponent corresponding to $t_{dry} = 0$. Recall that the flood scaling exponent is the slope of the regression line that describes the power-law relationship between peak discharge and drainage area across a range of spatial scales. As t_{dry} increases further, however, the peak discharge at the outlet starts decreasing, and the resulting flood scaling exponent will be less than the exponent calculated when $t_{dry} = 1$ day. This means that the flood scaling exponent initially increases with increasing t_{dry} before decreasing as t_{dry} continues to increase further. This simple exercise shows how the temporal intermittency of excess rainfall systematically controls the magnitude of peak discharge across a range of spatial scales in the basin.

Figure VI-9a recaps the results obtained after simulating storm cells of varying durations that are separated by a range of intra-storm dry periods. When the duration of the individual storm cells $T \leq 3$ hr, the flood scaling exponent initially increases with

increasing excess rainfall duration before starting to decrease as the duration increases. However, when $T > 6\,\text{hr}$, the flood scaling exponent is a decreasing function of the excess rainfall duration. The results also show that, for a given excess rainfall duration, the flood scaling exponent increases as the duration of the individual storm cells increases. Figure VI-9b shows that when $T \leq 3\,\text{hr}$, the flood scaling intercept decreases with increasing excess rainfall duration and converges to a certain value that is determined by the intensity of the individual storm cells. The convergence happens at t_{dry} values that lead to the maximum flood scaling exponent for a given storm cell duration. When $T > 6\,\text{hr}$, however, the intercept appears to slightly increase with increasing excess rainfall duration. These results highlight how the interplay between the storm cell duration and intra-storm dry period affects the scaling structure of peak discharge.

To further understand how the temporal intermittency of excess rainfall affects the scaling structure of peak discharge, I expanded the above analysis to an excess rainfall time series that has more than two storm cells. I fixed the total excess rainfall depth to 12.5 mm and divided it equally among a predetermined number of storm cells (*n*), each of which has a duration of 1 hr. The results presented in Figures VI-10a and b show that an increase in *n* leads to an increase in the flood scaling exponent and a decrease in the intercept. The exponent increases because an increase in *n* is equivalent to increasing the overall excess rainfall duration, as seen from the point of view of larger subcatchments. Moreover, the intercept decreases because, for a fixed total excess rainfall depth, the intensity of the individual storm cells decreases as *n* increases.

The results presented in Figures VI-9 and 10 show that the effect of the interplay among the number of storm cells, their duration, and the intra-storm dry period is manifested in the scatter observed in empirical data while relating the flood scaling exponent and intercept to excess rainfall duration (see Figures 5, 6, 7, and 8). This observation is further summarized in Figure VI-11, where the results obtained from both empirical data analysis and numerical simulation are superimposed on the same plot. In the plot, the blue line shows how the flood scaling exponent and intercept vary as a function of the duration of a single storm cell that has an excess rainfall depth of 12.5 mm, whereas the grey shaded area shows the range over which the flood scaling exponent and intercept obtained from the numerical simulation vary due to the effect of the temporal structure of rainfall. The grey circles depict the results obtained from empirical data discussed in earlier sections. It can be seen that a significant majority of the grey circles fall within the shaded area. Furthermore, it can be seen that a flood scaling exponent of greater than one is observed in empirical data, whereas the exponent obtained from numerical simulations is always less than one. This is because the numerical simulations used a spatially uniform rainfall input. I have already showed in Chapter-V that a flood scaling exponent of greater than one can occur due to spatially variable rainfall. To conclude, these results reveal the important role that the temporal structure of excess rainfall plays in shaping the scaling structure of peak discharges.

6.4.Conclusions

I analyzed 52 rainfall-runoff events from the Iowa River basin (A=32,400 km^2) to investigate how certain rainfall and catchment physical properties control the spatial scaling structure of peak discharges in a mesoscale river basin. I selected these events in

such a way that a single-peaked hydrograph is observed at the catchment outlet and that all the internal gauging sites exhibit a significant streamflow response at some point during a 15 days period leading up to the time when the peak discharge at the outlet is observed. This duration corresponds to the basin's time of concentration. I used the Stage-IV radar rainfall data to identify and characterize the rainfall time series that drives the observed peak discharges. The following are summary of the key findings:

(1) The flood scaling exponent generally increases with increasing excess rainfall duration where as it decreases with increasing excess rainfall depth. The results also show that the intercept increases with excess rainfall depth whereas it decreases with increasing excess rainfall duration. These results confirm the findings I reported in Chapters IV and V and other findings from simulation-based studies (Gupta and Waymire 1998; Mandapaka et al. 2009; Mantilla et al. 2006; Menabde and Sivapalan 2001; Menabde et al. 2001). Moreover, these results provide additional insights to findings from empirical studies (Furey and Gupta 2005; Furey and Gupta 2007; Gupta et al. 2007; Ogden and Dawdy 2003).

(2) The temporal intermittency of rainfall plays a significant role in determining the spatial scaling structure of peak discharges. The results, which are obtained from a systematic diagnostic simulation study that is guided by observations in empirical data, revealed that, for a fixed excess rainfall depth and shorter storm cell durations, the flood scaling exponent initially increases with increasing intra-storm dry period before starting to decrease when the inter-storm dry period increases beyond a certain point. However, the flood scaling exponent appears to always be a decreasing function of the intra-storm dry period for longer storm cell

durations. Furthermore, the results show that the flood scaling exponent increases with increasing duration of the individual storm cells and with increasing number of storm cells. The results also show that the intercept decreases with increasing inter-storm duration and the duration of individual storm cells and converges to a value that is determined by the intensity of the individual storm cells.

Table VI - 1. Results of the multiple linear regression of the flood scaling intercept on excess rainfall depth and duration

Variable	Coefficient	Std. Error	t value	P-value
(Intercept)	-4.604	0.869	-5.301	0.000
Log(Excess rainfall depth)	1.814	0.255	7.109	0.000
Log(Excess rainfall duration)	-0.751	0.233	-3.226	0.002
Residual standard error: 1.27 on 45 degrees of freedom Multiple R-squared: 0.538, Adjusted R-squared: 0.517 F-statistic: 26.16 on 2 and 45 DF, p-value: 0.000				

Table VI - 2. Results of the multiple linear regression of the flood scaling exponent on excess rainfall depth and duration

Variable	Coefficient	Std. Error	t value	P-value
(Intercept)	0.854	0.093	9.228	0.000
Log(Excess Rainfall Depth)	-0.108	0.027	-3.971	0.000
Log(Excess Rainfall Duration)	0.084	0.025	3.374	0.002
Residual standard error: 0.135 on 45 degrees of freedom Multiple R-squared: 0.323, Adjusted R-squared: 0.293 F-statistic: 10.72 on 2 and 45 DF, p-value: 0.0002				

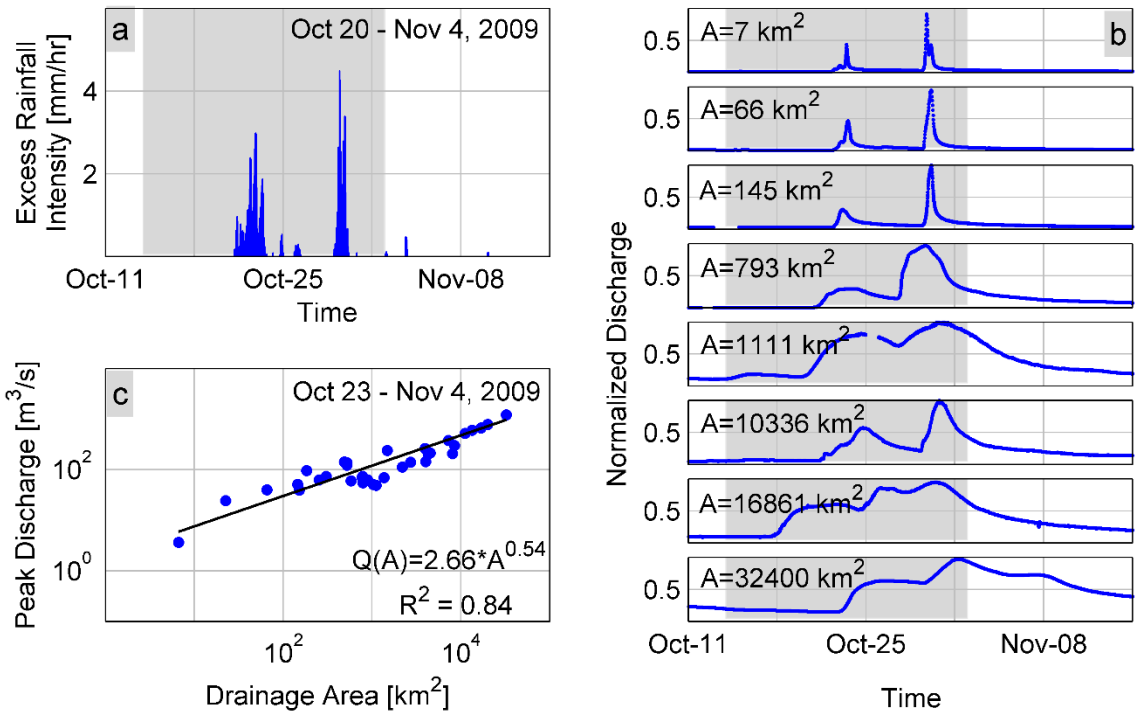

Figure VI - 1. (a) An example excess rainfall and (b) the associated streamflow time series at selected gauging sites in the Iowa River basin. The streamflow time series is normalized by the corresponding peak discharge of the event at each streamflow gauging site. The corresponding peak discharge scaling plot is also shown (c). The shaded region indicates the 15 day time window over which peak discharges in the basin were selected.

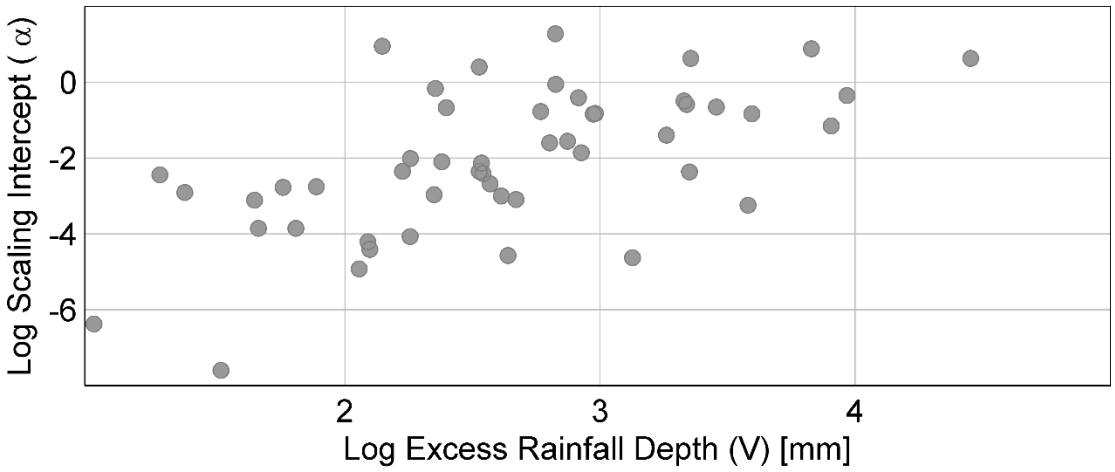

Figure VI - 2. A scatter plot depicting the relationship between the natural logarithms of flood scaling intercept (α) and excess rainfall depth (V).

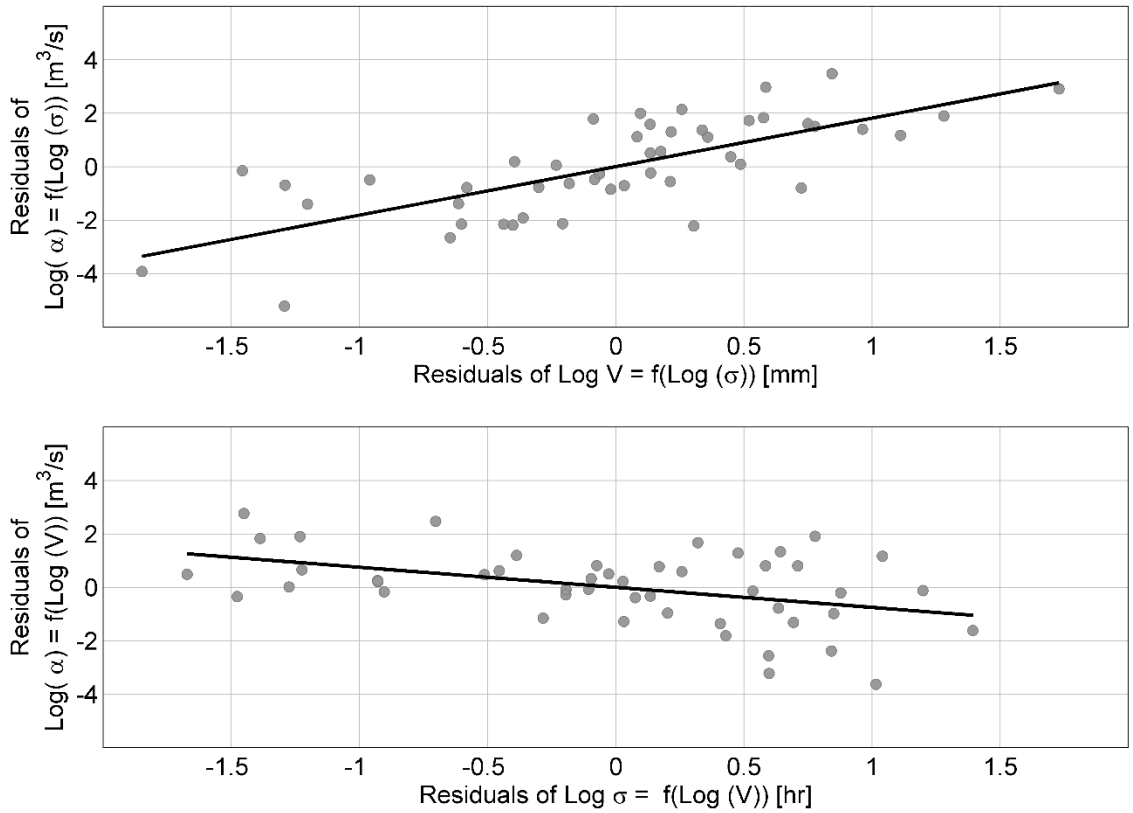

Figure VI - 3. Partial regression plots showing (a) the dependence of the flood scaling intercept on the excess rainfall depth after the effect of excess rainfall duration is taken out and (b) the dependence of the flood scaling intercept on the excess rainfall duration after the effect of excess rainfall depth is taken out.

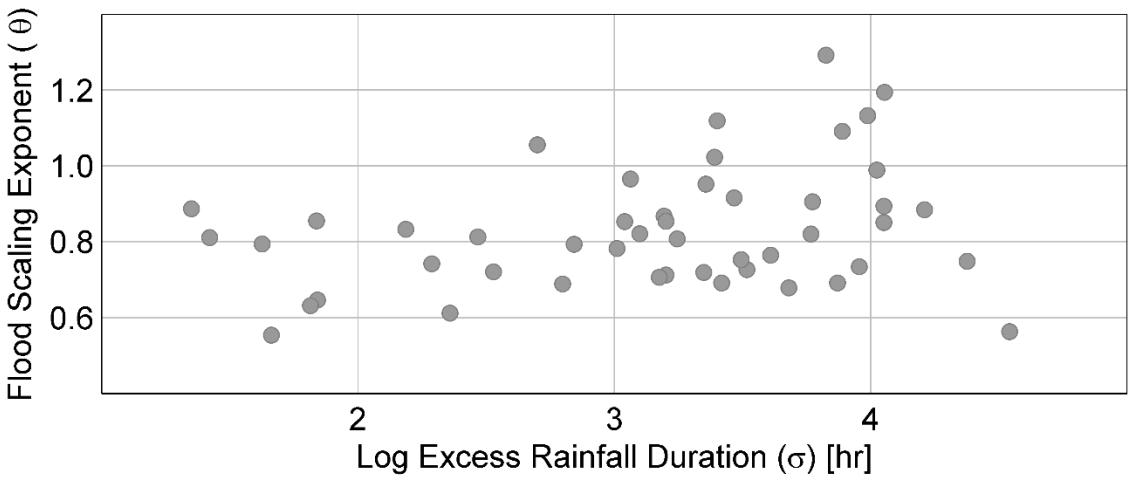

Figure VI - 4. A scatter plot depicting the relationship between the flood scaling intercept exponent and the natural logarithm of excess rainfall depth (V).

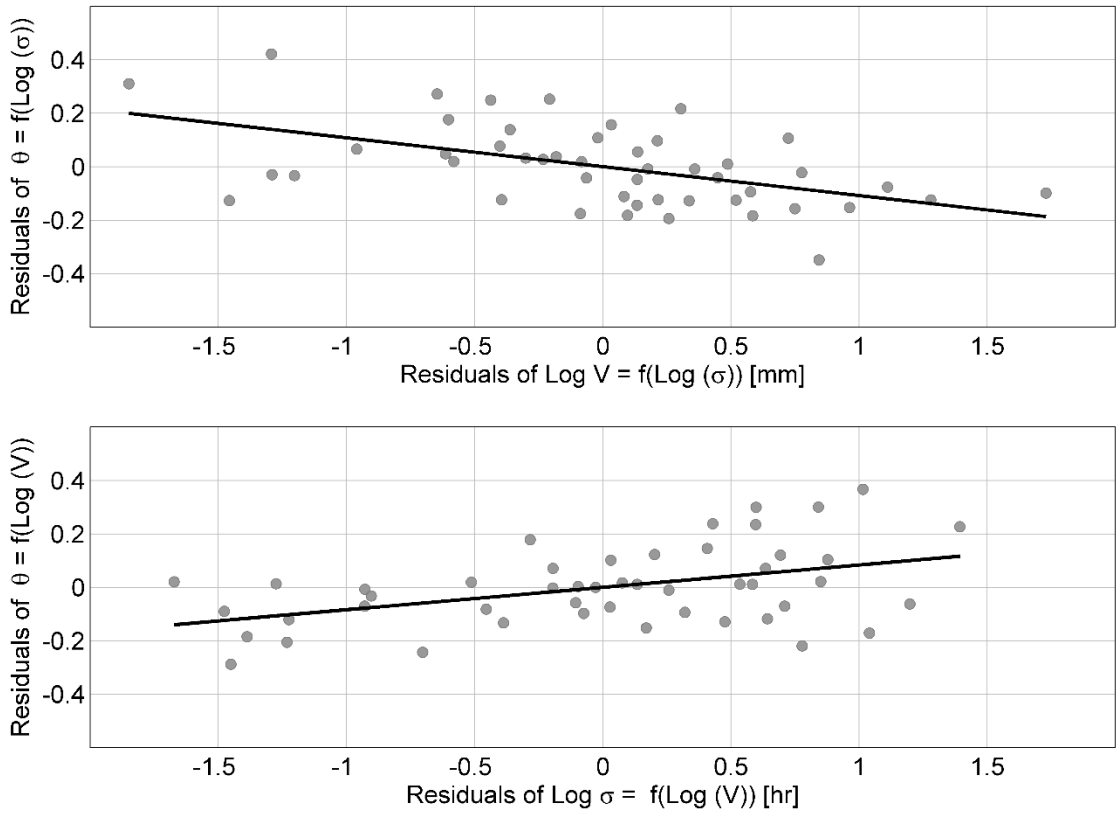

Figure VI - 5. Partial regression plots showing (a) the dependence of the flood scaling exponent on the excess rainfall depth after the effect of excess rainfall duration is taken out and (b) the dependence of the flood scaling exponent on the excess rainfall duration after the effect of excess rainfall depth is taken out.

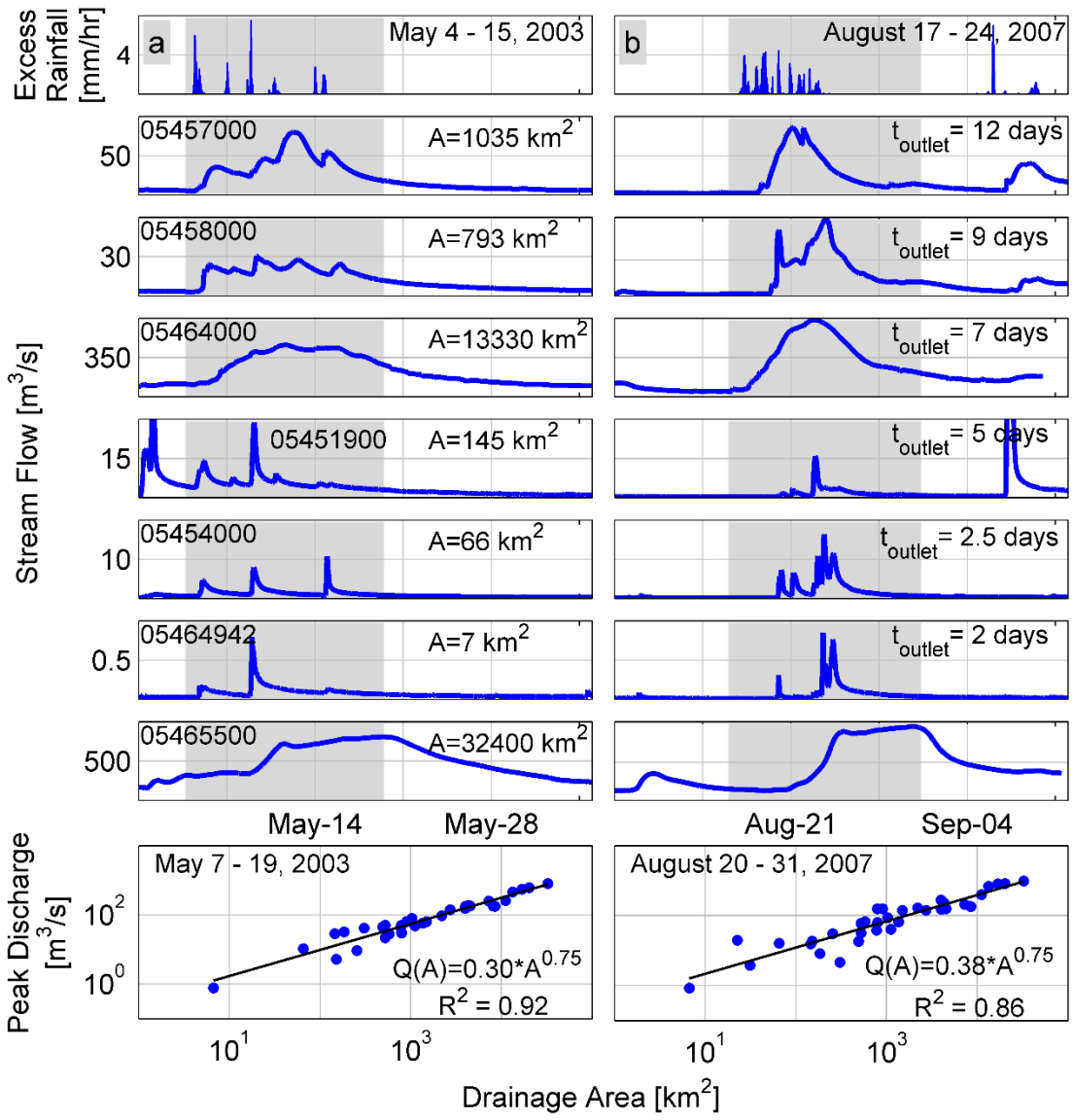

Figure VI - 6. Comparison of two different rainfall-runoff events and the associated peak discharge scaling plots. The shaded region depicts the 15 day time window preceding the time when the peak discharge at the catchment outlet is observed.

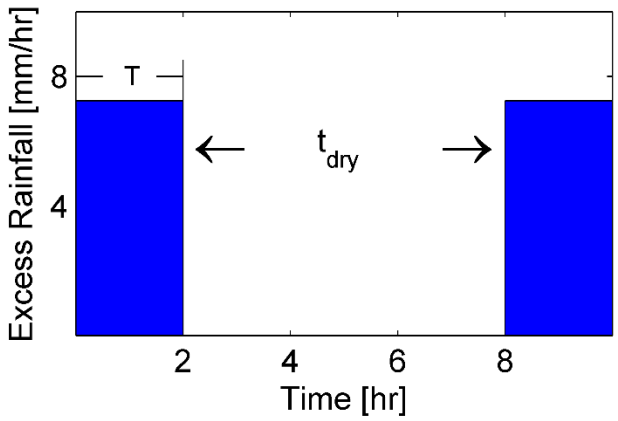

Figure VI - 7. A schematic of the excess rainfall temporal structure that is simulated in this study.

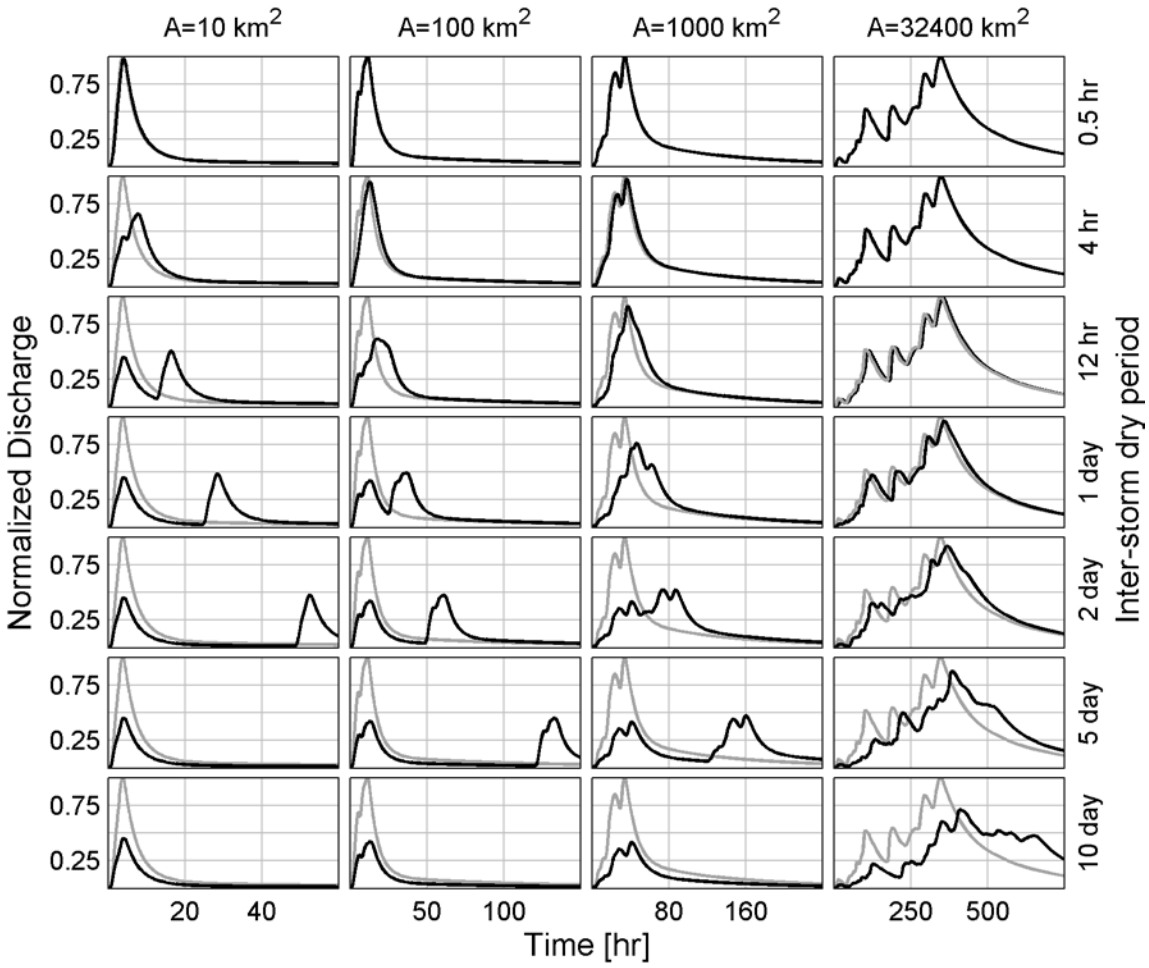

Figure VI - 8. The effect of an intra-storm dry period on the streamflow response, as seen across four representative spatial scales. In order for the hydrographs to be comparable, the discharge in each panel is normalized by the peak discharge obtained when the intra-storm dry period is zero (grey lines).

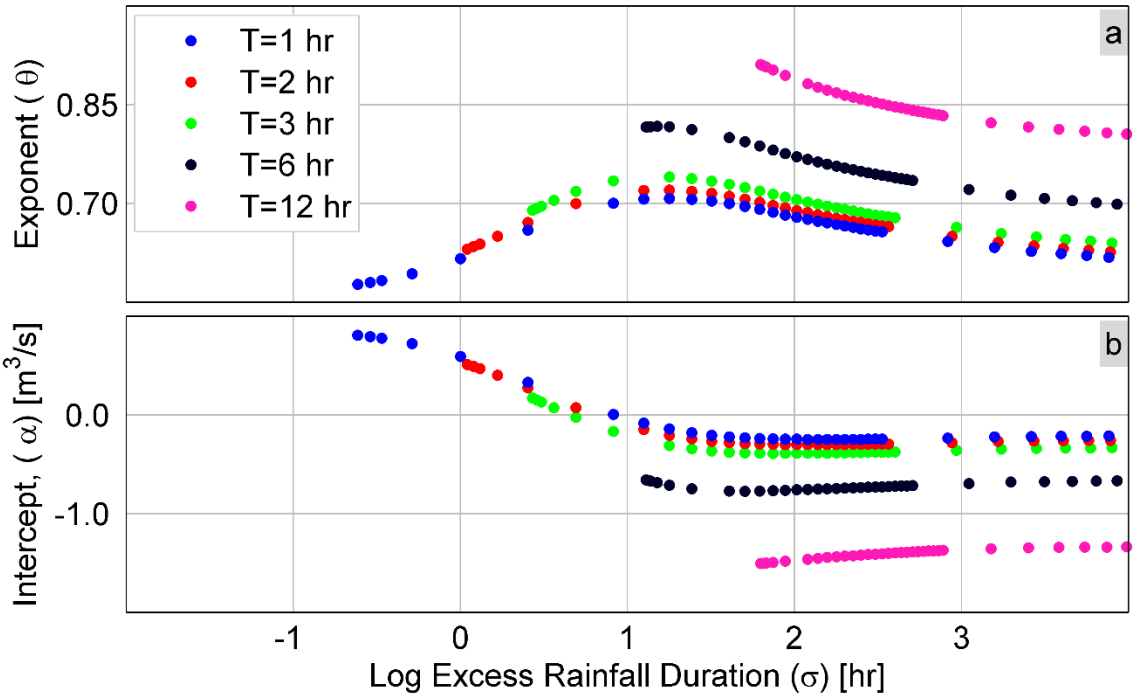

Figure VI - 9. Event-to-event variability of (a) the flood scaling exponent and (b) the natural logarithm of the flood scaling intercept as a function of the natural logarithm of the excess rainfall duration. The different colors depict the duration of the individual storm cells (T).

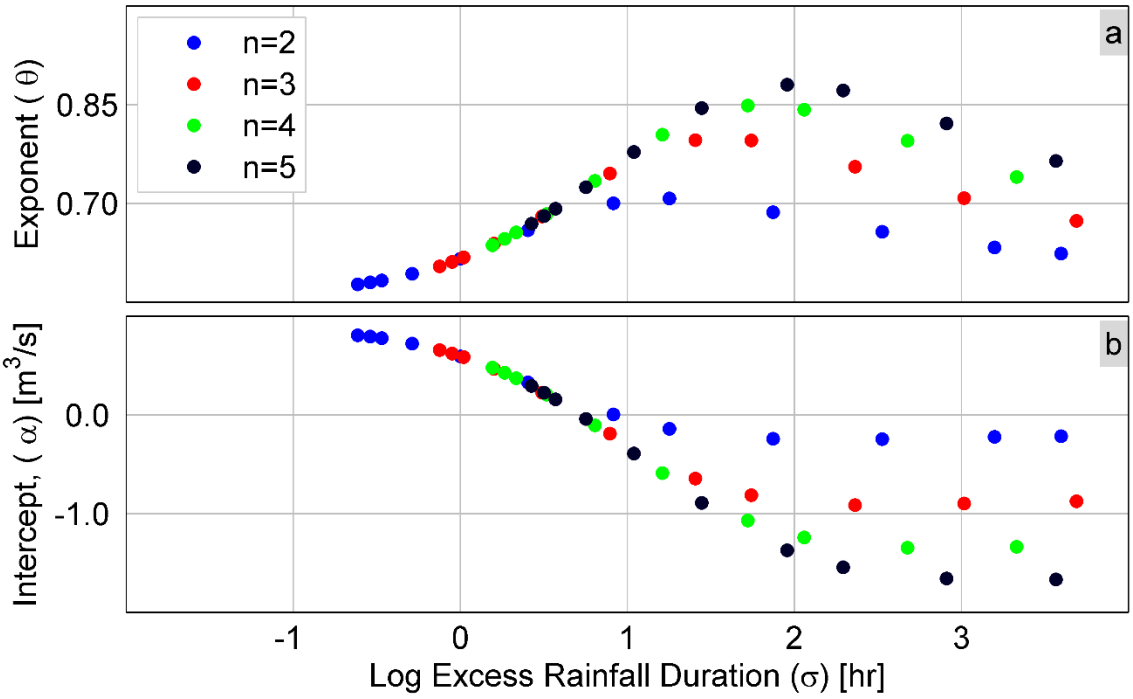

Figure VI - 10. Event-to-event variability of (a) the flood scaling exponent and (b) the natural logarithm of the flood scaling intercept as a function of the natural logarithm of the excess rainfall duration. The different colors indicate the number of storm cells (n) associated with a single storm.

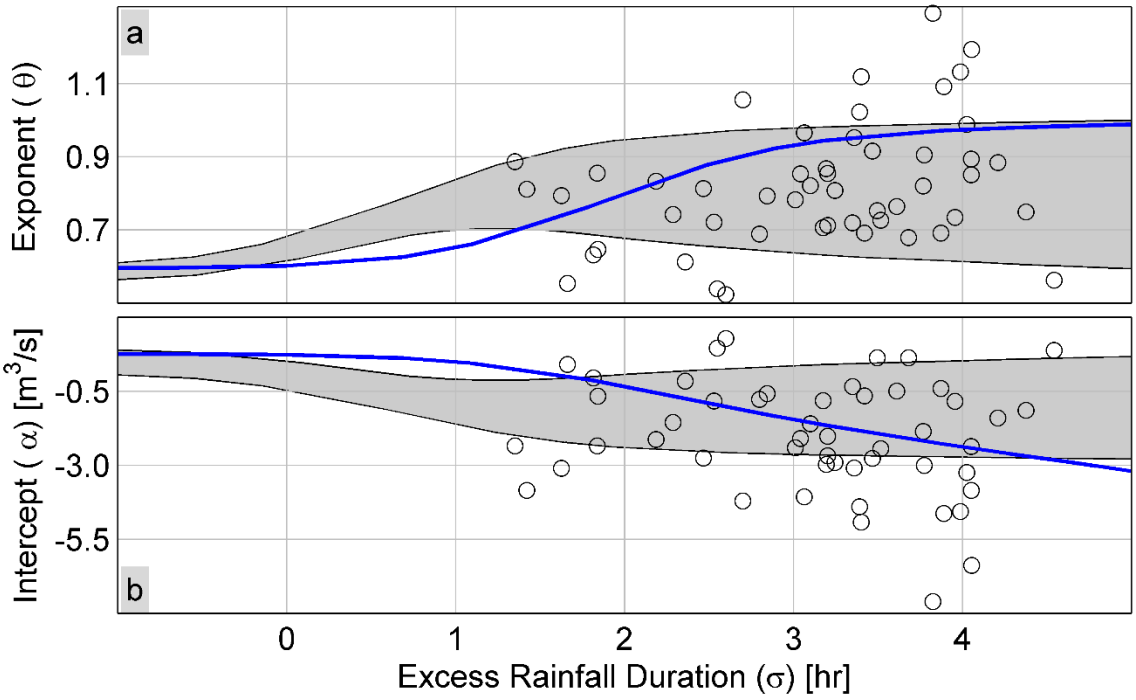

Figure VI - 11. Comparison of the range over which (a) the flood scaling exponent and (b) the intercept obtained from empirical data analysis (grey circles) and numerical simulations (grey shaded area) vary. The blue line depicts how the flood scaling parameters obtained from numerical simulation of a single storm cell vary as a function of its duration for a fixed rainfall volume.

CHAPTER VII

THE EFFECT OF CATCHMENT SHAPE ON FLOOD FREQUENCY – INSIGHTS FROM TWO CATCHMENTS IN THE IOWA RIVER BASIN

7.1. Introduction

Regional flood frequency equations are established for the purpose of predicting peak flood magnitudes in ungauged basins. These peak flood magnitudes, which are calculated for a range of exceedance probabilities, are used to design hydraulic structures such as bridges and culverts and to delineate flood inundation zones for flood risk assessment purposes. In the United States, the regional flood frequency equations are established by the U.S. Geological Survey (USGS) on a state by state basis. These equations are defined for hydrologically similar regions that are identified based on physical and statistical reasoning. The regional flood frequency equations relate peak discharge quantiles to rainfall and catchment physical properties such as drainage area, basin shape, basin length, drainage density, main channel slope, soil hydraulic conductivity, temperature, and mean annual precipitation. Among these, drainage area is the most important and is often used as the single explanatory variable to predict peak discharge quantiles. A close examination of the regional flood frequency equations established for all the 52 states of the U.S. indicate that the shape of the drainage basin is a largely ignored catchment property. In this case, catchments with the same drainage area but different shape and drainage network geometry are expected to have the same peak discharge quantiles. This is contrary to the long standing hydrologic knowledge that the shape of a basin affects the magnitude of peak flow at the outlet (Horton 1932; Morisawa 1958; Sherman 1932; Strahler 1964; Taylor and Schwarz 1952). The main objective of this chapter is therefore to show, using two equally sized catchments from

Iowa River basin, how the shape and the resulting network geometry affects the peak discharge at the single rainfall-runoff event and annual time scale.

7.2.Study area and data source

To demonstrate the effect of catchment shape on flood frequency, I use two catchments that have the same drainage area but markedly different shapes. These catchments are: Old Mans Creek (USGS ID: 05455100) and Salt Creek (USGS ID: 05452000). They are shown in Figure VII-1. Both of the catchments drain a catchment area of 521 km2. The geometric distance between the centroid of the two catchments is about 65 km, indicating their geographical proximity. In terms of shape, Old Mans Creek is elongated whereas Salt Creek is fairly circular. Both of the catchments are located in the Iowa River basin, Iowa and belong in the same hydrologic region, which is called Region 2 according to a USGS report on regional flood frequencies in Iowa (Eash et al. 2013). Hence, the same set of regional flood frequency equations are used to predict peak flood quantiles in these catchments.

The catchments are monitored by two USGS stream gauging sites whose unique gauge identification number is shown above. Old Mans Creek has 64 annual maximum peak discharge observations that occurred in the years between 1951 and 2014 whereas Salt Creek has 70 annul maximum peak discharge observations that occurred in the years between 1944 and 2014. There is an instantaneous streamflow observation data available since 1990 for Old Mans Creek and 1986 for Salt Creek. To check for the similarity of the rainfall over the two basins, we selected the closest available rain gauge station to each of the catchments. Data from the rain gauge stations is obtained through the National Climatic Data Center (NCDC) web service. Figure VII-2 presents a statistical

comparison of daily rainfall accumulation from the two rain gauge sites. As expected, the rainfall statistics are similar and hence the catchments are subject to the same rainfall regime.

7.3. At site flood frequency analysis

I begin by estimating the flood frequency curve for each of the catchments using the annual maximum peak discharge obtained from the USGS streamflow gauging sites located at the outlet of the catchments. We use the PeakFQ (Veilleux et al. 2014) software that is freely provided by the USGS to undertake the at site flood frequency analysis. In this step, I used annual maximum peak discharge data from the 64 years when peak flow information is available at both sites. The results presented in Figure VII-3 show plot of the Log-Pearson Type-III distribution fitted to the annual maximum peak discharges according to the procedure outlined in Bulletin-17B (IACWD 1982). The confidence interval of the fitted curve is also shown. It can be seen that the flood magnitudes calculated for the two catchments are significantly different although the confidence intervals overlap. Given that these two catchments are located in the same hydroclimatic region, and share similar land use and soil type, the observed difference in peak flood magnitudes across a range of exceedance probabilities calls for the investigation of other catchment physical properties that control the generation of the streamflow response in space and time. In this regard, one obvious difference between the two catchments is their shape. The role that the shape of the catchments played in the observed difference in peak flood magnitudes is discussed in the following section.

7.4. Effect of the drainage network geometry on the observed difference in peak flood magnitudes in the two catchments

It is long known that the shape of the catchment affects the peak of the streamflow hydrograph through its effect on the drainage network geometry (Black 1972; Chorley et al. 1957; Horton 1932; Morisawa 1958; Sherman 1932; Taylor and Schwarz 1952). All rainfall and catchment physical properties being equal, catchments that have rounded shape exhibit higher peak discharges than catchments that have an elongated shape (Strahler 1964). This is because of the difference in the resulting geometry of the drainage network, along which the fundamental processes of streamflow aggregation, translation, and attenuation occurs, and, as a result, is intimately connected to the hydrograph (Gupta et al. 1980; Rinaldo et al. 1995; Rodríguez-Iturbe and Valdés 1979). The drainage network geometry is described by the width function, which is defined as the number of channel links at a given distance from the outlet (Kirkby 1976; Lee and Delleur 1976). It is equivalent to the streamflow hydrograph under the assumptions that a spatially uniform rainfall is instantaneously injected to all channel links and the resulting streamflow travels with constant velocity and without attenuation (Gupta et al. 2010; Kirkby 1976).

Figure VII- 4 shows plot of the width functions of the two catchments that are estimated from a 30 m digital elevation model (DEM) obtained from the USGS. It can be seen that longest travel distance in Salt Creek is about 52 km whereas it is 75 km in Old Mans Creek. The plot also shows that the peak of the width function of the Salt Creek catchment, which has rounded shape, is greater than the peak of the width function of the Old Mans Creek catchment by a factor of 2.5. This indicates that, given the same rainfall input and simillar catchment physical properties such as catchment soil moisture state,

soil type, and land use, higher peak discharge magnitudes can be observed in Salt Creek than in Old Mans Creek. Can peak discharges in Salt Creek be greater than peak discharges from Old Mans Creek by the same factor? We will address this question in the following sections.

It is discussed above that the width function resembles the hydrograph observed at the outlet under the assumption that a spatially uniform rainfall instantaneously enters the drainage network and the resulting flow moves with constant velocity and without attenuation. However, this is a highly idealized case because rainfall is spatially and temporally variable over its duration and streamflow attenuates as it propagates in the downstream direction. With this view in mind, I remove the above assumptions by (1) allowing for a finite duration rainfall whose rate of delivery to the channel network is controlled by a spatially and temporally constant hillslope overland flow velocity and (2) a constant channel flow velocity that is incorporated in a channel transport formulation (i.e., channel storage discharge relationship) that allows for flow attenuation. Furthermore, we deliberately assume that rainfall and runoff coefficient are spatially constant. These assumptions will enable us to separately characterize the effects of the interplay among rainfall duration and drainage network geometry on the observed peak discharge differences in the two study catchments.

I simulated the two catchments using the hydrologic model presented in Chapter-IV. I used 25 mm rain as input and applied it over a range of durations. This allows for the rainfall volume to remain constant while the intensity changes with duration. I used a runoff coefficient of 0.5, a hillslope overland flow velocity of 0.02 m/s, and a channel flow velocity value of 0.4 m/s. These values are within the range of what is observed in

reality (Botter and Rinaldo 2003; Di Lazzaro and Volpi 2011; Grimaldi et al. 2010; Gupta and Waymire 1998; Huff et al. 1982). The simulation results presented in Figure VII- 5 show that the difference in the peak discharges observed at the outlet of the two catchments decrease with increasing rainfall duration. These results indicate that it is not only the shape of the catchments but also the rainfall duration that affects the peak discharge difference that could be observed in these two catchments and by extension in any other catchments that have the same drainage area.

The results presented above showed how the interplay among the drainage network geometry and rainfall duration affects the peak discharge. An additional question is: how do these rainfall and catchment properties affect the spatial scaling properties of peak discharges? To address this question, we simulated the two catchments using a spatially uniform rainfall depth of 25 mm that is applied over a range of durations. Peak discharges corresponding to each simulation experiment are computed at the bottom of complete order Horton-Strahler streams. The resulting peak discharges exhibit scaling invariance with drainage area that is described by the power law relation $Q(A) = \alpha A^{\theta}$ where Q is the peak discharge observed at a drainage area A, α is the scaling intercept and θ is the scaling exponent. The results presented in Chapter-IV and V showed that the scaling exponent and intercept increase with rainfall duration and rainfall intensity, respectively. While these results are evident in Figure VII- 6a, it can be seen that significantly different scaling exponents are observed in the two catchments at shorter rainfall durations. This is because, shorter time to peak means that less time is required to arrive to equilibrium state. As expected for the case of a spatially uniform rainfall application, the scaling exponents converge to unity at larger rainfall durations.

Figure VII- 6b shows that the scaling intercept values estimate for the two catchments appear to be similar. Given that the intercept is equivalent to the expected value of peak discharges observed in subcatchments that have a unit drainage area (i.e., 1 km^2 when metric units are used) and there are a lot of them in each of the study catchments, the similarity of the scaling intercept in these two catchments is a manifestation of the fact that there are a number of subcatchments and hence the expectation of peak discharges from these subcatchments converges to a similar value.

7.5. Effect of the drainage network geometry on flood frequency

I have showed in the previous section how the interplay among rainfall duration and drainage network geometry affects the peak discharge at the rainfall-runoff event scale. The results were obtained under the assumption that the rainfall intensity is constant over its duration. However, this is an unrealistic assumption as rainfall exhibits significant temporal variability. This leads us to the main objective of this study, which is to investigate how the interplay among the temporal structure of rainfall and the network geometry affect the peak discharge at the annual time scale and hence the flood frequency. To this end, I adopted a continuous simulation approach where a stochastically generated 5000 years long rainfall time series is used to derive the rainfall-runoff model. In such a way, a random combination of rainfall intensities and storm durations can lead the annual maximum peak discharge. Furthermore, the rainfall intensity, runoff coefficient, hillslope overland flow velocity, and channel flow velocity values are kept constant in space with the objective of studying the role of the network geometry alone.

The stochastic rainfall generator is based on the well-known Bartlett-Lewis Rectangular pulse model (Rodriguez-Iturbe et al. 1987; Rodriguez-Iturbe et al. 1988), which belongs to the family of Poisson-cluster processes. The model is fitted to the rainfall time series observed at the Iowa City airport (NCDC Station ID: COOP 134101) that is located closer to the outlet of the Old Mans Creek. The rainfall data, which has a temporal resolution of 15 min and covers the period between 1979 and 2013, is obtained from the National Climatic Data Center (NCDC). By fitting the stochastic rainfall generator to a point rainfall time series that is observed within close proximity of the study catchments, some elements of the local rainfall temporal pattern is preserved.

The results of the continuous simulation experiment is shown in Figure VII- 7. It can be seen that the simulated peak discharges at the outlet of Salt Creek are greater than those simulated at the outlet of Old Mans Creek across all exceedance probabilities. This result suggests that the effect of the drainage network geometry on peak-discharge at the rainfall-runoff event scale also propagates to the annual time scale.

7.6. Conclusion

The main objective of this chapter is to show how the drainage network geometry affects the peak discharge magnitude at the rainfall-runoff event scale and at the annual time scale. To demonstrate this, I used two catchments that have the same drainage area and different drainage network geometry. The catchments are Old Mans Creek and Salt Creek, both of which are located in the Iowa River basin. These catchments are also located in the same hydrologic region and hence the same regional flood frequency equations are used to estimate peak discharge quantiles at any location in these

catchments. The catchments also exhibit similar soil type and land use patterns. Analysis of daily rainfall accumulation data from rain gauge sites located closer to the catchments indicate that they receive similar rainfall depths.

The at site flood frequency analysis conducted using 64 years of annual maximum peak discharge data since 1951 shows a significant difference of peak discharge magnitudes for all the exceedance probabilities considered. Given that the two catchments are located in the same hydroclimatic region, the observed difference in the flood frequency at the outlet of the two catchments is attributed to the observed difference in the drainage network geometry of the two catchments. To further substantiate this claim, I conducted a systematic simulation experiment by using the same rainfall depth, runoff coefficient, hillslope overland flow velocity and channel flow velocity values as input. The results show how the interplay among drainage network geometry and rainfall duration affect the simulated peak discharge at the outlet. The analysis is expanded to the annual time scale by simulating a stochastically generated 10,000 years long rainfall time series as input. Analysis of the simulation results show that the effect of the network geometry at the rainfall-runoff scale propagates to the annual time scale. The results show the significant effect that the drainage network geometry has on flood frequency.

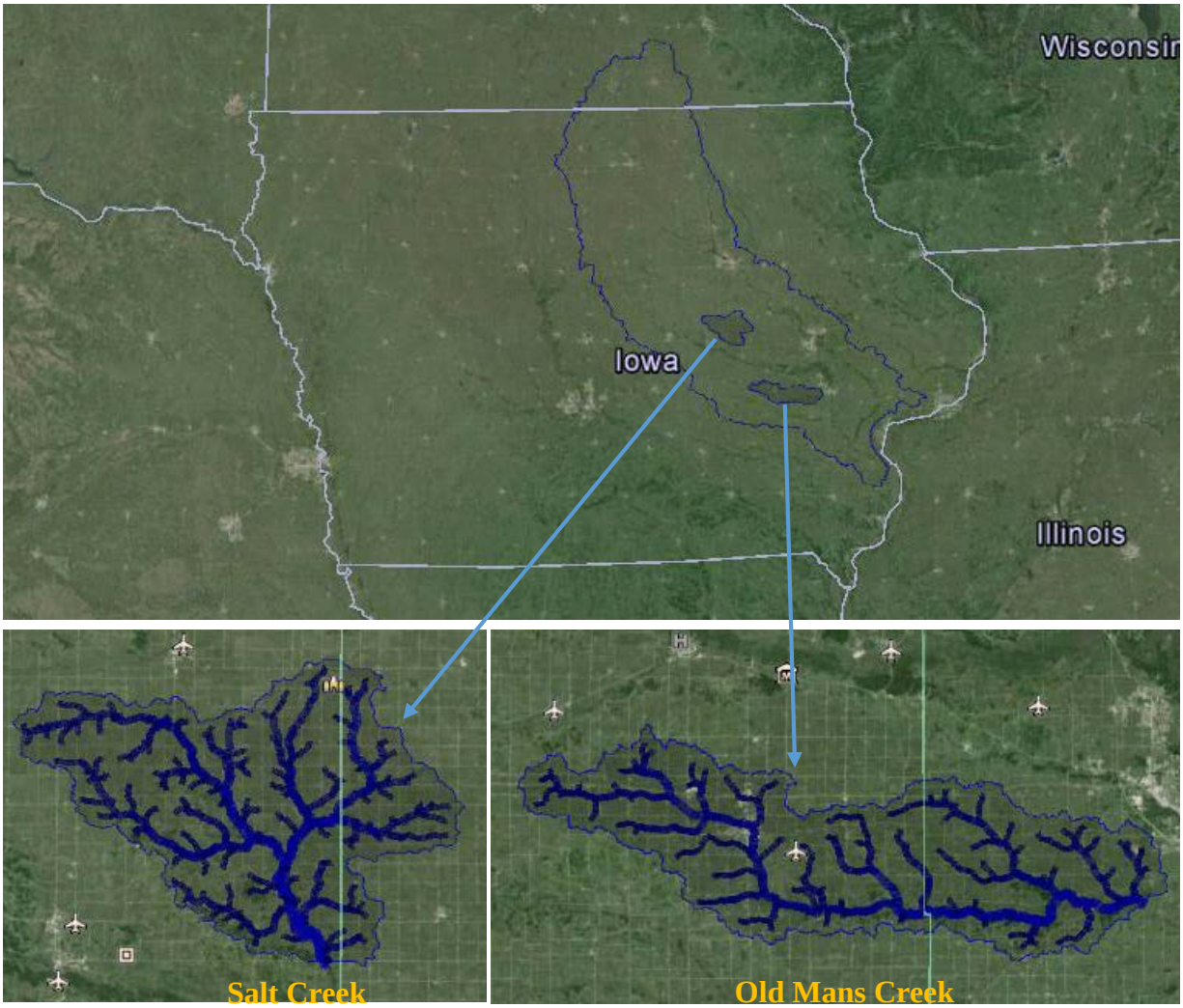

Figure VII - 1. The geographic location of the two catchments. Streams of Horton-Strahler order 4 and beyond are shown for the sake of clarity.

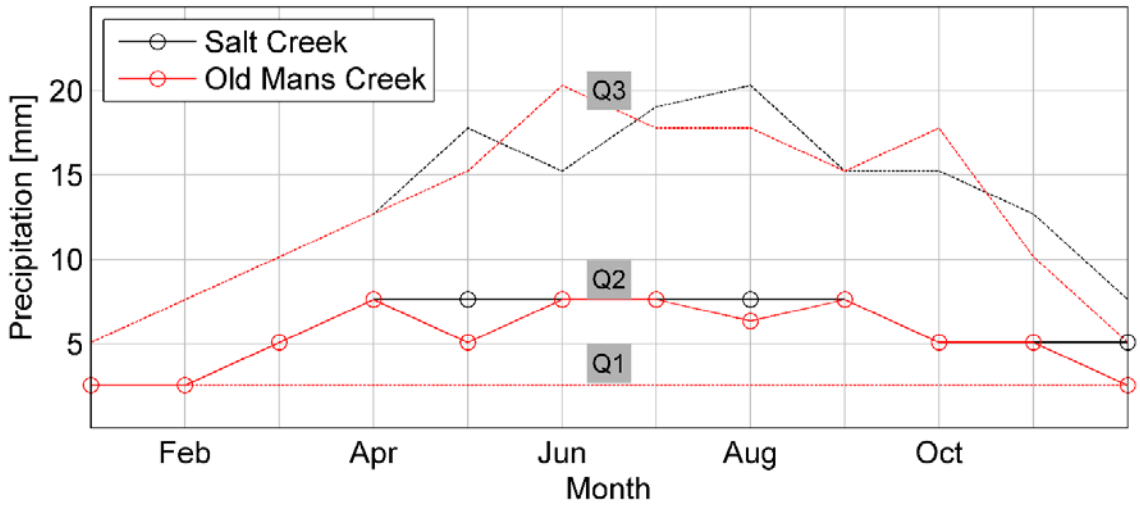

Figure VII - 2. Comparison of the first (Q1), second (Q2), and third(Q3) quantiles of the daily rainfall accumulation estimated using data from two rain gauge sites that are each located close to the catchments.

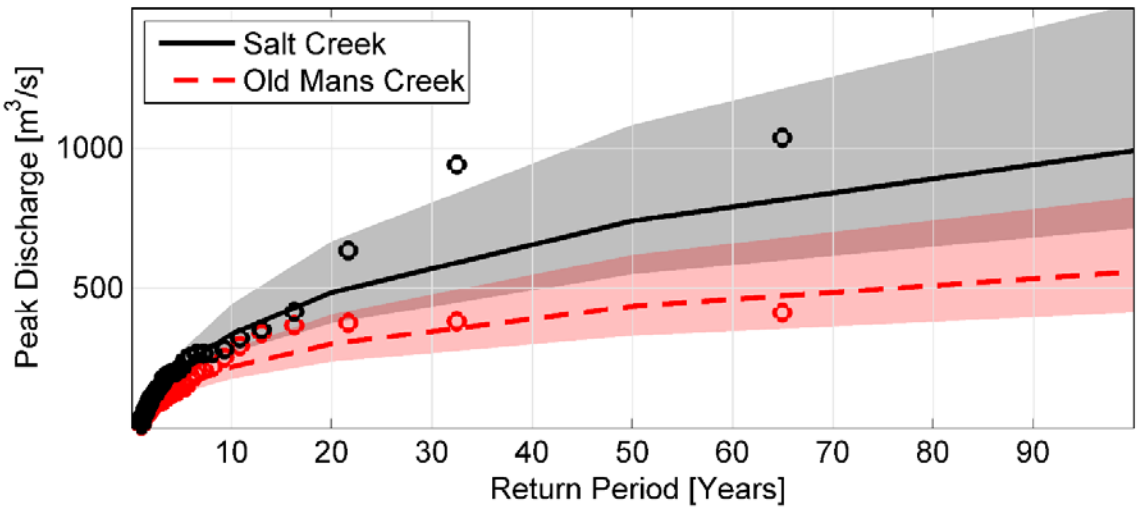

Figure VII - 3. Comparison of the at site flood frequency computed at the outlet of the Old Mans Creek and Salt Creek catchments. The shaded region is the confidence interval. The hollow circles are the annual maximum peak discharges used for the analysis. Weibull's plotting position formula is used to calculate the exceedance probabilities.

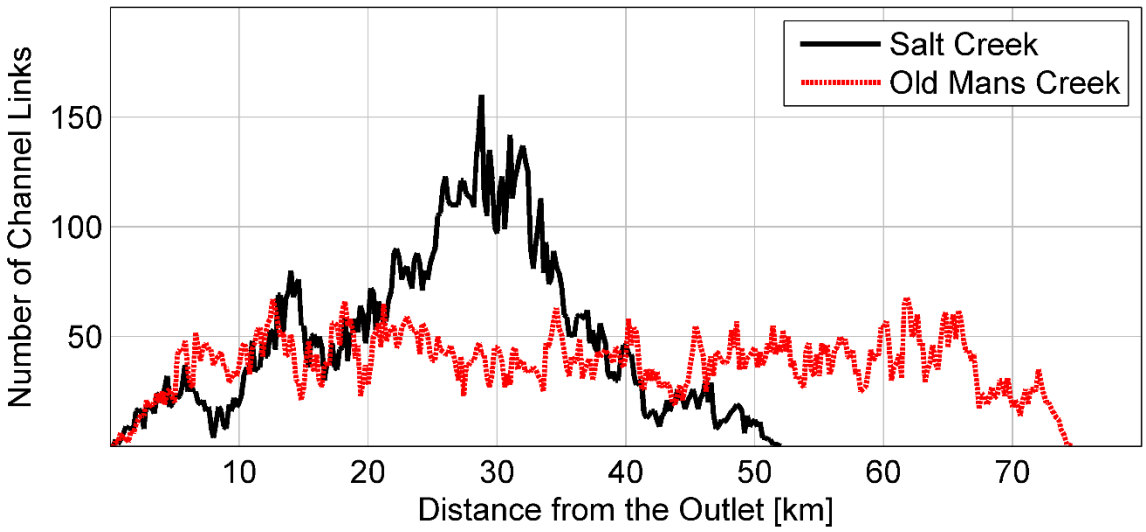

Figure VII - 4. Comparison of the geometric width function estimated at the outlet of the Old Mans Creek and Salt Creek catchments

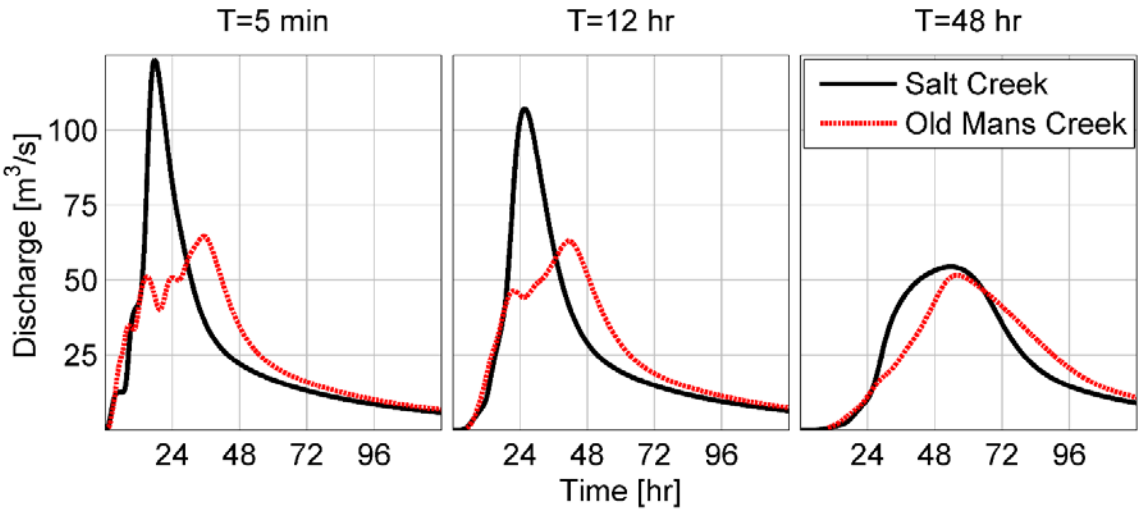

Figure VII - 5. Comparison of the hydrographs at the outlet of the two catchments that are simulated using a fixed rainfall depth of 25 mm that is applied over a range of durations.

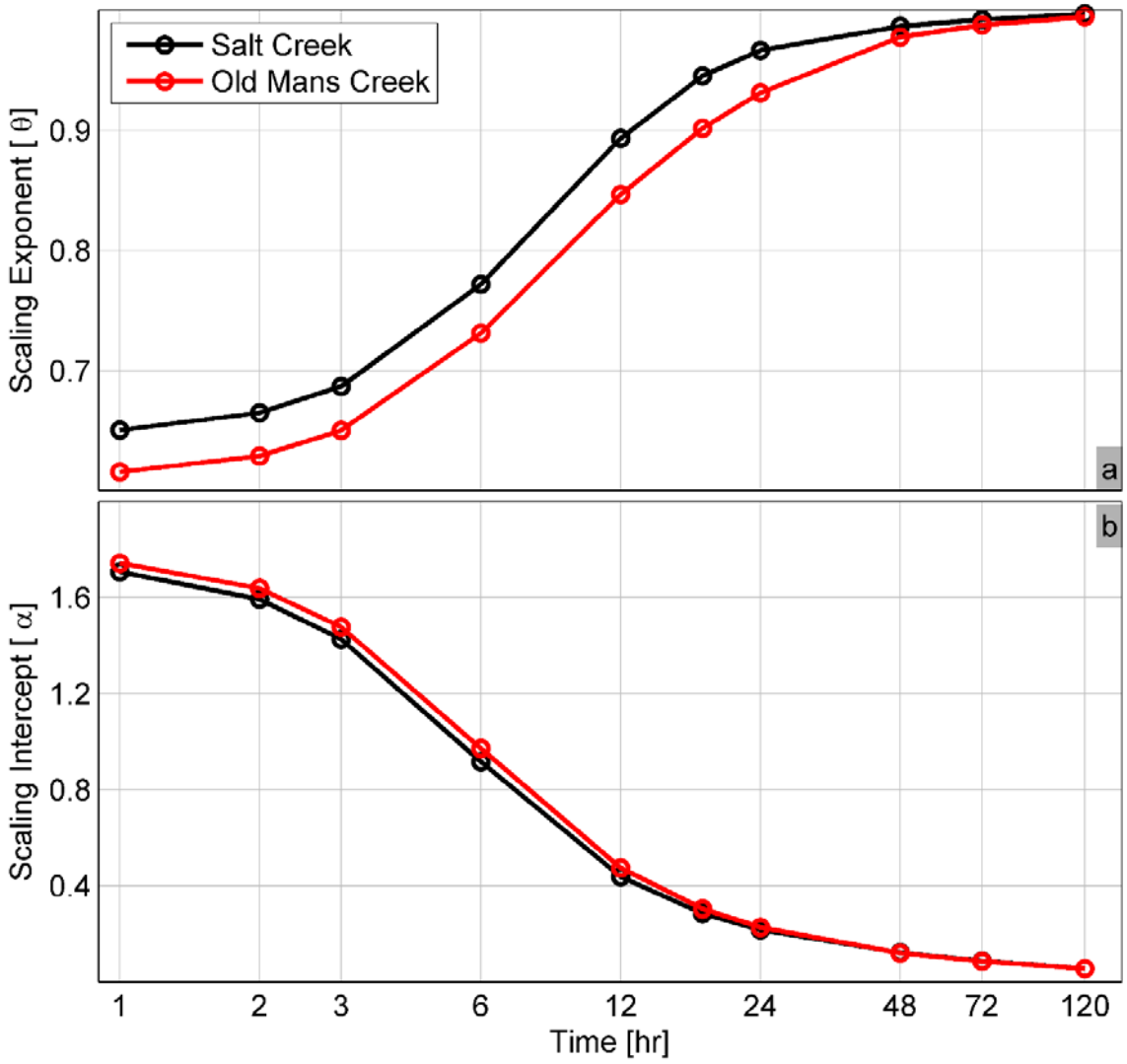

Figure VII - 6. Comparison of the flood scaling exponent and intercept estimated for the two catchments using a fixed rainfall depth of 25 mm that is applied over a range of durations.

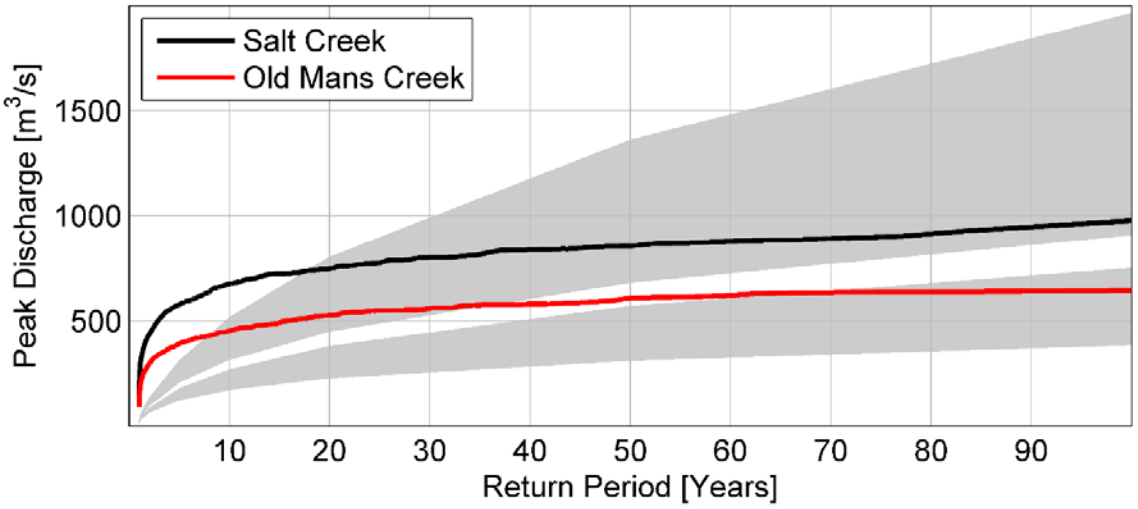

Figure VII - 7. Comparison of simulated flood frequencies computed at the outlet of Old Mans Creek and Salt Creek catchments.

CHAPTER VIII

CONNECTING EVENT AND QUANTILE SCALING OF PEAK FLOODS: IMPLICATIONS TO REGIONAL FLOOD FREQUENCY ESTIMATIONS

8.1. Introduction

I showed in previous chapters how the interplay among rainfall intensity, duration, antecedent soil moisture state, hillslope overland flow velocity, channel flow velocity, and drainage network geometry affect the spatial scaling structure of peak discharges. In Chapter-VII, I showed how the effect of the drainage network geometry on the peak discharge at the rainfall-runoff event scale propagates to the annual time scale affecting flood frequencies. A remaining question is to test if, for a given catchment, the effect of rainfall intensity and duration at the rainfall-runoff event scale can describe the spatial scaling structure of peak discharges of a given quantile at the annual time scale and hence flood frequencies. I address this issue in this chapter.

In Chapter-III, I showed that the scaling structure of peak discharges at the rainfall-runoff event scale can be connected to the scaling of peak-discharge quantiles provided that peak discharges are selected in such a way that they come from the same basin wide rainfall-runoff event. However, our attempt to fully understand the connection between single event peak discharge scaling and peak discharge quantile scaling is limited by the lack of sufficient empirical data. To circumvent this problem, I used the hydrologic model presented in Chapter-IV as a diagnostic tool. The reminder of the chapter is organized as follows. I begin by discussing the study area. This is followed by the model setup used to systematically address the question I posed earlier and an in depth

discussion of the simulation results. I conclude the chapter by summarizing the main findings.

8.2. Study area

I use the 21 km^2 Goodwin Creek Experimental Watershed (GCEW) as a test catchment. The catchment, which is heavily instrumented to a level not seen elsewhere in the world, is located near Batesville, Mississippi. The catchment is continuously monitored by 31 rain gauges and 14 stream gauges. Ogden and Dawdy (2003) analyzed 279 rainfall-runoff events and showed for the first time the existence of a scale invariant spatial organization of peak flows at the rainfall-runoff event scale. Furey and Gupta (2005) later on investigated 148 rainfall-runoff events from the same catchment and showed how the event to event variability of the scaling exponent and intercept is controlled by the event to event variability of excess rainfall duration and depth. There is an ongoing effort to empirically connect peak discharge event scaling to quantile scaling using data from the GCEW (Furey et al. submitted). I selected the same study site to complement this ongoing effort.

8.3. Model setup

I simulated a spatially variable runoff response by introducing a spatially variable runoff coefficient (C_r) that was sampled from a uniform distribution $C_r \sim U[0,1]$. This will allow for a spatially variable runoff response. As a result, when this experiment is conducted within a Monte Carlo simulation framework, peak discharges that have the same probability of exceedance can come from different realizations (events). In this Monte Carlo simulation experiment, rainfall is kept spatially uniform and temporally

constant over its duration. This is a reasonable assumption given the basin's small size. Two cases of channel velocities were then considered: constant (linear) and nonlinear. The channel velocity is constant both in space and time for the constant channel velocity case whereas it is a nonlinear function of upstream area and channel storage for the nonlinear channel velocity case which results in a channel flow velocity that is variable both in space and time. The later case has its root in hydraulic geometry (Leopold et al. 1964; Mantilla 2007). Furthermore, two cases of hillslope velocities were considered: constant (linear) and nonlinear. A spatially uniform and temporally constant hillslope overland flow velocity was used in the first case. In the second case, a spatially uniform but temporally variable hillslope overland flow velocity was used by dynamically calculating the velocity using the Manning's equation. These different channel and hillslope overland flow velocity cases are important to show how different channel and hillslope overland flow velocity setups could lead to different results as the rainfall intensity and duration changes.

8.4. Results

Before I embark on discussing the relationship between single peak discharge event scaling and quantile scaling, it is imperative to discuss how the spatial variability of the runoff coefficient introduced at the hillslope scale affects the runoff response at different spatial scales in the basin. The results presented in FigureVIII-1 show that the spatially variable C_r introduced at the hillslope scale led to a significant variability of the runoff response in small-scale sub-basins (FigureVIII-1, top row). However, the variability of the runoff response decreases with increasing spatial scale and appear to converge to the mean runoff response at the GCEW outlet (FigureVIII-1, bottom row). The same result

is reported in Chapter V where the combined effect of spatially variable rainfall, C_r, and v_h on the runoff response is shown to decrease with increasing spatial scale. The results reported in Chapter V further show that, as the drainage area gets larger, the runoff response converges to the mean hydrograph that is obtained by using a spatially uniform mean rainfall intensity, C_r, and v_h values as input.

8.4.1. Peak discharge event scaling: effect of rainfall intensity

Quantile-based analyses of peak discharge scaling have shown that the scaling exponent (θ) decreases with decreasing probability of occurrence in some regions of the continental US and it increases with decreasing probability of occurrence in other regions of the US (Gupta and Dawdy 1995). However, to the best of my knowledge, there is no study that looked into how the scaling statistics changes with probability of occurrence of peak discharges at the rainfall-runoff event scale. How θ changes with changing probability of occurrence of peak discharge events can be studied by simulating different rainfall intensity values and assuming that higher rainfall intensity is associated with less frequent peak discharge events. To this end, I simulated several combinations of rainfall intensity and duration and the results are presented in FigureVIII-2.

The results presented in FigureVIII-2 show that θ is independent of the rainfall intensity when both v_c and v_h are constant (FigureVIII-2, left column). FigureVIII-2 (middle column) shows that, when the hillslope is linear and channel flow velocity is nonlinear, θ increases with increasing rainfall intensity before converging to some limiting value that is largely determined by the rainfall duration. The observed increase in θ with increasing rainfall intensity is due to the fact that v_c increases as a function of

rainfall intensity. An increase in v_c means that more subcatchments achieve saturation for a given rainfall duration. FigureVIII-2 (right column) shows that θ decreases with increasing rainfall intensity for shorter rainfall durations whereas it increases with increasing rainfall intensity for longer rainfall durations. This result is a manifestation of the increasing v_h with increasing rainfall intensity. The results also show that the intercept is a linear function of rainfall intensity except when the hillslope is nonlinear. All these results are reported in greater detail in Chapters IV and V

We can conclude from the above results that θ is independent of the probability of occurrence of peak discharges when the runoff generation and transport mechanism is linear. When the runoff generation mechanism is linear and transport in channels is nonlinear, θ increases with decreasing probability of occurrence of peak discharges. Note that the rainfall intensity is used as a proxy for probability of exceedance of peak flows. Furthermore, for the more realistic case of nonlinear runoff generation and transport mechanism, results show that θ decreases with decreasing probability of exceedance at shorter rainfall durations whereas it increases with decreasing probability of occurrence at longer rainfall durations. The results also show that α increases with decreasing probability of exceedance irrespective of the type of runoff generation and transport mechanism. These results provide a first order understanding into how the scaling statistics change with changing probability of occurrence of peak discharge events.

8.4.2. Peak discharge quantile scaling: effects of rainfall intensity

I simulated 100 realizations of spatially variable C_r that are sampled from $C_r \sim U[0,1]$ for different combinations of rainfall duration and intensity. For each realization, peak discharge data was obtained from different locations that represent a range of spatial scales in the basin. The probability of exceedance of each of the resulting peak discharges is then calculated using the Weibull plotting position formula. This means that peak discharges that represent different spatial scales in the basin and have the same exceedance probability can come from different realizations (rainfall-runoff events).

FigureVIII-3 shows the result for which the rainfall depth varies between 1 and 55 mm over a fixed duration of 1-minute. The results show that, for a given class of rainfall duration and intensity, θ decreases with decreasing probability of exceedance whereas α increases with decreasing probability of exceedance. The results discussed in section 8.4.1 are clearly at play in determining the scaling structure of peak discharge quantiles. FigureVIII-3 (left column) shows that θ is independent of rainfall intensity when both v_c and v_h are constant. However, for each non-exceedance probability, θ increases with increasing rainfall intensity when v_c is nonlinear and v_h is constant (FigureVIII-3, middle column) whereas it decreases with increasing rainfall intensity when both v_c and v_h are nonlinear (FigureVIII-, right column). This later result would change when the rainfall duration is greater than or equal to 120-min. For example, FigureVIII-4 (right column) shows that θ increases with increasing rainfall intensity when the rainfall duration gets

longer which in this case is 360-min. Note here that the same result was obtained from analysis of peak discharge events (FigureVIII-1, right column).

8.4.3. Peak discharge quantile scaling: effects of rainfall duration

Few empirical studies (Furey and Gupta 2005; Furey and Gupta 2007) and several theoretical studies of an event scale peak discharge scaling analysis (e.g., Gupta and Waymire 1998; Menabde and Sivapalan 2001) including the results reported in Chapters IV, V, And VI have shown that θ increases with increasing rainfall duration. In this section, we look into how peak discharge quantile scaling statistics change with rainfall duration. To this end, I simulated 100 realizations of C_r for a range of rainfall durations that have a fixed volume of 5-mm. The results shown in FigureVIII-5 show that, for a given rainfall duration, θ decreases with decreasing probability of exceedance whereas α increases with decreasing probability of exceedance. The results also show that, for a given probability of exceedance, θ increases with increasing rainfall duration whereas α decreases with increasing rainfall duration. I have shown in Chapter IV that this later result is a direct consequence of the decreasing rainfall intensity, which is a result of the fixed rainfall volume that is applied over a range of durations.

8.4.4. Connecting single event peak discharge scaling to quantile scaling

The results I presented so far indicate that rainfall intensity and duration affect the scaling statistics of peak discharge quantiles in the same way they affect the scaling statistics of peak discharges at the rainfall-runoff event scale. This means that there is indeed a physical connection between quantile scaling and single event scaling of peak discharges provided that the peak discharges are selected on a rainfall-runoff event basis. In other words, peak discharges observed at all locations in the basin following a basin

wide runoff generating event make it to the sample used to calculate peak discharge quantiles. I have called such quantiles as Type-I quantiles in Chapter-III. In this case, since multiple basin wide runoff generating rainfall event can occur in any given year, the approach leads to the selection of multiple peak discharges at each gauging site per year. This approach can be compared to the peak over threshold approach of flood frequency analysis, with the threshold in this case being the occurrence of a basin wide runoff-generating rainfall event over the time window that is equivalent to the basin's concentration time. In such a way, we can make sure that the peak discharges that are observed at all gauging sites are driven by rainfall and catchment physical properties that have similar characteristics.

In order to show the physical connection between quantile scaling and single event scaling of peak discharges, I started by assuming that each realization of C_r represents a single rainfall-runoff event. A probability of exceedance was then assigned to each event based on the plotting position of the peak discharge obtained at the outlet. The grey circles in FigureVIII-6 show the scaling statistics for individual realizations of rainfall-runoff events that are driven by rainfall that has 1-min duration and 5-mm depth. The dark black circles are peak discharge quantile scaling statistics calculated using the same set of results as above but a probability of exceedance was assigned to individual peak discharge values obtained from individual locations of different spatial scales in the basin. Peak discharge values that have the same exceedance probability were then used to calculate the peak discharge quantile scaling statistics. The results show that single event peak discharge scaling statistics are bounded by the scaling statistics of peak discharge quantiles. More specifically, the expected value of single event peak discharge

scaling statistics is equal to the 50^{th} percentile of the peak discharge quantile scaling statistics. Similar results were obtained for different combinations of rainfall intensity and duration.

The connection between single event scaling and quantile scaling exists only when they belong to the same class of rainfall intensity, duration, and other catchment physical characteristics that determine the magnitude of the runoff response at the event scale. In order to demonstrate this, I simulated 100 realizations of C_r for each class of rainfall depth (1, 5, 10, 15, 20, 25, 30, 35, 40, 45, 50, and 55 mm) and duration (1, 5, 10, 15, 30, 60, 120, 180, 360, and 720 minutes) combination. This has resulted in 1200 rainfall-runoff events that are simulated using the nonlinear hillslope overland flow and channel flow routing equations. Finally, I mixed all these simulations into a single group and calculated both event and quantile scaling statistics. For both cases, probability of exceedance was calculated based on the peak discharge obtained at the basin outlet. The results presented in FigureVIII-7 show that it is difficult to predict single event scaling statistics from quantile scaling statistics and vice versa. Based on this, we can say that the scaling statistics of peak discharge quantiles reported by the USGS in their regional flood frequency studies lack physical meaning since they combine different classes of rainfall and catchment physical properties that are responsible for driving the streamflow response at the event scale.

8.5. Conclusions

Using the Goodwin Creek Experimental Watershed (GCEW) as a study catchment, I conducted a Monte Carlo simulation experiment where I simulated 100

realizations of runoff coefficient that is randomly variable in space. For each set of 100 realizations, I used rainfall that has a unique intensity and duration. In this setup, each realization produces a spatially variable streamflow response and can be considered as representing a single basin wide rainfall-runoff event. The experiment is repeated using various combinations of rainfall intensity and duration. Using the simulated peak discharges at 14 streamflow gauging sites that are extracted for each realization, the following analysis was undertaken. First, for each realization that is forced by a unique combination of rainfall intensity and duration, I calculated the flood scaling exponent and intercept. I assigned a probability of exceedance for each rainfall-runoff event based on the simulated peak discharge at the catchment outlet. Second, I ranked the streamflow response simulated at each streamflow gauging site and calculated the peak discharge quantiles. I previously called these quantiles, which are selected based on the occurrence of a basin wide single rainfall-runoff event, as *Type-I quantiles*. In this step I also calculated the flood scaling exponent and intercept corresponding to peak discharges that have the same exceedance probability. Finally, I compared the scaling exponents and intercepts calculated for individual rainfall-runoff events (realizations) with the corresponding scaling parameters calculated for *Type-I quantiles*. The results show that the expected values of the flood scaling exponent and intercept of single rainfall-runoff events are equivalent to the expected values of the flood scaling exponent and intercept calculated using Type-I peak discharge quantiles. This indicates that there is indeed a connection between event scaling and quantile scaling provided that peak discharges used for quantile based analysis are selected from nested watersheds on a rainfall-runoff event basis than selecting only one peak discharge event per year per streamflow gauging site.

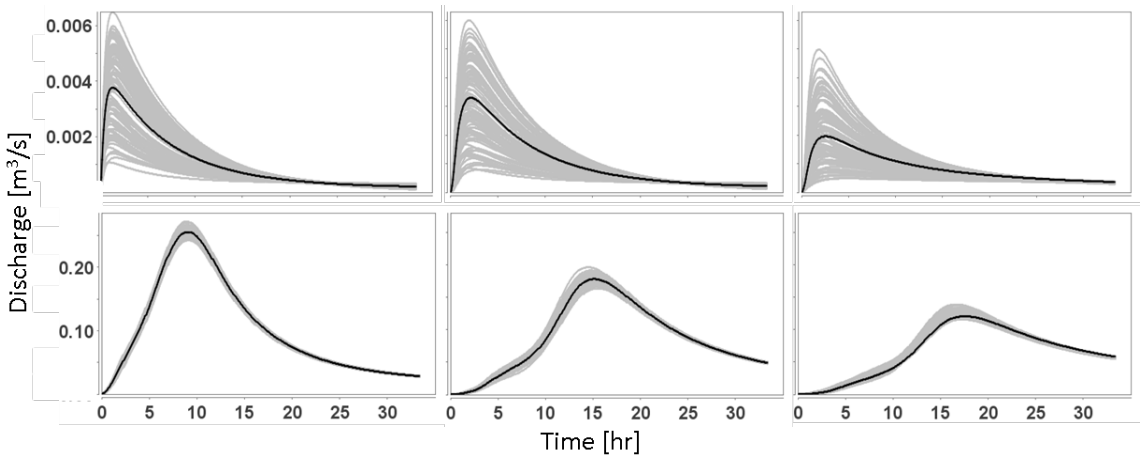

Figure VIII - 1. The runoff response at two different spatial scales in the basin (0.18 km^2 (top row) and 21.39 km^2 (bottom row)) and three different cases of channel and hillslope overland flow velocity combinations (constant v_c and v_h (left column); nonlinear v_c and constant v_h (middle column); and nonlinear v_c and v_h (right column)). The grey lines show the runoff response for each of the 100 realizations of runoff coefficient we simulated. The dark black line is for the case where a spatially uniform mean runoff coefficient value of 0.5 was used.

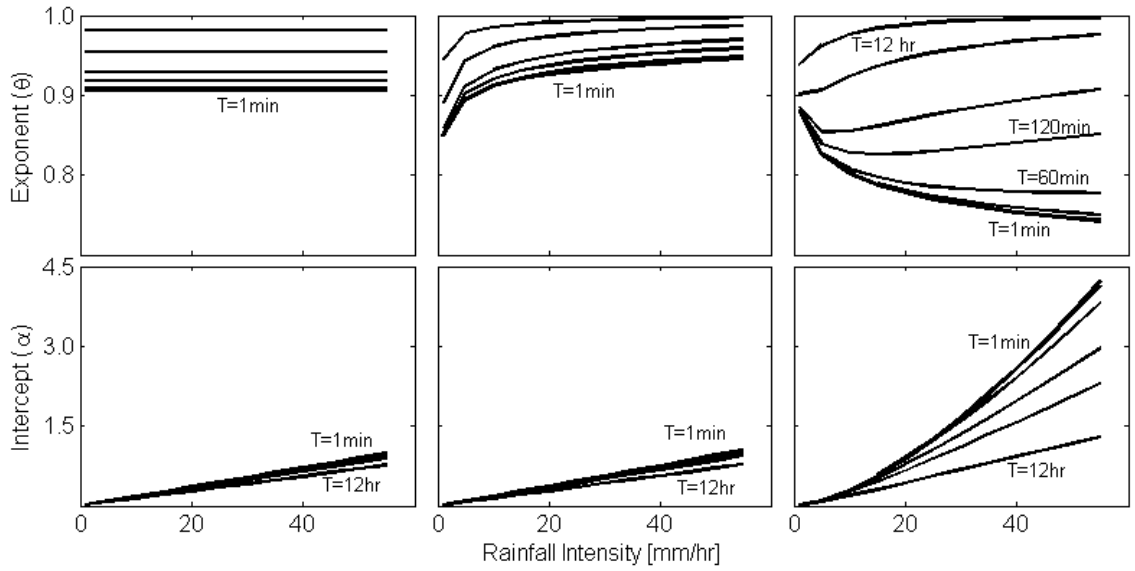

Figure VIII - 2. Effect of rainfall intensity on the power-law scaling structure of peak discharge events. The results shown here are for the cases of constant v_c and v_h (left column); nonlinear v_c and constant v_h (middle column); and nonlinear v_c and v_h (right column).

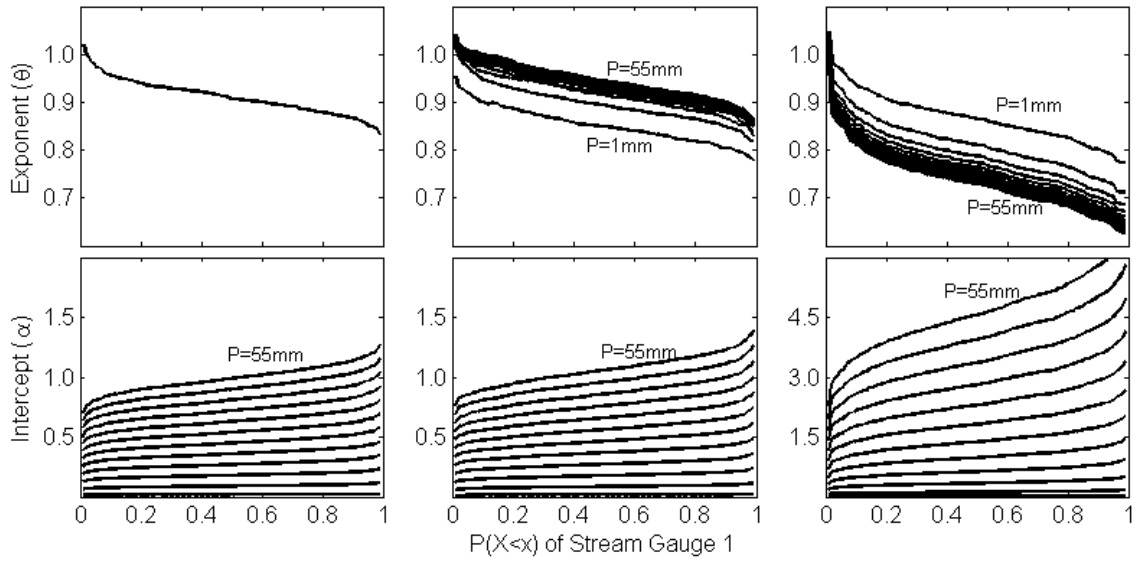

Figure VIII - 3. Peak discharge quantile scaling statistics for rainfall duration of 1-min and rainfall depths of 1, 5,10,15,20,25,30,35,40,45,50, and 55 mm. 100 realizations of C_r were simulated for each rainfall depth group. The results shown here are for the cases of constant v_c and v_h (left column); nonlinear v_c and constant v_h (middle column); and nonlinear v_c and v_h (right column).

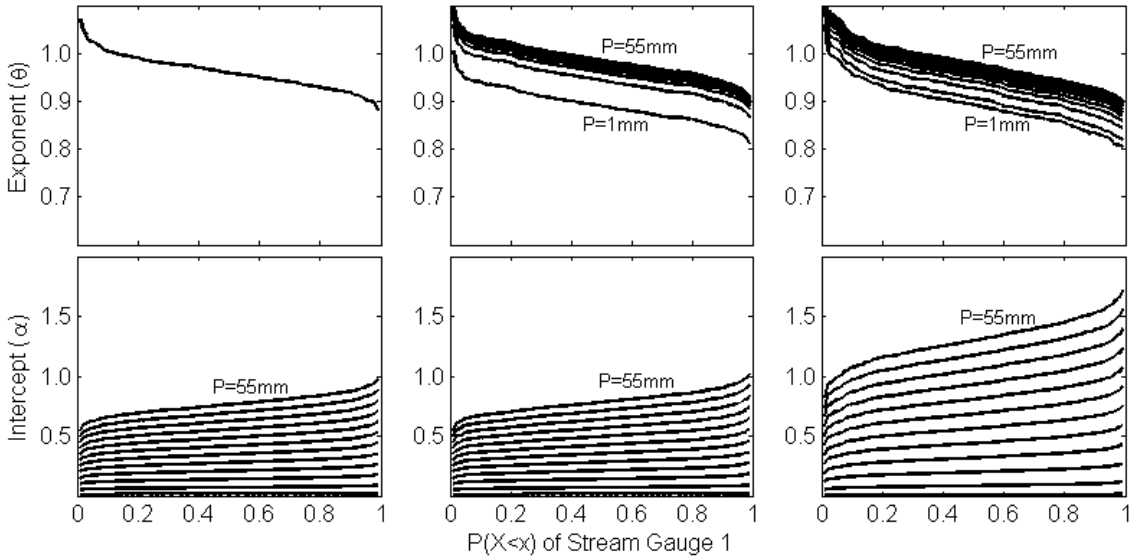

Figure VIII - 4. Peak discharge quantile scaling statistics for rainfall duration of 360-min and rainfall depths of 1, 5,10,15,20,25,30,35,40,45,50, and 55 mm. 100 realizations of C_r were simulated for each rainfall depth group. The results shown here are for the cases of constant v_c and v_h (left column); nonlinear v_c and constant v_h (middle column); and nonlinear v_c and v_h (right column).

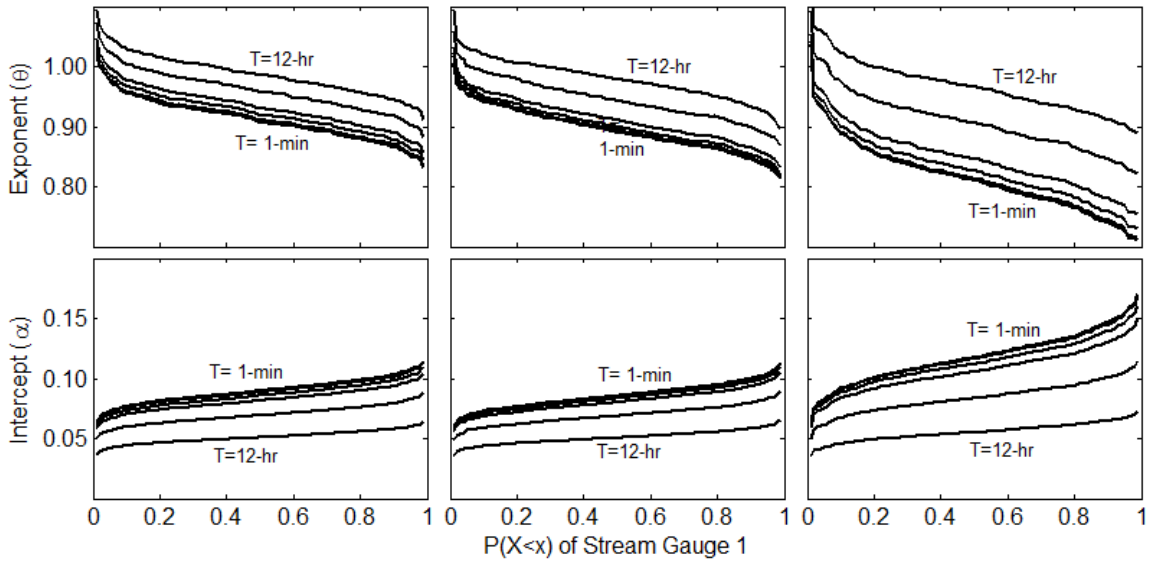

Figure VIII - 5. Peak discharge quantile scaling statistics for constant rainfall depth of 5-mm that occur over durations of 1,5,10,15,30,60,120,180,360, and 720 minutes. 100 realizations of C_r were simulated per each rainfall duration. The results shown here are for the cases of constant v_c and v_h (left column); nonlinear v_c and constant v_h (middle column); and nonlinear v_c and v_h (right column).

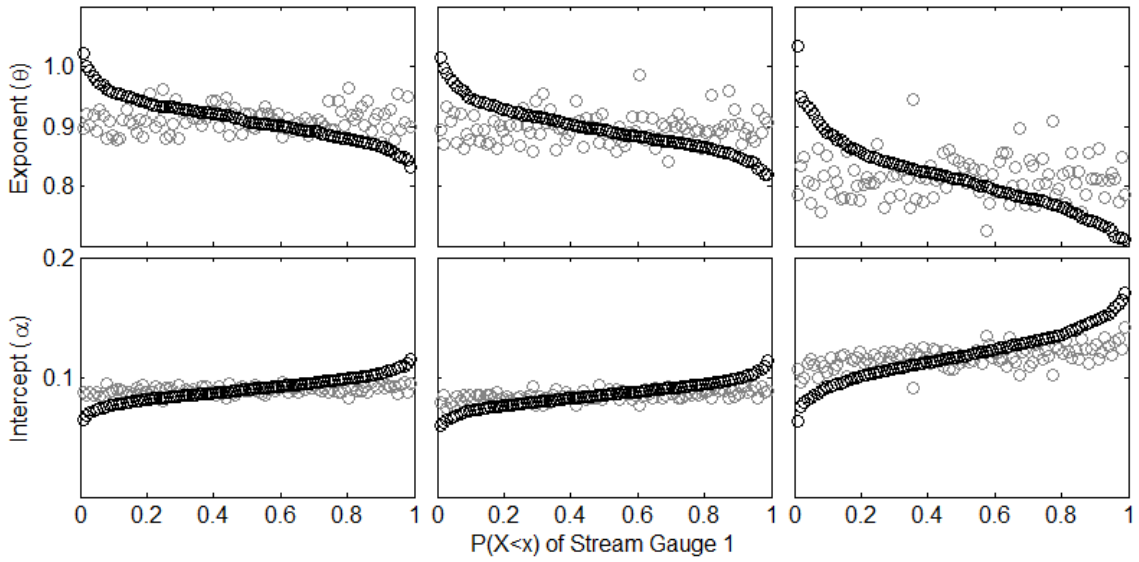

Figure VIII - 6. Peak discharge quantile scaling statistics (dark circles) and peak discharge event scaling statistics (grey circles) for rainfall duration of 1-min and rainfall depths of 5 mm. 100 realizations of C_r were simulated. The results shown here are for the cases of constant v_c and v_h (left column); nonlinear v_c and constant v_h (middle column); and nonlinear v_c and v_h (right column).

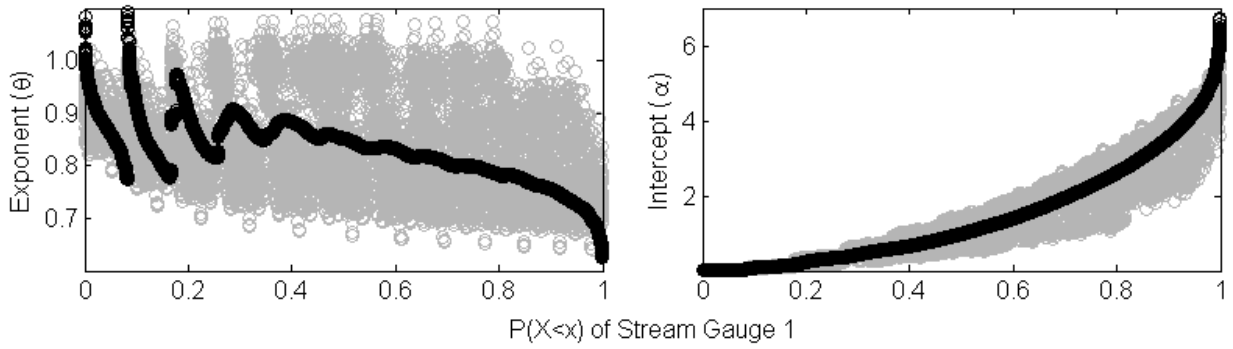

Figure VIII - 7. Peak discharge quantile scaling statistics (dark circles) and peak discharge event scaling statistics (grey circles) for rainfall depths of 1, 5, 10, 15, 20, 25, 30, 35, 40, 45, 50, and 55 mm that are each applied over durations of 1, 5, 10, 15, 30, 60, 120, 180, 360, and 720 minutes. 100 realizations of C_r were simulated for all rainfall depth and duration combinations.

CHAPTER IX

CAN FLOODS IN LARGE RIVER BASINS BE PREDICTED FROM FLOODS OBSERVED AT SMALL SUBBASINS?

9.1. Introduction

Foundational analyses of peak discharge data from rainfall-runoff events from *nested* watersheds have been driving the development of a *nonlinear geophysical theory of floods* over the past couple of decades (Dawdy et al. 2012; Gupta 2004; Gupta et al. 1996; Gupta et al. 2010; Gupta et al. 2007; Gupta and Waymire 1998; Ogden and Dawdy 2003). The main hypothesis of the theory is that, provided that the entire basin receives a runoff generating rainfall event, the solution of the coupled mass and momentum conservation equations over the self-similar drainage network leads to a scale invariant spatial organization of peak discharges that is described by a power law relation as,

$$E[Q_e \mid A] = \alpha(e) A^{\theta(e)} \qquad \text{Equation IX-1}$$

where Q_e is peak discharge [m^3/s] for a given rainfall-runoff event *'e'*, A is upstream drainage area [km^2], $\alpha(e)$ is the scaling intercept [m^3/s], $\theta(e)$ is the scaling exponent. This hypothesis is validated through the results presented in Chapters III and VI as well as a host of other empirically based studies (Furey and Gupta 2005; Gupta et al. 2010; Ogden and Dawdy 2003) and numerical rainfall-runoff simulations in synthetic and natural river basins (Furey and Gupta 2007; Gupta et al. 1996; Gupta et al. 2007; Gupta and Waymire 1998; Mandapaka et al. 2009; Mantilla et al. 2006; Mantilla et al. 2011; Menabde and Sivapalan 2001; Menabde et al. 2001).

Recent studies have been geared towards describing the event to event variability of the scaling intercept $\alpha(e)$ and scaling exponent $\theta(e)$ in terms of rainfall and catchment

physical properties that govern the generation of streamflow in space and time, contributing towards the long standing hydrologic problem of *predictions in ungauged basins* (PUB) (Hrachowitz et al. 2013; Sivapalan et al. 2003). The importance of the problem ranges from addressing the effect of climate change on flood frequency to predicting floods in ungauged basins, which is typical of developing regions of the world. Provided that the physical connection between the flood scaling parameters (i.e., α and θ) and rainfall and catchment physical properties is established, the *nonlinear geophysical theory of floods* can be used to predict peak floods using rainfall and catchment physical properties that can be measured either directly or indirectly. To this end, few studies have been undertaken to investigate how the interplay among the network geometry, excess rainfall duration, depth, antecedent soil moisture, hillslope overland flow velocity, and channel flow velocity control the flood scaling parameters. Chapters IV to VIII were devoted to contribute to the understanding of these issues.

The review of the literature presented in Chapter II indicates that the efforts have been focused on examining the physical connections that both the scaling exponent and intercept have with rainfall and catchment physical properties. In particular, much attention has been given to the scaling exponent in comparison to the scaling intercept (Gupta et al. 1996; Gupta and Waymire 1998; Mandapaka et al. 2009; Mantilla et al. 2006; Menabde and Sivapalan 2001; Menabde et al. 2001). The study presented in this chapter is inspired by a recent discovery by Gleason and Smith (2014), who proposed a framework that can be used for accurate estimation of river discharge from measurements of the flow width that is obtained from satellite images. At the core of their proposed methodology is the largely ignored empirical relationship between the intercepts and

exponents of the hydraulic geometry power law equations first proposed in the seminal work of Leopold and Maddock (1953). Specifically, their proposed streamflow measurement framework uses the observed at-many-stations relationship between the intercept *a* and exponent *b* in the power law hydraulic geometry relation $w = aQ^b$, where *w* is the river's flow width and *Q* is discharge.

Motivated by this breakthrough, I investigated if there exists a physically meaningful relationship between the scaling intercept $\alpha(e)$ and scaling exponent $\theta(e)$ in the power law relation between peak discharges and drainage area shown in Equation IX-1. If a physically meaningful relationship between the scaling intercept and exponent exists, it would suggest that the problem of flood prediction in ungauged basins using this power law relationship between peak discharge and drainage area is simplified to estimating only the scaling intercept from rainfall and catchment physical properties. Interestingly, the intercept appears to be simpler to measure or estimate as it is equivalent to the observed peak discharge at the outlet of subcatchments that have a unit drainage area, i.e., 1 km^2 when metric units are used (Furey and Gupta 2005).

The chapter is organized as follows. In section 9.2 I discuss the results from the data analysis conducted to test if there is a physically meaningful relationship between the scaling exponent and intercept. In section 9.3 I provide further evidence for the results reported in section 9.2 using peak discharge data obtained from observations and numerical simulations of the study basin. In section 9.4 I present a methodology for predicting the scaling intercept from small-scale peak discharge observations in the basin. Finally, in section 9.5 I demonstrate how the relationship between the scaling exponent and intercept can be used to predict peak discharges across a range of spatial scales in the

basin. I close the chapter with summary of the main findings and concluding remarks in section 9.6.

9.2. Relationship between the scaling intercept and exponent

I use the 52 rainfall-runoff events that occurred in the Iowa River basin between 2002 and 2013, which I identified and reported in detail in Chapter-III. Figure IX-1 shows the scaling plot of peak discharges resulting from each of these rainfall-runoff events. I used the 52 pairs of scaling intercepts and scaling exponents shown in Figure IX-1 to test if a statistically significant relationship exists between the two. To this end, I regressed the scaling exponent on the natural logarithm of the scaling intercept. The results presented in Figure IX-2 show that there is a strong log-linear relationship between the scaling exponent and the scaling intercept. The resulting linear regression model is summarized by the following equation

$$\theta = 0.655 - 0.0845 \ln(\alpha) \qquad \text{Equation IX-2}$$

A Student's t-test on the coefficients of equation (2) indicate that they are statistically significant at the 99% confidence interval. Examination of the Q-Q plot of the residuals and the Shapiro-Wilk test for normality, W=0.99 and p=0.93, show that the residuals are normally distributed. Also, the Breusch-Pagan test for homoscedasticity, BP=0.03 and p=0.87, indicate that the residuals have constant variance. These results confirm the robustness of the statistical inference of the scaling exponent from the natural logarithm of the scaling intercept.

The log-linear relationship between the scaling exponent and scaling intercept shown in Figure IX-2 is an important finding because it essentially reduces the problem of flood

prediction in ungauged basins to a one-parameter estimation problem, i.e., the scaling intercept from rainfall and catchment physical properties. This is of course based on the assumption that the log-linear relationship between the scaling exponent is already parametrized using either some physical reasoning or following the same procedure that I followed to arrive at Equation IX-2 using hisorical peak discharge observations.

An additional interesting insight is that, in the flood scaling relationship shown in Equation IX-1, the scaling intercept $\alpha(e)$ is equivalent to the expected value of peak discharges observed at subcatchments that have a drainage are of 1 km^2 (Furey and Gupta 2005). This can be easily shown by setting the value of the drainage area in Equation IX-1 to unity. Because of this, the scaling intercept appears to be simpler to estimate than the scaling exponent. I postulate that, if the observed log-linear relationship is physically meaningful, we can use this relationship to predict floods across a range of spatial scales in the basin by only estimating the scaling intercept from rainfall and catchment physical properties that control the magnitude of peak dicharges in small scale subcatchments.

9.3. Physical basis of the relationship between the scaling exponent and intercept

Figure IX-2 shows that the scaling exponent decreases as the scaling intercept increases. Why? Is this observation physically meaningful? Or is it simply the consequence of the OLS regression procedure used to estimate $\alpha(e)$ and $\theta(e)$ in our attempt to describe the spatial scaling properties of observed peak discharges in terms of the upstream drainage area? I address these questions in the following sections using evidence in empirical data and results from the numerical simulation of hypothetical rainfall-runoff events in the Iowa River basin.

9.3.1. Evidence based on empirical data

Let us begin with inspecting observational peak discharge data from the Iowa River basin. Figure IX-3 shows the combined scatter plot of all of the peak discharges resulting from the 52 rainfall-runoff events shown in Figure IX-1. The grey lines in Figure IX-3 depict the power law regression line fitted to each rainfall-runoff events. The dark solid regression lines, which are fitted to the corresponding peak discharges shown in blue and light blue colors, depict rainfall-runoff events that resulted in the smallest and highest peak discharge values observed at the smallest gauged subcatchment in the basin. Visual examination of Figure IX-3 reveals that the variance of observed peak discharges at each stream gauge site decrease with increasing catchment spatial scale. Although not shown here for the sake of brevity, my calculation of the coefficient of variation (CV) of observed peak discharges at each stream gauge sites indicates that it decreases with drainage area. This property is also reported to exist in annul maximum peak discharges, whose CV exhibit a tendency to decrease with drainage area (Bloschl and Sivapalan 1997; Smith 1992).

The consequence of the decreasing CV with drainage area of peak discharges shown in Figure IX-3 is that an increase in the peak discharge at smaller scale subcatchments do not necessarily lead to an equivalent increase in the peak discharges observed at larger catchment scales. In other words, the rate at which peak discharges increase with drainage area decreases as the streamflow response at smaller catchment scales increases. This implies that the rate at which peak discharges increase with excess rain decreases with drainage area.

In Chapter-VI, I analyzed the same dataset and showed that the excess rainfall depth has a statistically significant positive relationship with the scaling intercept and negative relationship with the scaling exponent. In Chapter-V, I showed that an increase in the hillslope overland flow velocity, which itself has a positive relationship with excess rainfall depth, leads to a higher rate of increase of peak discharges at smaller catchment scales than at larger catchment scales leading to a decrease in the scaling exponent. These results suggest that the effect of hillslope overland flow velocity, which is a function of the excess rainfall depth for a given catchment topography, land use and land cover, on peak discharge decreases with increasing drainage area. Note also that the streamflow response is affected more and more by attenuation as the flood wave moves downstream. As a direct consequence of these physical phenomena, the scaling intercept increases with excess rainfall depth whereas the scaling exponent decreases with excess rainfall depth. Similarly, Robinson et al. (1995) also showed that the hillslope overland flow velocity dominates the streamflow response of smaller catchments whereas drainage network geomorphology, along which the fundamental process of flow aggregation, attenuation and translation occurs, dominates the streamflow response at larger catchment scales. These results show that the decreasing relationship between the scaling exponent and intercept is explained by rainfall and catchment physical processes that govern the generation of streamflow in space and time.

9.3.2. Evidence from numerical simulations

To further demonstrate how rainfall and catchment physical properties control the relationship between the scaling exponent and intercept, I undertook a numerical simulation experiment in the Iowa River basin using the hydrologic model that is based

on the decomposition of the landscape to hillslopes and channel-links as discussed in Mantilla and Gupta (2005), which I described in Chapter-IV. I setup a systematic simulation experiment where I altered the model configuration by using different formulations of hillslope overland flow and channel flow velocities. These simulations are designed with the objective of testing if different approximations of hillslope overland flow and channel flow velocities could lead to different relationships between the scaling exponent and scaling intercept. If different model formulations lead to different results that are either similar or dissimilar to the result shown in Figure IX-2, it will then mean that the log-linear relationship between the scaling exponent and scaling intercept is controlled by the physics behind the generation of streamflow in space and time.

The results presented in Figure IX-4 show that different model configurations of hillslope and channel flow velocity values result in a different relationship between the scaling exponent and scaling intercept. Specifically, when constant hillslope and channel flow velocities are used (Figure IX-4a), the scaling exponent is independent of the scaling intercept. This is because, the increasing excess rainfall depth has no effect on the hillslope and channel velocity values, which are set to always be constant. This is similar to the Unit Hydrograph theory (Sherman 1932), which postulates that the streamflow response as depicted by the hydrograph is a linear function of the excess rainfall depth for a given excess rainfall duration. Additional results show that when the constant hillslope velocity and a nonlinear channel flow velocity formulation is used (Figure IX-4b), the scaling exponent increases with scaling intercept as the excess rainfall depth increases. This is because of the nonlinear channel flow velocity formulation (see Equation IV-11) which allows for the increase in channel flow velocity as a function of drainage area and

discharge. The results shown in Figure IX-4a and b are contrary to the findings from empirical data analysis shown in Figure IX-2.

Results from the simulation of the Iowa River basin using nonlinear hillslope overland flow (i.e., Manning's equation) and constant channel flow velocity formulations (Figure IX-4c) suggest that the scaling exponent decreases with the scaling intercept as the excess rainfall depth increases. This is because the hillslope overland flow velocity increases with increasing excess rainfall depth and, as a result, peak discharges at smaller catchment scales increase at a much faster rate than peak discharges observed at larger catchment scales. Finally, when nonlinear hillslope overland flow and channel flow velocity formulations are used (Figure IX-4d), which are reasonable approximations of reality, the scaling exponent decreases with the scaling intercept as the excess rainfall depth increases. Together, all these results confirm that the decreasing log-linear relationship between the scaling exponent and intercept shown in Figure IX-2 is a result of rainfall and catchment physical processes that control the streamflow response in space and time, and not a statistical artifact.

9.4. How the scaling intercept can be predicted from observational data

The results presented in Section 9.3 suggest that the log-linear relationship between the scaling exponent and scaling intercept is a product of the physics of runoff generation in space and time. The next step is to explore how the scaling intercept can be predicted from certain observables in the basin. To this end, I propose an avenue that is based on the physical meaning of the scaling intercept, which equates the intercept to the expected value of peak discharges observed at subcatchments that have a unit drainage area (Furey and Gupta 2005). I use this concept to predict the scaling intercept using peak discharges

observed at the smallest available gauged subcatchment in the Iowa River basin whose drainage area is 7 km^2 (USGS ID: 05464942).

Using data from the 52 rainfall-runoff events shown in Figure IX-1, I regressed the natural logarithm of the scaling intercept on the natural logarithm of the peak discharge observed at the 7 km^2 subcatchment in the basin. The results presented in Figure IX-5 show that there is a strong log-log relationship between the scaling intercept and the peak discharge observed at the smallest gauged subcatchment in the basin. The following equation summarizes the resulting linear regression model:

$$\ln(\alpha) = 1.09 \ln(Q_{7km^2}) - 1.21 \qquad \text{Equation IX-3}$$

A Student's t-test on the coefficients of Equation IX-3 indicate that they are statistically significant at the 99% confidence interval. Examination of the Q-Q plot of the residuals and the Shapiro-Wilk test for normality, W=0.96 and p=0.12, show that the residuals are normally distributed. Similarly, the Breusch-Pagan test for homoscedasticity, BP=0.02 and p=0.88, indicate that the residuals have constant variance. These results confirm the robustness of the regression model presented in Equation IX-3 and demonstrates that the scaling intercept can be predicted using the peak discharge observed at the smallest gauged subcatchments in the basin.

9.5. Application of the log-linear relationship between the scaling exponent and intercept to predict peak discharges across scales

I now propose a flood prediction framework that is based on the log-linear relationship between the scaling exponent and intercept. I demonstrate the framework using four example rainfall-runoff events that occurred in the basin over the spring and

summer of 2014. This period includes the flood event of June-July 2014, which is the third largest flood event recorded at the basin's outlet (USGS ID 05465500) over the past 112 years of record. I followed the following procedure to estimate the expected value of peak discharges across different spatial scales in the basin. First, I obtained the observed peak discharge at the 7 km^2 subcatchment (USGS ID 05464942) that corresponds to the particular rainfall-runoff event. Second, I used the regression model presented in Equation IX-3 to estimate the scaling intercept from the observed peak discharge at the 7 km^2 subcatchment. Third, the regression model presented in Equation IX-2 is used to estimate the corresponding scaling exponent from the natural logarithm of the scaling intercept estimated in step two. Finally, the estimated scaling exponent and scaling intercept are used to predict the expected value of peak discharges across a range of spatial scales in the basin using Equation IX-1. The steps presented so far provide the estimate of the expected value of peak discharges across a range of spatial scales for a given rainfall-runoff event in the basin. However, the data presented in Figure IX-1 shows that peak discharges exhibit variability around their expected value that is shown in black line in Figure IX-1. Gupta et al. (submitted) recently introduced a framework that can be used to quantify the variability (uncertainty) of peak discharges around their expectation that is calculated using Equation IX-1. They called the proposed framework the Natural Uncertainty Measure for Peak Discharges (NUMPD). I briefly review the framework here.

The NUMPD framework for quantifying the natural variability of peak discharges is based on two important findings. The first is the finding by Peckham and Gupta

(1999) who showed that drainage area exhibits a *'Generalized Horton Law'* that is written as follows.

$$A_\omega / \overline{A}_\omega = A_\omega / \overline{A}_1 (R_A)^{\omega-1} \overset{d}{=} Z, \qquad \omega = 1,2,... \qquad \text{Equation IX-4}$$

where ω is the Horton-Strahler stream order, A_ω is the drainage area for stream order ω, $\overline{A}_1$ is the expected value of drainage area for order 1 streams, R_A is the area ratio, and Z is a random variable whose expected value $E[Z] = 1$. The symbol $\overset{d}{=}$ denotes equality in probability distributions of random variables. The second finding is due to Gupta et al. (submitted) who showed that peak discharges exhibit a *'Generalized Horton Law'* as follows.

$$\frac{Q_{\omega,e}}{\overline{Q}_{\omega,e}} \overset{d}{=} \frac{Z^{\theta(e)}}{E[Z^{\theta(e)}]} = Y(e), \qquad \omega = 1,2,... \qquad \text{Equation IX-5}$$

where '*e*' denotes a rainfall-runoff event and it is used to index the 52 rainfall-runoff events used in this study, $Q_{\omega,e}$ is the peak discharge observed in a catchment that is drained by an order ω stream, $\theta(e)$ is the scaling exponent, and *Y(e)* is a random variable whose expectation $E[Y(e)] = 1$. To arrive at Equation IX-5, they postulated that $Q_{\omega,e} \overset{d}{=} \alpha(e) A_\omega^{\theta(e)}$ and after substituting Equation IX-4 for A_ω they obtained the following relation.

$$Q_{\omega,e} \overset{d}{=} \alpha(e) A_\omega^{\theta(e)} \overset{d}{=} \alpha(e) (\overline{A}_1)^{\theta(e)} (R_A^{\theta(e)})^{\omega-1} Z^{\theta(e)} \qquad \text{Equation IX-6}$$

Similarly, after combining and manipulating Equations IX-4 and IX-1 that is rewritten as $E[Q_{\omega,e} \mid A_\omega] = \alpha(e) A_\omega^{\theta(e)} = c(e) (\overline{A}_1)^{\theta(e)} (R_A^{\theta(e)})^{\omega-1} Z^{\theta(e)}$ to account for the Horton-Strahler

stream orders, they obtained the expression for the expected value of peak discharge for a stream of order ω that is written as,

$$\overline{Q}_{\omega,e} = E[Q_{\omega,e}] = E\{E[Q_{\omega,e} \mid A_\omega]\} = \alpha(e)E[A_\omega^{\theta(e)}] = \alpha(e)(\overline{A}_1)^{\theta(e)}(R_A^{\theta(e)})^{\omega-1}\mathrm{E}[Z^{\theta(e)}] \quad \text{Equation IX-7}$$

Combining Equations IX-6 and IX-7 yields Equation IX-5. An important finding of Gupta et al. (submitted), which is obtained through the analysis of the empirical distribution of $Y(e)$ obtained from the 52 rainfall-runoff events shown in Figure IX-1, is that the probability distribution of $Y(e)$ is event independent suggesting the statistical simple scaling of Y in the limit of large Horton-Strahler order ω. This discovery sets the foundation for quantifying the natural variability of peak discharges in nested catchments.

Finally, the following procedure is used to establish the natural variability bound (confidence interval) for peak discharge predictions made using Equation IX-1. First, the empirical distribution of Z (see Equation IX-4) is obtained by processing a 30 m digital elevation model (DEM) of the Iowa River basin obtained from the USGS. This is done using CUENCAS (Mantilla and Gupta 2005). The Horton-Strahler stream orders (ω) of the streams along which the USGS stream gauges are located are also determined. It turns out that the stream gauges monitor flows from streams whose ω ranges between 4, at the smallest gauged subcatchments in the basin, and 9, at the outlet. Analysis of the extracted drainage network shows that the values of $\overline{A}_1$ and R_A for the Iowa River basin are 0.045 km^2 and 4.81, respectively. Second, the empirical distribution of Y (Equation IX-5) is determined from the 52 rainfall-runoff events shown in Figure IX-1. Third, $\overline{A}_\omega$ is estimated using the classical Horton law for drainage area $\overline{A}_\omega = \overline{A}_1(R_A)^{\omega-1}$. $\overline{Q}_{\omega,e}$ is also estimated using equation (15) for all stream orders (ω=1,2,3…,9) in the basin. Note

that Equation IX-7 uses as an input the scaling exponent $\theta(e)$ and the scaling intercept $\alpha(e)$ that are predicted using Equations IX-2 and IX-3. Finally, the 95% confidence interval over which peak discharges naturally vary is estimated by combining the results from step three and the empirical probability distributions of the random variables Z and Y obtained in steps one and two, respectively.

The results presented in Figure IX-6 depict comparison of the observed and predicted peak discharges for the four rainfall-runoff events that occurred in the Iowa River basin in the spring and summer of 2014. The grey circles depict the peak discharges observed at the USGS stream gauge stations. The black solid lines represent the power law fitted to the observed peak discharges. The blue line is the expected value of peak discharges estimated using Equations IX-2 and IX-3. The red lines depict the 95% confidence interval over which peak discharges naturally vary and are estimated using the NUMPD framework proposed by Gupta et al. (submitted). The observed (α_{obs}, θ_{obs}) and predicted (α_{pred}, θ_{pred}) flood scaling parameters are also shown on each panel. It can be seen that the log-linear relationship between the scaling exponent and scaling intercept shown in Equations IX-2 and the log-log dependence of the scaling intercept on the peak discharge that is observed in the smallest gauged subcatchments in the basin can be used in conjunction with the NUMPD framework to reasonably predict peak discharges across scales in the basin. This is an important discovery that can be used to predict peak floods in ungauged basins. Considering the fact that there is a time delay between the time when peak discharges are observed in small scale subbasins and the time when peak floods are observed at large scale basins, the flood prediction framework proposed in this study can also be used for short term flood forecasting purposes.

9.6. Summary and Conclusion

Using 52 rainfall-runoff events observed in the Iowa River basin over a 12-year period between 2002 and 2013, I revealed an entirely overlooked log-linear relationship between the exponent and intercept of the power law relationship that characterizes the scaling invariance of peak discharges with drainage area, which is often observed in *nested* watersheds following a basin wide runoff generating rainfall event. This finding reduces the number of flood scaling parameters we need to infer from rainfall and catchment physical properties in order to predict floods across a range of spatial scales in the basin using the *nonlinear geophysical theory of floods*. I demonstrated the potential application of the discovery by formulating a framework that can be used to predict the expected value of peak discharges at large basin scales using peak discharges observed at the smallest gauged subcatchment in the basin.

The proposed flood prediction framework is a four step process. First, the scaling intercept is estimated from the peak discharge observed in the smallest gauged subcatchment in the basin, which in this case has a drainage area of 7 km^2. This step is based on the fact that the scaling intercept is equivalent to the expected value of peak discharges observed at the outlet of subcatchments that has a unit drainage area (Furey and Gupta 2005). Second, the scaling exponent is estimated from the scaling intercept using the log-linear relationship observed between the two. The log-linear relationship between the scaling exponent and intercept is established using peak discharge data from 52 rainfall-runoff events. Third, the expected value of peak discharges across a range of spatial scales is predicted using the estimated scaling exponent and scaling intercept that are used to parametrize the power law relationship between peak discharge and drainage

area. Finally, the uncertainty (natural variability) of the predicted peak discharges is quantified by using a methodology that is recently proposed by Gupta et al. (submitted) and called Natural Uncertainty Measure for Peak Discharges (NUMPD). The results show that peak floods at large basin scales can be reasonably predicted from peak floods observed in small scale subcatchments which typically have short streamflow response time. These results suggest that the flood prediction framework that I proposed provides reasonable estimates of peak discharges across a range of spatial scales.

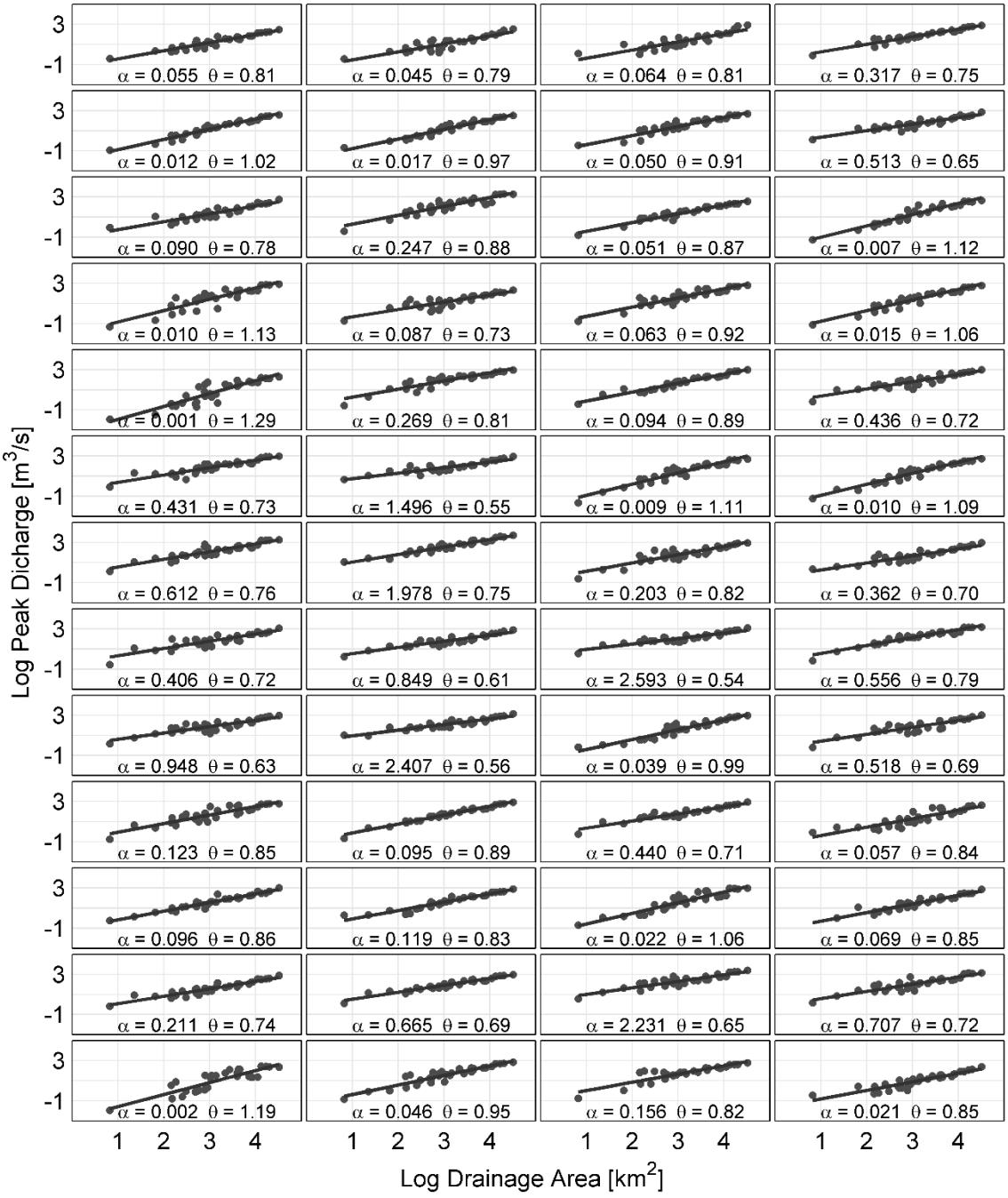

Figure IX - 1. Scaling plot of peak discharges for 52 rainfall-runoff events that occurred in the Iowa River basin over the period 2002-2013. Note that scaling intercept and exponent change from event to event.

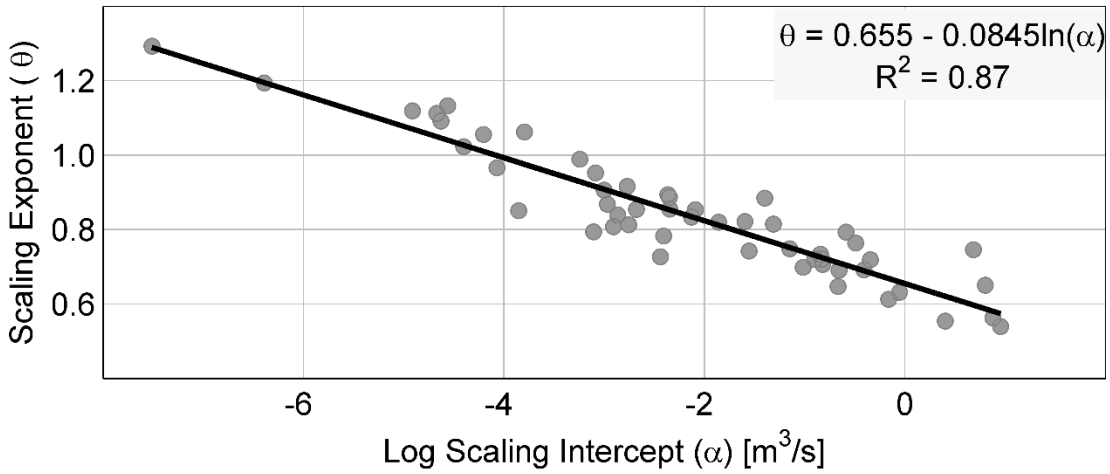

Figure IX - 2. Scatter plot of the scaling exponent versus the natural logarithm of the scaling intercept. The ordinary least squares regression line is shown in black solid line.

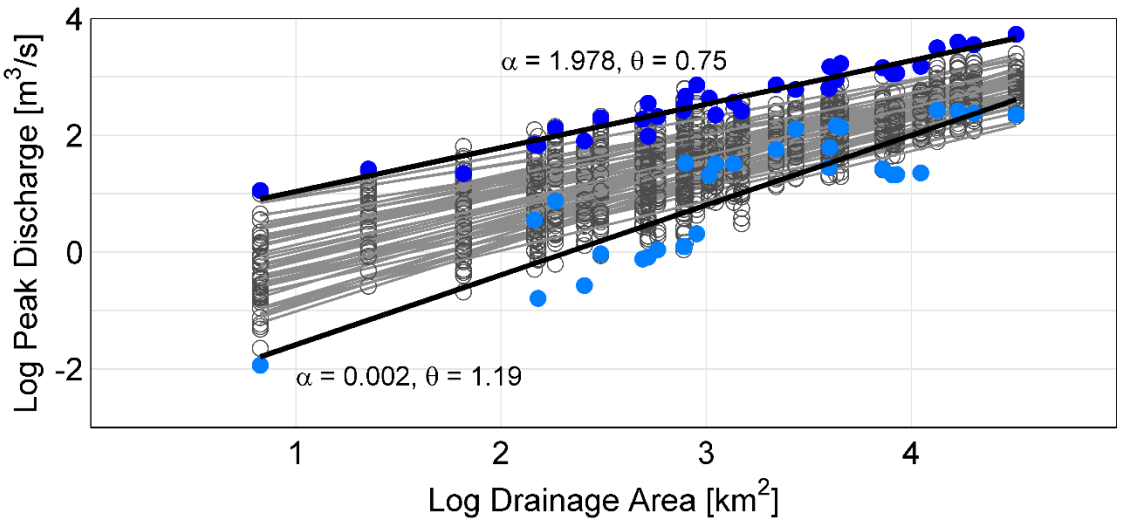

Figure IX - 3. Scatter plot of all the 52 peak discharge events observed in the basin following a single rainfall-runoff event.

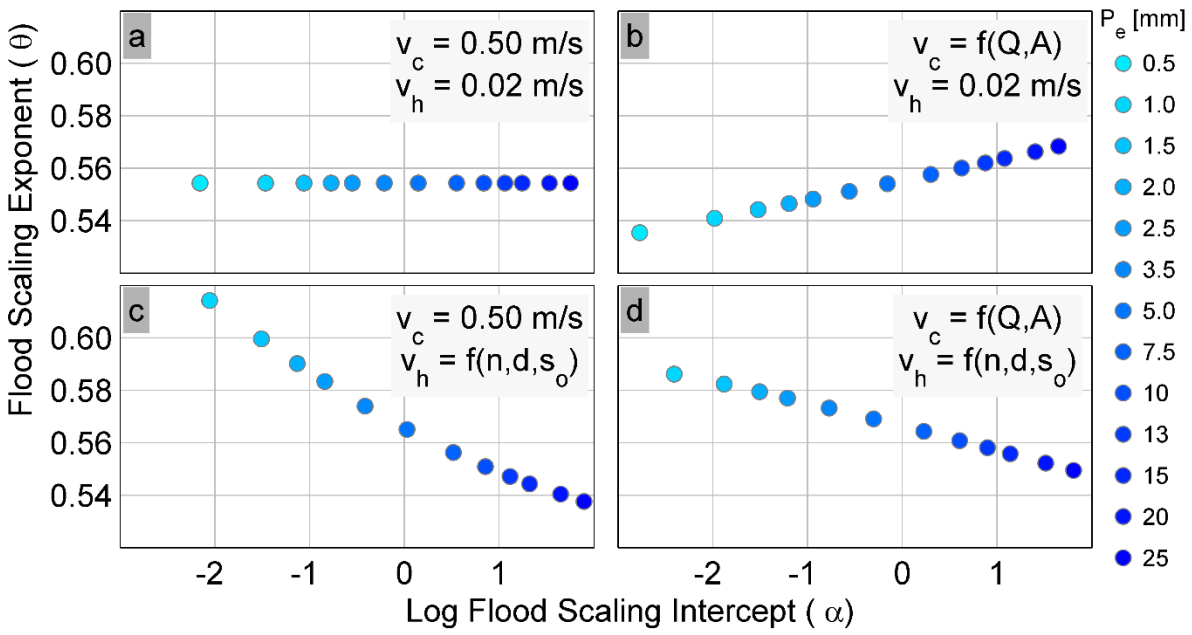

Figure IX - 4. Plot of simulation results that show how different formulations of the hillslope overland flow and channel flow velocities lead to different relationships between the scaling intercept and exponent. The rainfall duration is set to one hour for all the simulations. The excess rainfall depth is shown in the legend.

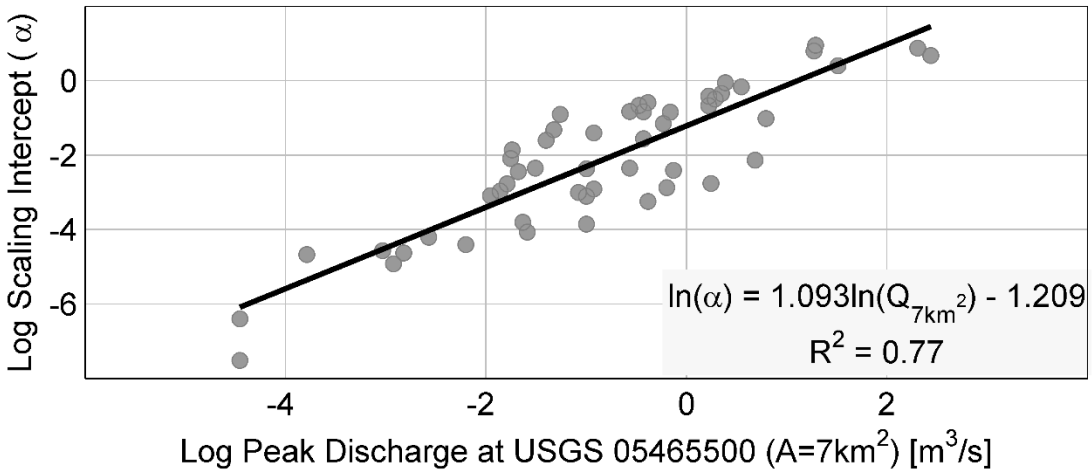

Figure IX - 5. Scatter plot of the natural logarithm of the scaling intercept versus the natural logarithm of peak discharges observed at a 7 km^2 subcatchment of the Iowa River basin (USGS ID: 05465500). The OLS regression line is shown in black solid line.

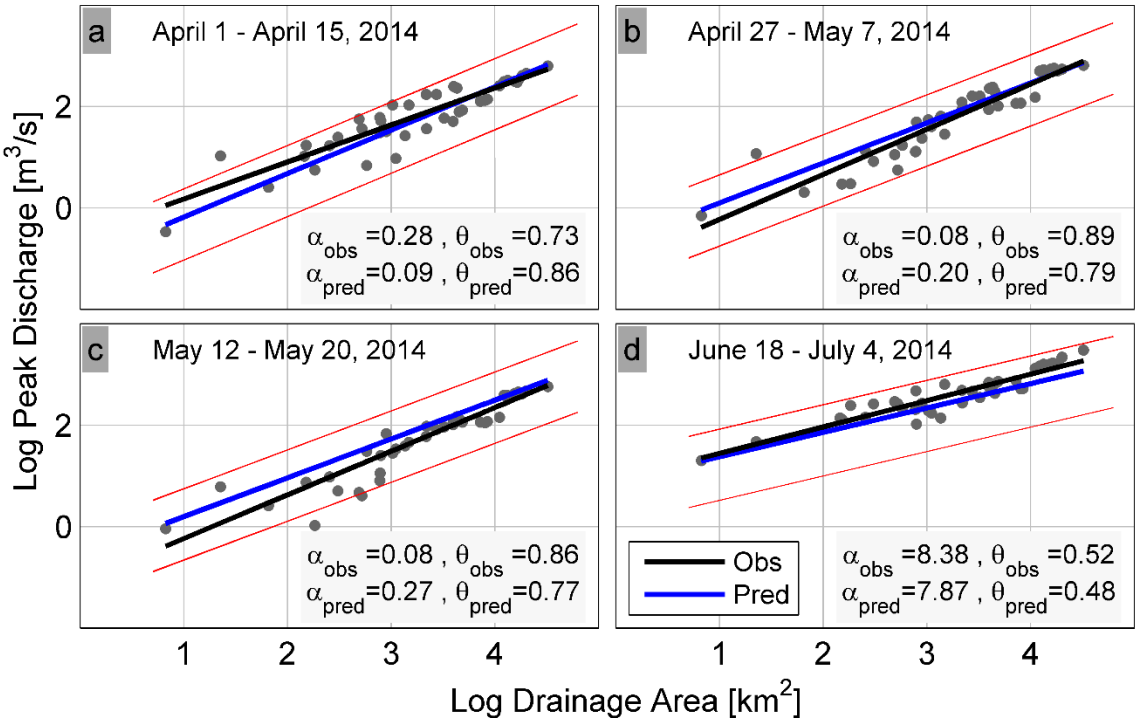

Figure IX - 6. Comparison of observed and predicated peak discharges for four rainfall-runoff events that occurred in the Iowa River basin in the spring and summer of 2014. Grey circles are observed peak discharges, solid black line is the power law fitted to observation whose parameters are shown on the plot (α_{obs}, θ_{obs}), the dotted blue line connects the expected value of peak discharges that are calculated using the predicted flood scaling parameters (α_{pred}, θ_{pred}), and the dotted red lines are the 95% confidence intervals estimated using the NUMPD framework.

CHAPTER X

DISCUSSION AND CONCLUSIONS

Conservation of mass dictates that the magnitude of peak discharge should increase with drainage area provided that there is no significant abstraction or other losses (storages) as the streamflow propagates downstream. It is perhaps because of this simple fact that drainage area is the single most important explanatory variable that is used in regional flood frequency equations. Empirical evidence from basins across different hydroclimatic regions show that the magnitude of peak discharges of a given probability of exceedance increases as a power-law function of drainage area suggesting the existence of a scale invariant spatial organization of peak discharge quantiles time (Bloschl and Sivapalan 1997; Goodrich et al. 1997; Gupta and Dawdy 1995; Gupta et al. 2010; Lima and Lall 2010; Ogden and Dawdy 2003; Smith et al. 2010). These studies also show that the parameters describing the power-law relationship, which we call the flood quantile scaling intercept and exponent, vary from one geographic region to another. This observation has been the subject of a number of fundamental research efforts that addressed the following two important questions: why do peak discharges exhibit scaling invariance with drainage area? Why is it that the parameters of the power-law relationship between peak discharge quantiles and drainage area vary from one geographic region to another? The answer to the first question cites the observed self-similarity of the river network, along which the fundamental processes of streamflow aggregation, translation, and attenuation occurs, as the reason behind the observed scaling invariance of peak discharge with drainage area (Gupta 2004; Gupta et al. 1996; Gupta and Waymire 1998; Menabde et al. 2001). Researches that were geared to addressing the

second question revealed that the geographic variability of rainfall and catchment physical properties that control the magnitude of peak discharge at the rainfall-runoff event scale is the reason behind the observed variability of the flood quantile scaling parameters from one region to another and as a function of the probability of exceedance of flood peaks (Bloschl and Sivapalan 1997; Gupta and Dawdy 1995; Merz and Bloschl 2003; Sivapalan et al. 2005; Smith 1992).

Although the regional flood frequency methodology has been successfully used for design flood estimations in ungauged basins, it remains a statistical tool that is largely detached from the physics of runoff generation at the rainfall-runoff event scale (Bloschl and Sivapalan 1997; Dawdy et al. 2012; Gupta and Dawdy 1995). This means that it is dependent on availability of historical data and as a result cannot be used in ungauged basins that are located in ungauged regions, which is typical of developing countries. Even in gauged regions, the regional flood frequency equations are changing every time they are updated to include newly available peak discharge data or use newly available statistical methods. Eash et al. (2013) recently compared the 100 year flood that is estimated using the regional flood frequency equations that they established for the state of Iowa in 2013 with the 100 year flood that is estimated using the regional flood frequency equations that were established in 2001 and showed that they are different by roughly ±40%. This has a huge implication on the overall cost of hydraulic infrastructure building and flood risk mitigation initiatives. Moreover, the assumption of stationarity may no longer be valid as the hydroclimate is changing and hence the past may no longer be used to predict the future. Under such circumstances, understanding the physical

mechanisms that control the spatial scaling property of peak floods is of paramount importance. It is this challenge that inspired this dissertation.

The physics behind the scaling invariance of peak discharges with drainage area can be understood by analyzing observed peak discharges at the rainfall-runoff event scale within a nested watershed. There are very few studies that are conducted under this premise because of the lack of observational data. The first empirical evidence for the existence of a scale invariant spatial organization of peak discharges at the rainfall-runoff event scale within a nested watershed is due to Ogden and Dawdy (2003) who analyzed observational data from the 21 km^2 Goodwin Creek Experimental Watershed (GCEW). They showed also that the flood scaling exponent and intercept change from one rainfall-runoff event to another. Furey and Gupta (2005) analyzed the same dataset and showed that the event to event variability of the flood scaling parameters can be partly explained by the intensity and duration of the excess rainfall that is associated with the peak discharge events. Their study clearly showed the need to investigate the role of other catchment physical properties and to expand the spatial scale of the analysis. Progress in this line of research that will lead to the complete understanding and description of the physical reasons as to why the flood scaling intercept and exponent change from one rainfall-runoff event to another is tantamount to solving the long standing hydrologic problem of prediction in ungauged basins (PUB). With this goal in mind, I conducted extensive analysis of empirical data obtained from the mesoscale Iowa River basin. I also undertook extensive diagnostic rainfall-runoff simulations to address questions that otherwise are very difficult to address using empirical data alone. I will summarize the main findings of my study as follows.

I began by analyzing streamflow data from the 32,400 km^2 Iowa River basin for the period between 2002 and 2013. I defined a rainfall-runoff event by following a two-step process. First, I check if a single peaked hydrograph is observed at the basin outlet. Second, based on the answer from the first step, I check if all the internal streamflow gauging sites also exhibit a significant streamflow response over the time window that is equivalent to the concentration time of the basin. If these two criteria are met, it means that a basin wide runoff generating rainfall event has occurred. Based on these two criteria, I have identified 52 rainfall-runoff events over the 13 years period of record. The results indicate that a scale invariant spatial organization of peak discharges frequently occurs in a mesoscale river basin such as the Iowa River basin. In this Chapter, I also investigated if a connection exists between scaling of peak discharges obtained from single rainfall-runoff events and scaling of peak discharge quantiles. To this end, I defined two type of peak discharge quantiles which I called Type-I and Type-II quantiles. Type-I quantiles are peak discharge quantiles that I calculated using peak discharges that are obtained using the rainfall-runoff event definition described above. As such, there could be multiple peak discharges observed at all gauging sites in any given year. This is similar to the peak over threshold method of flood frequency analysis with the threshold in this case being the basin wide occurrence of a runoff generating rainfall event. Type-II quantiles are the traditional peak discharge quantiles estimated based on the annual maximum peak discharge observed at each gauging sites. The results indicate that the expected value of the flood scaling parameters describing the spatial scaling propertied of peak discharges resulting from individual rainfall-runoff events is equivalent to the flood quantile scaling parameters estimated for Type-I

quantiles, suggesting for the possibility of a physically meaningful connection between the two. The results also show that the flood scaling parameters estimated for individual events and Type-I quantiles are different from those estimated for Type-II quantiles. This later result confirms the apparent disconnect of the traditional flood frequency estimation methodology from the physics governing the generation of the streamflow response in space and time at the rainfall runoff event scale.

In Chapter IV, I conducted an extensive diagnostic simulation experiment using a hydrologic model that is based on the decomposition of the landscape to hillslopes and channel-links as discussed in Mantilla and Gupta (2005). The experiments were conducted using three different watersheds from the state of Iowa representing different catchment spatial scales. Moreover, I conducted the numerical experiments under the assumption that rainfall, runoff coefficient, and hillslope overland flow velocity are constant in space and time. The results revealed how the interplay among rainfall intensity, duration, hillslope overland flow velocity, and channel flow velocity control the flood scaling intercept and exponent. In particular, the results show that the flood scaling exponent increases with increasing rainfall duration and channel flow velocity. The effect of hillslope overland flow velocity on the flood scaling exponent is shown to be a function of the rainfall duration. For shorter duration rainfall events, the scaling exponent decreases with increasing hillslope overland flow velocity whereas the opposite is true for longer duration rainfall events with the transition occurring at a rainfall duration of about 3 hr. When it comes to the flood scaling intercept, the results show that, while it is mainly an increasing function of the rainfall intensity (excess rainfall depth), it also increases with increasing hillslope overland flow velocity and channel flow

velocity. In this Chapter, I also investigated how the scale break in the relationship between peak discharge and drainage area is controlled by the interplay among rainfall duration, hillslope overland flow velocity and channel flow velocity. In particular, I showed that the spatial scale at which the scale break occurs decreases with increasing hillslope overland flow velocity whereas it increases with increasing rainfall duration and channel flow velocity. The results also show that the flood scaling exponent is always greater than the exponent of the scaling of the width function maxima and converges to unity as the rainfall duration approaches the catchment's concentration time. The fact that the scaling exponent converges to unity when the catchment is in dynamic equilibrium (steady state) is in agreement with the Rational Formula, which is extensively used to predict design floods in small ungauged catchments and predicts that the peak discharge linearly increases with drainage area for a given excess rainfall intensity that is applied over a duration that is equivalent to the concentration time of the catchment (Mulvany 1850).

In Chapter V, I expanded the diagnostic study by relaxing some of the assumptions I used in Chapter IV. Specifically, I allowed the rainfall intensity, runoff coefficient, and hillslope overland flow velocity to randomly vary in space. Additionally, I introduced a nonlinear hillslope overland flow formulation by using the Manning's formula. By varying the Manning's *n* in space, this formulation allows for a hillslope overland flow velocity that varies both in space and time. The most important finding of this chapter is the result that shows the contrasting effects of hillslope overland flow velocity and channel flow velocity on the magnitude of peak discharges as a function of scale. In particular, the results show that the effect of hillslope overland flow velocity on

the magnitude peak discharges decreases with increasing catchment spatial scale whereas the opposite is true with increasing channel flow velocity. This means that small scale catchment responses are dominated by hillslope processes whereas large scale catchment responses are dominated by the channel flow velocity and the river network geometry. As a result, the flood scaling exponent decreases with increasing hillslope overland flow velocity whereas it increases with increasing channel flow velocity. An additional insight that emerged due to the use of a nonlinear hillslope overland flow velocity is that rainfall and catchment physical properties that lead to an increase in hillslope overland flow velocity will result in a decrease in the flood scaling exponent. In this regard, I showed that the flood scaling exponent generally decreases with increasing excess rainfall depth and runoff coefficient, which I used as a proxy to antecedent soil moisture content. Finally, the results show that a scaling exponent of greater than unity occurs when rainfall and other catchment physical properties are spatially variable.

While the diagnostic simulation studies reported in Chapter IV and V revealed several insightful results, it is important to test if the simulation results can be supported by empirical observations. To this end, I used the 52 rainfall-runoff events that occurred in the Iowa River basin over the 13 years period between 2002 and 2013. The methodology used to identify these events is discussed in Chapter III. In Chapter VI, I analyzed the rainfall data that corresponds to each of the 52 rainfall-runoff events. I used the Stage-IV radar rainfall data as my data source. The results show that the flood scaling exponent increases with increasing rainfall duration whereas it decreases with increasing excess rainfall depth. The opposite is shown to be true for the flood scaling exponent. These results confirm the simulation results I reported in Chapters IV and V.

This chapter also uncovered the fundamental role played by the temporal intermittency of rainfall. Specifically, using a diagnostic simulation that is supported by evidence in empirical data, I showed that the flood scaling exponent initially increases with increasing intra-storm period before starting to decrease as the intra-storm period increases further. This later result qualifies the temporal intermittency structure of rainfall as an important rainfall property that controls the event to event variability of the flood scaling exponent and calls for an in depth exploration of the problem.

The results reported in Chapters IV, V, and VI show how certain properties of rainfall and the catchment affect the spatial scaling properties of peak discharges at the rainfall-runoff event scale. A remaining question was how the effect of these and other catchment physical properties on the magnitude of peak discharge at the rainfall-runoff event scale propagates to the annual time scale and hence affect flood frequency. Such line of enquiry will provide an avenue to connect the scaling of peak discharges resulting from single rainfall-runoff events to the scaling of peak discharge quantiles at the annual time scale. To this end, I investigated in Chapter VII how the interplay among rainfall duration and the drainage network geometry, which is intimately connected to the streamflow hydrograph, affect the magnitude of peak discharge at the rainfall-runoff event scale and how this propagates to the annual time scale and affects flood frequency. I used two catchments that have the same drainage area (521 km^2) and different shape. These catchments, which are called Old Mans Creek and Salt Creek, are both located within the same flood frequency region and hence the same set of regional flood frequency equations are used to predict floods in these catchments. Analysis of the respective drainage network geometry show that the peak of the width function of Salt

Creek, which has circular shape, is higher than the peak of the width function of Old Mans Creek by a factor of 2.5, which has an elongated shape. Moreover, the peak of the width function is closer to the outlet in Salt Creek than it is in Old Mans Creek. Simulation of the catchments using the same spatially constant rainfall input indicates that the peak discharge at the outlet of Salt Creek is greater than the peak discharges at the outlet of Old Mans Creek at shorter rainfall durations. This result is expected due to the obvious difference in the drainage network geometry and has been reported upon for quite a while (Black 1972; Chorley et al. 1957; Horton 1932; Morisawa 1958; Sherman 1932; Taylor and Schwarz 1952). However, as the rainfall duration gets longer, the hydrographs observed at the outlet of the two catchments appear to converge. Analysis of the scaling structure of peak discharges in these catchments show that the flood scaling exponent in Salt Creek is greater than the scaling exponent in Old Mans Creek and these values converge to unity as the rainfall duration increases. This indicates the role the interplay among rainfall duration and drainage network geometry affects the magnitude of peak discharges across scales at the rainfall-runoff event scale.

I expanded the above analysis to the annual time scale by computing the at site flood frequency using the Bulletin 17B methodology (IACWD 1982) implemented in PeakFQ software (Veilleux et al. 2014) and 64 years of annual maximum peak discharge data observed at the outlet of the catchments indicated that peak discharges at the outlet of Salt Creek are always greater than those at the outlet of Old Mans Creek for all exceedance probabilities. To show that this difference is mainly due to the drainage network geometry, I conducted a continuous simulation experiment using a stochastically generated 10,000 year point rainfall time series by keeping everything the same in the

two catchments except the drainage network geometry. The results show that the drainage network geometry can significantly affect the flood frequency. Comparison of the simulated and observed at site flood frequency with the flood frequency estimated using the regional flood frequency equations reported in Eash et al. (2013) indicate that the metric used to account for the shape of the catchment, which is the ratio of the square of the catchment length to its drainage area, do not adequately address the effect of the drainage network geometry on flood frequency. This later result calls for a review or search of a better drainage network geometry metric that can be used in regional flood frequency equations.

In Chapter VIII, I revisit the results from Chapter III and investigate how the effect of the interplay among rainfall duration and intensity on the peak discharge at the rainfall-runoff event scale affects the scaling of Type-I peak discharge quantiles. Recall that I defined Type-I peak discharge quantiles as those calculated from peak discharges that are selected from nested watersheds under the condition that they result from a basin wide runoff generating rainfall event that occurs over the time window that is equivalent to the basin's concentration time. Results from my Monte Carlo simulation experiment, which is based on the simulation of runoff coefficients that are randomly variable in space that are set up to mimic a spatially variable runoff response, show that the flood scaling exponent describing the spatial organization of Type-I quantiles decreases with probability of exceedance. This is in support of the result I reported in Chapter III based on the analysis of observational data from the Iowa River basin. The results also show that for a given probability of exceedance, the flood quantile scaling exponent increases with increasing rainfall duration and decreases with increasing excess rainfall depth.

This later result shows how the effect of rainfall and catchment physical properties that control the peak discharge at the rainfall-runoff event scale affect the spatial scaling properties of peak discharge. This is further confirmed through the finding that showed the expected value of the flood scaling parameters of individual rainfall-runoff events is equivalent to the expected value of the flood scaling parameters corresponding to peak discharge quantiles. These results indicate that how we select and organize peak discharge events may go a long way in helping establish a physically meaningful regionalization of flood frequencies.

Through extensive analysis of empirical data and diagnostic simulation experiments, I have uncovered a host of insights pertaining to the mechanism through which selected rainfall and catchment physical properties control the event to event variability of the flood scaling exponent and intercept and how these effects propagate from the rainfall-runoff event scale to the annual time scale and affect flood frequency. These results, which are reported in Chapters III to VIII, indicate that the flood scaling exponent and intercept can be predicted from rainfall and catchment physical properties and hence can be used to predict floods across a range of spatial scales. In Chapter IX, using the 52 rainfall-runoff events I reported upon in Chapters III and VI, I discovered the existence of a physically meaningful log-linear relationship between the flood scaling exponent and intercept, which will essentially reduce the problem of flood prediction using the scaling theory of floods to a one parameter estimation problem. The fact that the flood scaling intercept, which is equivalent to the peak discharge observed at $1km^2$ when metric units are used, is easier to estimate than the flood scaling exponent highlights the potential use of the discovery for flood prediction (forecasting) across

scales. To this end, I proposed a flood forecasting framework that has three major components. First, the flood scaling intercept is predicted from the peak discharge that is observed at the smallest gauged subcatchments in the basin of interest. Second, the flood scaling exponent is predicted using the flood scaling intercept estimated in step one. Third, using the flood scaling exponent and intercept estimated in steps one and two, predict the expected value of peak discharges across scales. I used the Natural Uncertainty Measure of Peak Discharges (NUMPD) recently introduced by Gupta et al. (submitted) to estimate the confidence interval for the predicted peak discharge. I have successfully demonstrated the capability of the framework using four rainfall-runoff events that occurred in the Iowa River basin in the spring and summer of 2014.

Although, in my proposed flood prediction framework, the scaling intercept is estimated from peak discharges that are observed in the smallest gauged subcatchment in the basin, the results presented in Chapters IV to VII studies show that it can also be predicted from rainfall and catchment physical properties. Advances in this line of research will provide an alternative approach to estimate the scaling intercept. This will enhance our capability to predict peak floods using rainfall forecasts at some lead time before the first peak discharge in the smallest gauged subcatchment in the basin is observed without the need to run expensive numerical models. This later information, i.e., peak discharges that occur in small scale subcatchments of the basin within few hours of the occurrence of the rain event due to the short catchment response time, can be used to refine the forecasted peak discharges as the rainfall event unfolds in the basin. Several interesting questions arise from this work. Are the parameters of the log-linear relationship between the scaling exponent and scaling intercept universal? Or are they

regional? If the latter is the case, can they be used for regionalization of flood frequencies? I am making progress in addressing some of these questions and it is my hope that this study will inspire many more studies that will contribute towards solving the grand hydrologic problem of predictions in ungauged basins (PUB) (Hrachowitz et al. 2013; Sivapalan et al. 2003).

APPENDIX A

EXPLORING THE EFFECT OF A SINGLE FLOOD STORAGE RESERVOIR ON FLOOD FREQUENCY [4]

A.1. Introduction

I have showed in the preceding three chapters how the event-to-event variability of the flood scaling exponent and the intercept can be described by rainfall and catchment physical variables that also vary from event to event. These results were obtained under the assumption that both the simulated and observed peak discharges are not regulated. The USGS also uses streamflow data obtained from unregulated gauging sites while establishing the regional flood frequency equations for homogeneous hydrologic regions. In their analysis, they only ignore stream flow data obtained from those gauging sites that are located in the immediate downstream of major reservoirs (Eash 2001). However, this appears to be an unrealistic assumption because it ignores the effect of the numerous small dams that are scattered across the US. Data from the US Army Corps of Engineers' National Inventory of Dams show that there are more than 87,035 dams already built in the US. In Iowa, where the study basins of this dissertation are located, there are more than 3,927 dams and the trend appears to suggest that the construction of small dams is continuing. There is essentially no study that addressed how these dams are affecting the flood frequency in the river basin of their location. Understanding how these spatially distributed dams affect the flood frequency is of paramount importance in managing our water resources. One potential application is to provide a statistical

[4] Adapted from Ayalew, T. B., Krajewski, W. F., and Mantilla, R. (2013). "Exploring the Effect of Reservoir Storage on Peak Discharge Frequency." *Journal of Hydrologic Engineering*, 18(12), 1697-1708.

framework that can be used to correct flood frequencies that are estimated using the *scaling theory of floods* or any other methodology that ignores the existence of these dams.

This and the following two chapters are devoted to understanding how flood retention reservoirs affect flood frequency. I use a continuous simulation approach to systematically address this problem by first studying the effect of a single reservoir on flood frequency. The results will serve as a building block to Chapter VIII where I investigate how the spatial organization of two dams and their storage and release capacities relative to their location in the drainage network affect the flood frequency at different locations in the basin. Chapter IX will expand the analysis to the 660 km^2 Soap Creek catchment located in southeastern Iowa that hosts more than 132 dams.

This chapter is organized as follows. I begin with review of the current literature as regard to the effect of storage reservoirs on downstream flood frequency followed by a brief discussion of reservoir-regulated flows obtained from the Iowa River. This is followed by a description of the continuous simulation methodology I adopted in this study. The methodology section details the stochastic rainfall model and the simple but realistic rainfall-runoff model that is used to generate stream flow time series data that serve as the input to the reservoir model. I also describe the reservoir routing module that I used to derive reservoir regulated flow time series data. I then present the data analyses of the synthetic regulated streamflow time series and show how reservoirs modify the peak discharge frequency. Following this, I discuss how the reservoir operation rule, reservoir storage size, and size of its release structures affect the regulated flood frequency. Finally, I detail the existing method of estimating regulated flood frequency

that is being used by the USACE to estimate regulated flood frequencies and show why the approach may lead to incorrect results. I end the chapter with a summary of the major findings.

A.2. Review of the effect of flood storage reservoirs on flood frequency

The regional flood frequency equations discussed in section 2.2 are established using streamflow records that are not affected by flow regulation due to reservoirs or other engineered structures (e.g., Eash 2001). Moreover, the *nonlinear geophysical theory (or scaling theory) of floods* that has been developing over the past two decades, to which this dissertation will significantly contribute, also assumes that there is no regulation of flow along the river network. This means that these flood prediction methods cannot be used to predict peak discharge quantiles or events for those locations downstream of a flood storage reservoir. To put the problem into perspective, according to the United States Army Corps of Engineers (USACE) national inventory of dams (NID) there are more than 79,000 dams built in the continental U.S. of which about 4,000 are built in the state of Iowa. This highlights the need to study how a single and a system of distributed flood storage reservoirs modify the flood frequency across different spatial scales in the basin.

It is common (hydrologic) knowledge that reservoirs attenuate incoming flood peaks. The magnitude of the attenuation depends on the reservoir's available storage capacity at the time of flood wave arrival, the release capacity, and the operation rules determined by the purpose of the reservoir. Other factors pertain to the dynamics of the incoming flood waves and are characterized by their total water volume and the inter arrival time. The manner in which all these factors combine determines how flood

frequency is modified for locations immediately downstream from the reservoir. What is not well known is how exactly the flood frequency is modified and how to best estimate it. Despite its practical significance, this problem has not been fully discussed in the literature. It was partially addressed by Bradley and Potter (1992), but we still lack an in-depth understanding. Currently, the standard methodology for estimating regulated flow frequencies is empirical (Goldman 2001; USACE 2010). Therefore, a more complete analysis of this problem is required to quantify the limits of reservoirs in reducing flood peak frequencies and the associated flood risk for downstream locations.

Bradley and Potter (1992) proposed a runoff volume-based approach, which they called a peak-to-volume approach, to estimate regulated flood frequency from peak discharges obtained using a continuous rainfall-runoff simulation of watersheds regulated by distributed engineered storages. To illustrate their approach, they chose the 47.4 km^2 Salt Creek watershed in Illinois as an example and simulated flows with and without a hypothetical reservoir placed at the outlet of the catchment. The peak-to-volume relationship they established using the 41 years of data was incomplete as it lacked the low frequency events that are most important in terms of flood frequency estimation. To resolve this issue and construct an accurate peak-to-volume relationship, they transposed and simulated extreme rainfall events of various durations from around the region where the study site was located. Hess and Inman (1994) used an event based rainfall-runoff model to study the effects of urban flood-detention reservoirs on peak discharges and flood frequencies. They had access to 68 years of daily rainfall data from which they selected four to eight rainfall events per year. They then modeled each of these events with and without reservoirs and later fitted the log Pearson Type III distribution to the

resulting annual peak flood time series. The flood frequency of the two cases, with and without reservoirs, indicated no sign of convergence for the calculated annual flood exceedance probabilities between 0.01 and 0.5.

The existing Volume-Duration-Frequency (VDF)-based methodology that is being used by the United States Army Corp of Engineers (USACE) for estimating reservoir regulated flood frequency is a four step process. The first step involves the estimation of site-specific VDF relationships using a methodology that is closely connected to the Bulletin 17B guidelines (IACWD 1982). The second step involves the estimation of the critical inflow duration that leads to peak annual regulated flows. This step is often achieved by analyzing existing reservoir inflow-outflow data or by performing reservoir routing studies. The third step deals with the development of a relationship between unregulated inflow volume and peak outflow for the critical inflow duration identified earlier. Finally, this relationship is used to translate an inflow volume of a given frequency to peak outflow of the same frequency. In this way, the regulated flood frequency is estimated from the inflow volume frequency.

The traditional method discussed above has two methodological shortcomings that could lead to the underestimation of the peak of the regulated outflow. The first shortcoming is due to the assumption made about the initial water level in the reservoir when extending the inflow volume to peak outflow relationship to low frequency events which are often missing from observed data. According to this method, to determine the inflow volume to peak outflow relationship for low frequency events, historical flood events are scaled up and then routed through the reservoir. The reservoir routing is achieved by assuming that the initial water level in the reservoir is at the bottom of the

flood control pool. However, for a given reservoir, the initial water level is determined by the antecedent inflow condition and how the reservoir was operated prior to and during the arrival of such an event. This means that the initial water level is a random function of time that varies between the bottom of the reservoir (for purely flood control reservoirs) or the bottom of the flood control pool (for multi-purpose reservoirs) and the reservoir's spill level. Goldman (2001) acknowledges this challenge and argues that assuming the initial water level to be at the bottom of the flood control pool is "the simplest and most defensible approach." The second shortcoming of the method is the implicit assumption made during the development of the relationship between inflow volume and peak outflow. It assumes that the relationship between inflow volume and peak outflow is unique for a given reservoir and can be determined by relating inflow volume to peak outflow of individual flood events. However, depending on the initial water level and how the reservoir is operated, a given inflow volume could lead to a range of peak outflows. This makes it impossible to determine a reservoir specific unique curve that relates inflow volume to peak outflow. Moreover, due to the stochastic nature of the initial water level in the reservoir, assigning the same exceedance probability to both inflow volume and peak outflow leads to incorrect results. For example, a high frequency inflow volume that occurs when the reservoir is full leads to a low frequency peak outflow.

The methodological shortcomings of the existing VDF-based approach can be overcome using a continuous simulation of a catchment-reservoir system using either observed or synthetically generated rainfall time series. Nehrke and Roesner (2004) used the continuous simulation of 50 years of hourly rainfall records to investigate how

different configurations and sizes of orifices in a single flood detention pond affect the flood frequency curve. They designed the detention pond so that it had multiple vertically-stacked orifices whose size increased with increasing elevation. Each of these orifices controls peak discharges that have different return periods. They showed that the size and configuration of the orifices systematically control the departure of the regulated flood frequency curve from the unregulated flood frequency curve, its slope, and the return period at which a break in the slope occurs.

The literature reviewed above has discussed the limited studies that have been made to investigate how a single reservoir modifies the flood frequency in the immediate downstream of a flood storage dam. However, a survey of reservoirs built in the U.S. indicates that there could be a number of reservoirs scattered across a given river basin, with the spatial density of reservoirs varying across geographic regions. For example, there are over 3,928 dams built across the state of Iowa. Moreover, due to the acknowledged economic, environmental, and safety limitations of large reservoirs, the construction of distributed small retention ponds has become an alternative approach to reducing flood risk in urban and rural watersheds (Chen et al. 2007; Verstraeten and Poesen 1999). In the United States, the Environmental Protection Agency (EPA) recommends such ponds as an alternative best management practice (BMP) for stormwater management, because, in addition to attenuating flood peaks, retention ponds contribute to improved water quality (Bottcher et al. 1995; Guo and Urbonas 1996). Furthermore, when distributed across the watershed, these ponds provide distributed flood reduction benefits, a feature that large reservoirs lack due to their typically benefitting only locations immediately downstream from the dam. Despite their wide use

for stormwater management, little is known about how a system of flood retention ponds affects the flood frequency at different locations in the watershed. Understanding this problem is of paramount importance as it addresses such questions as: what is the best spatial configuration of retention ponds? and what are the best sizes of storage and outlet structures of ponds given their location in the drainage network? Answers to these questions would greatly assist floodplain managers in planning, designing, and managing systems of retention ponds.

There is no study, to the best of my knowledge, which addressed how distributed reservoirs modify the flood frequency across scales in the watershed that host them. The only related study is conducted by Kusumastuti et al. (2008b) who investigated a catchment that has a chain of natural lakes connected *in series*. As a first step, Kusumastuti et al. (2008a) investigated the catchment and lake physical properties that affect the magnitude and frequency of lake-overflow in a catchment that has a single lake located at its outlet. They used a continuous simulation approach that employed a stochastic rainfall model and a simple conceptual rainfall-runoff model. The lake can be considered as a reservoir that doesn't have an outlet (orifice) at the bottom, and its spillway is therefore the only outflow structure. Their study revealed that the most dominant catchment and lake threshold driven processes that determine the magnitude and frequency of lake overflow are the antecedent catchment-lake storage condition, the magnitude of storm depth, and the catchment area to lake area ratio, *AC/AL*. The latter determines the size of the storm events that fill and overflow the catchment-lake storage system. Kusumastuti et al. (2008b) built on this study and investigated a catchment that has a chain of lakes connected *in series*. In addition to the threshold driven processes

identified in Kusumastuti et al. (2008a), the follow-up study by Kusumastuti et al. (2008b) revealed that the spatial organization of lakes in the landscape, which determines their connectivity, plays a determining role in the magnitude and frequency of lake overflow. In particular, they showed that when the AC/AL of the chain of lakes decreases in the downstream direction, i.e., when the lake area increases in the downstream direction relative to the catchment area it drains, the resulting peak discharge at the outlet of the catchment-lake system is greater than the peak discharge obtained when the AC/AL either increases in the downstream direction or remains constant.

Research Gap: Based on the current literature, it is clear that there is a need to investigate how the design and operational aspects of a single and a system of geographically distributed flood storage reservoirs affect the flood frequency at different spatial scales in the catchment.

A.3. How does a single reservoir modify flood frequency?

Consider a single reservoir built with the main purpose of flood mitigation. If the inflows can be characterized by a given peak discharge frequency, how is the frequency modified by the existence of the reservoir? Furthermore, how can we best estimate the reservoir regulated flood frequency based on available data? While these questions appear straightforward and easily answered by reservoir design analysis, they are actually quite complicated. Answering the first question requires a model of the dynamic interactions of the inflows with the reservoir. We can gain insight into the answer through a theoretical analysis or a computer simulation. Note that answering the first question does not necessarily lead to answering the second one. This is mainly due to observed data limitations. First, our knowledge of the frequency of the inflows is based either on observed record of discharge at the site upstream from the reservoir or by a

regional peak discharge analysis. In either case, the estimated frequency is subject to significant uncertainty. Second, the observational records of reservoir outflows are often too short to reveal the effect of the reservoir on low frequency flows associated with extreme floods. Third, hydrologic models that could be used in a simulation framework to provide simulated inputs into the reservoir require long records of data for the parameter calibration necessary for the models to perform satisfactorily. Fourth, reservoirs modify the inflow peaks indirectly through storage volume, where the relationship between peak inflow volumes and peak outflow rate is non-unique due to the stochastic nature of the initial water level in the reservoir at the time of flood wave arrival. Therefore, the downstream probability distribution of peak flows is not a trivial derived distribution of the probability density of the inflows. Clearly, there are several factors that complicate our ability to answer the questions we have posed.

What should we expect based on general reasoning? A conceptual answer is presented in Figure VII-1(a), which shows the expected shape of the relationship between peak inflow (Q_I) and peak outflow (Q_O) for a hypothetical reservoir. For low inflows, which correspond to high probability of exceedance, we would not want to change the outflow due to the environmental considerations associated with the low-flow regime of the river (stream). Consequently, the inflows and outflows will have a one-to-one relationship, as will their frequencies. For higher flows that could potentially cause flooding downstream, we want to reduce the outflow peak as appropriate (i.e. to keep it below the (significant) flood level). Therefore, the associated outflow will veer to the right of the 1:1 line so that lower outflows correspond to higher inflows. However, as the inflow increases in peak and volume, the potential for reducing the outflow is diminished

because the remaining storage capacity is limited. For very high flows, such reduction is a small (insignificant) portion of the inflow, and the corresponding flows will come back to the 1:1 line.

The degree of departure from the 1:1 line depends on the operating rules of the reservoir and the initial water level in the reservoir at the time of flood wave arrival. Assuming that the black envelope line describes the maximum possible reduction in inflow peaks, which would happen if the reservoir is empty at the time of flood wave arrival, the grey area represents other possibilities. In the opposite limit, keeping the reservoir full would be equivalent to staying on the 1:1 line. Note that all possible combinations of inflow vs. outflow in the grey area are possible, though not equally likely. Thus, answering the question, "what is the frequency of peak outflow given a frequency of peak inflows?" depends upon whether we know how the reservoir is operated and if we consider all possible combinations of initial water storage and inflow volume. This question is best answered by the grey line in Figure VII-1(a) that corresponds to pairs of inflow-outflow values (let's say q_I vs. q_O) for which $P(Q_I > q_I) = P(Q_O > q_O)$. The grey line is simply the quantile-quantile plot of possible inflow-outflow pairs in the grey area.

To further illustrate the effect of reservoirs, we use data collected upstream and downstream from the Coralville Reservoir located 12 miles upstream (north) from Iowa City, Iowa on the Iowa River. The dam was built in the early 1950s to provide flood protection for Iowa City, where The University of Iowa is located. The dam was designed based on 49 years of streamflow data collected by the US Geological Survey (USGS) at Marengo, Iowa, located further upstream and north of Iowa City. For our

analysis, I selected 54 years (1957-2010) of annual flood peak time series of the Iowa River from the gauging stations located in Marengo and Iowa City, which are upstream and downstream of the dam, respectively. These two gauging stations provide real-time measurement of inflow to and outflow from the reservoir. The quantile-quantile plot of the two datasets shown in Figure VII-(1b) reveals a hint of the outflow and the inflow converging. The two highest values correspond to the historic floods of 1993 and 2008 (Galloway 1994; Gupta et al. 2010; Mutel 2010; Smith et al. 2013), when water had to be released through the emergency spillway. Clearly, the reservoir's flow control ability was compromised during these two flood events.

If the qualitative behavior discussed so far is correct, full understanding of the problem implies our ability to describe the above relationships in quantitative terms by relating the characteristics of the inflow, outflow, storage capacity, flow dynamics, and operating rules to each other. I will address these issues using a continuous simulation approach that is discussed in the following sections.

A.4. Simulation methodology

To explore the important problem of estimating reservoir regulated flood frequency and to gain insight into the associated issues, I use a stochastic rainfall model to generate long and statistically homogeneous rainfall time series with high temporal resolution. The long length of the generated rainfall time series allows us to get around the problem of having short periods of observed data. I use a simple rainfall-runoff model to convert the generated rainfall to runoff. The generated runoff forms the reservoir inflow time series. I use a numerical model of reservoir routing to calculate the outflow time series for a given reservoir operation rule, reservoir storage size, and release

capacity. Stochastic rainfall generators in combination with rainfall-runoff models have been extensively used in the literature to estimate flood frequency in data limited gauged catchments (e.g., Aronica and Candela 2007; Blazkova and Beven 1997; Cameron et al. 1999) and ungauged catchments (e.g., Blazkova and Beven 2002) and to study the effect of land use change on flood frequency (Brath et al. 2006). Reservoir routing is also a well-established technique used to transform inflow hydrographs to outflow hydrographs.

I illustrate how storage affects peak flow frequency by using a simplified case of reservoir operation and inflows where the roles of specific problem variables can be separated. First, I consider a hypothetical catchment that is regulated by a small reservoir built at the outlet and has storage capacity of 140,000 m. The storage capacity is comparable with some of the small dams built in Iowa. The hypothetical catchment has an area of 3.75 km^2 and a catchment storage coefficient of about 1.3-hour. The small size of the catchment implies that the point rainfall time series generated using the stochastic rainfall model can be reasonably assumed to be uniformly distributed in space (see Seo and Krajewski (2011)for a study of rainfall variability). By studying a small reservoir, we can use very simple rainfall and rainfall-runoff models without compromising the general mechanism of how storage modifies peak discharge frequency. Second, I propose a rainfall-runoff generation model for our hypothetical catchment. The relatively fast catchment response time and the size of the reservoir necessitate the use of a high resolution rainfall time series. Therefore, I chose a stochastic rainfall model with the capacity to generate synthetic rainfall time series at 5-minute resolution. Finally, I specify deterministic routing and operation rules for a reservoir with a unique storage vs. elevation relationship. We discuss these three distinct components, i.e. the stochastic

rainfall generator, the simple rainfall-runoff model, and the reservoir flood routing module in the following subsections.

A.4.1. The stochastic rainfall model

A variety of stochastic rainfall models of varying complexity exist in the literature. Some of these models, which are relatively simple, use an event based approach that requires minimal parameterization, where distributions of inter-storm arrival time, storm duration, and storm intensity are treated as random variables described by a parametric probability distribution function, often the exponential distribution, to mimic the alternating wet-dry characteristics of rainfall (e.g., Acreman 1990; Eagleson 1972). These approaches consider the inter-storm arrival and storm depth processes separately and superimpose them to form the rainfall model. More complex models are based on the Neyman-Scott or Bartlett-Lewis cluster processes (Cox and Isham 1980). In these approaches, storm origins arrive in a Poisson process, with each storm origin leading to the formation of a random number of storm cells that have random cell duration and depth. In the Neyman-Scott clustered model, no storm cell exists at the storm origin. The cell arrival times, which are independently and identically distributed, are measured from the storm origin. Unlike the Neyman-Scott clustered model, the Bartlett-Lewis clustered model assumes the existence of a storm cell at the storm origin. The cell arrival times are then the interval times between successive cells, which are also independently and identically distributed. Two well-developed cluster-based rainfall models are the Neyman-Scott Rectangular Pulses model (NSRP) and the Bartlett-Lewis Rectangular Pulses (BLRP) model, first developed by Rodriguez-Iturbe et al. (1987). An

important characteristic of these models is their ability to generate a continuous rainfall time series that can consistently be further aggregated to different time scales.

The BLRP model is extensively used in the literature to generate hourly point rainfall with good success, preserving rainfall statistics at different aggregation levels (e.g., Islam et al. 1990; Khaliq and Cunnane 1996; Onof and Wheater 1993; Rodriguez-Iturbe et al. 1987). More recent efforts have been geared towards modifying the model to reproduce the sub-hourly rainfall variability that is evident in historical data that rectangular pulse models are unable to reproduce (Cowpertwait et al. 2007; Kaczmarska 2011). Models of this kind allow us to study the behavior of hydrologic systems that have a quick response time, such as small watersheds and urban storm water sewerage systems. Herein, I adopt the modified Bartlett-Lewis pulse (BLP) model proposed by Cowpertwait et al. (2007).

The modified BLP model uses three Poisson processes to reproduce the sub-hourly rainfall structure and has a total of six parameters. First, it assumes that storm origins arrive at time T_i in a Poisson process of rate λ. A storm lasts for an independent random duration of length D_i that is exponentially distributed with parameter γ. During the duration of the storm, cell origins arrive at time T_{ij}, which is described by a secondary Poisson process of rate β, and their arrival process terminates at the end of the storm duration, i.e. $T_{ij} < T_i + D_i$. The model assumes that the cells have a random duration of L_{ij} that is also exponentially distributed with parameter η. A third Poisson process is used to describe the arrival of pulses of random duration and intensity during the lifetime of a cell. The model further assumes that each cell origin (T_{ij}) leads to the

onset of a sequence of pulses that arrive at time T_{ijk} in a Poisson process of rate ξ. Each of these pulses has random rainfall depths X_{ijk} that are exponentially distributed with parameter θ and are terminated at the end of the cell duration. This approach replaces the constant cell intensity assumption of the original BLRP model. It follows that, in the modified BLP model, the mean number of cells per storm is β/γ and the mean number of pulses embedded in each cell is $\xi/(\gamma+\eta)$, leading to the mean number of pulses in each storm $\mu_P = \beta\xi\{\gamma(\gamma+\eta)\}^{-1}$. The expected total rainfall depth per storm is, therefore, $\mu_P\mu_X$, where $\mu_P\mu_X = E(X_{ijk})$. The interested reader is referred to Cowpertwait et al. (2007) for an in-depth description of the model.

In this study, I made no attempt to fit the model to any particular site. Instead, I assigned sensible values to the model parameters to generate a hypothetical rainfall regime with a sub-hourly structure similar to what we observe in historical data. I referred to the modified BLP model fitted to 5-minute rainfall data at Kelburn (near Wellington in New Zealand) to learn the order of magnitudes the modified BLP model parameters could assume and to inform our parameter selection accordingly (Cowpertwait et al. 2007).

A.4.2. The rainfall-runoff model

Hydrologic models that have a varying range of complexity and calibration requirements are used in the literature for continuous simulation-based flood frequency estimation studies. Examples include the grid based spatially distributed hydrologic model used by Brath et al. (2006); the semi-distributed hydrologic model called TOPMODEL used by Cameron et al. (1999) as well as Blazkova and Beven (1997; 2002;

2004); and the unit hydrograph theory based simple model used by Aronica and Candela (2007). As the main intention of this study is not to estimate flood frequency for a specific site but rather to study how a single reservoir modifies flood frequency, I gave little attention to the accuracy of runoff generation and, hence, used a simple hydrologic model. A good candidate for our requirement is the simple conceptual hydrologic model that was proposed by Chow et al. (1988) that is based on the determination of runoff hydrograph by the linear-reservoir method.

In the linear-reservoir method, the storage (S) in the catchment is assumed to be linearly related to the runoff (R) as,

$$S = kR, \qquad \text{Equation A-1}$$

where k is a constant commonly called a storage coefficient. The storage in the catchment is also a function of the effective precipitation (P) and runoff (R), as described by the continuity equation as

$$\frac{dS}{dt} = P(t) - R(t) \qquad \text{Equation A-2}$$

Differentiating Equation A-1 with respect to time and substituting the result into Equation VII-2, we will have:

$$k\frac{dR(t)}{dt} = P(t) - R(t) \qquad \text{Equation A-3}$$

This is a first-order linear differential equation that has a well-known solution as follows (Chow et al. 1988):

$$R(t) = R_O e^{-t/k} + \int_0^t P(\tau)\frac{1}{k}e^{-(t-\tau)/k}d\tau$$ Equation A-4

where R_O is the initial runoff condition and τ is the integration variable. If we assume that the initial condition $R_O = 0$, the above equation turns into the convolution integral,

$$R(t) = \int_0^t P(\tau)\frac{1}{k}e^{-(t-\tau)/k}d\tau$$ Equation A-5

Let us now define $g(t) = \int_0^t \frac{1}{k}e^{-(t-\tau)/k}d\tau$ in the above equation. This is called a step response function and its solution is similar to what is commonly called the S-hydrograph in hydrology. One can easily show

$$g(t) = 1 - e^{-t/k}$$ Equation A-6

The runoff hydrograph $\left(R_h(t)\right)$ corresponding to an effective precipitation of duration T_d can therefore be calculated from Equation A-6 using the principle of superposition as follows:

$$R_h(t) = \frac{P}{T_d}\left(g(t) - g(t - T_d)\right)$$ Equation A-7

where $g(t - T_d) = 0$ for $0 \le t \le T_d$. This leads to the following set of equations

$$R_h(t) = \begin{cases} \frac{P \cdot A}{T_d}\left(1 - e^{-t/k}\right) & \text{for } 0 \le t \le T_d \\ \frac{P \cdot A}{T_d}e^{-t/k}\left(e^{\frac{T_d}{k}} - 1\right) & \text{for } t > T_d \end{cases}$$ Equation A-8

where A is the catchment area and $R_h(t)$ has a unit of volume per time. Equation A-8 forms the basis of the simple rainfall-runoff model used in this study.

The storage coefficient, k, for a single linear reservoir model is equal to the hydrograph time lag and can be determined from the relationship between a stream flow hydrograph and the related effective precipitation hyetograph. The reader can refer to Chow et al. (1988) for the detailed derivations of the above set of equations. I further simplified the model by assuming that the runoff coefficient is 0.2. This simplification was made to ensure that we have a realistic stream flow time series that is proportional to the catchment size considered in this study. We can check this by comparing the results with estimation made using the rational method (Brutsaert 2005). Using rainfall intensity and rational method C runoff coefficient values appropriate for the study area, the 10, 50, and 100 year return period peak discharge values estimated using the rational method were 21, 31, and 35 m/s, respectively. These results are in good agreement with the results obtained in this study (see Figure A-8).

A.4.3. Reservoir routing

Reservoir routing determines the outflow hydrograph from a given inflow hydrograph and known reservoir characteristics. It is often accomplished by means of hydrologic routing, which is a method that considers the reservoir as a lumped system and computes the flow as a function of time at the reservoir outlet. The method solves the mass conservation (continuity) equation (Chow et al. 1988). The continuity equation as applied to a reservoir system is a first-order differential equation that can be solved numerically. Fenton (1992) showed that the second-order Runge-Kutta method can be

used to solve this problem with an acceptable degree of accuracy. In this work, I use the Runge-Kutta method to calculate the reservoir outflow time series.

The continuity equation for storage in a reservoir is expressed as

$$\frac{dV}{dt} = I(t) - Q(t,V) \qquad \text{Equation A-9}$$

where V is the volume of water stored in the reservoir; $I(t)$ is the inflow into the reservoir as a function of time; and $Q(t,V)$ is the outflow from the reservoir.

The outflow from the reservoir is computed as a function of the water level, which is itself a function of the stored volume in the reservoir. I established the relationship between storage and water level, often called the elevation-area-storage relationship, for our hypothetical reservoir site in the Clear Creek watershed, Iowa, using ArcGIS tools for terrain data processing. Based on this relationship, I selected a reservoir that has a maximum storage capacity of 140,000 m and a total dam height of 4.6 m. I further assumed that the reservoir has a spillway weir length of 2 m and an outflow orifice diameter of 762 mm.

The relationship between the outflow and storage is non-linear and is described by the following set of equations for the outflow:

$$Q(t,h) = \begin{cases} c_1 A_c \sqrt{2gh} & \text{for} \quad 0 \le h \le H_{spill} \\ c_1 A_c \sqrt{2gh} + c_2 L (h - H_{spill})^{3/2} & \text{for} \quad H_{spill} < h < H_{dam} \end{cases} \qquad \text{Equation A-10}$$

where c_1 is the orifice coefficient; A_c is the orifice cross-sectional area; h is the water level in the reservoir; H_{spill} is the reservoir spill level; H_{dam} is the total dam height; c_2

is the weir coefficient; and L is the length of the weir crest. We assumed the outflow to be equal to the inflow when the reservoir is full.

Using the Runge-Kutta method, the storage volume at the $(i+1)^{th}$ time step is expressed as:

$$S_{i+1} = S_i + k_2, \text{ where } k_2 = \Delta t * f\left(t_i + \frac{\Delta t}{2}, S_i + \frac{k_1}{2}\right);\ k_1 = \Delta t * f\left(t_i, S_i\right) \qquad \text{Equation A-11}$$

In addition to the above set of equations, we need to specify a reservoir operation rule to complete the reservoir routing model.

The optimal operation of a reservoir is a well-researched study area. For a flood control reservoir, optimal operation implies the maximum reduction of flood risk in downstream areas. Research has shown that reliable forecasts and adaptive decision systems can substantially contribute to optimal reservoir operation endeavors (Yao and Georgakakos 2001). In this work, I make no effort to find the optimal operation rule for the single flood control reservoir that formed the basis of the study. Instead, I investigate two basic types of reservoir operation rules: passive control and active control. In the passive control strategy, the reservoir gate was set to remain fully open for the entire simulation period. In this case, the reservoir regulates the flow based only on its storage-discharge relationship, which means that the reservoir is operating at its maximum release potential at any given time during the simulation period. In the active control strategy, the outflow is regulated by dynamically changing the opening size of the reservoir gate in such a way that the outflow should not exceed a prescribed flow magnitude that is assumed to create downstream flooding. For the case of active control,

I assumed a simple streamflow forecast methodology known as persistence. In this case, the inflow to the reservoir for the coming 1-hour duration is assumed to be the same as the inflow over the past 1-hour duration leading up to the current time. This allows for decisions to be made to either partially or fully open the sluice gate of the reservoir based on available reservoir storage space. This strategy works as long as there is enough space left in the reservoir to store some portion of the incoming flood wave which otherwise could create flooding at downstream areas. In the simulation, there were also instances when the outflow was set to be equivalent to the inflow because the reservoir was already full. It is important to note here that the reservoir operation rules investigated in this work are very simple types of reservoir control strategies in which the reservoir under consideration is a single purpose (flood control) reservoir with a single constraint (downstream flood level) as opposed to a multi-purpose reservoir with a multi-objective operation, which is a common situation in practice.

A.5. Statistical analysis of simulated inflow and outflow time series

Using the stochastic rainfall model, I generated a 5-minute rainfall time series for a period of 1000 years. The notion of time and its units is unimportant for the conclusions of this study; we could as easily talk in terms of sample size only. However, to bring a degree of realism to our hypothetical example, I use time units commensurate with the watershed and the reservoir at hand. The generated rainfall was then used as an input to generate runoff with a temporal resolution similar to the rainfall data. Finally, the runoff was routed through a hypothetical reservoir characterized by the size of its storage capacity, outlet gate, dam height, and spillway length. The inflow and outflow time series were then treated as unregulated and regulated streamflow data, respectively.

I further analyzed the data to study the effect of the reservoir on the immediate downstream flood frequency.

There are two well-established techniques of flood peak data selection for estimating flood quantiles: the block maxima (BM) and the peak-over-threshold (PoT) methods (Coles 2001). In the BM method, we need to specify the time window from which the peak flow value is selected. The selected BM peaks are independently and identically distributed random variables that follow the Generalized Extreme Value (GEV) distribution (Fisher and Tippet, 1928). In the PoT method, we need to specify some threshold flow value above which peak flow value is selected. Flood peak values selected in such a way follow the Generalized Pareto (GP) distribution (Pickands 1975). In the BM approach, too small of a block size leads to bias, whereas too large of a block size leads to high variance. Similarly, in the PoT approach, too small of a threshold value leads to bias whereas too large of a threshold value leads to high variance. Therefore, the choice of optimum block size or threshold value is based on a compromise between bias and variance (Coles 2001; Engeland et al. 2004).

I used both the BM and PoT methods. I selected peak flow values from both regulated and unregulated streamflow data using different magnitudes of block size and threshold value. I assigned exceedance probability values to the selected peak flow time series according to the Weibull plotting position formula and plotted the resulting peak flow quantile estimates of regulated and unregulated flows against each other. Figure A-2 and Figure A-3 show the results for different peak threshold values and block sizes, respectively.

I found that the PoT method is very sensitive to selected threshold values, making it an inappropriate approach to compare the peak flow quantile estimates of regulated and unregulated flows. This is because the PoT data of regulated and unregulated streamflow time series will have uneven sample sizes which will lead to a distorted relationship between the two. Fig. 2 shows cases when an increased threshold value yields results in which the outflow is greater than the inflow for a given quantile value. However, both PoT and BM approaches give comparable results when the block size and the threshold value are very small (see Figure A-2(a) and Figure A-3(a)).

Once I ruled out the PoT method, I decided to use a block size equivalent to one month for all of our subsequent analyses using the BM method. Although flood frequency is often estimated based on annual peak flows in conformance with the assumption of stationarity (to mitigate against the effects of annual cycle in runoff regime), the small reservoir being investigated here requires a smaller block size to understand the complete picture of flood frequency modification due to the reservoir. This is evident in Figure A-3 where the quantile-quantile relationship corresponding to high frequency events does not exist when we use a block size of one year. This part of the curve corresponds to low flows, which could have been captured if the block size was smaller. Hence, in order to preserve the stationary assumption and make sure that "monthly" peak flows are independently and identically distributed, the same rainfall model parameters were used for all 12 months of the year while generating the stochastic rainfall time series.

The Weibull plotting position formula is used to calculate monthly unregulated and regulated flow exceedance probabilities. Figure A-4 shows the flood frequency of

unregulated and reservoir regulated flows for a given reservoir size and operation rule. Our findings here clearly reveal how reservoirs modify flood frequency. They also show how the flood frequency of regulated and unregulated flows converge for large floods. This marks the upper limit beyond which reservoirs no longer contribute to regulating flood events.

The regulated flood frequency discussed thus far is only an estimation of flood frequency for a unique set of stationary climate, reservoir operation rule, reservoir size, and size of the reservoir's release structures. For a reservoir with a given storage and release capacities, the operation rule will be the single most important factor contributing to uncertainty in the estimation of the regulated flood frequency. The problem becomes further complicated when the uncertainty related to the estimation of the inflow time series is factored in. In the following sections, I will use simple examples to explain how the reservoir operation rule, the reservoir storage size, and the size of its orifice affect the regulated flood frequency.

A.5.1. Active vs. passive reservoir operation

As we discussed in the reservoir routing section, I considered two cases of reservoir operation strategies: passive control and active control. In the passive control case, the gate of the reservoir is kept open throughout the simulation time. In the active control case, the reservoir is operated in such a way that the discharge from the reservoir, where possible, did not exceed the threshold peak discharge level that could cause flooding downstream. Analysis of both sets of results showed that the manner in which the reservoir modifies flood frequency depends on how it is operated.

For both reservoir operation strategies, the flood frequency of the regulated flow converges to the flood frequency of the unregulated flow both at the lower and upper ends of the flow quantiles. However, for the case of active control, there is a flattening of the regulated flood frequency at the specified threshold discharge level that was assumed to cause flooding at downstream locations. In some instances, while operating at this threshold level, the reservoir gets filled and no sufficient storage space is left for incoming flows. This situation leads to the release of water at a much higher rate than the threshold discharge level due to the combined use of the spillway and the now fully open sluice gate. This is shown in the quantile-quantile plot of Figure A-5 where the outflow jumped drastically for a small increase in inflow.

The result also showed an interesting aspect of the tradeoff a reservoir operator makes between choosing different operation strategies. Interestingly, in comparison to the passive control strategy, the active control strategy was able to reduce the magnitude of higher frequency events by partially closing the sluice gate and holding back more water in the reservoir. However, as a direct consequence of the reduced storage space left in the reservoir, the active control strategy led to the magnitude of relatively low frequency flood events being higher than when passive control strategy was used. This result confirms the fact that the best reservoir operation strategy for flood control purposes is to keep as much spare storage space as possible. This result also indicates how a reservoir operation rule contributes to the uncertainty related to the regulated flood frequency estimate.

A.5.2. Effects of release gate size and storage capacity

I investigated the effects of the reservoir's release gate size and storage capacity on the regulated flood frequency by using the passive control strategy only. The simulation result (Figure A-6) indicates that increased gate size, for a given storage capacity, reduced the magnitude of some low frequency flood events while increasing the magnitude of some other high frequency flood events. The reason behind this result is that, by releasing flow at a much higher rate, the reservoir has some storage space left that is later used to regulate incoming low frequency flood events. An alternative interpretation of the results from this simple experiment is that the area bound between the 1:1 line and the quantile-quantile curve for the biggest gate size represents the uncertainty related to the reservoir's capability to modify flood frequency. This uncertainty is partly determined by the reservoir's operation rule, which is, in this case, how wide its gate is allowed to remain open. The result also shows that, in keeping with existing hydrologic knowledge, increasing the reservoir storage capacity offers a greater degree of control over the outflow flood peaks. However, we have shown that the upper limit at which any flood frequency intersects with the 1:1 line depends on the specific conditions of the reservoir. This is shown in Figure A-6, where all flood quantile curves of regulated flows corresponding to different reservoir storage capacities converge to the unregulated flow quantile curve for different values of the flood frequency.

A.6. Connecting results to the VDF-based traditional method of estimating regulated flood frequencies

As we discussed earlier, there is scarce literature on the issue of reservoir regulated flood frequency analysis. However, there is an empirical methodology that is based on inflow volume-duration-frequency (VDF) analysis and its relationship to peak

outflow. This method is currently used in practical applications by the USACE and other agencies (Goldman 2001; USACE 2010). We also discussed earlier that, when low frequency peak outflows are estimated by simulating rainfall events that are scaled up from historical extreme events, the VDF-based traditional methodology proposes that routing of the incoming flood wave be conducted under the assumption that the reservoir is at the bottom of the flood control pool. An important connection that must be made here is that the relationship proposed by the traditional methodology to relate peak inflow volumes and peak outflows of the same frequency corresponds to the lower envelope of the peak inflow to peak outflow relationship (red line in Figure A-1(a)).

I argue that the traditional method is incorrect, due primarily to the implicit assumption made about the relationship between unregulated inflow volume and regulated outflow. The methodology assumes that the relationship between unregulated inflow volume and regulated outflow for the critical inflow duration is unique, when in actuality it is non-unique. The non-uniqueness arises because: (1) the reservoir's water level at the time of flood wave arrival is a random variable that is determined by antecedent inflow sequences and (2) the operation rule of a reservoir is often a function of the water level, which implies that the operation rule is also a random variable. Consequently, there are instances where the same inflow volume will lead to different peak outflow values. Hence, the use of a single inflow volume to peak outflow relationship may lead to incorrect results. This non-uniqueness is confirmed using the results from the Monte Carlo simulations for a range of inflow durations (Figure A-7 (b), (c), and (d)). It is important to highlight that for the synthetic example we used in this work, i.e., a small 3.75 km^2 catchment with a catchment storage coefficient of 1.3-hour, it

appears that the critical inflow duration is between 2-hour and 4-hour. Figure A-7(a) also shows that the same non-uniqueness is observed in the relationship between peak inflow and peak outflow. Hence, the correct curve to relate equally likely peak inflows to peak outflows is the curve of the most likely peak flow reduction that is depicted using the grey line in Figure A-1(a) and Figure A-7(a). In Figure A-7(a), all the simulated inflow-outflow pairs (light grey dots), the maximum possible attenuation curve (black envelop line), and the quantile-quantile inflow-outflow relationship (grey line) are shown to illustrate the differences I mentioned previously.

Another questionable conjecture in the VDF based traditional method arises from the assumption that unregulated inflows and regulated outflows share the same probability of occurrence. As discussed above, a given inflow volume will lead to a peak outflow that has a probability of occurrence that is either lower or higher than the probability of occurrence of the inflow volume. Figure A-8 shows how a peak inflow of a given exceedance probability could lead to a peak outflow that has a range of exceedance probabilities.

In addition to showing the dynamics of the inflow-outflow relationship, this work also reveals that the quantile-quantile relationship between inflow and outflow is unique for a given reservoir's design specification and operation rule. To show this, I simulated three independent realizations of 1000-year inflow time series and found that their quantile-quantile curves fall on top of each other (Figure A-9). We already demonstrated that the quantile-quantile plots became non-unique when the reservoirs are operated differently (Figure A-6). In this case, the different operation strategies were assumed to have come from using different orifice sizes for each simulation. Finally, I compared the

regulated flood frequency estimates that would be calculated using the traditional method with the regulated frequency estimated using the simulated results. I found that the traditional methodology leads to an underestimation of the flood risk. For example, when the lower envelope curve in Figure A-7(a) is used, the inflow with a 2% exceedance probability (30 m/s) would correspond to an outflow of 15 m/s that has the same exceedance probability. In contrast, the quantile-quantile plot established using the Monte Carlo simulation (the green line in Figure A-7(a)) yields an outflow of 29 m/s. This difference would lead to an incorrect perception of flood risk for locations downstream of the reservoir. This result can easily be extrapolated to other flood frequency estimations by realizing that the inflow to outflow transformation proposed by the traditional methodology corresponds to the lower envelope shown in Figure A-7(a). This underestimation of risk is not unique to our simulation but is a general feature of the empirical methodology that is rooted in its implicit assumptions. However, the generalization of my conclusion would require a more sophisticated study in which each of the components of the estimation framework (stochastic rainfall, hydrologic model, and reservoir routing and operation) are closer approximations to realistic conditions.

Although more research needs to be conducted before we can translate the simulation framework illustrated here into practice, this work provides a road map for understanding how reservoirs regulate peak flows and, hence, a statistically sound methodology for quantifying reservoir regulated flood frequency. The use of a stochastic rainfall-runoff model for estimating flood frequency in poorly gauged catchments has already shown promise (Aronica and Candela 2007), and this work extends the

methodology to the estimation of a reservoir regulated flood frequency where regulated flow data is often characterized by short record length.

A.7. Summary and Conclusions

A simple Monte Carlo simulation approach is used to investigate the effect of flood control reservoirs on downstream flood frequency. The simulation is necessary because sufficiently large samples of observations are not available for a data-based study of the problem. By limiting the scope to small watersheds and, thus, to small storages, the complexities of modeling the spatial and temporal variability aspects of rainfall and runoff is avoided. I also ignored the seasonal cycle of the rainfall-runoff process while assuming a perfect short-term forecast of inflows. These simplifications do not compromise the generic insights we gained into the relationship between the quantile estimates of inflows to and outflows from storage reservoirs.

Two distinct cases of reservoir operation rules are analyzed: (1) passive control where the reservoir specifications determine the outflow and (2) active control where a reservoir "operator" adjusts the gate opening according to some operating rules. Analysis of the two cases revealed that the flood frequency of unregulated and regulated flows converge for low probability flood events. In addition, the results revealed that there exists a break in the regulated flood frequency estimate. The observed break marks the point where the outflow transitions from a sluice gate (orifice) only controlled outflow to sluice gate and spillway controlled outflow. It is important to acknowledge here that a detailed study of sophisticated operation rules used to operate multipurpose reservoirs might further reveal additional properties of the regulated flood frequency.

By using a simple hydrologic example, the study also showed that the VDF-based traditional methodology used in current engineering practice could lead to an underestimation of flood risk for locations downstream of reservoirs. This underestimation is primarily due to the implicit assumption made about the relationship between unregulated inflow volume and regulated outflow. In the VDF methodology, it is assumed that the relationship between unregulated inflow volume and regulated outflow for the critical inflow duration is unique, when in actuality it is non-unique. The non-uniqueness arises because: (1) the reservoir's water level at the time of flood wave arrival is a random variable that is determined by antecedent inflow sequences, and (2) the operation rule of a reservoir is often a function of the water level, which implies that the operation rule is also a random variable. Consequently, there are instances where the same inflow volume will lead to different peak outflow values. The results also show that the VDF-based methodology can lead to incorrect results.

Finally, this study marks a significant step towards determining how passive and active storage systems modify flood frequency for locations downstream from reservoirs and how this modification could be quantified. While the benefits of skillful reservoir operation have been well documented in the literature, a better understanding of frequency modifications could aid discussions on flood mitigation policy. The problem is difficult, as extending the case to large single reservoirs that regulate drainage from complex basins or to a system of reservoirs would invalidate many of the simplifying assumptions this study was able to justify.

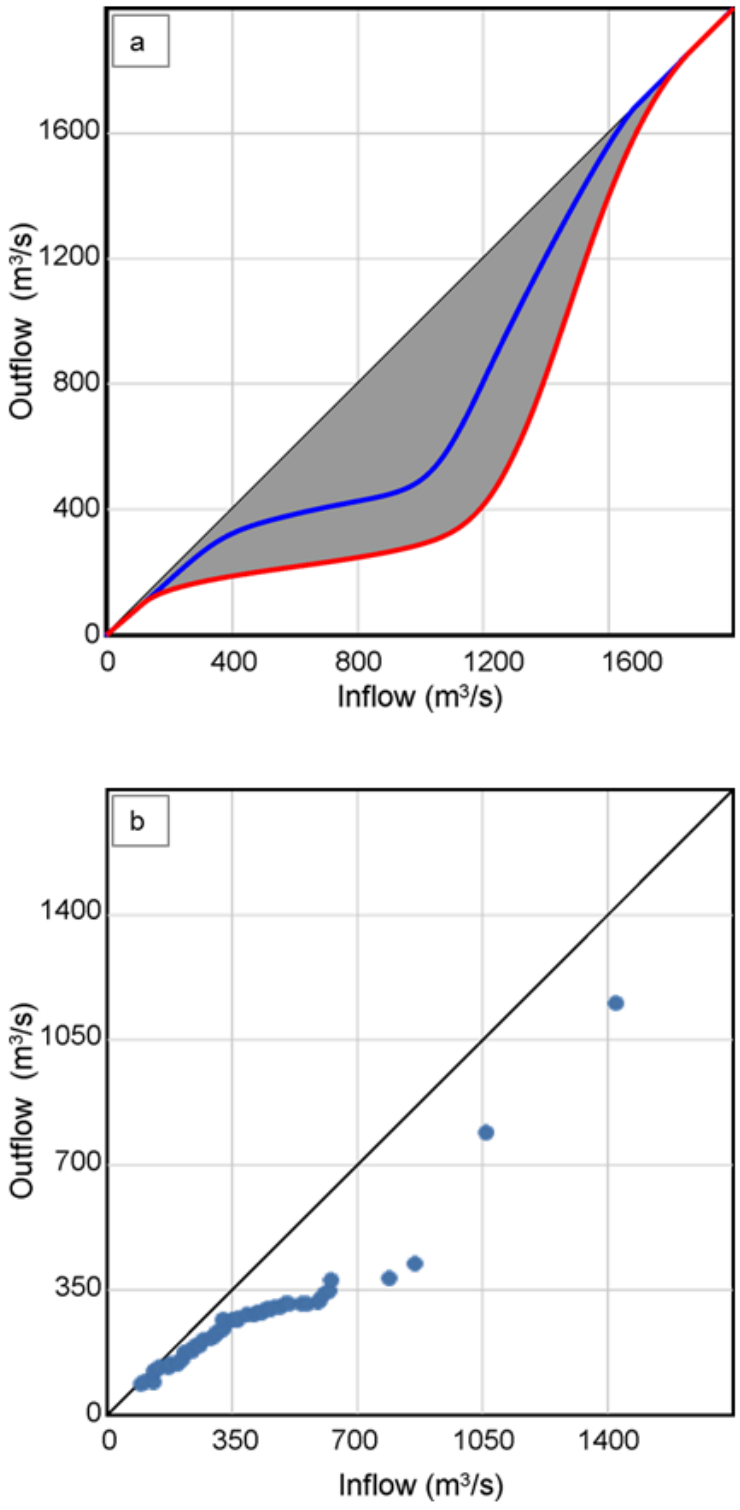

Figure A - 1. (a) Hypothesized inflow-outflow relationship and (b) a quantile-quantile relationship between inflow and outflow data of the Coralville dam.

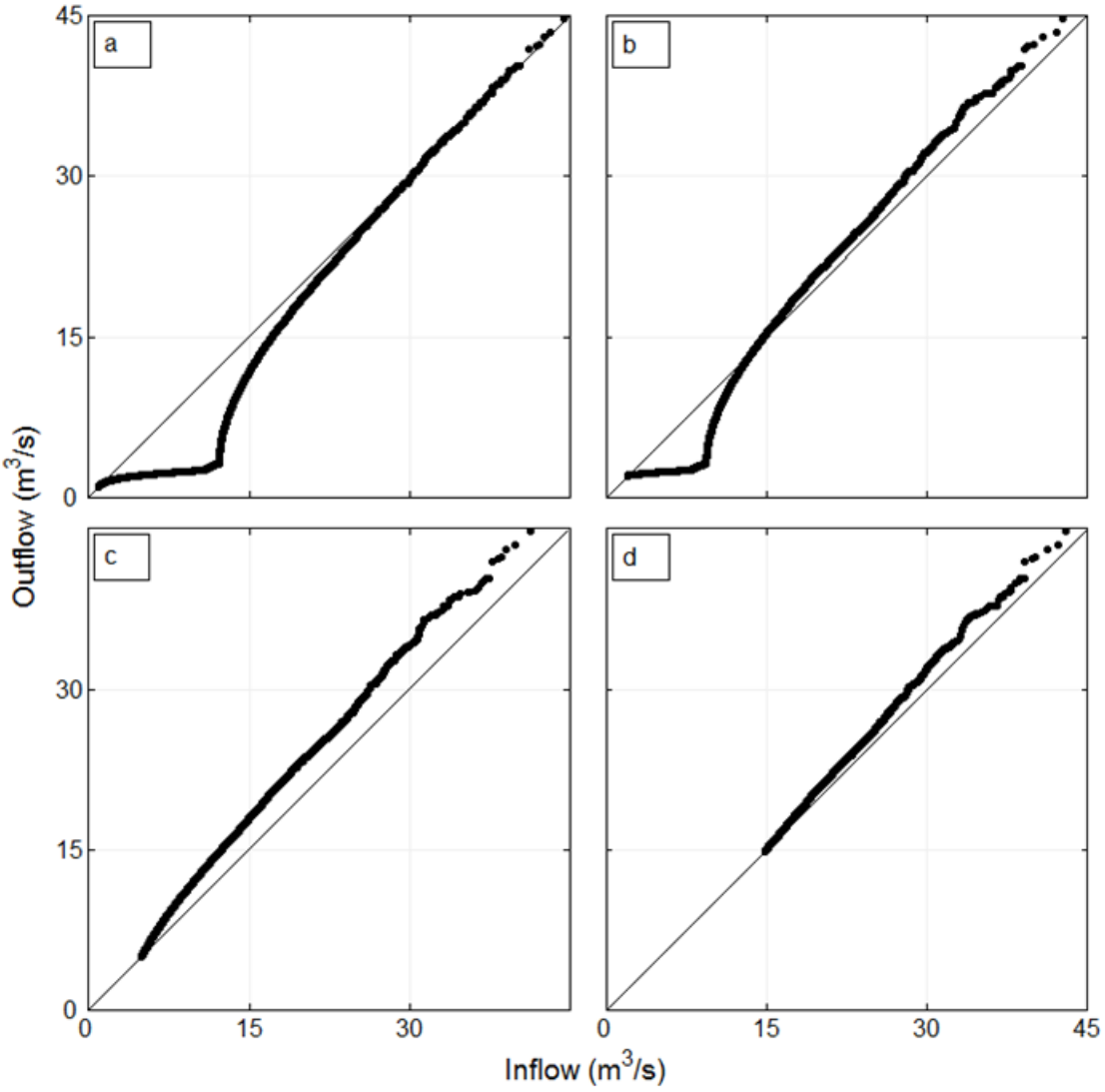

Figure A - 2. The quantile-quantile relationship between unregulated (inflow) and regulated (outflow) flows based on the peak over threshold approach using threshold values of 1 m/s (a), 2 m/s (b), 5 m/s (c), and 15 m/s (d).

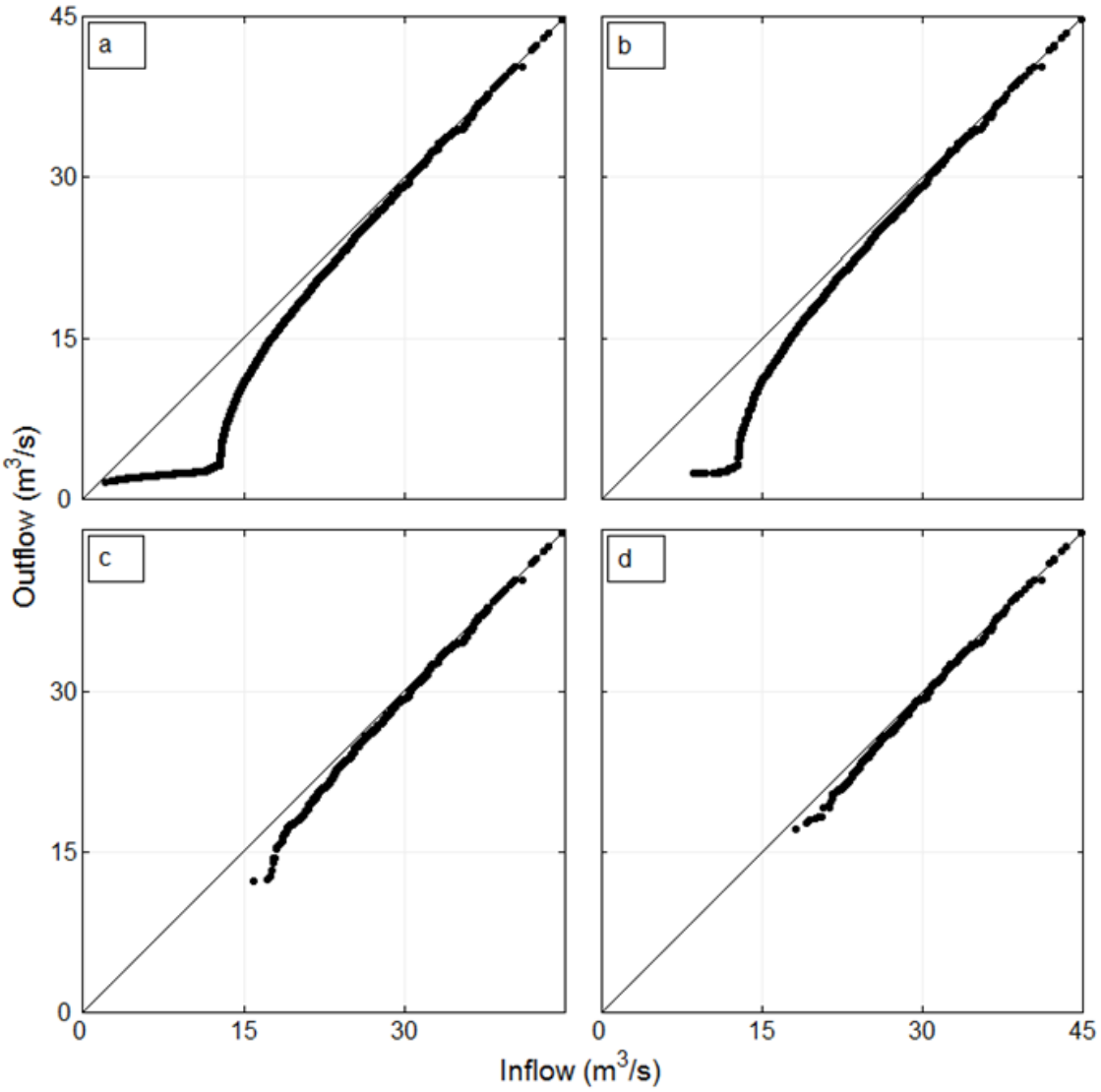

Figure A - 3. The quantile-quantile relationship between unregulated (inflow) and regulated (outflow) flows based on the block-maxima approach using block sizes of 1 month (a), 3 months (b), 1 year (c), and 2 years (d).

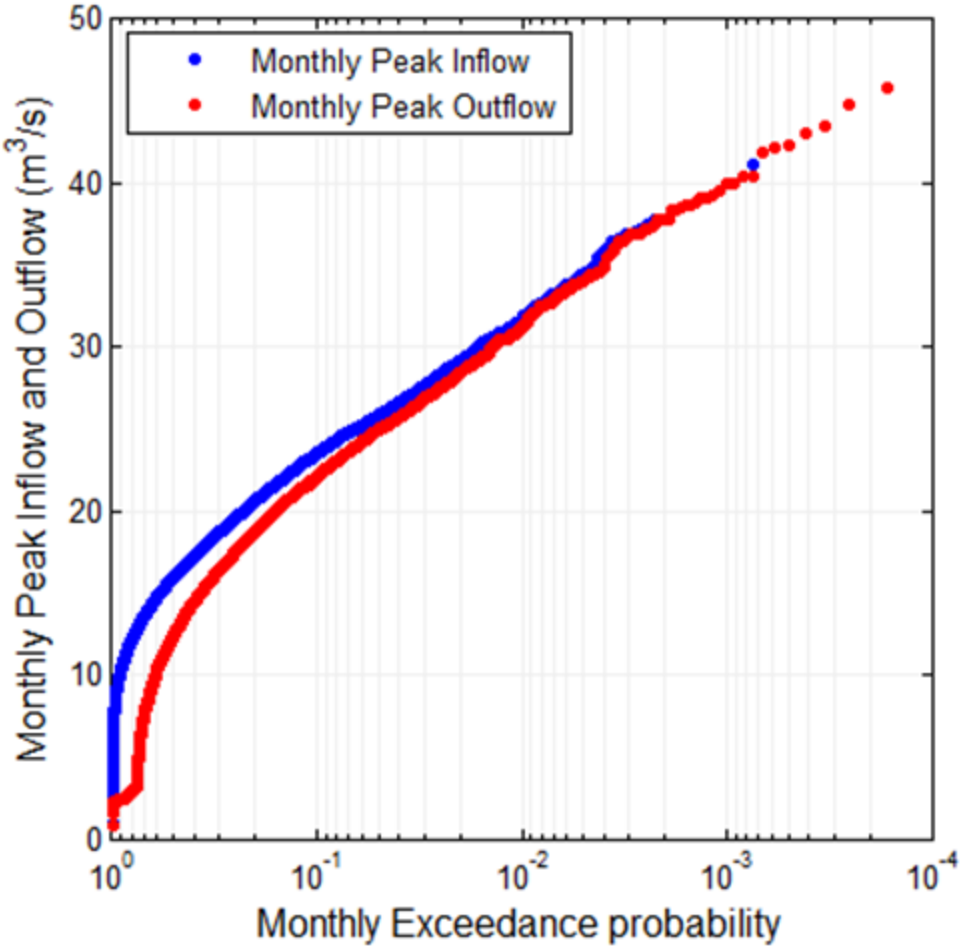

Figure A - 4. An illustration of the reservoir regulated flood frequency curve.

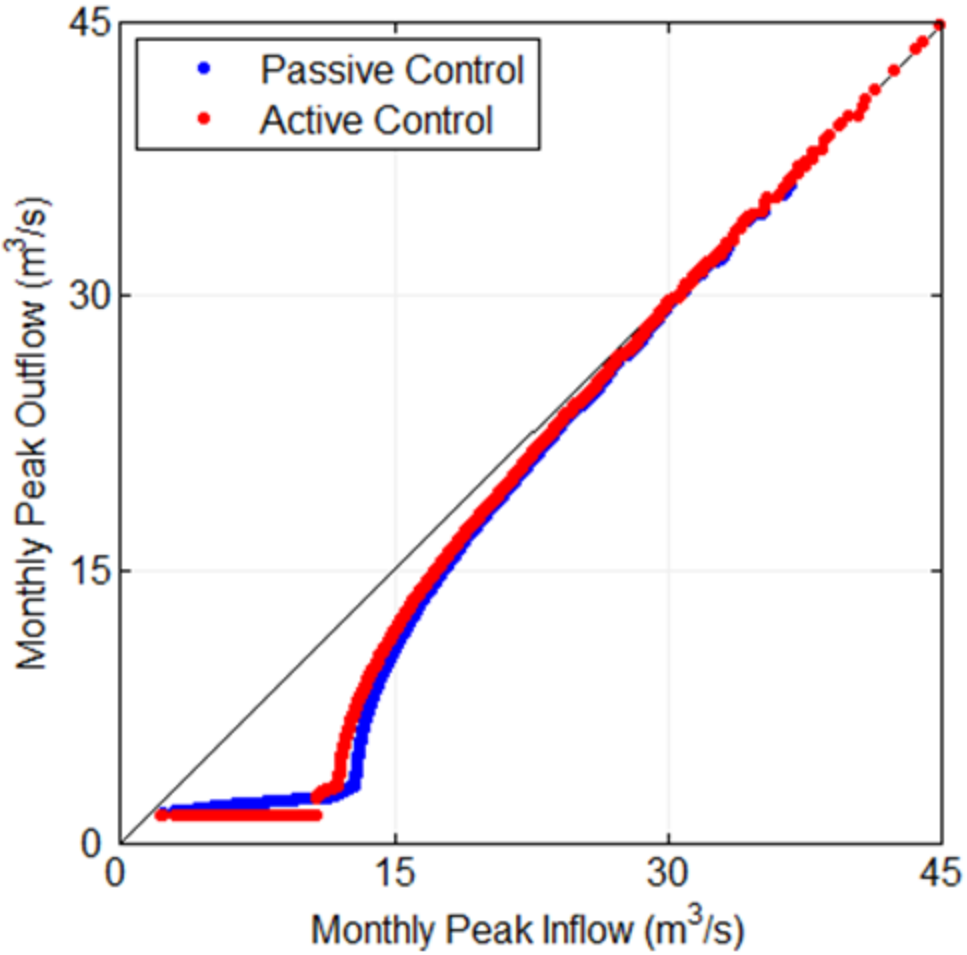

Figure A - 5. The quantile-quantile relationship between unregulated (inflow) and regulated (outflow) flows for active and passive reservoir control strategy.

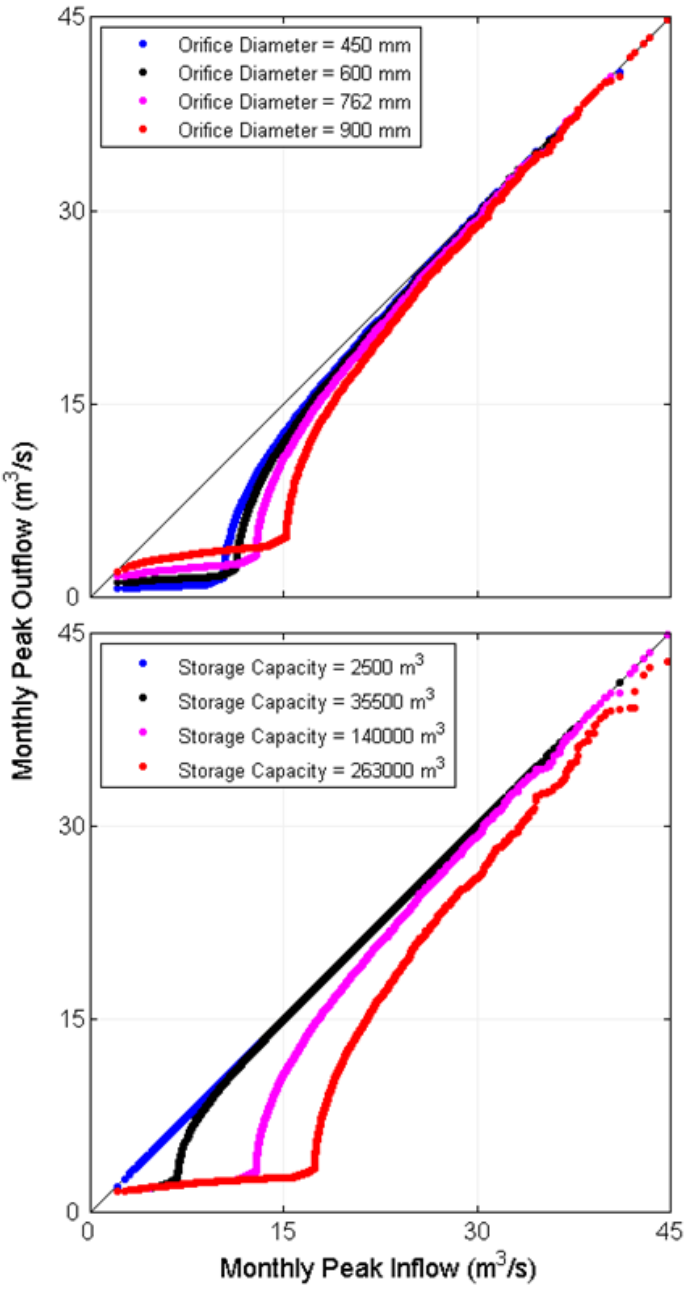

Figure A - 6. The quantile-quantile relationship between unregulated and regulated flows for different outflow gate diameters (450, 650, 762, 900 mm from light to dark, respectively) with a constant storage capacity of 140000 m (top) and for different reservoir storage capacities (2500, 35500, 140000, and 263000 m from light to dark, respectively) with a constant outflow gate diameter of 762 mm (bottom).

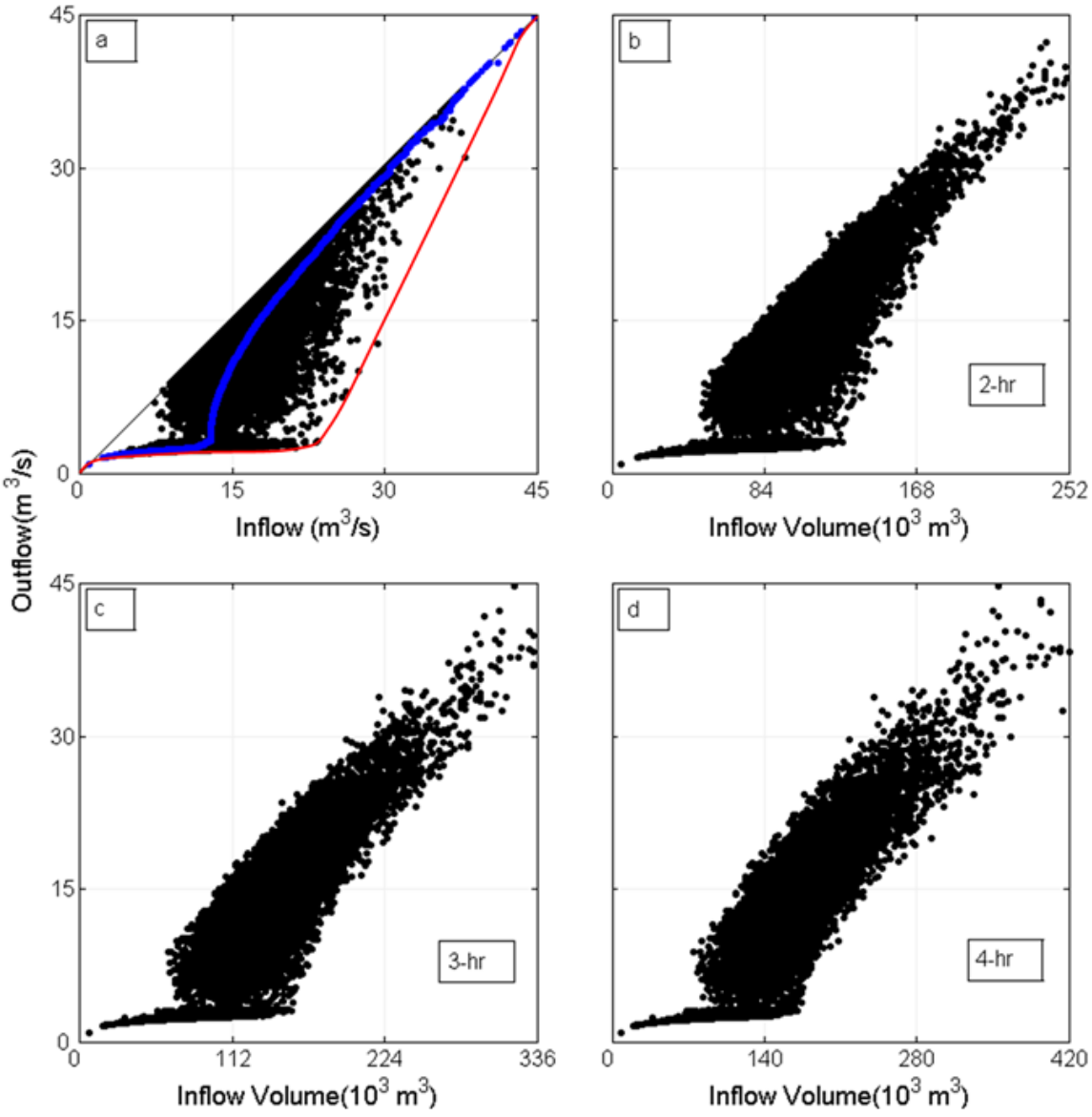

Figure A - 7. The peak monthly inflow to peak monthly outflow event to event and quantile-quantile relationship (a). The remaining plots show the event to event relationship between peak monthly outflow and peak monthly inflow volume of 2-hour (b), 3-hour (c), and 4-hour durations (d).

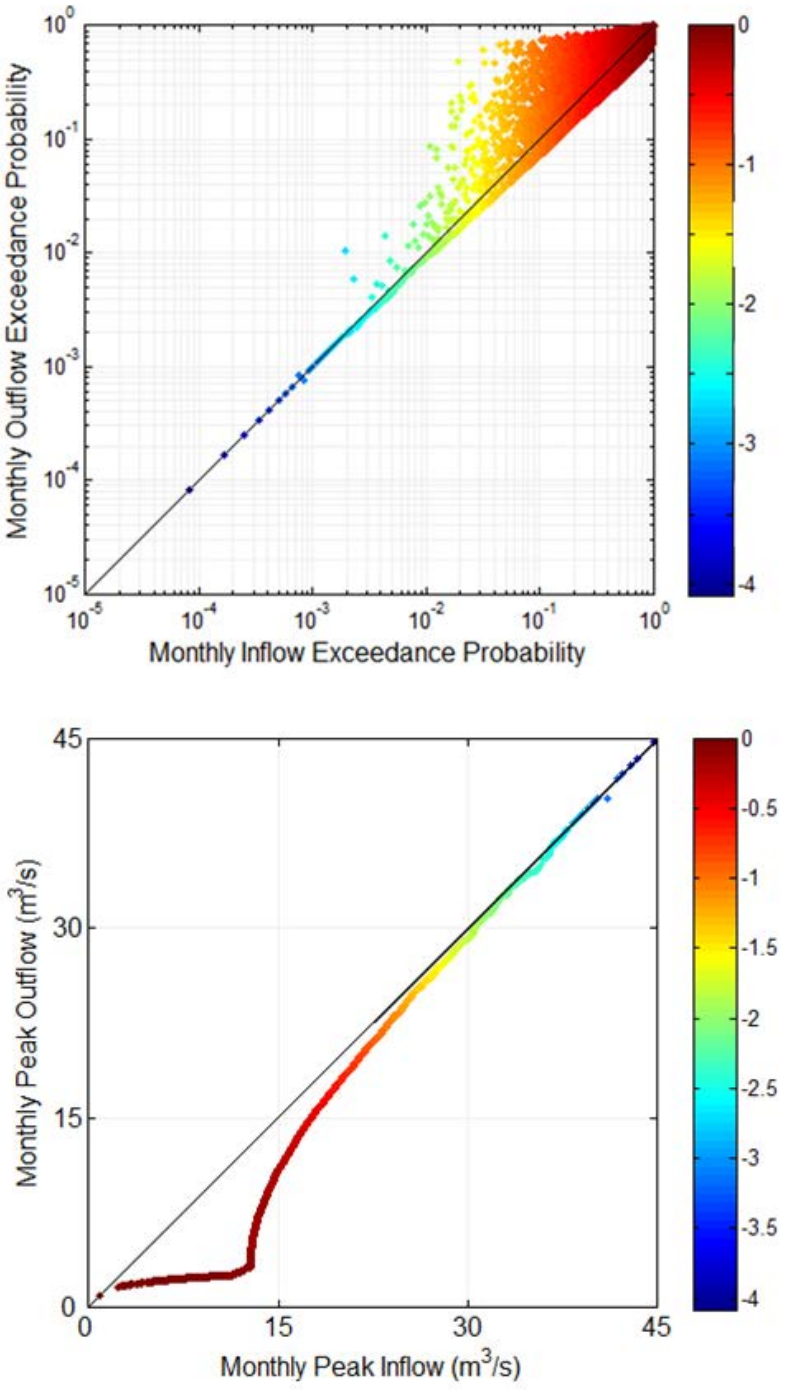

Figure A - 8. The plot of an event to event relationship between monthly inflow and outflow exceedance probabilities (top) and monthly inflow and the outflow quantile-quantile relationship (bottom). The grayscale bar represents the common logarithm of inflow exceedance probabilities.

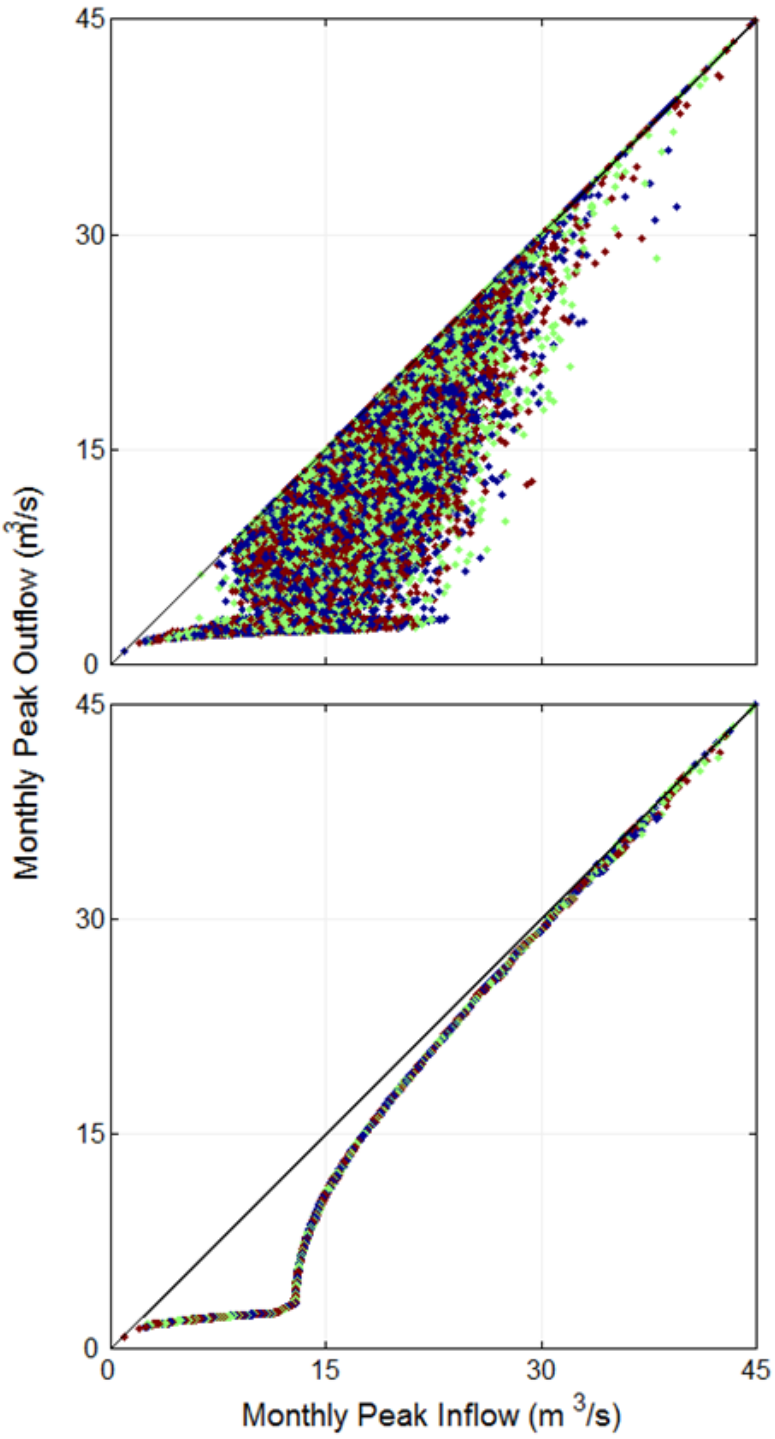

Figure A - 9. A plot of the peak monthly inflow and outflow relationship for three independent realizations of 1000 year inflow-outflow time series (top) and their quantile-quantile plot following the same reservoir operation rule (bottom).

APPENDIX B

ANALYZING THE EFFECT OF THE SPATIAL CONFIGURATION OF FLOOD STORAGE PONDS ON FLOOD FREQUENCY [5]

B.1. Introduction

The results discussed in Appendix A has shown how the design and operation aspects of a single flood storage reservoir affect the flood frequency in the immediate downstream of the dam. Based on the current literature reviewed in section 2.5, it is clear that there is a need to investigate how distributed flood storage reservoirs affect the flood frequency at different locations in the catchment. The main objective of this chapter is, therefore, to build on the results reported in Appendix A and expand the analysis to multiple retention ponds that are spatially organized either *in series* or *in parallel*. In addition to the spatial configuration of flood storage reservoirs, I also address how the storage and release capacity of the reservoirs relative to their location in the drainage network change the regulated flood frequency curve. The remainder of the paper is organized as follows: I begin with a detailed description of the continuous simulation methodology. I then present the results from the simulation of regulated and unregulated peak discharges. Specifically, I discuss the effects of spatial configuration, storage capacity, and release capacity of distributed flood storage reservoirs on flood frequencies. I conclude with a summary of the major findings.

[5] Adapted from Ayalew, T. B., W. F. Krajewski, and R. Mantilla (2015), Insights into expected changes in regulated flood frequencies due to the spatial configuration of flood retention ponds, *Journal of Hydrologic Engineering*, 04015010.

B.2. Experimental setup

Two important factors need to be considered in our experimental setup in order to provide definitive conclusions and to meet the objectives of this study. First, retention ponds get filled and emptied quickly due to their small size. Second, since the catchments that are regulated by the retention ponds are also small, they have a quick runoff response time following a runoff generating rainfall event. These two factors impose the requirement of using high-resolution rainfall-runoff data over long periods of time (~ hundreds of years). This precludes the use of historically observed data because such time series do not exist. To circumvent this problem, I use a continuous simulation approach that has two main components. First, a stochastic rainfall model is used to generate a 1000 year-long rainfall time series with 5-minute resolution. The stochastic rainfall model is discussed in detail in section 7.3.1. Second, the rainfall is used as input into a rainfall-runoff model that is capable of generating both the regulated and unregulated streamflow time series with a temporal resolution of 5-minutes. In this chapter, I use the physically based distributed hydrologic model CUENCAS (Mantilla and Gupta 2005). Outflow from the flood storage reservoirs is calculated according to Equation A-10.

To make a fair comparison among different spatial configurations of retention ponds, it is imperative that ponds that have the same flood storage capacity regulate flows from subcatchments that have the same drainage area. In addition to this, the ponds should be located at an equal distance from the outlet where their effect on the flood frequency is evaluated. This requirement is introduced to discount the effect of flood peak attenuation as the streamflow propagates downstream. With these requirements in

mind, I constructed an artificial catchment drained by a river network that is consistent with the deterministic Mandelbrot-Viseck tree (Mandelbrot and Vicsek 1989). Mandelbrot-Viseck trees have been successfully used in numerous studies that have advanced our understanding of catchment hydrologic processes (e.g., Menabde and Sivapalan 2001).

Figure B-1(a) shows an embedded order four Mandelbrot-Viseck tree (Mantilla et al. 2012). I set each of the channel-links to have the same length (1.4 km) and their associated hillslopes to have the same drainage area (1 km^2). This means that our study basin has a total drainage area of 29 km^2. Also shown in the figure are the proposed sites for retention ponds. I considered two ponds that have the same storage capacity and placed them either *in parallel* or *in series*. Ponds are said to be configured *in parallel* when they are located at sites A and B, and *in series* when they are placed at sites A and D. For comparative purposes, I also simulated one large pond whose flood storage and release capacity is twice as large as those placed either *in parallel* or *in series*. This large pond is placed either at site C or D. Figure B-1(b) shows the width function of the drainage network. As discussed in earlier chapters, the width function is defined as the total number of links in the catchment at a given distance from the outlet (Rodriguez-Iturbe and Rinaldo 1997), and it resembles the instantaneous streamflow response at the outlet following an instantaneous injection of rainfall to the drainage network, assuming that the resulting hydrographs from hillslopes propagate downstream with constant velocity and without attenuation (Gupta et al. 2010).

B.3. Results and Discussion

I begin by first simulating a single "big" pond that is located near the outlet (location D in Fig. 1(a)). It has a storage capacity of 600,000 m^3 and an orifice diameter (OD) of 1.0 m. This will help us evaluate the benefits of the two small ponds that are configured either *in parallel* or *in series* in comparison to a single big pond located near the outlet. The small ponds used in this study have a storage capacity of 300,000 m^3 and an orifice diameter of 0.5 m. To make the comparison fair, the orifice diameter and spillway dimensions of the big pond are selected in such a way that the pond's storage-discharge relationship is equivalent to the storage-discharge relationship of the small ponds that is scaled up by a factor of two (see Figure B-2).

I selected peak discharges from the simulated time series by using the block maxima method to estimate flood frequency. In this method, the maximum peak discharge over a specified time window is selected (Coles 2001), and the resulting peak discharges are independently and identically distributed and follow the generalized extreme value (GEV) distribution (Fisher and Tippett 1928). I used a time window of 30 days as the block size. Using a comparable spatial basin scale and flood retention pond, I have showed in Chapter A that time windows longer than 30 days reduce the selection chance of low flows that directly pass through the pond's orifice, and the resulting flood frequency curve would consequently be incomplete. Figure B-3 shows how a single pond located near the catchment outlet modifies the flood frequency for downstream locations. It can be seen that the regulated flood frequency curve is the same as the unregulated flood frequency curve for low flows of high exceedance probability that go directly through the orifice and for high flows of low exceedance probability that arrive

while the pond is full from an earlier rainfall event. The sharp break in the regulated flood frequency curve marks the transition from orifice-only regulated flows to flows regulated by both the orifice and the spillway.

B.3.1. Ponds configured in parallel

To study the effect of ponds that are configured *in parallel* on the regulated flood frequency, I placed two ponds at locations A and B (shown in Fig. 1(a)) and simulated the following three cases: *i*) both ponds have the same storage (S=300,000 m) and release capacity (OD=0.5 m); *ii*) both ponds have the same storage capacity (S=300,000 m), but the orifice diameter of pond A (OD=1.0 m) is twice the orifice diameter of pond B (OD=0.5 m); and *iii*) pond A (S=450,000 m, OD=0.75 m) has 1.5 times the storage and release capacity of pond B (S=300,000 m, OD=0.5 m). As discussed earlier, a single "big" pond (S=600,000 m, OD=1.0 m) located at D (Figure B-1(a)) is also simulated for the purpose of comparison.

The results presented in Figure B-4(a) show how two ponds that have the same storage and release capacity and are configured *in parallel* change the regulated flood frequency curve in comparison to a single but bigger pond located at the catchment outlet. The results show that, for peak discharge events whose exceedance probability is greater than 0.1, the two small ponds configured *in parallel* control the flood frequency at the catchment outlet in a comparatively similar way to the single but bigger pond located at the outlet. However, the two small ponds configured *in parallel* appear to have a better control over peak discharge events whose exceedance probability is less than 0.1. Note also that, in comparison to the single "big" pond located at the catchment outlet, the ponds configured *in parallel* have the added benefit of reducing flood risk for locations

along the main stem of the river, which do not benefit from the pond located at the catchment outlet. The reason why the two ponds *in parallel* control the regulated flood frequency curve better than the single "big" pond located at the outlet is explained by their locations in the drainage network, which allows them to regulate peak discharges from locations that contribute directly to the maxima of the width function. This means that these ponds regulate the portion of the streamflow response that directly contributes to the peak of the hydrograph at the outlet. This result is consistent with a related and recent study by Yang et al. (2011), who showed that land use and land cover changes in regions that contribute to the peak of the width function of a catchment significantly affect the magnitude of peak discharge at the outlet.

Figure B-4 (b) shows the effect of two ponds configured *in parallel* that have the same storage capacity but different release capacities (OD=1.0 m and OD=0.5 m). The results show that the resulting regulated flood frequency curve is different from the one obtained when the two ponds have the same release capacity. It can be seen that, in comparison to the results presented in Figure B-4 (a), this configuration offers better control over unregulated peak discharges with a lower probability of exceedance. This shows that the release capacity of the two ponds can be configured to systematically control peak discharges that have a wider range of probability of occurrence. This result highlights the added advantage of having multiple ponds rather than having a single bigger pond that offers the capability of regulating peak discharges over a narrower range of exceedance probability. Figure B-4(c) shows the results for the case in which one small pond (S=300,000 m, OD=0.5 m) and one bigger pond (S=450,000 m, OD=0.75 m)

are placed *in parallel*. The resulting regulated flood frequency curve is qualitatively similar to the earlier case ($S = S_B$ =300,000 m, OD=1.0 m, and OD=0.5 m).

I would like to highlight that the better flood reduction capability of the two ponds configured *in parallel* in comparison to the single "big" pond located at the catchment outlet does not imply that the two small ponds make a better flood mitigation project. I acknowledge that a more detailed cost-benefit analysis of the two alternatives may yield a different result. For example, a preliminary analysis of the construction costs using the wet retention pond construction cost formula presented in Young et al. (1996) reveals that the single "big" pond is approximately 15% cheaper than the two small ponds configured *in parallel*. However, as discussed above, the two small ponds benefit a larger proportion of areas along the main stem of the drainage network. This simple exercise indicates that any final decision should be based on quantifying costs and benefits corresponding to the sets of flood retention pond design alternatives being considered. Such an analysis is beyond the scope of this study.

B.3.2. Ponds configured in series

Two ponds were placed at locations A and D (Figure B-1(a)), and the following five cases were investigated: *i*) both ponds have the same storage (S=300,000 m) and release capacity (OD=0.5 m); *ii*) both ponds have the same storage capacity (S=300,000 m) but the orifice diameter of the upstream pond (OD=1.0 m) is twice the orifice diameter of the downstream pond (OD_D=0.5 m); *iii*) both ponds have the same storage capacity (S=300,000 m) but the orifice diameter of the upstream pond (OD=0.5 m) is half the orifice diameter of the downstream pond (OD_D=1.0 m); *iv*) the upstream pond (S=450,000m, OD=0.75 m) has 1.5 times the storage and release capacity of the

downstream pond (S_D=300,000m, OD_D=0.5 m); and *v*) the downstream pond (S_D=450,000 m, OD_D=0.75 m) has 1.5 times the storage and release capacity of the upstream pond (S=300,000m, OD=0.5 m). For comparative purposes, a single "big" pond (S=600,000m, OD=1.0 m) that is located at D is also simulated.

The results presented in Figure B-5(a) show that, when compared to the single bigger pond located at the outlet, the two ponds *in series* perform better than the single "big" pond in terms of controlling peak discharges whose probabilities of exceedance is less than 0.05. However, the single pond located at the outlet controls peak discharges with high exceedance probability ($0.05<p<0.3$) better than the ponds *in series*. The results also show that the regulated flood frequency curve of flows controlled by ponds *in series* has a different feature than when the flow is controlled by ponds *in parallel*. It can be seen in Figure B-5(a) that the regulated flood frequency curve (black line) appears to converge towards the unregulated flood frequency curve for exceedance probability value of around 0.5 before diverging again. This characteristic becomes more apparent when the upstream pond has higher release capacity (black line in Figure B-5(b)) or higher storage capacity (black line in Figure B-5(c)) than the downstream pond. This means that the spatial configuration of ponds and their storage and release capacities relative to their location in the drainage network will introduce additional breaks in the slope of the regulated flood frequency curve.

An important operational question regarding ponds *in series* concerns which of the two ponds should be emptied first during a flood event. I simulated two cases where the release capacity of one of the ponds is greater than the other. In this way, I was able to mimic what happens to the regulated flood frequency curve when either of the ponds is

emptied faster than the other. The results presented in Figure B-5(b) show that better control over peak discharges that have lower exceedance probability is achieved when the upstream pond has a greater release capacity than the downstream pond (black line). This is contrary to the existing reservoir operation strategy where it is recommended to empty the downstream pond first (Lund and Guzman 1999 and literature cited therein). The physical reason behind our result is rooted in the location of the upstream pond in the drainage network, which allows it to control the bulk of the streamflow that contributes to the peak discharge at the outlet. This means that waiting for the next flood event with the maximum possible available flood storage capacity in the upstream pond warrants the maximum possible reduction in peak discharges of low probability of exceedance at the outlet.

An additional important question concerning ponds *in series* is that, given the possibility of building two ponds with different storage capacities, where should the bigger pond be placed relative to the smaller pond? To address this, I simulated two ponds *in series* where one of the ponds has 1.5 times the storage and release capacity of the other. The results presented in Figure B-5(c) show those peak discharges with lower exceedance probability are better controlled when the bigger pond is placed in the upstream section (black line). This result is again explained by the location of the upstream pond in the drainage network. Kusumastuti et al. (2008b) arrived at a similar conclusion after investigating the effect of multiple lakes *in series* on the peak discharge frequency at the catchment outlet.

B.3.3. Comparison of the effects of ponds in series and in parallel

All of the results discussed thus far have revealed how retention ponds configured either *in parallel* or *in series* control the regulated flood frequency curve. Additional important questions that are not yet addressed include: which of the two spatial configurations of retention ponds (i.e., ponds *in parallel* or *in series*) is better at controlling the regulated flood frequency? and if we have the resource to build only one pond, where in the drainage network should it be placed?

Figure B-6(a) shows the results from simulating two ponds that have the same flood storage and release capacity but are configured either *in parallel* or *in series*. It can be seen that, when compared at the catchment outlet, ponds configured *in parallel* perform better at controlling peak discharges with exceedance probability ranging between 0.05 and 0.5. It can also be seen that both spatial configurations of ponds control peak discharges with lower probabilities of exceedance comparatively equally. However, it is intuitively clear that the ponds configured *in parallel* offer larger reductions of flood peaks for those locations along the main stem of the drainage network (i.e, from location A/B to D as shown in Figure B-1). These locations will not experience similar flood risk reduction benefit if the ponds are configured *in series*. Considering the fact that the two ponds have the same storage and release capacities and hence the same construction cost, the parallel configuration of the ponds warrant a better flood mitigation project due to its above mentioned superior capability of reducing peak discharges for larger portions of the catchment.

I also simulated a bigger pond (S=600,000m; OD=1.0 m) that is placed either at C or D (see Fig. 1). The results presented in Figure B-6(b) show that a single pond located

at C performs better than a single pond that is located at D (i.e., closer to the outlet) at controlling peak discharges whose probability of exceedance is less than 0.1, whereas the pond placed at the outlet does a better job of controlling peak discharges of higher probability of exceedance ($p>0.1$). This is again attributed to the fact that the pond at location C has greater control over flows that contribute to the peak of the hydrograph observed at the catchment outlet. The same argument is behind the reason why ponds configured *in parallel* and placed in the upstream section of the catchment outperform ponds configured *in series*. These results show that, in addition to the storage and release capacities of a pond; its location in the drainage network plays a significant role in determining its peak discharge reduction capability.

B.3.4. Effect of ponds on peak flood reduction at different catchment spatial scales

The results discussed thus far reveal how different spatial configurations of retention ponds modify the flood frequency at the outlet. The resulting regulated flood frequency comparisons at the catchment outlet has enabled us to gain insights into the optimal spatial configuration of retention ponds and the design of their release structures, or their operation, according to their location in the drainage network. An important remaining question is, how do the different spatial configurations of ponds affect the flood frequency at different locations in the catchment? To address this question, I calculated the percentage peak discharge reduction due to the ponds as a function of the probability of exceedance of the regulated peak discharge at two different locations in the catchment, namely location C and D (see Figure B-1). It is clear that the catchment drainage area increases as we move from C to D. I calculated the percentage peak discharge reduction as the ratio of the difference between unregulated and regulated peak

discharges to the unregulated peak discharge. This is done for ponds configured *in parallel*, *in series*, and a single "big" pond located in the upstream section of the catchment (location C).

The results presented in Figure B-7 show that the percentage peak discharge reduction due to construction of retention ponds initially increases with decreasing probability of exceedance before starting to decrease as the probability of exceedance decreases further. The maximum peak discharge reduction occurs at a probability of exceedance value that corresponds to the point where the flow transitions from orifice only regulated flow to orifice and spillway regulated flow, i.e., when the spillway is overtopped. This point also marks the break observed in the slope of the regulated flood frequency curve (see, for example, Figure B-6). In particular, the results presented in Figure B-7(a) show that when the ponds are configured *in parallel* the percentage peak discharge reduction reduces in the downstream direction for events whose probability of exceedance range between 0.06 and 0.8. Figure B-7(b) show the percentage peak discharge reduction for the case where the ponds are configured *in series*. It can be seen that the percentage peak discharge reduction increases in the downstream direction for peak discharges with exceedance probability of greater than 0.3 whereas the opposite is true for peak discharges whose exceedance probability is between 0.02 and 0.3, in which case the percentage peak discharge reduction in the upstream section of the catchment (black line) is greater than the corresponding reduction at the outlet (broken grey line). Comparison of the percentage peak discharge reduction due to ponds configured *in series* (Figure B-7(b)) and *in parallel* (Figure B-7(a)) reveals that, as discussed earlier, ponds configured *in parallel* offer greater reduction of peak discharge magnitude over a wider

range of exceedance probability at both locations in the catchment. Finally, the results shown in Figure B-7(c) reveal how the effect of a single bigger pond located in the upstream section of the catchment on the flood frequency changes in the downstream direction. It can be seen that the percentage peak discharge reduction reduces in the downstream direction for peak discharges whose exceedance probability ranges between 0.04 and 0.7.

The results discussed above shows that the flood reduction benefit of the retention ponds generally decreases in the downstream direction for peak discharge events whose exceedance probability range approximately between 0.05 and 0.8. However, for those events whose probability of exceedance is less than 0.05, it appears that the percentage peak discharge reduction at the upstream section of the catchment (location C) and the catchment outlet are similar. This is true due to the small size of the catchment I have investigated. However, it should be expected that the percentage peak discharge reduction should also decrease in the downstream direction for low exceedance probability events as the catchment gets bigger. This is because two important catchment processes become dominant as the catchment gets bigger and the number of retention ponds remains constant. First, the proportion of streamflow that comes from unregulated subcathments and contributes to the peak discharge at bigger catchment scales increases with increasing catchment area. This leads to a reduction in the flood mitigation benefit of the retention ponds in the downstream direction. Secondly, the role of the space-time rainfall variability on the observed peak discharge reduction becomes significant as the catchment gets bigger. As a result, a scenario in which peak discharges observed at bigger catchment scales results from a rainfall event that occurred in subcatchments that

are not regulated by the retention ponds will become more common. This means that peak discharges with a lower probability of exceedance could occur at downstream locations purely due to a rainfall event that occurred in the subcatchments that are not regulated by the retention pond(s). This will also result in the reduction of the flood mitigation benefits of the ponds at locations far downstream. Our argument is supported by the findings of Smith et al. (2010) who showed through analysis of observational data from the Delaware River basin (USA) that the effect of reservoirs on flood frequency for locations far downstream from a dam is limited. To conclude, an important insight that we gained from these results is that, since the effect of reservoirs on the flood frequency is primarily local, distributed storages will have the added value of distributing the flood mitigation benefits across the catchment.

B.4. Summary and Conclusion

A continuous simulation approach is adopted in order to investigate how different spatial configurations of retention ponds control the regulated flood frequency curve. This approach used a stochastic rainfall model that is capable of reproducing a sub-hourly rainfall structure (Cowpertwait et al. 2007) to generate a 1000 year-long rainfall time series that has 5 minute resolution, which is an important requirement when simulating small scale catchments such as the one used in this study. The rainfall time series was used as input into the hydrologic model CUENCAS (Mantilla and Gupta 2005) that is configured for an order four Mandelbrot-Viseck tree (Mandelbrot and Vicsek 1989). The resulting regulated and unregulated streamflow time series at the catchment outlet were analyzed by selecting peak discharges using the method of block maxima. The results showed that the spatial configuration of the retention ponds and the storage and release

capacity of the ponds relative to their location in the drainage network systematically control the magnitude of the departure of the regulated flood frequency curve from the unregulated flood frequency curve, its slope, and the recurrence interval at which the slope breaks. Three important insights emerge from analysis of the results:

1) Retention ponds that are configured *in parallel* have greater control over flood peaks with low to medium probabilities of exceedance when compared to ponds that have the same storage and release capacity but are configured *in series*. The results also show that ponds *in parallel* regulate the flood frequency comparatively similarly to a single, bigger pond whose storage and release capacity is twice that of the small ponds and that is located at the catchment outlet. Considering also that the comparison is made at the catchment outlet, the ponds configured *in parallel* have the added value of reducing the flood risk for locations between the ponds and the catchment outlet where the bigger pond is located. Furthermore, the results also show that the parallel configuration of ponds enables control over a wider range of peak discharge recurrence intervals, which can be achieved by setting the two ponds to have different storage and/or release capacities. This superior capability of ponds configured *in parallel* is attributable to their location in the drainage network that enables them to regulate flows that contribute to the width function maxima. These results highlight the need to account for the geomorphic structure of the drainage network while selecting potential flood retention pond sites.

2) When the retention ponds are configured *in series*, the results show that emptying the upstream pond before the downstream pond, which can be achieved by setting the upstream pond to have a greater release capacity than the downstream pond, offers

greater control over low probability peak discharges. This finding is contrary to existing operational practices that recommend emptying the downstream reservoir first (Lund and Guzman 1999 and literature cited therein). Furthermore, the results also show that, if we have to build two ponds that have different storage capacities *in series*, putting the bigger pond upstream of the smaller pond will lead to better control over low probability peak discharges. Moreover, the results show that if we only have to build a single big pond, it is better to place it at the upstream sections of the catchment that contribute to the maxima of the width function. In this way, greater control over lower probability peak discharges can be achieved.

3) The results also show that, for locations downstream from the retention ponds, the percentage peak discharge reduction initially increases with decreasing probability of exceedance before starting to decrease as the probability of exceedance increases further. The maximum possible reduction happens for those events that fill the ponds but do not flow over the spillway. The results also show that the flood control benefit of ponds is mainly local as their flood reduction benefits quickly reduce in the downstream direction. This is mainly because, for a fixed number of retention ponds, the proportion of unregulated subcatchments that contribute to the peak discharge at the outlet increases in the downstream direction. Moreover, we argue that the flood reduction benefits of retention ponds will further reduce in the downstream direction, i.e., as the catchment gets bigger, at which scale the effect of the space-time variability of rainfall on the regulated flood frequency becomes significant. This insight can explain findings from data analyses by Smith et al.

(2010), who demonstrated that flood control reservoirs have little peak discharge reduction capability at locations farther downstream from the reservoirs.

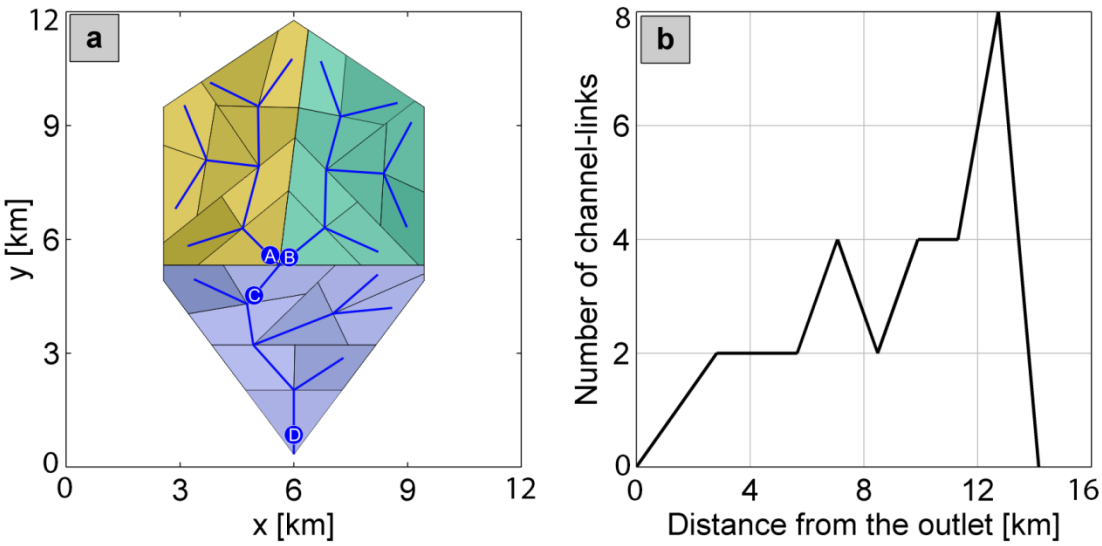

Figure B - 1. (a) The drainage network of the hypothetical watershed and the proposed flood retention pond sites and (b) the width function of the drainage network as evaluated at the outlet.

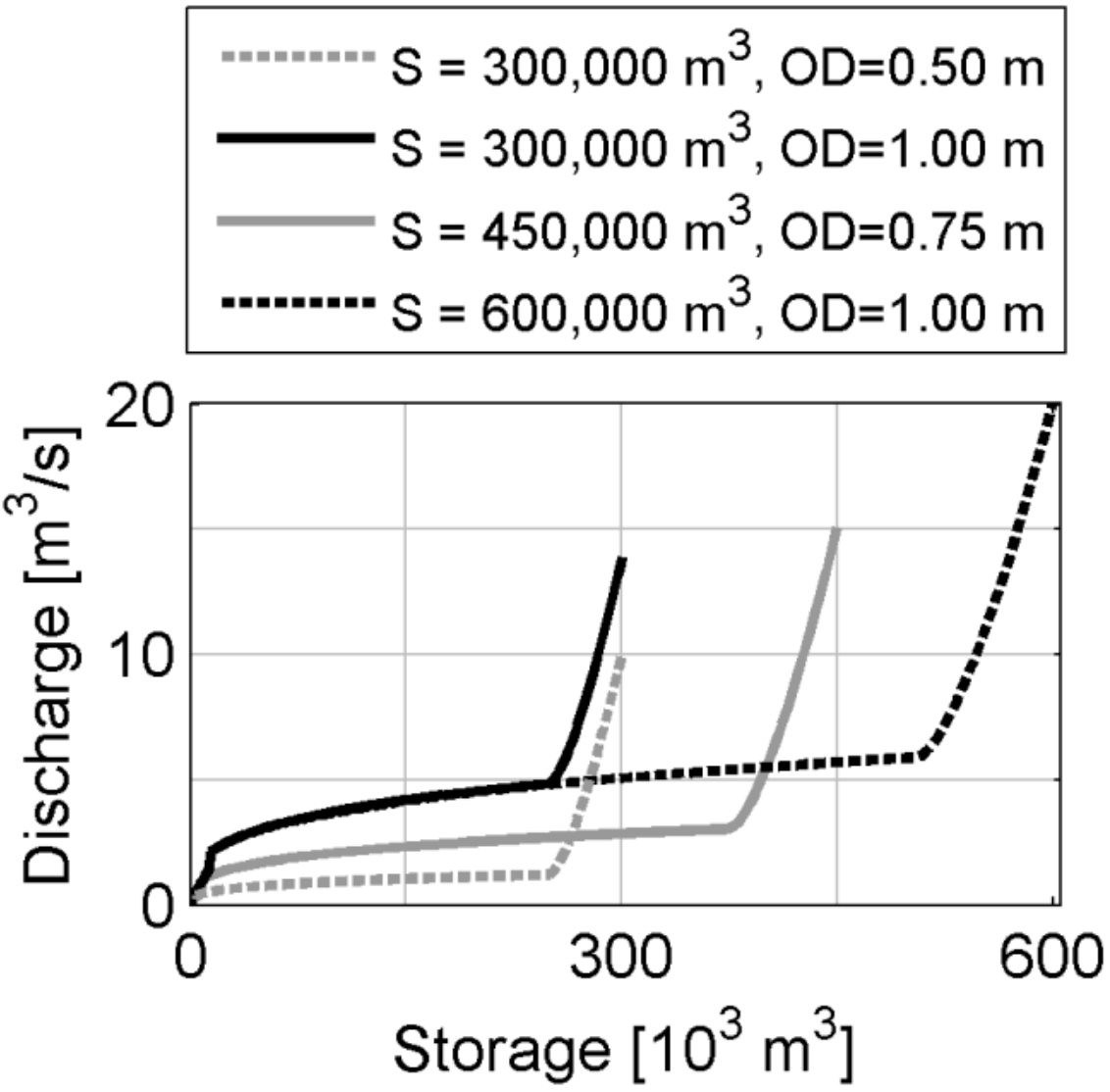

Figure B - 2. Storage-discharge relationships of all the retention ponds used in this study.

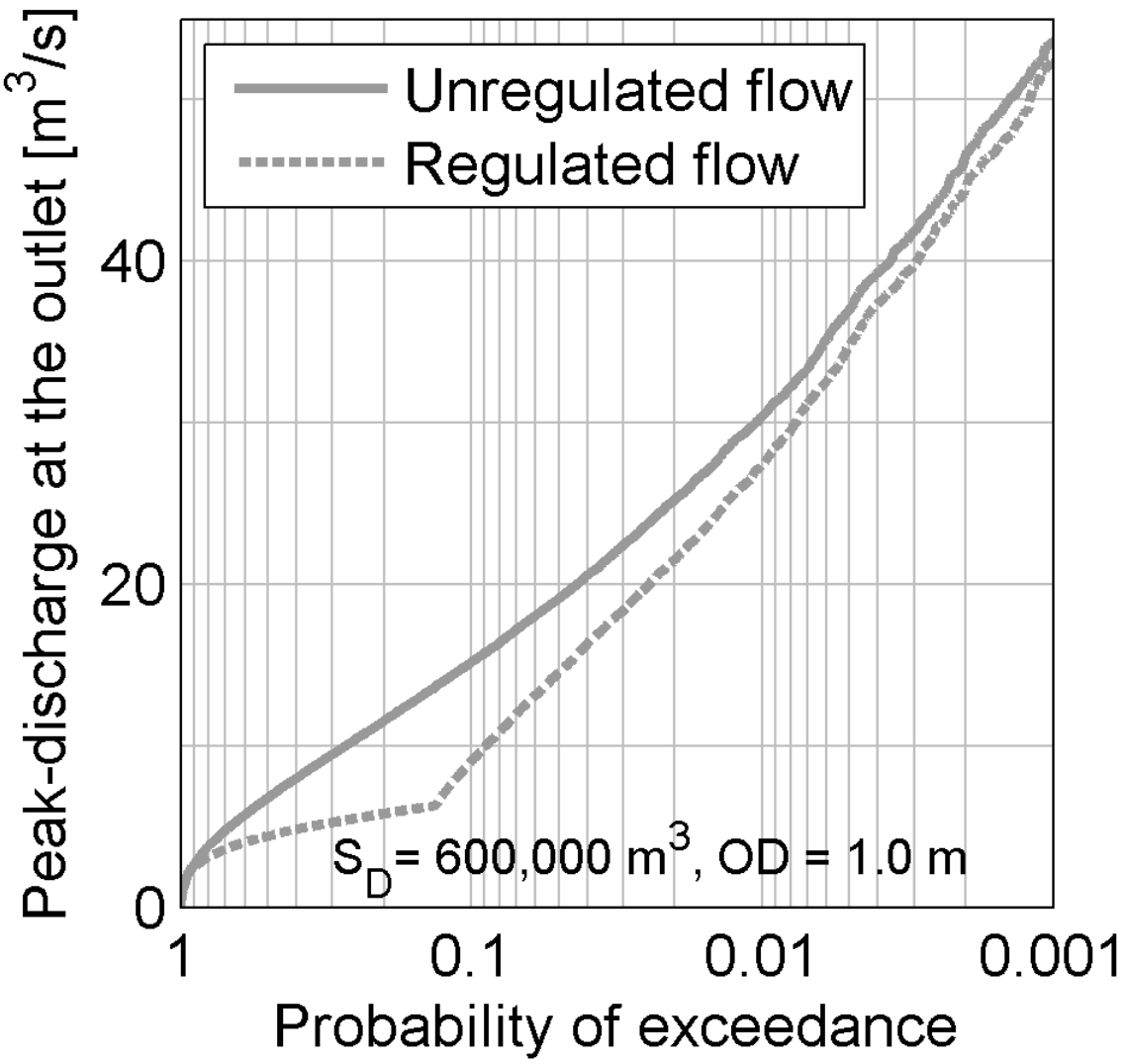

Figure B - 3. Comparison of the regulated and unregulated flood frequency curve at the catchment outlet. The flow is regulated by a single flood retention pond located near the outlet (location D in Figure B-1) that has a storage capacity (S) of 600,000 m^3 and an orifice diameter (OD) of 1.0 m.

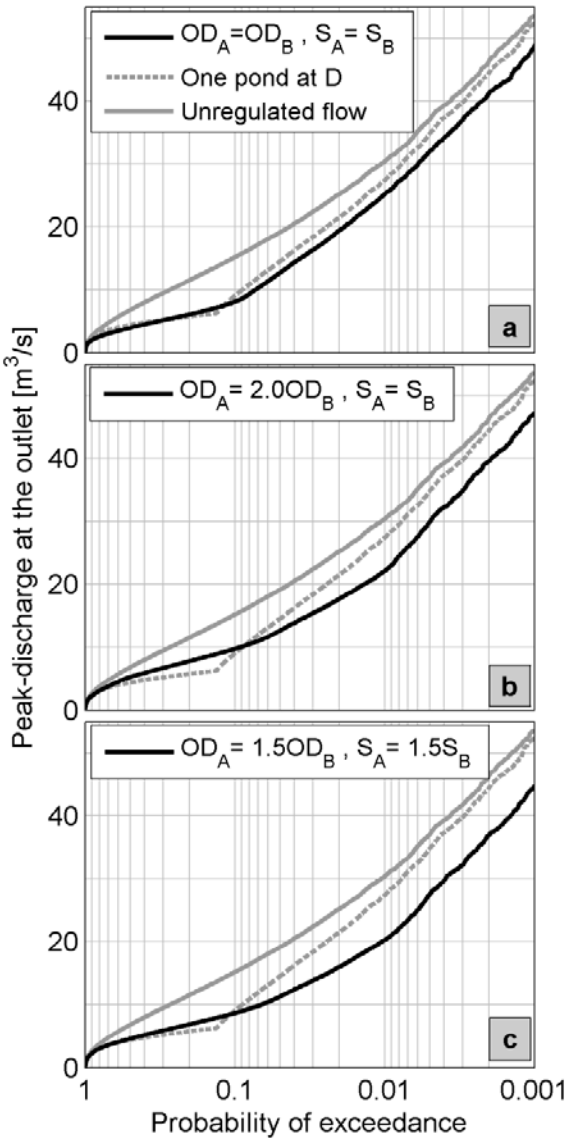

Figure B - 4. Probability of exceedance plot of unregulated and regulated flows for the cases where the two ponds configured in parallel have (a) the same storage (S=300,000 m^3) and release capacity (OD=0.5 m); (b) the same storage capacity (S=300,000 m^3) but the orifice diameter of pond A (OD_A=1.0 m) is twice the orifice diameter of pond B (OD_B=0.5 m); and (c) pond A (S_A=450,000 m^3, OD_A=0.75 m) has 1.5 times the storage and release capacity of pond B (S_B=300,000 m^3, OD_B=0.5 m). The locations of the ponds is shown in Figure B-1.

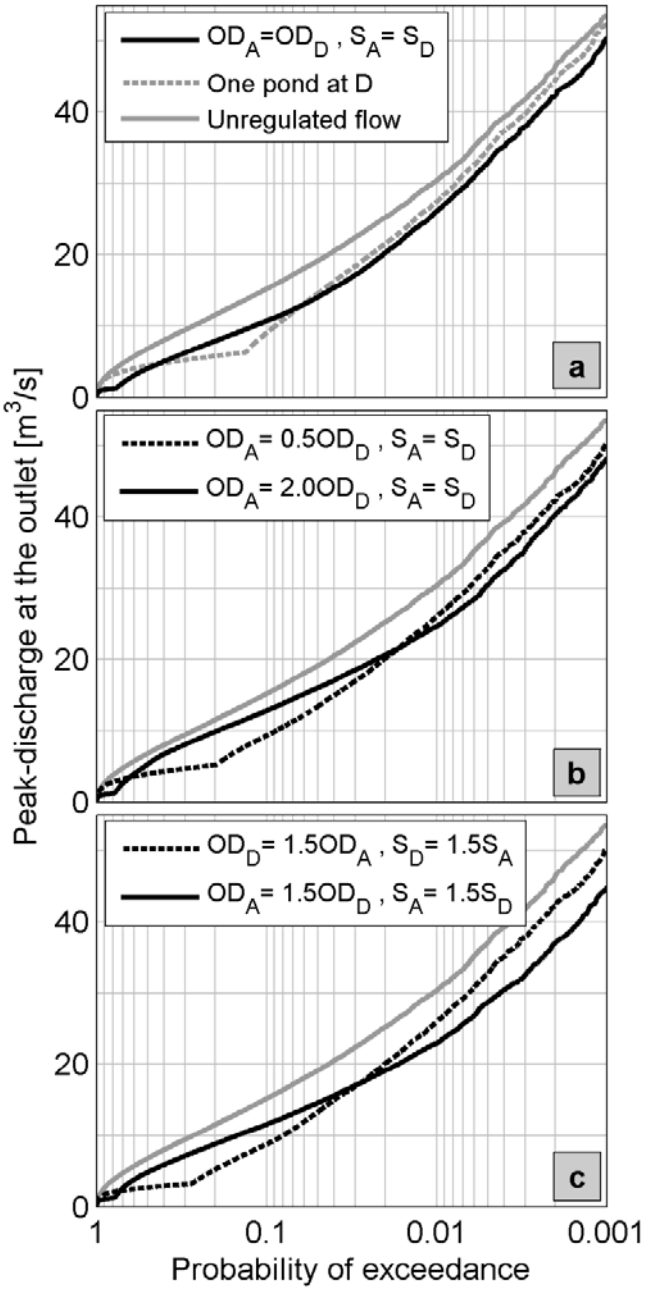

Figure B - 5. Probability of exceedance plot of unregulated and regulated flows for the cases in which the two ponds configured in series have (a) the same storage (S) and release capacity (orifice diameter, OD); (b) the same storage capacity but different release capacities; and (c) different storage and release capacities. The locations of the ponds is shown in Figure B-1.

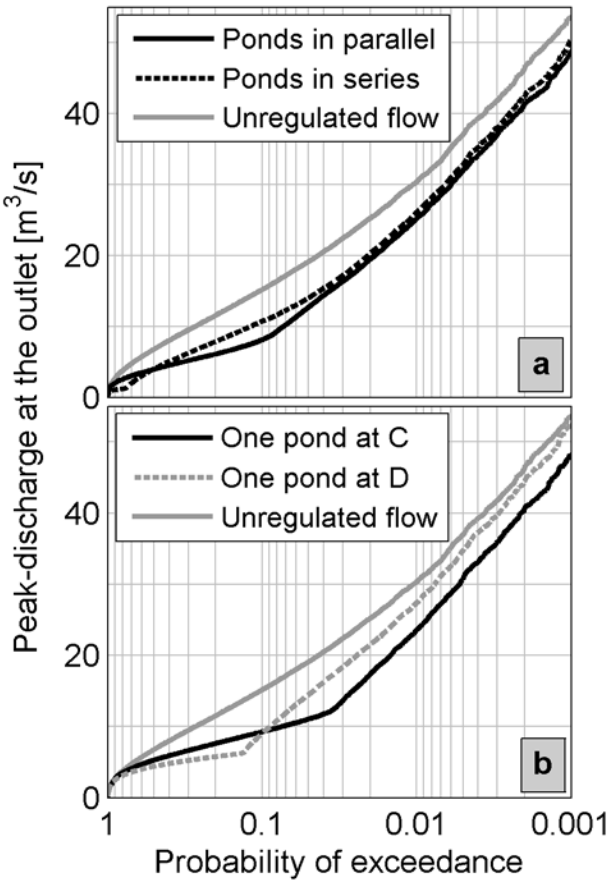

Figure B - 6. Comparison of (a) the flood frequency controlling capability of ponds in parallel and in series (storage capacity S=300,000 m^3 and orifice diameter OD=0.5 m) and (b) a single pond (S = 600,000 m^3 and OD = 1.0 m) placed at different locations in the catchment. The comparisons are made at the catchment outlet.

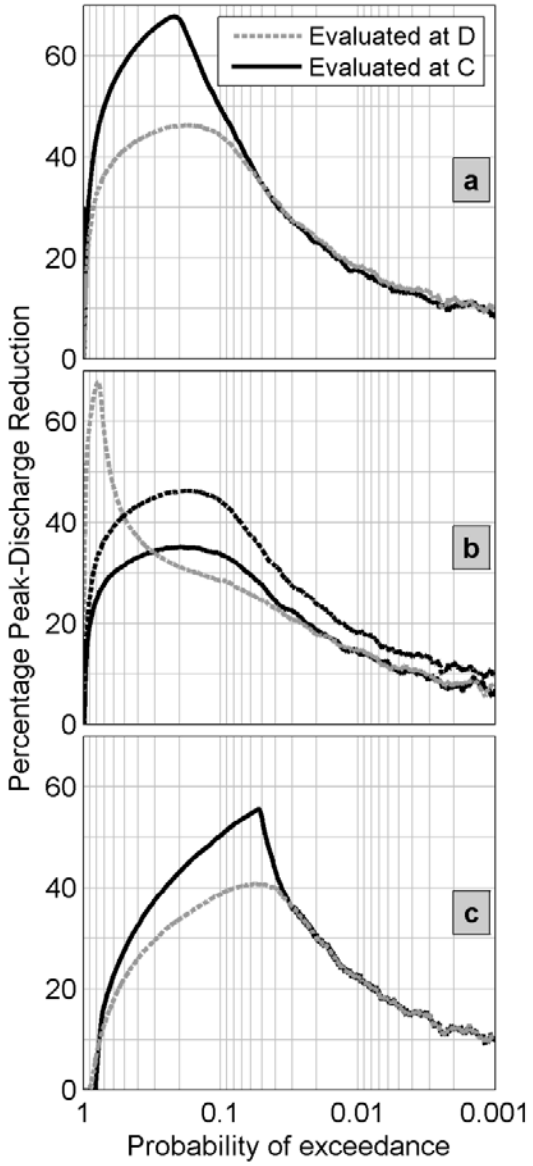

Figure B - 7. Comparison of the percentage peak-discharge reduction of flood retention ponds that are configured (a) in parallel; (b) in series; and (c) a single bigger pond that is located at location C in the upstream section of the catchment. The comparisons are made at locations C and D as shown in Figure B-1. The ponds that are configured either in parallel or in series have a storage capacity of 300, 000 m^3 and an orifice diameter of 0.5 m whereas the single "big" pond located at C has a storage capacity of 600,000 m^3 and an orifice diameter of 1.0 m.

REFERENCES

Acreman, M. C. (1990). "A Simple Stochastic-Model of Hourly Rainfall for Farnborough, England." *Hydrolog Sci J*, 35(2), 119-148.

Anderson, A. E., Weiler, M., Alila, Y., and Hudson, R. O. (2009). "Subsurface flow velocities in a hillslope with lateral preferential flow." *Water Resources Research*, 45(11), W11407-W11407.

Anderson, S. P., Dietrich, W. E., Montgomery, D. R., Torres, R., Conrad, M. E., and Loague, K. (1997). "Subsurface flow paths in a steep, unchanneled catchment." *Water Resources Research*, 33(12), 2637-2653.

Aronica, G. T., and Candela, A. (2007). "Derivation of flood frequency curves in poorly gauged Mediterranean catchments using a simple stochastic hydrological rainfall-runoff model." *Journal of Hydrology*, 347(1–2), 132-142.

Asquith, W. H., and Slade, R. M. (1997). *Regional equations for estimation of peak-streamflow frequency for natural basins in Texas*, US Department of the Interior, US Geological Survey.

Ayalew, T. B., Krajewski, W. F., and Mantilla, R. (2013). "Exploring the Effect of Reservoir Storage on Peak Discharge Frequency." *Journal of Hydrologic Engineering*, 18(12), 1697-1708.

Ayalew, T. B., Krajewski, W. F., and Mantilla, R. (2014). "Connecting the power-law scaling structure of peak-discharges to spatially variable rainfall and catchment physical properties." *Advances in Water Resources*, 71(0), 32-43.

Ayalew, T. B., Krajewski, W. F., and Mantilla, R. (2015). "Insights into Expected Changes in Regulated Flood Frequencies due to the Spatial Configuration of Flood Retention Ponds." *Journal of Hydrologic Engineering*, 04015010.

Ayalew, T. B., Krajewski, W. F., and Mantilla, R. (2015). "Analyzing the effects of excess rainfall properties on the scaling structure of peak-discharges: Insights from a mesoscale river basin." *Water Resources Research*.

Ayalew, T. B., Krajewski, W. F., Mantilla, R., and Small, S. J. (2014). "Exploring the Effects of Hillslope-Channel Link Dynamics and Excess Rainfall Properties on the Scaling Structure of Peak-Discharge." *Advances in Water Resources*, 64, 9-20.

Benson, M. A. (1962). "Factors influencing the occurrence of floods in a humid region of diverse terrain." *Water Supply Paper*, 1580-B.

Benson, M. A. (1964). "Factors influencing the occurrence of floods in the Southwest." *Water Supply Paper*, 1580-D.

Benson, M. A. (1968). "Uniform Flood-Frequency Estimating Methods for Federal Agencies." *Water Resources Research*, 4(5), 891-908.

Benz, R. W., Swamidass, S. J., and Baldi, P. (2008). "Discovery of power-laws in chemical space." *J Chem Inf Model*, 48(6), 1138-1151.

Black, P. E. (1972). "Hydrograph responses to geomorphic model watershed characteristics and precipitation variables." *Journal of Hydrology*, 17(4), 309-329.

Blazkova, S., and Beven, K. (1997). "Flood frequency prediction for data limited catchments in the Czech Republic using a stochastic rainfall model and TOPMODEL." *Journal of Hydrology*, 195(1-4), 256-278.

Blazkova, S., and Beven, K. (2002). "Flood frequency estimation by continuous simulation for a catchment treated as ungauged (with uncertainty)." *Water Resources Research*, 38(8), 1-14.
Blazkova, S., and Beven, K. (2002). "Flood frequency estimation by continuous simulation for a catchment treated as ungauged (with uncertainty)." *Water Resources Research*, 38(8).
Blazkova, S., and Beven, K. (2004). "Flood frequency estimation by continuous simulation of subcatchment rainfalls and discharges with the aim of improving dam safety assessment in a large basin in the Czech Republic." *Journal of Hydrology*, 292(1-4), 153-172.
Bloschl, G., and Sivapalan, M. (1997). "Process controls on regional flood frequency: Coefficient of variation and basin scale." *Water Resources Research*, 33(12), 2967-2980.
Bottcher, A. B., Tremwel, K., and Campbell, K. L. (1995). "Best management practices for water quality improvement in the Lake Okeechobee watershed." *Ecol Eng*, 5(2-3), 341-356.
Botter, G., and Rinaldo, A. (2003). "Scale effect on geomorphologic and kinematic dispersion." *Water Resources Research*, 39(10), 1286-1286.
Botter, G., and Rinaldo, A. (2003). "Scale effect on geomorphologic and kinematic dispersion." *Water Resources Research*, 39(10).
Bradley, A. A., and Potter, K. W. (1992). "Flood Frequency-Analysis of Simulated Flows." *Water Resources Research*, 28(9), 2375-2385.
Brath, A., Montanari, A., and Moretti, G. (2006). "Assessing the effect on flood frequency of land use change via hydrological simulation (with uncertainty)." *Journal of Hydrology*, 324(1-4), 141-153.
Brown, J. H., Gillooly, J. F., Allen, A. P., Savage, V. M., and West, G. B. (2004). "Toward a metabolic theory of ecology." *Ecology*, 85(7), 1771-1789.
Brown, J. H., Gupta, V. K., Li, B. L., Milne, B. T., Restrepo, C., and West, G. B. (2002). "The fractal nature of nature: power laws, ecological complexity and biodiversity." *Philos T R Soc B*, 357(1421), 619-626.
Brutsaert, W. (2005). *Hydrology : an introduction*, Cambridge University Press, Cambridge ; New York.
Brutsaert, W. (2005). *Hydrology: an introduction*, Cambridge University Press.
Cameron, D. S., Beven, K. J., Tawn, J., Blazkova, S., and Naden, P. (1999). "Flood frequency estimation by continuous simulation for a gauged upland catchment (with uncertainty)." *Journal of Hydrology*, 219(3-4), 169-187.
Carpenter, T. M., and Georgakakos, K. P. (2004). "Impacts of parametric and radar rainfall uncertainty on the ensemble streamflow simulations of a distributed hydrologic model." *Journal of Hydrology*, 298, 202-221.
Chen, C.-N., Tsai, C.-H., and Tsai, C.-T. (2007). "Reduction of discharge hydrograph and flood stage resulted from upstream detention ponds." *Hydrological Processes*, 21(25), 3492-3506.
Chorley, R. J., Malm, D. E. G., and Pogorzelski, H. A. (1957). "A New Standard for Estimating Drainage Basin Shape." *Am J Sci*, 255(2), 138-141.
Chow, V. T., Maidment, D. R., and Mays, L. W. (1988). *Applied hydrology*, McGraw-Hill, New York.

Ciach, G. J., Krajewski, W. F., and Villarini, G. (2007). "Product-error-driven uncertainty model for probabilistic quantitative precipitation estimation with NEXRAD data." *Journal of Hydrometeorology*, 8(6), 1325-1347.
Coles, S. (2001). *An Introduction to Statistical Modeling of Extreme Values*, Springer London, London.
Coles, S. (2001). *An introduction to statistical modeling of extreme values*, Springer, London ; New York.
Cowpertwait, P., Isham, V., and Onof, C. (2007). "Point process models of rainfall: developments for fine-scale structure." *Proceedings of the Royal Society A: Mathematical, Physical and Engineering Sciences*, 463(2086), 2569-2587.
Cox, D. R., and Isham, V. (1980). *Point processes*, Chapman and Hall, London ; New York.
Cunha, L. K., Krajewski, W. F., and Mantilla, R. (2011). "A framework for flood risk assessment under nonstationary conditions or in the absence of historical data." *Journal of Flood Risk Management*, 4(1), 3-22.
Cunha, L. K., Mandapaka, P. V., Krajewski, W. F., Mantilla, R., and Bradley, A. A. (2012). "Impact of radar-rainfall error structure on estimated flood magnitude across scales: An investigation based on a parsimonious distributed hydrological model." *Water Resources Research*, 48(10).
D'Odorico, P., and Rigon, R. (2003). "Hillslope and channel contributions to the hydrologic response." *Water Resources Research*, 39(5), 1113-1113.
Dawdy, D. R., Griffis, V. W., and Gupta, V. K. (2012). "Regional Flood-Frequency Analysis: How We Got Here and Where We Are Going." *Journal of Hydrologic Engineering*, 17(9), 953-959.
De Lima, J. L. M. P., and Singh, V. P. (2002). "The influence of the pattern of moving rainstorms on overland flow." *Advances in Water Resources*, 25, 817-828.
Di Lazzaro, M., and Volpi, E. (2011). "Effects of hillslope dynamics and network geometry on the scaling properties of the hydrologic response." *Advances in Water Resources*, 34(11), 1496-1507.
Eagleson, P. S. (1972). "Dynamics of flood frequency." *Water Resources Research*, 8(4), 878-898.
Eash, D. A. (2001). "Techniques for estimating flood-frequency discharges for streams in Iowa." *Water Resources Investigations Report.United States Geological Survey*(4233).
Eash, D. A., Barnes, K. K., and Veilleux, A. G. (2013). "Methods for estimating annual exceedance-probability discharges for streams in Iowa, based on data through water year 2010." *USGS Scientific investigations report 2013-5086*, U.S. Geological Survey,, Reston, Va., 63.
Eaton, B., Church, M., and Ham, D. (2002). "Scaling and regionalization of flood flows in British Columbia, Canada." *Hydrological Processes*, 16, 3245-3263.
Engeland, K., Hisdal, H., and Frigessi, A. (2004). "Practical Extreme Value Modelling of Hydrological Floods and Droughts: A Case Study." *Extremes*, 7(1), 5-30.
Faraway, J. J. (2004). *Linear models with R*, CRC Press, Boca Raton.
Fenton, J. D. (1992). "Reservoir Routing." *Hydrolog Sci J*, 37(3), 233-246.
Ferguson, R. I. (1986). "Hydraulics and Hydraulic Geometry." *Progress in Physical Geography*, 10(1), 1-31.

Fisher, R. A., and Tippett, L. H. C. (1928). "Limiting forms of the frequency distribution of the largest or smallest member of a sample." *Mathematical Proceedings of the Cambridge Philosophical Society*, 24(02), 180-190.

Furey, P. R., and Gupta, V. K. (2005). "Effects of excess rainfall on the temporal variability of observed peak-discharge power laws." *Advances in Water Resources*, 28(11), 1240-1253.

Furey, P. R., and Gupta, V. K. (2007). "Diagnosing peak-discharge power laws observed in rainfall–runoff events in Goodwin Creek experimental watershed." *Advances in Water Resources*, 30(11), 2387-2399.

Furey, P. R., Troutman, B. M., Gupta, V. K., and Krajewski, W. F. (submitted). "Connecting event-based scaling of flood peaks to regional flood frequency relationships." *Journal of Hydrologic Engineering*.

Gabaix, X. (2009). "Power Laws in Economics and Finance." *Annu Rev Econ*, 1, 255-293.

Gallant, A. L., Sadinski, W., Roth, M. F., and Rewa, C. A. (2011). "Changes in historical Iowa land cover as context for assessing the environmental benefits of current and future conservation efforts on agricultural lands." *J Soil Water Conserv*, 66(3), 67a-77a.

Galloway, G. E. (1994). "Sharing the challenge: Floodplain management into the 21st century." *Rept. of the Interagency Floodplain Management Review Committee to the Administration Floodplain Management Task Force.*, U.S. Army Corps of Engineers, Washington D.C., 191p.

Gleason, C. J., and Smith, L. C. (2014). "Toward global mapping of river discharge using satellite images and at-many-stations hydraulic geometry." *Proceedings of the National Academy of Sciences*.

Goldman, D. M. "Quantifying uncertainty in estimates of regulated flood frequency curves." *Proc., Bridging the Gap@ sMeeting the World's Water and Environmental Resources Challenges*, ASCE, 1-13.

Goodrich, D. C., Lane, L. J., Shillito, R. M., Miller, S. N., Syed, K. H., and Woolhiser, D. A. (1997). "Linearity of basin response as a function of scale in a semiarid watershed." *Water Resources Research*, 33(12), 2951-2965.

Grimaldi, S., Petroselli, A., Alonso, G., and Nardi, F. (2010). "Flow time estimation with spatially variable hillslope velocity in ungauged basins." *Advances in Water Resources*, 33(10), 1216-1223.

Guo, J. C. Y., and Urbonas, B. (1996). "Maximized detention volume determined by runoff capture ratio." *J Water Res Pl-Asce*, 122(1), 33-39.

Gupta, V., Waymire, E., and Rodríguez-Iturbe, I. (1986). "On Scales, Gravity and Network Structure in Basin Runoff." *Scale Problems in Hydrology*, V. K. Gupta, I. Rodríguez-Iturbe, and E. F. Wood, eds., Springer Netherlands, 159-184.

Gupta, V. K. (2004). "Emergence of statistical scaling in floods on channel networks from complex runoff dynamics." *Chaos, Solitons & Fractals*, 19(2), 357-365.

Gupta, V. K., Castro, S. L., and Over, T. M. (1996). "On scaling exponents of spatial peak flows from rainfall and river network geometry." *Journal of Hydrology*, 187(1-2), 81-104.

Gupta, V. K., and Dawdy, D. R. (1995). "Physical interpretations of regional variations in the scaling exponents of flood quantiles." *Hydrological Processes*, 9(3-4), 347-361.

Gupta, V. K., Mantilla, R., Krajewski, W. F., and Ayalew, T. B. (submitted). "Natural uncertainty measure for forecasting floods in ungauged basins." *Chaos*.

Gupta, V. K., Mantilla, R., Troutman, B. M., Dawdy, D., and Krajewski, W. F. (2010). "Generalizing a nonlinear geophysical flood theory to medium-sized river networks." *Geophysical Research Letters*, 37(11), L11402-L11402.

Gupta, V. K., and Mesa, O. J. (1988). "Runoff Generation and Hydrologic Response Via Channel Network Geomorphology - Recent Progress and Open Problems." *Journal of Hydrology*, 102(1-4), 3-28.

Gupta, V. K., and Mesa, O. J. (2014). "Horton laws for hydraulic–geometric variables and their scaling exponents in self-similar Tokunaga river networks." *Nonlin. Processes Geophys.*, 21(5), 1007-1025.

Gupta, V. K., Troutman, B. M., and Dawdy, D. R. (2007). "Towards a nonlinear geophysical theory of floods in river networks: an overview of 20 years of progress." *Nonlinear dynamics in geosciences*, 121-151.

Gupta, V. K., and Waymire, E. (1983). "On the Formulation of an Analytical Approach to Hydrologic Response and Similarity at the Basin Scale." *Journal of Hydrology*, 65(1-3), 95-123.

Gupta, V. K., and Waymire, E. (1998). "Spatial variability and scale invariance in hydrologic regionalization." *Scale dependence and scale invariance in hydrology*, 88-135.

Gupta, V. K., Waymire, E., and Wang, C. T. (1980). "A representation of an instantaneous unit hydrograph from geomorphology." *Water Resources Research*, 16(5), 855-862.

Habib, E., Qin, L., Seo, D.-J., Ciach, G. J., and Nelson, B. R. (2013). "Independent Assessment of Incremental Complexity in NWS Multisensor Precipitation Estimator Algorithms." *Journal of Hydrologic Engineering*, 18(2), 143-155.

Hardison, C. H. (1974). "Generalized skew coefficients of annual floods in the United States and their application." *Water Resources Research*, 10(4), 745-752.

Hess, G. W., and Inman, E. J. (1994). *Effects of urban flood-detention reservoirs on peak discharges and flood discharges and flood frequencies, and simulation of flood-detention reservoir outflow hydrographs in two watersheds in Albany, Georgia*, U.S. Dept. of the Interior

U.S. Geological Survey, Earth Science Information Center, Open-file Reports Section, Atlanta, Ga.

Denver, Colo.

Horton, R. E. (1932). "Drainage-basin characteristics." *Eos, Transactions American Geophysical Union*, 13(1), 350-361.

Horton, R. E. (1945). "Erosional Development of Streams and Their Drainage Basins - Hydrophysical Approach to Quantitative Morphology." *Geol Soc Am Bull*, 56(3), 275-370.

Hrachowitz, M., Savenije, H. H. G., Bloschl, G., McDonnell, J. J., Sivapalan, M., Pomeroy, J. W., Arheimer, B., Blume, T., Clark, M. P., Ehret, U., Fenicia, F.,

Freer, J. E., Gelfan, A., Gupta, H. V., Hughes, D. A., Hut, R. W., Montanari, A., Pande, S., Tetzlaff, D., Troch, P. A., Uhlenbrook, S., Wagener, T., Winsemius, H. C., Woods, R. A., Zehe, E., and Cudennec, C. (2013). "A decade of Predictions in Ungauged Basins (PUB)a review." *Hydrolog Sci J*, 58(6), 1198-1255.

Huff, D. D., O'Neill, R. V., Emanuel, W. R., Elwood, J. W., and Newbold, J. D. (1982). "Flow variability and hillslope hydrology." *Earth Surface Processes and Landforms*, 7(1), 91-94.

Huff, F. A., and Angel, J. R. (1992). *Rainfall frequency atlas of the Midwest*, Midwestern Climate Center (Washington, DC and Champaign, Ill. 2204 Griffith Dr., Champaign 61820-7495).

IACWD (1982). *Guidelines for determining flood flow frequency: Bulletin 17B*, U.S. Water Resources Council, Washington, D.C.

Islam, S., Entekhabi, D., Bras, R. L., and Rodriguez-Iturbe, I. (1990). "Parameter-Estimation and Sensitivity Analysis for the Modified Bartlett-Lewis Rectangular Pulses Model of Rainfall." *J Geophys Res-Atmos*, 95(D3), 2093-2100.

Kaczmarska, J. (2011). "Further development of Bartlett–Lewis models for fine-resolution rainfall." University College London, London.

Kalin, L., and Hantush, M. M. (2006). "Hydrologic Modeling of an eastern Pennsylvania watershed with NEXRAD and rain gauge data." *Journal of Hydrologic Engineering*, 11(6), 555-569.

Khaliq, M. N., and Cunnane, C. (1996). "Modelling point rainfall occurrences with the Modified Bartlett-Lewis Rectangular Pulses Model." *Journal of Hydrology*, 180(1-4), 109-138.

Kirchner, J. W. (1993). "Statistical inevitability of Horton's laws and the apparent randomness of stream channel networks." *Geology*, 21(7), 591-594.

Kirkby, M. J. (1976). "Tests of the random network model, and its application to basin hydrology." *Earth Surface Processes*, 1(3), 197-212.

Kitzmiller, D., Miller, D., Fulton, R., and Ding, F. (2013). "Radar and Multisensor Precipitation Estimation Techniques in National Weather Service Hydrologic Operations." *Journal of Hydrologic Engineering*, 18(2), 133-142.

Krajewski, W. F., and Mantilla, R. (2010). "Why Were the 2008 Floods So Large?", C. F. Mutel, ed., University of Iowa Press, Iowa City, 19-30.

Kusumastuti, D. I., Sivapalan, M., Struthers, I., and Reynolds, D. A. (2008). "Thresholds in the storm response of a lake chain system and the occurrence and magnitude of lake overflows: Implications for flood frequency." *Advances in Water Resources*, 31(12), 1651-1661.

Kusumastuti, D. I., Sivapalan, M., Struthers, I., Reynolds, D. A., Murray, K., and Turlach, B. A. (2008). "Thresholds in the storm response of a catchment-lake system and the occurrence and magnitude of lake overflows: Implications for flood frequency." *Water Resources Research*, 44(2).

Lee, M. T., and Delleur, J. W. (1976). "A variable source area model of the rainfall-runoff process based on the Watershed Stream Network." *Water Resources Research*, 12(5), 1029-1036.

Leopold, L. B., and Maddock, T. (1953). "The hydraulic geometry of stream channels and some physiographic implications." *USGS professional paper*(252).

Leopold, L. B., and Miller, J. P. (1956). "Ephemeral streams: Hydraulic factors and their relation to the drainage net." *USGS professional paper*(282-A).
Leopold, L. B., Wolman, M. G., and Miller, J. P. (1964). *Fluvial processes in geomorphology*, W.H. Freeman, San Francisco.
Lima, C. H. R., and Lall, U. (2010). "Spatial scaling in a changing climate: A hierarchical bayesian model for non-stationary multi-site annual maximum and monthly streamflow." *Journal of Hydrology*, 383(3-4), 307-318.
Lund, J. R., and Guzman, J. (1999). "Derived Operating Rules for Reservoirs in Series or in Parallel." *Journal of Water Resources Planning and Management*, 125(3), 143-153.
Main, I. G., Leonard, T., Papasouliotis, O., Hatton, C. G., and Meredith, P. G. (1999). "One slope or two? Detecting statistically significant breaks of slope in geophysical data, with application to fracture scaling relationships." *Geophysical Research Letters*, 26(18), 2801-2804.
Mandapaka, P. V., Krajewski, W. F., Mantilla, R., and Gupta, V. K. (2009). "Dissecting the effect of rainfall variability on the statistical structure of peak flows." *Advances in Water Resources*, 32(10), 1508-1525.
Mandelbrot, B. B. (1983). *The fractal geometry of nature*, W.H. Freeman, New York.
Mandelbrot, B. B., and Vicsek, T. (1989). "Directed recursion models for fractal growth." *Journal of Physics A: Mathematical and General*, 22(9), L377-L383.
Mantilla, R. (2007). "Physical basis of statistical scaling in peak flows and stream flow hydrographs for topologic and spatially embedded random self-similiar channel networks." The University of Colorado.
Mantilla, R., and Gupta, V. K. (2005). "A GIS Numerical Framework to Study the Process Basis of Scaling Statistics in River Networks." *IEEE Geoscience and Remote Sensing Letters*, 2(4), 404-408.
Mantilla, R., Gupta, V. K., and Mesa, O. J. (2006). "Role of coupled flow dynamics and real network structures on Hortonian scaling of peak flows." *Journal of Hydrology*, 322(1-4), 155-167.
Mantilla, R., Gupta, V. K., and Troutman, B. M. (2011). "Scaling of peak flows with constant flow velocity in random self-similar networks." *Nonlinear Processes in Geophysics*, 18(4), 489-502.
Mantilla, R., Gupta, V. K., and Troutman, B. M. (2012). "Extending generalized Horton laws to test embedding algorithms for topologic river networks." *Geomorphology*, 151, 13-26.
Menabde, M., and Sivapalan, M. (2001). "Linking space–time variability of river runoff and rainfall fields: a dynamic approach." *Advances in Water Resources*, 24(9-10), 1001-1014.
Menabde, M., Veitzer, S., Gupta, V. K., and Sivapalan, M. (2001). "Tests of peak flow scaling in simulated self-similar river networks." *Advances in Water Resources*, 24(9-10), 991-999.
Merz, B., and Plate, E. J. (1997). "An analysis of the effects of spatial variability of soil and soil moisture on runoff." *Water Resources Research*, 33, 2909-2922.
Merz, R., and Bloschl, G. (2003). "A process typology of regional floods." *Water Resources Research*, 39(12).

Merz, R., and Blöschl, G. (2009). "A regional analysis of event runoff coefficients with respect to climate and catchment characteristics in Austria." *Water Resources Research*, 45, 1-19.
Merz, R., Blöschl, G., and Parajka, J. (2006). "Spatio-temporal variability of event runoff coefficients." *Journal of Hydrology*, 331, 591-604.
Mesa, O. J., and Mifflin, E. R. (1986). "On the Relative Role of Hillslope and Network Geometry in Hydrologic Response." *Scale Problems in Hydrology*, V. K. Gupta, I. Rodríguez-Iturbe, and E. F. Wood, eds., Springer Netherlands, 1-17.
Mitzenmacher, M. (2003). "A Brief History of Generative Models for Power Law and Lognormal Distributions." 226-251.
Morisawa, M. (1958). "Measurement of Drainage-Basin Outline Form." *J Geol*, 66(5), 587-591.
Morrison, J., and Smith, J. (2001). "Scaling Properties of Flood Peaks." *Extremes*, 4(1), 5-22.
Mulvany, T. J. (1850). "On the use of self-registering rain and flood gauges." *Making Observations of the Relations of Rain Fall and Flood Discharges in a Given Catchment.Transactions and Minutes of the Proceedings of the Institute of Civil Engineers of Ireland, Dublin, Ireland, Session*, 1.
Mutel, C. F. (2010). *A watershed year : anatomy of the Iowa floods of 2008*, University of Iowa Press, Iowa City.
Nehrke, S. M., and Roesner, L. A. (2004). "Effects of Design Practice for Flood Control and Best Management Practices on the Flow-Frequency Curve." *Journal of Water Resources Planning and Management*, 130(2), 131-139.
Newman, M. E. J. (2005). "Power laws, Pareto distributions and Zipf's law." *Contemporary Physics*, 46(5), 323-351.
Niemczynowicz, J. (1984). "Investigation of the Influence of Rainfall Movement on Runoff Hydrograph."
O'Connell, P. (1868). "On the relation of the freshwater floods of rivers to the areas and physical features of their basins and on a method of classifying rivers and streams with reference to the magnitude of their floods." *Minutes Proceedings of the Institution of Civil Engineers*, 27(1868), 204-217.
Ogden, F. L., and Dawdy, D. R. (2003). "Peak Discharge Scaling in Small Hortonian Watershed." *Journal of Hydrologic Engineering*, 8(2), 64-73.
Ogden, F. L., Richardson, J. R., and Julien, Y. (1995). "Similarity in catchment response 2. Moving rainstorms." *Water Resources Research*, 31, 1543-1547.
Onof, C., and Wheater, H. S. (1993). "Modeling of British Rainfall Using a Random Parameter Bartlett-Lewis Rectangular Pulse Model." *Journal of Hydrology*, 149(1-4), 67-95.
Peckham, S. D. (1995). "New Results for Self-Similar Trees with Applications to River Networks." *Water Resources Research*, 31(4), 1023-1029.
Peckham, S. D., and Gupta, V. K. (1999). "A reformulation of Horton's Laws for large river networks in terms of statistical self-similarity." *Water Resources Research*, 35(9), 2763-2777.
Pickands, J. (1975). "Statistical-Inference Using Extreme Order Statistics." *Ann Stat*, 3(1), 119-131.

Poveda, G., Vélez, J., Mesa, O., Cuartas, A., Barco, J., Mantilla, R., Mejía, J., Hoyos, C., Ramírez, J., Ceballos, L., Zuluaga, M., Arias, P., Botero, B., Montoya, M., Giraldo, J., and Quevedo, D. (2007). "Linking Long-Term Water Balances and Statistical Scaling to Estimate River Flows along the Drainage Network of Colombia." *Journal of Hydrologic Engineering*, 12(1), 4-13.

Rinaldo, A., and Rodriguez-Iturbe, I. (1996). "Geomorphological theory of the hydrological response." *Hydrological Processes*, 10(6), 803-829.

Rinaldo, A., Vogel, G. K., Rigon, R., and Rodriguez-Iturbe, I. (1995). "Can One Gauge the Shape of a Basin." *Water Resources Research*, 31(4), 1119-1127.

Robinson, J. S., and Sivapalan, M. (1997). "An investigation into the physical causes of scaling and heterogeneity of regional flood frequency." *Water Resources Research*, 33(5), 1045-1059.

Robinson, J. S., Sivapalan, M., and Snell, J. D. (1995). "On the relative roles of hillslope processes, channel routing, and network geomorphology in the hydrologic response." *Water Resources Research*, 31(12), 3089-3101.

Robinson, J. S., Sivapalan, M., and Snell, J. D. (1995). "On the relative roles of hillslope processes, channel routing, and network geomorphology in the hydrologic response of natural catchments." *Water Resources Research*, 31(12), 3089-3101.

Rodriguez-Iturbe, I., Cox, D. R., and Isham, V. (1987). "Some Models for Rainfall Based on Stochastic Point-Processes." *Proc R Soc Lon Ser-A*, 410(1839), 269-288.

Rodriguez-Iturbe, I., Cox, D. R., and Isham, V. (1987). "Some Models for Rainfall Based on Stochastic Point Processes." 269-288.

Rodriguez-Iturbe, I., Cox, D. R., and Isham, V. (1988). "A Point Process Model for Rainfall: Further Developments." *Proceedings of the Royal Society of London A: Mathematical, Physical and Engineering Sciences*, 417(1853), 283-298.

Rodriguez-Iturbe, I., Febres De Power, B., and Valdés, J. B. (1987). "Rectangular pulses point process models for rainfall: Analysis of empirical data." *Journal of Geophysical Research*, 92(D8), 9645-9645.

Rodriguez-Iturbe, I., and Rinaldo, A. (1997). *Fractal river basins: chance and self-organization*, Cambridge University Press, Cambridge.

Rodríguez-Iturbe, I., and Valdés, J. B. (1979). "The geomorphologic structure of hydrologic response." *Water Resources Research*, 15(6), 1409-1420.

Saco, P. M., and Kumar, P. (2004). "Kinematic dispersion effects of hillslope velocities." *Water Resources Research*, 40(1), W01301-W01301.

Schilling, K. E., Jha, M. K., Zhang, Y.-K., Gassman, P. W., and Wolter, C. F. (2008). "Impact of land use and land cover change on the water balance of a large agricultural watershed: Historical effects and future directions." *Water Resources Research*, 44(7), W00A09.

Schroeder, M. R. (1991). *Fractals, chaos, power laws : minutes from an infinite paradise*, W.H. Freeman, New York.

Seo, B.-C., Cunha, L. K., and Krajewski, W. F. (2013). "Uncertainty in radar-rainfall composite and its impact on hydrologic prediction for the eastern Iowa flood of 2008." *Water Resources Research*, 49(5), 2747-2764.

Seo, B.-C., and Krajewski, W. F. (2011). "Investigation of the scale-dependent variability of radar-rainfall and rain gauge error covariance." 152-163.

Seo, Y., Schmidt, A. R., and Sivapalan, M. (2012). "Effect of storm movement on flood peaks: Analysis framework based on characteristic timescales." *Water Resources Research*, 48(5), W05532-W05532.

Sherman, L. K. (1932). "The relation of hydrographs of runoff to size and character of drainage-basins." *Eos, Transactions American Geophysical Union*, 13(1), 332-339.

Sherman, L. K. (1932). "Streamflow from rainfall by the unit graph method." *Eng. News Rec.*, 108, 501-505.

Shreve, R. L. (1967). "Infinite topologically random channel networks." *The Journal of Geology*, 178-186.

Sivapalan, M., Bloschl, G., Merz, R., and Gutknecht, D. (2005). "Linking flood frequency to long-term water balance: Incorporating effects of seasonality." *Water Resources Research*, 41(6).

Sivapalan, M., Takeuchi, K., Franks, S. W., Gupta, V. K., Karambiri, H., Lakshmi, V., Liang, X., McDonnell, J. J., Mendiondo, E. M., O'Connell, P. E., Oki, T., Pomeroy, J. W., Schertzer, D., Uhlenbrook, S., and Zehe, E. (2003). "IAHS decade on Predictions in Ungauged Basins (PUB), 2003-2012: Shaping an exciting future for the hydrological sciences." *Hydrolog Sci J*, 48(6), 857-880.

Small, S. J., Jay, L. O., Mantilla, R., Curtu, R., Cunha, L. K., Fonley, M., and Krajewski, W. F. (2013). "An asynchronous solver for systems of ODEs linked by a directed tree structure." *Advances in Water Resources*, 53(0), 23-32.

Smith, J. A. (1992). "Representation of basin scale in flood peak distributions." *Water Resources Research*, 28(11), 2993-2999.

Smith, J. A., Baeck, M. L., Villarini, G., and Krajewski, W. F. (2010). "The Hydrology and Hydrometeorology of Flooding in the Delaware River Basin." *Journal of Hydrometeorology*, 11(4), 841-859.

Smith, J. A., Baeck, M. L., Villarini, G., Wright, D. B., and Krajewski, W. (2013). "Extreme Flood Response: The June 2008 Flooding in Iowa." *Journal of Hydrometeorology*, 14(6), 1810-1825.

Strahler, A. N. (1964). "Quantitative geomorphology of drainage basins and channel networks." *Handbook of Applied Hydrology*, V. T. Chow, ed., McGraw-Hill, New York, 4-39/34-76.

Tarboton, D. G., Bras, R. L., and Rodriguez-Iturbe, I. (1988). "The fractal nature of river networks." *Water Resources Research*, 24(8), 1317-1322.

Tasker, G. D., and Stedinger, J. R. (1986). "Regional Skew with Weighted Ls Regression." *J Water Res Pl-Asce*, 112(2), 225-237.

Taylor, A. B., and Schwarz, H. E. (1952). "Unit-hydrograph lag and peak flow related to basin characteristics." *Eos, Transactions American Geophysical Union*, 33(2), 235-246.

USACE (2010). "Des Moines River regulated flow frequency study." U.S. Army Corps of Engineers Rock Islands District, Rock Island, Illinois, 82p.

Veilleux, A. G., Cohn, T. A., Flynn, K. M., Mason, R. R., Jr., and Hummel, P. R. (2014). "Estimating magnitude and frequency of floods using the PeakFQ 7.0 program: U.S. Geological Survey Fact Sheet 2013–3108." *U.S. Geological Survey Fact Sheet*, 2.

Veitzer, S. A., and Gupta, V. K. (2001). "Statistical self-similarity of width function maxima with implications to floods." *Advances in Water Resources*, 24(9-10), 955-965.

Verstraeten, G., and Poesen, J. (1999). "The nature of small-scale flooding, muddy floods and retention pond sedimentation in central Belgium." *Geomorphology*, 29(3-4), 275-292.

Villarini, G., and Krajewski, W. F. (2010). "Review of the Different Sources of Uncertainty in Single Polarization Radar-Based Estimates of Rainfall." *Surv Geophys*, 31(1), 107-129.

Villarini, G., Smith, J. A., Baeck, M. L., and Krajewski, W. F. (2011). "Examining Flood Frequency Distributions in the Midwest U.S." *JAWRA Journal of the American Water Resources Association*, 47(3), 447-463.

Yang, G., Bowling, L. C., Cherkauer, K. A., and Pijanowski, B. C. (2011). "The impact of urban development on hydrologic regime from catchment to basin scales." *Landscape and Urban Planning*, 103(2), 237-247.

Yao, H., and Georgakakos, A. (2001). "Assessment of Folsom Lake response to historical and potential future climate scenarios 2. Reservoir management." *Journal of Hydrology*, 249(1-4), 176-196.

Young, G. K., Stein, S., Cole, P., Kammer, T., Graziano, F., and Bank, F. (1996). "Evaluation and management of highway runoff water quality." *Tech. Rep. for the Federal Highway Administration*, Washington, DC.